# DESIGN AND PERFORMANCE OF STAY-IN-PLACE UHPC PREFABRICATED PANELS FOR INFRASTRUCTURE CONSTRUCTION

by

**Kamal H. Khayat, P. Eng., Ph.D.**
**Vernon and Maralee Jones Professor**
Department of Civil, Architectural, and Environmental Engineering
Missouri University of Science and Technology

**Weina Meng**
Ph.D. Candidate
Department of Civil, Architectural, and Environmental Engineering
Missouri University of Science and Technology

August 2014

## *Disclaimer*

The contents of this report reflect the views of the author(s), who are responsible for the facts and the accuracy of information presented herein. This document is disseminated under the sponsorship of the Department of Transportation, University Transportation Centers Program and the Center for Transportation Infrastructure and Safety NUTC program at the Missouri University of Science and Technology, in the interest of information exchange. The U.S. Government and Center for Transportation Infrastructure and Safety assumes no liability for the contents or use thereof.

## Technical Report Documentation Page

| 1. Report No.  NUTC R320 | | 2. Government Accession No. | 3. Recipient's Catalog No. | |
|---|---|---|---|---|
| 4. Title and Subtitle  Design and Performance of Stay-In-Place UHPC Prefabricated Panels for Infrastructure Construction | | | 5. Report Date  August 2014 | |
| | | | 6. Performing Organization Code | |
| 7. Author/s  Kamal H. Khayat and Weina Meng | | | 8. Performing Organization Report No.  Project #00040515 | |
| 9. Performing Organization Name and Address  Center for Transportation Infrastructure and Safety/NUTC program  Missouri University of Science and Technology  220 Engineering Research Lab  Rolla, MO 65409 | | | 10. Work Unit No. (TRAIS) | |
| | | | 11. Contract or Grant No.  DTRT06-G-0014 | |
| 12. Sponsoring Organization Name and Address  U.S. Department of Transportation  Research and Innovative Technology Administration  1200 New Jersey Avenue, SE  Washington, DC 20590 | | | 13. Type of Report and Period Covered  Final | |
| | | | 14. Sponsoring Agency Code | |
| 15. Supplementary Notes | | | | |

16. Abstract

This project aims at designing a stay-in-place formwork system for cast-in-place bridge applications using ultra-high performance concrete (UHPC) that can be used in the permanent formwork construction. Such panels can be used as permanent formwork system that can exhibit extended service life given the high impermeability and resistance of the cover-crete to cracking, increase the cost-effectiveness, and decrease of deleterious materials in concrete, including chloride ions. The stay-in-place formwork can be used for new construction as well as in the rehabilitation of concrete infrastructure, including bridges. It is anticipated that this design concept will lead to substantial savings and reduced energy costs associated with the production, handling, and whole life performance of the cast concrete elements.

The key characteristics and benefits of the proposed product are: (1) the units will be more durable and much lighter than current products (less than 25 kg per unit), light enough that one person can carry a single unit. (2) faster construction due to simplicity of use. (3) reduction in the volume of transport. (4) the units will be "lego-like", in that they can easily be linked together in modular forms. (5) smooth surface finish that reduces the need for further surface work (that is, additional finishing). (6) environmentally advantageous structures; reduced carbon emissions compared to conventional on-site casting methods. (7) versatility regarding application, usage is not restricted to bridge columns but other elements, such as conventional wall structures.

The pre-fabricated panels were made of UHPC reinforced with fibers, such as micro steel fibers or micro polyvinyl alcohol (PVA) fibers, and glass fiber reinforced polymer (GFRP) grids or carbon fiber reinforced polymer (CFRP) grids which can provide bi-directional reinforcement.

| 17. Key Words  Carbon Foot Print, Concrete, Fiber-Reinforced Plastic Rebar, Ultra-High Performance Concrete, Rapid Construction, Stay-in-Placed Formwork | | 18. Distribution Statement  No restrictions. This document is available to the public through the National Technical Information Service, Springfield, Virginia 22161. | | |
|---|---|---|---|---|
| 19. Security Classification (of this report)  unclassified | | 20. Security Classification (of this page)  unclassified | 21. No. Of Pages  167 | 22. Price |

Form DOT F 1700.7 (8-72)

# DESIGN AND PERFORMANCE OF STAY-IN-PLACE UHPC PREFABRICATED PANELS FOR INFRASTRUCTURE CONSTRUCTION

By

Kamal H. Khayat, P. Eng., Ph.D.

Vernon and Maralee Jones Professor

Department of Civil, Architectural, and Environmental Engineering

Missouri University of Science and Technology

Weina Meng

Ph.D. Candidate

Department of Civil, Architectural, and Environmental Engineering

Missouri University of Science and Technology

A Report on Research Sponsored by

August 2014

# Executive summary

**Objectives:** This project aims at designing a stay-in-place formwork system for cast-in-place bridge applications using ultra-high performance concrete (UHPC) that can be used in the permanent formwork construction. Such panels can be used as permanent formwork system that can exhibit extended service life given the high impermeability and resistance of the cover-crete to cracking, increase the cost-effectiveness, and decrease of deleterious materials in concrete, including chloride ions. The stay-in-place formwork can be used for new construction as well as in the rehabilitation of concrete infrastructure, including bridges. It is anticipated that this design concept will lead to substantial savings and reduced energy costs associated with the production, handling, and whole life performance of the cast concrete elements.

The key characteristics and benefits of the proposed product are: (1) the units will be more durable and much lighter than current products (less than 25 kg per unit) light enough that one person can carry a single unit. (2) faster construction due to simplicity of use. (3) reduction in the volume of transport. (4) the units will be "*lego-like*", in that they can easily be linked together in modular forms. (5) smooth surface finish that reduces the need for further surface work (that is, additional finishing). (6) environmentally advantageous structures; reduced carbon emissions compared to conventional on-site casting methods. (7) versatility regarding application, usage is not restricted to bridge columns but other elements, such as conventional wall structures.

The pre-fabricated panels were made of UHPC reinforced with fibers, such as micro steel fibers or micro polyvinyl alcohol (PVA) fibers, and glass fiber reinforced polymer (GFRP) grids or carbon fiber reinforced polymer (CFRP) grids which can provide bi-directional reinforcement.

**Scope of work:** The project is divided into two phases with specific objectives that are described below. Phase I is completed and is presented in this report. Phase II is work under way and will be reported elsewhere.

Phase I: Design of Panel Material. The UHPC was optimized by experimentally selecting appropriate material constituents, such as specialty cement, silica fume, fine sands, fibers, and chemical admixtures. In this research, it is proposed to use high volumes of supplemental cementitious materials (SCMs) and fillers, as partial replacements for portland cement. UHPC is incorporated with fibers to secure excellent performance in terms of cracking resistance, mechanical behavior, and durability. The mix design of this material is optimized using experimental design approach. The grading of the solid skeleton is investigated to obtain an optimum packing density, which is necessary to reduce viscosity. The composition of the cement paste/mortar is optimized to achieve suitable rheological properties and segregation resistance of solid particles during flow and thereafter until the onset of setting. Performance-based design was developed for the UHPC. It is anticipated to produce a highly flowable material with mini-slump flow consistency of 260-300 mm, a 56-day compressive strength close to 150 MPa as well as 56-day splitting tensile and flexural strengths greater or equal to 10 MPa and 20 MPa, respectively.

This task also involves the optimization of the reinforcement systems for the UHPC panels. The panel configuration is closed to the proposed permanent formwork panel, which is about $500 \times 500 \times 40$ mm. FRP grids are proposed to reinforce the panel elements to produce light-weight panels with minimum thickness that are not prone to corrosion. The bond between the concrete material and FRP grids was investigated by innovative de-bonding tests in the laboratory. Flexural performance of the FRP girds was evaluated by "three point bending" tests. Detailing of the reinforcement will be optimized using finite element analysis (FEA).

Phase II: Design of Panel System. The proposed panels will be designed to be assembled as Lego-like for ease and speed of construction. The configurations of the panel system will be designed and optimized by conducting FEA, including appropriate selection of element dimensions, innovative designs of joints, stiffeners, and anchorages. Detailed three-dimensional finite element models will be established and the

nonlinear contact behavior between joints will be taken into account. The precast panels will be designed to resist various loads including self-weight, construction loads, wind, and earthquake. As stated earlier, the mass of each panel should be limited to 25 kg. Considering the specific gravity for the UHPC material of 2500 kg/m$^3$, the dimension of the panel should be about $500 \times 500 \times 40$ mm. Stiffeners will be designed, and their effect on the structure performance will be evaluated.

**Main findings:** In this report, the design of stay-in-place permanent formwork panel materials is presented. Performance-based design was developed for the UHPC. The final mixtures has a mini-slump flow consistency of 260 to 300 mm, 28-day compressive strength greater than 120 MPa, as well as 28-day splitting tensile and flexural strengths greater or equal to 10 MPa and 20 MPa, respectively. This project also involved the optimization of the reinforcement system for the UHPC panels. Two layers of GFRP type I reinforced UHPC shows good flexural performance both in strength and ductility. The following main findings can be drawn based on the results presented in this report.

(1) Using a supplemental cementitious material (SCM) as a cement replacement can significantly improve the workability of binder.

(2) The workability and rheological properties of cement paste and UHPC are influenced by the mixer type, mixing energy, and mixing time. The mixing procedure should be adapted to provide proper dispersion. In this study, the optimized mixing involved the use of Omni and EIRICH high-shear mixers.

(3) A star plot method introduced in this study enable the display of multivariate data in the form of a two-dimensional chart of three or more quantitative variables. By applying this method, four cementitious compositions: G50 (powder portion of cement:GGBS of 1:1 by volume), G50SF5 (powder portion of cement: GGBS:silica fume of 0.45:0.5:0.05, by volume), FAC40SF5 (powder portion of cement:fly ash c:silica fume of 0.55:0.45:0.05, by volume), and FAC60 (powder portion of cement:FAC of 0.4:0.6, by volume), were selected as candidates of cementitious matrix to design UHPC panel product.

(4) According to the result of the flow test, FAC 60 mixture resulted in the lowest minimum water content (MWC), which corresponded to highest packing density. The mixture also exhibited the highest relative water demand (RWD), which corresponds to best level of robustness. From the results of the flow test, it can also be observed that for the ternary cementious composition, the G50SF5 mixture showed the lowest MWC and highest RWD.

(5) By setting a target spread value, the high ranged water reducer (HRWR) demand for cementious compositions and UHPC mixes can be determined and compared. FAC 60 mixture required the lowests HRWR demand.

(6) The G50 mixture had the lowest viscosity determined using a co-axial rheometer at 20 to 90 minutes. The G50SF5 mixture also showed relatively low viscosity at of 40 min to 90 min after water addition.

(7) The intensive gyration testing was used to optimize the packing of fine aggregate. In this study, the combination of 30% masonry sand with 70% river sand, by mass, was selected as the optimized sand combination.Rheology testing was conducted with the ConTec Viscometer 5 to optimize agg/cm ratio, by mass. The lowest viscosity was combined with the results of flow properties and compressive strength. The optimum agg/cm ratio was determined to be 1.

(8) The selection of fiber was based on the result of three point flexural testing. The addition of 2% of high strength steel fibers, by volume, led to a posted cracking flexural strength of 28 MPa, which is approximately twice that of concrete reinforced with 0.5% fibers. A deflection at peak load of 1.05 mm was obtained with the 2% fiber UHPC, which is more than 10 times that of the UHPC without any fibers.

(9) With high volume of SCMs as cement replacement (50% slag or higher than 40% fly ash), the flexural performance can be improved, compared with the commercial reference mixture which was replaced with 25% silica fume by mass, the toughness increased by around 15%.

(10)   No special treatment, such as heat curing, or pressure or vacuum mixing was used. Mechanical properties can be expected to enhace from some treatment, including steam curing at 80 - 90℃ for 2 - 3 days.

(11) For the optimization of UHPC mix design, a commercial product was cast for comparison purposes. According to the results, at the same w/cm, the reference was with the lowest viscosity while the UHPC matrix with 50% GGBS led to the highest viscosity. In terms of compressive strength, the reference UHPC had 135 MPa at 28-day which was the highest strength. The Mix-1 G50SF mixture achieved 125 MPa which was 93% of the reference values. For the splitting tensile strength, the G50SF5 mixture also achieved the highest strength of 14 MPa, which is 16% higher than the reference mixture. Moduli of elasticity value for all mixtures were 45 to 53 GPa.

(12) In this study, all UHPC mixtures expect the FAC40SF5 mixture can achieve low risk of corrosion, based on electrical resistivity test results.

(13) According to drying shrinkage measurements, the G50SF5 and FAC60 mixtures are all within 150 microstrains for 56 days of testing, which performed better than the reference mixture (151 microstrains). For the autogenous shrinkage, the G50 mixture had 100 microstrains of autogeneous shrinkage at 56 days, which was the lowest.

The characterization of UHPC elements reinforced with internally installed FRP grids was evaluated. The tensile strength of individual FRP specimen, bond strength of the interface between FRP grids and UHPC, and flexural strength of FRP enhanced UHPC panels reinforced with CFRP and GFRP are also determined using three-point loading. The main findings are summarized below.

(14) Three types of FRP (GFRP type I, GFRP type II, and CFRP) grids were investigated. The strength and stiffness of individual CFRP specimens was the highest (119.1 kN/$\varepsilon$), which is 102% higher than that of GFRP type I; the strength and stiffness of individual GFRP type II specimens was the lowest (17.0 kN/$\varepsilon$); the performance of GFRP type I were in between the other types of grids (57.6 kN/$\varepsilon$)..

(15) Bond between the FRP grid and UHPC matrix was investigated by evaluating the strength between the FRP grids and UHPC. Pull-out tests were carried out. Fracture of FRP grid was took place for the failure mode. No debonding/slipping at the interfaces was observed, meaning that the debonding would not happen when the grids are well embedded in UHPC with an embedment length of at least 250 mm.

(16) Flexural strength of panels with different reinforcement configurations was investigated. Three-point bending tests were carried out. When there was no steel fiber in the mortar, once cracking was initiated, it propagated quickly until the failure of the mortar. Even if FRP grids were used as reinforcement, the flexural capacity was not significantly increased. The FRP grids could benefit concrete by improving the ductility. When concrete fractured, the grids could hold the panel sections, thus preventing sudden/instant collapse.

(17) When steel micro fibers were used as reinforcement in the mortar, the performance of the panels was significantly improved compared with the reference panel, in terms of flexural capacity (increased by 33%), deflection at peak load (increased by 166%), and dissipated energy was 11 times of the reference panel. The effectiveness of the FRP grids could be significantly improved by the inclusion of steel fibers that could restrain the cracking and increase the ductility. Compared panel 6 which reinforced with CFRP with panel 4, the dispatted energy is increased by 70%. Which means the interlock between the grids and fibers benefited the panels by the full development of the grids' strength. However, the grids could not appreciably increase the cracking strain limit of the UHPC to postpone the onset of the cracking according to the test results.

(18) The performance demonstrated by the dual-layer of GFRP reinforced UHPC panel was comparable to that of the single-layer CFRP reinforced UHPC panel.

   **Keywords:** stay-in-place formwork system, FRP girds, UHPC, fibers, SCMs.

Table of Contents

# CHAPTER 1. INTRODUCTION

## 1.1 Background

This research project focuses on developing a novel fast repair and construction permanent formwork system. To evaluate the application, several relevant aspects of the design, such as the mix design of UHPC, shrinkage characteristics at early age, flexural behavior of fibers, including micro steel fibers or micro PVA fibers, and FRP grids reinforcement were determined.

The UHPC is a new class of high-performance cement-based materials with much higher mechanical properties and toughness than that of high-performance concrete (HPC). UHPC is typically a micro-mortar reinforced with micro fibers (typically steel fibers) resulting in extremely impermeable and crack-resistant material. Such material can be used to produce precast panels that can be assembled on-site for the construction of infrastructure elements, such as column, girder, and bridge pier elements.

In this report, the constitunent materials needed to produce the UHPC were selected. SCMs were used to replace a portion of the cement content in order to enhance material properties and decrease the carbon footprint of the UHPC. The mix design of the UHPC was also optimized with the use of various materials, including fibers.

The configurations of the panel system will be designed and optimized by conducting FEA, including appropriate selection of element dimensions, innovative design of the joints, stiffeners, and anchorages. Joints, shear keys, stiffeners, fibers and FRP were considered in the design. The mass of each panel was limited to 25 kg, and the dimension of the panel is about 50 cm × 50 cm × 4 cm.

Prefabrication of the panels made with UHPC reinforced with FRP grids system can serve as a permanent formwork system that can provide excellent durability and cracking resistance. The prefabrication of such a high-tech material in a well controlled prefabrication environment can enhance the quality of the final product. Economic considerations associated with greater productivity in prefabrication setting, together with greater control of the working environment, can lead to improved efficiency and lower carbon foot print for the production of UHPC prefabricated panels for fast bridge cast-in-place construction.

The proposed approach revolves around lightweight, fiber reinforced, UHPC units reinforced with fiber composite grids. Figure 1.1, (a) shows the preliminary design idea, including the fiber composite grids. Figure 1.1, (b) shows the same model from a different view point along with a construction worker model, to help emphasize the scale of the panel system. Figure 1.1, (c) shows the beginning of how a potential framework could be constructed, a framework that would be used to both assemble the mold and provide permanent strength against shear and flexural forces.



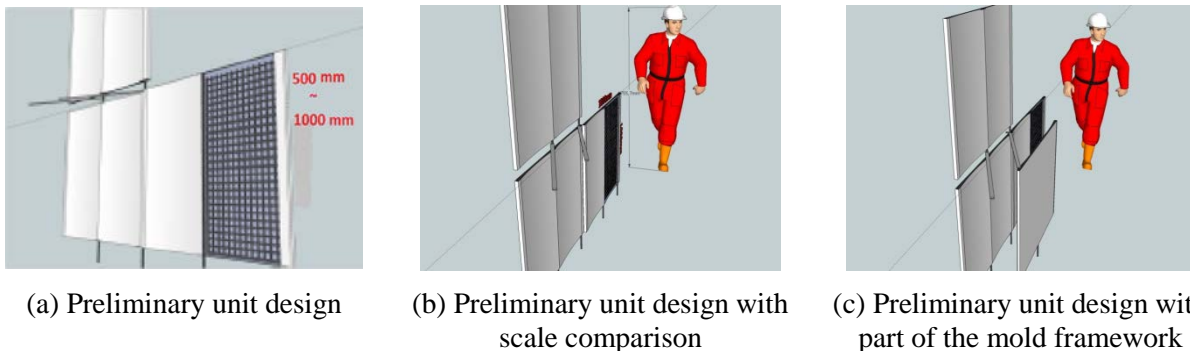| (a) Preliminary unit design | (b) Preliminary unit design with scale comparison | (c) Preliminary unit design with part of the mold framework |

Figure 1.1 Preliminary design and assembly of the permanent formwork system

The use of low carbon foot print prefabricated panels made with UHPC and reinforced with FRP can

result in several advantages transportation infrastructure systems, namely: (1) design of fast construction and rehabilitation system for transportation infrastructure that can exhibit extended service life given the high impermeability and resistance of the cover-crete to cracking; (2) the use of environmentally friendly UHPC can provide a rapid construction procedure that can increase the cost-effectiveness of this type of construction; (3) increasing the quality of the formwork system given greater  quality assurance and quality control are available in a prefabrication setting compared to cast-in-place concrete construction; (4) notable savings in labor and time by designing a permanent formwork system that eliminates the need for formwork removal and storage; (5) the system enables the design of architectural concrete with special surface treatment.

## 1.2 Literature review for UHPC and permanent formwork systems

Research work related to UHPC and the application has been underway at several universities and laboratories worldwide

### 1.2.1 Ultra-high performance concrete (UHPC)

The mechanical and durability properties of UHPC make it an ideal candidate for use in developing new solutions to pressing concerns about highway infrastructure deterioration, repair, and replacement (Graybeal, 2009).  The following section offers a brief review of some of the main properties of UHPC.

During the past four decades, researchers all over the world have been attempted to develop high performance cement-based materials, which include hot-pressed cement, macro-defect-free cement (MDF) (Birchall, et al., 1981), densified with small particles (DSP) (Bache, et al., 1981), and slurry infiltrated fiber concrete(SIFC) (Lankard and Newill, 1984), and etc. In 1993, Richard et al. in France used components with increased fineness and reactivity to develop reactive powder concrete (RPC) via heat treatment. RPC was characterized by high binder content, very low water-to-cement ratio, use of silica fume, fine quartz powder and high-rang water-reducing admixture (HRWR) and/or fine ductile fibers (Buck, et al., 2013). It generally gave over 150MPa for compressive strength, 5-15 MPa for uniaxial tension strength and 25-40 MPa for bending strength (Spasojevic, 2008). Furthermore, it exhibited high toughness and excellent durability (Habel, 2008). In the following year, De Larrard (1994) introduced the term "ultra high performance concrete" (UHPC). The production of UHPC often uses thermal curing at 90 ℃ or higher, which result in low production efficiency and high energy consumption (Feylessoufi, et al., 1997). Therefore, more and more researches have been conducted on the selection of raw materialsand curing regimes, and their influences on the microstructural characteristics, mechanical properties and durabilityof UHPC to facilitate their production and applications (Reda, et al., 1999).

In 2011, Graybeal defined UHPC is a cementitious composite material composed of an optimized gradation of granular constituents, a water-to-cementitious materials ratio (w/cm) less than 0.25, and a high percentage of discontinuous internal fiber reinforcement (Graybeal, 2011). The mechanical properties of UHPC include compressive strength greater than 21.7 ksi (150 MPa) and sustained post cracking tensile strength greater than 0.72 ksi (5 MPa). The most distinguishing characteristics of the composition of UHPC are the lack of coarse aggregate, the use of fibers, high proportion of cement/cementitious materials, and low volume of water. The use of only fine sand aggregate creates dense cement matrix with minimal voids that can be occupied by cementitious materialswhich results in a significant increase in strength (Graybeal, 2011).

The fibers in the cement matrix are designed to provide a bond at the micro level and minimize micro-cracking. In turn, the inclusion of fiber acts as micro-reinforcement similar to mild steel reinforcement in conventional reinforced concrete on the macro level.

### Mechanical Properties of UHPC

#### Compressive Strength

One of the most significant assets of UHPC is the improvement in compressive strength. UHPC uniaxial compressive strength is higher than 150 MPa. This improvement in compressive strength has far exceeded the results achieved with conventional concrete and can allow for the possibility of UHPC to be more competitive in markets that have been typically dominated by steel construction. Early age curing can have marked influence on mechanical properties, as discussed later. In tests conducted by Graybeal and Hartmann (2003), the curing method applied yielded significant variations in compressive strength, up to a 65% difference between steam curing and ambient air curing. While various curing methods can be applied in field applications, the quality control on curing methods makes UHPC more suitable for precast operations (Graybeal and Hartmann, 2003).

#### Tensile Strength / Flexural Strength

The significant improvements in compressive strength are complimented by the fact that UHPC also exhibits tensile strength that has not been demonstrated in conventional concrete. This tensile strength allows the material to support both pre-cracking and post-cracking loads without experiencing a brittle failure that is common in conventional concrete. Concrete materials produced with short, randomly distributed fibers may be superior to concrete reinforced using welded wire mesh or rebars. Both the tensile strength and toughness, especially the post-crack strength, can be improved when using fibers (Bentur and Mindess, 1990). It has been shown that due to the reduced specific spacing, the use of fibers can strengthen the composite at the micro level by bridging the microcracks before they reach the critical flaw size (Mobasher and Li, 1996). The small diameter of the individual fibers ensures a better and more uniform distribution of reinforcement. In addition, the high surface area offers significant bond capability. Since the bond strength of glass, steel, or even polymeric fibers is far superior to reinforcing bars, this increases the efficiency of reinforcement so that there is limited crack opening due to the debonding and pullout of the reinforcement. The fibers are distributed randomly, offering efficiency in load transfer by the fiber phase. Finally, because the fibers that bridge the matrix cracks are resilient and highly compliant, they can be oriented to carry the load across the crack faces. This can result in finely distributed and of fibers that can enhace durability of concrete and the service life of the structure.

UHPC can develop tensile strength ranging from 5-15 MPa with various curing regimes (Spasojevic, 2008). These tensile strength values are achieved as a result of the interaction of the steel fibers on the microscopic level and their ability to sustain load after the onset of cracking. In addition to the improvements in tensile strength, UHPC can also achieve flexural strengths ranging from 25-40 MPa (Spasojevic, 2008). This combination of the tensile and flexural strength makes UHPC an extremely ductile material, capable of supporting significant loads beyond cracking, which would be the ideal materials for a stay-in-place formwork system.

#### Modulus of elasticity

The UHPC can have a modulus of elasticity ranging between 50 and 60 GPa with an ultimate compressive strength between 150 to 180 MPa at 28-days and a compressive strength of 30 MPa after 24 hours of casting (Spasojevic, 2008). The density of the UHPC is 2500 kg/m$^3$ (Lafarge 2008).

#### Curing of UHPC

UHPC has a low w/cm, which increases its tendency to undergo shrinkage of early age. The risk of early age cracking in UHPC is complex and depends on thermal effects, drying, autogeneous strains and stresses, stress relaxation, and structural detailing and execution that capture the degree of restraint (Tang, 2004). The reduced water content in UHPC necessitates careful attention to curing practices to minimize water loss prior to a given degree of hydration. Proper curing of the surface eliminates the possibility of surface dehydration, which can lead to cracking and significant degradation of final material properties.

Immediately after casting, any exposed UHPC surface needs to be sealed with an impermeable layer, and perfectly in contact with curing water to avoid early drying the surface. When the material is sealed, the seal must rest against the UHPC and should not allow for any space between the covering material and the fresh concrete. Sealing of the surface eliminates the possibility of surface dehydration, which can lead to cracking and significant degradation of final material properties. Supplemental heat may be applied to UHPC castings after placement in order to accelerate setting behaviors and attainment of final properties.

Initial curing is required during the dormant period of cement hydration to prevent water loss and maintain the UHPC of an appropriate temperature until setting. The second curing phase may or may not involve elevated temperature conditions and a high moisture environment, depending on the desired level of strength gain. But if needed, the compressive strength of UHPC can be increased considerably by using post-set heat curing. Higher curing temperatures resulted in higher compressive strengths (Heinz, and Ludwig, 2004).

Room temperature water curing, heat curingunder atmospheric pressure and autoclave curing are often used for production of UHPC. During early age curing, concrete can absorb water from its environment. Hence, self-desiccation shrinkage can be delayed and cracking may be avoided. Based on the quality of the curing regime, UHPC can be subjected to wetting in lime water. It can be expected that the quality of the curing regime and the effects of the surrounding environment may be responsible for considerable dimensional instability due to moisture changes and can thus have major consequences on the long-term performance of the UHPC.Researches on hydration and pozzolanic reaction of UHPC showed that the average C-S-H chain length wasshort and the pozzolanic activity were weak when the curing temperature was 20 ℃ (Zhang, et al., 2008). If the curing ages was reasonably prolonged, the compressive strength could also reach to 150 MPa (Zhang, et al., 2008). Through 24 hours steam curing, about 15-30 MPa compressive strength was further gained when compared to that after 28-days room temperature curing (Zhang, et al., 2008). When steam curing, as the temperature increased to 90 ℃, it was important to prolong the heat curing duration which influenced not only the pozzolanic activity of silica fume, but also the chain length of C-S-H. Increasing the curing temperature could make the chain length longer as well (Masse, et al. 1993). Heat curing of UHPC usually consists of steam curing at 90℃ for 2 days, which is not always easy to apply in the precast industry (Staguet and Espion, 2004). Therefore, understanding the influence of in-place environmental conditions and normal temperature-curing regimes during the early-age stage is essential before taking UHPC from the laboratory to field application. The compressive strength of UHPC specimens after autoclave curing was larger than those after room temperature curing (23 ℃) and heat curing (90 ℃) (Zhang, et al., 2008). This extreme differenc in compressive strength reached up to 30 MPa (Zhang, et al., 2008). It was only through 8 hours autoclave curing that over 200 MPa compressive strength was achieved for UHPC (Yang, et al., 2009). Yazici (2007) found that compressive strengths at UHPC mixtures with high volume mineral admixtures after 8 hours of high-pressure steam curing at 20 ℃ were higher than that of the specimens cured in water at room temperature (23 ℃) (Yazici, et al., 2007). Massidda et al. (2001) found that the flexural strength of specimens reached 30 MPa after 3 hours of high-pressure steam curing. However, Yazici found that autoclave curing greatly reduced the flexural strength compared with those after room temperature curing at 28-days (Yazici, et al., 2009).

Curing methods also affect shrinkage and creep of UHPC. About 87% of the total autogenous shrinkage occurred during the thermal treatment due to accelerated rate of early hydration at higher temperature (Garas, 2009). However, its complicated operationand high energy consumption limit its applicationin practice. Development of UHPC production at room temperature is a key for its wide applications.

### Effect of fibers on the behavior of UHPC

Fibers are added to cementitious materials to improve the characteristics in the hardening or the hardened state. To optimize the performance of a single fiber, fibers need to be homogeneously distributed; clustering of fibers has to be counteracted.

The mixture composition of fiber-reinforced concrete (FRC) often is a compromise between the requirements on the fresh and the hardened states. The shape of the fibers differs from that of the aggregates; due to the long elongated shape and/or a higher surface area, the workability of concrete is affected. The practical fiber content is limited: a sudden decrease of workability occurs at a certain fiber content, which depends on the mixture composition and the applied fiber type.

The incorresponding of fibers can affect workability. The shape of the fibers is more elongated compared with aggregates; the surface area at the same volume is higher. Stiff fibers can change the structure of the granular skeleton, while flexile fibers can fill the space between them. Stiff fibers push apart particles that are relatively large compared with the fiber length, the porosity of the granular skeleton increases. Furthermore, the surface characteristics of fibers differ from that of cement and aggregates, e.g. plastic fibers might be hydrophilic or hydrophobic. Finally, fibers often are deformed to improve the anchorage between a fiber and the surrounding matrix. Steel fiber-reinforce concrete (SFRC) appears stiffer compared with conventional concrete without fibers, even when the workability is the same (Johnston, 2011). Vibration is needed to increase density, decrease air void content, and improve bond between the cemment matrix and fibers. The fiber aspect ratio (Lf/df) as well as the fiber volume should be optimized to enhance mechanical properties and workability (Johnston, 2011). A given fiber diameter and volume fraction, the proformance of the SFRC is related to the aspect ratio of the fibers. The relative fiber to coarse aggregate volume and the "balling up" phenomenon govern the maximum possible content of steel fibers (Swamy & Mangat, 1974).

### Typical composition of UHPC

With the significantly improved physical properties of UHPC, there are a number of advantages when compared to conventional concretes and even steel for structural applications. The high strength of UHPC allows designing smaller sections and thus reducing the weight of the products. UHPC structures are expected to have a longer service life than conventional reinforced concrete structures. UHPC is designed to be able to resist the effects of damaging environments and save money over the life of a project.

UHPC formulations often consist of a combination of portland cement, fine sand, silica fume, HRWR, fibers, and water. Small aggregates are sometimes used, as well as a variety of chemical admixtures. Different combinations of these materials may be used, depending on the application and supplier. Some commercial products are listed in Table 1.1.

In a study of the durability of UHPC, Teichmann and Schmidt used the mix proportioning shown in Table 1.1, UHPC type 1.  It had a maximum aggregate size of 8 mm (Teichmann and Schmidt, 2002). The UHPC type 2 shown in Table 1.1 used most often in North America for both research and application. In 2005, Rossi developed the UHPC type 3. The proportions of this UHPC are presented in Table 1.1. By optimizing the cementious matrix for compressive strength, packing density, and flowability; using high tensile strength, fine-diameter steel fibers; and tailoring the mechanical bond between the steel fiber and cement matrix, 28-day compressive strength in excess of 200 MPa on 50 mm cubes were achieved with no heat or pressure curing (Wille, 2011). Table 1.1 also gives this UHPC type 4 mix proportion. UHPC type 5 was developed by researchers at the U.S. Army Corps of Engineer Research and Development Center. The proportions of this UHPC are also presented in Table 1.1.

Table 1.1 Typical compositions of UHPCs

| Type | Materials | kg/m$^3$ |
|---|---|---|
| UHPC type 1 (Teichmann and Schmidt, 2002) | Portland cement | 733 |
| | Fine quartz | 183 |
| | Silica powder | 230 |
| | Sand | 1008 |
| | HRWR | 32.9 |
| | Steel fibers | 194 |

| Type | Materials | kg/m³ |
|---|---|---|
| | Water | 161 |
| UHPC type 2 (Graybeal, 2006) | Portland cement | 712 |
| | Fine sand | 1020 |
| | Silica fume | 231 |
| | Ground quartz | 211 |
| | HRWR | 30.7 |
| | Accelerator | 30.0 |
| | Steel fibers | 156 |
| | Water | 109 |
| UHPC type 3 (Rossi, et al., 2005) | Portland cement | 1050 |
| | Sand | 514 |
| | Silica fume | 268 |
| | HRWR | 44 |
| | Steel fibers | 858 |
| | Water | 180 |
| Type | Materials | Proportions (by weight) |
| UHPC type 4 (Wille, et al., 2011) | Portland cement | 1.0 |
| | Fine sand | 0.92 |
| | Silica fume | 0.25 |
| | Glass powder | 0.25 |
| | HRWR | 0.0108 |
| | Steel fibers | 0.22 to 0.31 |
| | Water | 0.18 to 0.20 |
| UHPC type 5 (Williams, et al., 2009) | Portland cement | 1.0 |
| | Sand | 0.967 |
| | Silica fume | 0.389 |
| | Silica flour | 0.277 |
| | HRWR | 0.0171 |
| | Steel fibers | 0.31 |
| | Water | 0.208 |

### Recent applications

Applications of UHPC in Europe, North America, Australia, Asia and New Zealand have been reported as well (Rebentrost and Wight, 2008; Schimidt and Fehling, 2005; Graybeal, 2008). The high compressive and tensile strengths allow for the redesign and optimization of structural elements. Concurrently, the enhanced durability properties facilitate a lengthening of design life and allow for potential use as thin overlays, claddings, shells, or formwork. The flexural toughness of UHPC enhanced with fine steel fibers is greater than 200 times that of conventional fiber reinforced concrete (Ngo, et al, 2005). Furthermore, under very high strain rates (>250 1/sec), the ultimate compressive and tensile capacities can increase up to 1.5 times (Fujikake, et al, 2005). The Bourg-Les-Valence bridges in France are claimed to be the first UHPC road bridges (Hajar, et al., 2004). The Horikoshii Highway C-Ramp Bridge was Japan's first highway bridge using UHPC (Tanaka, et al., 2009). The use of UHPC in the girders allowed reduction of the number of girders from 11 to 4. The overall weight of the bridge was reduced by 30% (Tanaka, et al., 2009). In the United States, the two-way ribbed precast slab system (Figure 1.2), uses the mechanical and durability properties of UHPC to create a resilient, lightweight deck. This concept has been tested and was scheduled to be deployed by the Iowa Department of Transportation in 2011(Aaleti, et al., 2011). UHPC is also being investigated for use in a variety of other applications. These applications include precast concrete piles, seismic retrofit of substandard bridge substructures, thin-bonded overlays on

deteriorated bridge decks, and security and blast mitigation applications (Massicotte and Boucher, 2010). Figure 1.3 shows the panels for the first structure incorporating blast resistant optimized UHPC panels were manufactured in 2005 Melbourne (Lafarge, 2011). In general, UHPC has proven to be particularly relevant in applications where conventional solutions are lacking.



Figure 1.2 Typical UHPC panel

(Aaleti, et al., 2011)

Figure 1. 3 UHPC blast resisting panels

(Lafarge, 2011)

Figure 1.4 shows UHPC was delivered via truck chute to a precast girder form.



Figure 1. 4 UHPC  delivery (Graybeal, B., 2011)

However, there are numerous challenges before wide spread implementation due to lack of commonly accepted standards for the selectionof the materialsand test methods, design guidesf or engineers and quality control methods in manufacturing facilities (Ahlborn and Steinberg, 2012).

1.2.2 Fiber reinforced polymer (FRP) grids reinforced structures

The proposed precast, permanent stay-in-place UHPC panel system can be reinforced with FRP. By using FRP, the weight of the panel can be significantly reduced.The following part reviews FRP reinforced concrete structure.

**Overview of hybrid FRP concrete systems**

In recent years, newer methods of construction using high performance structural materials, including FRP, have been investigated. Advantageous properties of FRP include high strength-to-weight ratio, high machanical strength, resistance to corrosion, and ease of installation relative to other structural materials.

FRP composite systems are created by fabricating a resinous matrix into which continuous fibers are embedded. The fibers, which provide the strength and stiffness to the composite system, are typically carbon fibers, glass fibers, or aramid fibers. The type of fiber dictates the nomenclature of the composite system: glass fibers are used in glass fiber reinforced polymer (GFRP) composites; carbon fibers are used in carbon fiber-reinforced polymer (CFRP) composites; and aramid fibers are used in aramid fiber-reinforced polymer (AFRP) composites. The resinous matrix, which provides rigidity and protection to the embedded fibers, is typically made from epoxy, polyester, or vinylester resin (Teng et al., 2002).

CFRP composites are generally durable, have excellent fatigue characteristics, and can exhibit high durability in most environmental conditions. They are highly stiff and brittle and are susceptible to galvanic corrosion. GFRP composites provide exceptional thermal insulation and low cost, but are susceptible to moisture in high alkaline environments. AFRP composites exhibit excellent toughness, damage tolerance, and have good fatigue characteristics. Challenges related to AFRP composites include high costs, high moisture absorption, and poor compressive properties (Ortega, 2009).

Tests on hybrid FRP-concrete structural members, many for the purpose of bridge applications, have been performed at institutions internationally with promising results. When used in the fabrication of a hybrid structural member, the FRP section often has the added advantage of acting as a stay-in-place formwork for the concrete. The short and long-term performance of hybrid FRP-concrete structural members was investigated by Deskovic et al. (1995), with emphasis on maximizing the advantageous properties of each material used. Kim et al. (2006) performed experimental tests on modular hybrid FRP-concrete bridge deck systems, using shear connecting plates fabricated monolithically with the FRP module as well as coarse sand coating to generate sufficient bond between the concrete and the FRP. Cheng and Karbhari (2005) studied the performance of a composite FRP-concrete deck panel system that utilizes a series of shear ribs perpendicular to a series of vertical stiffeners bonded on top of a FRP deck panel fabricated from a combination of carbon and E-glass FRPs. An FRP bridge deck system can weigh about 20% of a similar deck (Keller 2005).

Non-prestressed and prestressed internal FRP reinforcements for concrete have been under development since as early as the 1970s in Europe (Taerwe and Matthys, 1999; and Japan Fukuyama, 1999), although the overall level of research, demonstration, and commercialization has increased markedly since the 1980s. FRP reinforcements have been used primarily in concrete structures requiring improved corrosion resistance or electromagnetic transparency. Internal FRP reinforcements have been fabricated in a variety of one-dimensional and multidimensional shapes (Nanni, 1993).

To date, most commercially prefabricated multidimensional reinforcements are orthogonal, two-dimensional grids, although three-dimensional grids of various configurations have been proposed for certain precast structures. As with steel reinforcements, multidimensional FRP reinforcements can also be fabricated onsite by hand placement and tying of one-dimensional shapes. Grid reinforcements have been made by winding resin impregnated bundles of fibers into prescribed two and three dimensional shapes using a variety of manufacturing processes (Nanni, 1993). The grids are often used as flat, two-dimensional flexural reinforcement in slabs or three-dimensional cages for combined shear and axial reinforcement in beams. The joints of FRP grids dominate bond stiffness and strength, in effect providing a periodically bonded reinforcement system in cases where minimal bonding exists between the cross-over points (Matthys and Taerwe, 2000).

### Hybrid FRP grids reinforced structural members

An FRP grid is a multidirectional prefabricated composite. FRP grids are typically produced in large rolls and then cut into the required dimensions. The improved performance is due to the aligned fibers in a certain direction and that there are no unpenetrated fibers of fiber bundles with would prematurely fail. Furthermore, the thinner grids can are flexible and can be adapted to curved surfaces.

The grids are often used as flat, two-dimensional flexural reinforcement in slabs or three-dimensional

cages for combined shear and axial reinforcement in beams. In 2000, Mathys and Taerwe concluded that, when FRP grids were used in non-prestressed concrete structures, the design was mainly governed by serviceability criteria. To ensure enough flexural stiffness for deflection control, higher reinforcement ratios of depths are needed. The advantage of the high tensile strength of FRP can, therefore, only be partly utilized. As a result, FRP is not attractive to be used only as a substitute of steel. Its use would be mainly related to specific characteristics, such as resistance to classical corrosion, low weight, and nonconductivity (Matthys and Taerwe, 2000.)

The flexural behavior of concrete beams reinforced with 2D FRP grids was evaluated using simply supported concrete beams subjected to four-point monotonic loading The study concluded that, the grids was shown to provide an effective force transfer mechanism (Yost, et al., 2001). In 2007, Taljsten implemented pilot tests where the epoxy was replaced with a cement bonding agent for retrofitting. (Taljsten and Blanksvard, 2007.) Lining Ding et al. studied the behavior of concrete piles confined with CFRP grids, indicating that the specified C-Grid can provide equivalent performance or more than typical spiral steel reinforcement for precast prestressed concrete piles (Ding and Hatem, 2010). In 2012, Maria Rosa Valluzzi et al. successed to develope a standardized, reliable procedure for characterizing the bonding mechanism of masonry elements strengthened with cementitious composites under shear actions.

The performance of FRP reinforced systems in UHPC matrix will be strongly depended on the bond between the fiber and UHPC. When using strain-hardening mortars, there is a chemical bond between the mortar fine-grain aggregates and the fibers, which affects bond of the embedded FRP reinforcement in the UHPC. Bond characteristics influence the mechanism of load transfer between reinforcement and concrete, and therefore control the concrete crack spacing, crack width, required concrete cover to the reinforcement, and the reinforcement development length. The behavior of strengthened concrete structures thus depends on the integrity of the bond. Most literature to date has been published about bond of FRP bars in concrete or other cementitious matrix. Very little literature is found on bond of FRP grids to cementitious material which is more complex because of the geometry of the grid. The innovative testing method successfully performed by Carozzi (Carozzi, et al., 2014) to estimate the bond between concrete and the FRP grid.

Hybrid systems range from open or closed stay-in-place formwork to hybrid structural systems, incorporating FRP and concrete elements (ACI 440.2R–02). For hybrid systems in particular, connectionsof FRP-to-concrete, represent a critical research need (ACI 440.3R–07). Hybrid materials leverage the beneficial properties of different FRP materials in a single element, often such an approach is used to develop "pseudo-ductility." Despite promising developments in the implementation of FRP grids for construction of concrete structures, many challenges exist that have prevented additional growth of this market. Such challenges include: brittle failure of FRP-strengthened concrete structures due to sudden failure modes, such as FRP rupture or debonding (Galal and Mofidi, 2010); deterioration of the mechanical properties of FRP due to harsh environmental conditions such as wet-dry cycles and freeze-thaw conditions (Belarbi and Bae, 2007); a reduction in strength due to the effects of improper installation procedures (Orton, 2007); and lack of agreement among debonding behavior and bond length models (Ben Ouezdou et al., 2009).

## 1.2.3 Permanent formwork

### Introduction

Permanent formwork, or stay-in-place formwork, are formwork left in place that may become an integral part of the structural frame. The use of short fiber and continuously reinforced cementitious panels as stay-in-place panels for formwork has been examined by a number of researchers and organizations (Wrigley, 2001). Such panels may form part of the final structural load-carrying system or may only be used to carry the construction loads and the weight of the wet concrete. Thin, cementitious panels reinforced only with short bare fibers of glass, and synthetic polymers have been studied for many years

(True, 1985; PCI, 2001; Bentur and Mindess, 2007). Both flat and corrugated panels have been produced for use in the construction industry and are reported to be used in a number of European countries. Very thin (less than 15 mm) panels, whether corrugated or flat must be produced using an automated spray-up process and are therefore quite expensive. Somewhat thicker flat panels (from 25 to 45 mm) that are produced in regular molds, using conventional concrete mixures (typically with aggregate less than 12 mm) are more economical. These panels are typically brittle and have poor impact resistance. In order to improve their impact resistance and ductility, they can be reinforced with a separate continuous reinforcement system, such as a reinforcing bar, grid, or textile (Reinhardt, 2000; Brameshuber et al., 2002; Bramshuber, 2006). In order to prevent corrosion in these thin cementitious panels, nonmetallic bars and grids are preferable. In bridge construction where the formwork is often placed at high elevations with no scaffolding below, guaranteeing the safety of the construction workers is of paramount concern.

There is a lack of published work for the vertical element of permanent formwork, such as wall and bridge columns. Recently, research focused on the use of permanent formwork panels for bridge decks or slabs. Kim et al. (2008) used glass fiber reinforced concrete (GFRC) for permanent formwork for bridge deck which was limited to relatively short spans due to the material's modest flexural capacity. These limitations were overcome by reinforcing GFRC with rod reinforcement. They developed the thin GFRC permanent formwork capable of spanning up to 3 m (Kim, et al., 2008; Kim. 2006). The investigation of a structural FRP stay-in-place (SIP) form used to construct and reinforce a deck for a prototype military bridge system was discussed, and design guide equations were developed (Hanus, et al., 2009). Leung and Cao (2008) investigated a new approach for the construction of durable concrete structures. They fabricated bridge deck permanent formworks using pseudo-ductile cementitious composites (PDCC) of relatively low w/cm. Normal concrete was then cast to farbricate structural components for testing. With low permeability and high crack resistance, the permanent formwork acts as effective surface cover to prevent the corrosion of steel reinforcements. In their work, the PDCC formwork incorporated GFRP rods. In some structural components, the GFRP reinforcement was found to provide sufficient loading-carrying capacity. Test results on concrete beams made with GFRP reinforced PDCC formwork was compared to theoretical prediction values. Leuang and Cao (2010) also presented that the bonding between the formwork system and concrete cast within the formwork improved significantly by treating surface of the formwork with transverse and longitudinal grooves stiffeners that can be introduced in the formwork (Leung and Cao, 2010). In 2012, a novel joining method for permanent formwork involving the embedment of GFRP in high-strength fiber reinforced cementitious composites (HSFRCC) was proposed by Jin and Leung. Direct pull-out tests were carried out to investigate the bonding capacity between the HSFRCC and GFRP reinforcement. The required embedded length of GFRP bars was determined and the joint width can then be determined. (Jin, et al., 2013). Gai, et al. (2013) investigated a novel FRP stay-in-place structural formwork system for concrete slabs with particular emphasis on the ductility of the system. The system consists of a molded glass fiber reinforced polymer (GFRP) grating bonded to square pultruded GFRP box sections as structural stay-in-place formwork for a concrete slab (Xian Gai, et al., 2013).

### Design considerations

Specification is required for the design of SIP panel systems (ACI 347-04, 2004). Size, span, fastenings, and other special features pertinent to this type of form, such as being water repellent and protected against chemical attack from wet concrete; and the minimum requirements should be followed. Particular care should be taken in the design of such forms to minimize distortion or deformation of the form or supporting members under the construction loads. In the structural analysis of permanent rigid forms, both the construction dead and live loads on the form, as well as the structure's stability during construction, should be considered, in addition to consideration of the form's performance in the finished structure (ACI 347-04, 2004). When a metal deck is used as a permanent form to become an integral part of the structure, its shape, depth, gage, coating, physical dimensions, properties, and intermediate temporary support should be according to contract documents. If structural continuity is assumed in the

design of the form, the required number of permanent supports over which the form material should be continuous should be specified (PCI Committee on Tolerances, 1985).

### Use of precast concrete for stay-in-place panels

Precast concrete panels or molds have been used as formworks for cast-in-place and precast concrete, either as permanent formwork, integrated formwork, or as removable and reusable formwork (ACI 347-04, 2004). They have been used for both structural and architectural concrete, designed as structurally composite with the cast-in-place material or to provide a desired quality of outer surface and, in some cases, to serve both of these purposes (Bank, et al., 2008). Concrete form units can be plain, reinforced, or prestressed, and either cast in the factory or at the job site. The most common use of precast concrete form units has been for elevated slabs acting compositely with topping concrete, as in bridge and commercial or institutional construction (Bank, et al., 2008). Precast units are also common as ground holding systems in tunneling and as stay-in-place forms for rehabilitation of navigation lock walls.

Effective bond between precast form unit and the concrete structure is essential and can be achieved by: 1) special treatment, such as grooving or roughening the form face in contact with the structure concrete; 2) use of anchoring devices extending across the interface between form panel and structure concrete; 3) a combination of 1) and 2); and 4) use of paint-on or spray-on bonding chemicals (ACI 347-04, 2004). Lifting hooks in a form unit can be designed to serve also as anchors or shear connectors.

**Vibration**-Thorough consolidation of site-cast concrete is required to prevent voids that would interrupt the bond of the form to structure concrete, but sufficient care should be used to prevent damage of concrete panels by contact with vibrators.

**Protection of architectural finish**-Care should be taken to avoid spilling fresh concrete on exposed surfaces, and any spilled or leaked concrete should be thoroughly removed before it has hardened. After concreting, protection of precast architectural concrete form facings may need to be considered.

### Design Method

Most of the current standards are devoted to the design of the formwork for normal vibrated concrete. Currently, standards are being updated to include provisions for the newly adapted concrete, such as the flowable concrete and self-consolidating concrete (SCC). Formwork should be designed for the ultimate as well as the serviceability limit states. Different loads, such as wind, equipment/construction loads, snow, dead loads, live loads and the lateral pressure of concrete have to be considered (ACI 347-04). The system stability and member buckling should also be investigated. The design of the formwork takes into accounts the service loads or loads magnified by a safety factor. The bearing capacity of the formwork has to be calculated according to the materials used and the existing design concept. It should be noted that the calculation of the loads as well as the bearing capacity of the formwork should be based on the same design concept（Proske, et al., 2013）.

"ACI 347-04: Guide to Formwork for Concrete. American Concrete Institute, 2004.", "CAN/CSA S269.3: Concrete formwork, 1992." and "DIN 18218:1980-09 Frischbetondruck auf Lotrechte Schalungen (Pressure of Fresh Concrete on Vertical Formwork). Berlin, 1980." are considered to be the most widely used regulations for the calculation of form pressure. Most documents consider only concrete with ordinary consistency. Specific regulations for highly workable concrete and SCC are not included in the standards. In this case, hydrostatic pressure should be assumed for the design of the formwork, unless the concrete is pumped from the bottom where an additional of 25% pressure should be used to allow for pressure submerges. To achieve a more economic formwork design, a number of research efforts have been made to investigate form pressure characteristics exerted by highly flowable concrete, including SCC. These approaches take into consideration a number of concrete flow characteristics, including thixotropy, loss of slump flow, and initial setting time. More recently, the German Standard DIN 18218:2010-01 "Pressure of Fresh Concrete on Vertical Formwork'' was modified to include some of

these findings.

Concrete columns are usually one of five shapes: square, rectangular, L-shaped, octagonal, or round. For the design method of bridge columns, it is specified by the shape of the columns. The design procedures can follow the American Concrete Institute recommendation (ACI 318, ACI 347).

Some common design deficiencies that can lead to failure are: (1) lack of allowance in design for loadings, such as wind, powderbuggies, placing equipment, and temporary material storage; (2) inadequate reshoring; (3) overstressed reshoring; (4) insufficient anchorage against uplift due to battered form faces; (5) insufficient allowance for eccentric loading due to placement sequences; (6) failure to investigate bearing stresses in members in contact with shores or struts; (7) failure to provide proper lateral bracing or lacing of shoring; (8) failure to investigate the slenderness ratio of compression members; Formwork coatings; (9) temporary openings or attachments for climbing crane or other material handling equipment.

Unless the rate of placement can be controlled to a design specified rate, column forms shall be designed for full hydrostatic pressure. Determining the lateral pressure of the freshly placed concrete against the column forms is the first step in the design of column forms. Because forms for columns are usually filled rapidly, frequently in less than 60 min, the pressure on the sheathing will be high, especially for tall columns.

The formwork design is according to ACI 347-04. The lateral pressure diagram of concrete is trapezoidal in shape, as shown in Figure 1.5. The diagram is presumed to be a triangular distribution from the upper free surface of the casting down to some limiting depth, beyond which the value of pressure reached is considered constant until the bottom of the formwork. The significant variables considered are the rate of placement, consistency of concrete, coarse aggregate concentration, aggregate nominal size, concrete temperature, smoothness and permeability of the formwork material, size and shape of the formwork, consolidation method, pore-water pressure, content and type of cement, as well as the depth of the concrete placement, or concrete head.
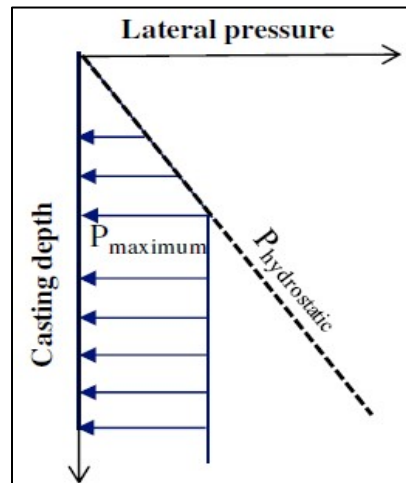


Figure 1.5 Lateral pressure diagram for concrete

Vertical loads

Vertical loads consist of dead and live loads. The weight of formwork plus the weight of the reinforcement and freshly placed concrete is dead load. The live load includes the weight of the workers, equipment, material storage, runways, and impact. Vertical loads assumed for shoring and re-shoring design for multi-story construction should include all loads transmitted from the floors above as dictated by the proposed construction schedule. The formwork should be designed for a live load of not less than 2.4 kPa of horizontal projection. When motorized carts are used, the live load should not be less than 3.6

kPa. The design load for combined dead and live loads should not be less than 4.8 or 6.0 kPa if motorized carts are used.

Horizontal loads

Braces and shores could be designed to resist all horizontal loads, such as wind, cable tensions, and inclined supports, dumping of concrete, and starting and stopping of equipment. Wind loads on enclosures or other wind breaks attached to the formwork should be considered in addition to these loads. Wall form bracing should be designed to meet the minimum wind load requirements of the local building code ANSI/SEI/ASCE-7 with adjustment for shorter recurrence intervals as provided in SEI/ASCE 37. For wall forms exposed to the elements, the minimum wind design load should be not less than 0.72 kPa. Bracing for wall forms should be designed for a horizontal load of at least 1.5 kPa of wall length, applied at the top. Wall forms of unusual height or exposure should be given special consideration.

Lateral pressure of concrete

Unless the conditions discussed below for the wall and column elements are met, the ACI 347 recommends that formwork be designed for its full hydrostatic lateral pressure as given by the following equations:

$$p = \rho g h \qquad \text{Equation (1.1)}$$

Where, $p$ = lateral pressure (kPa); $\rho$ = density of concrete (kg/m$^3$); $g$ = gravitational constant (9.81 N/kg); and $h$ = depth of fluid or plastic concrete from top of placement to point of consideration in form (m).

For columns or other forms that can be filled rapidly before stiffening of the concrete takes place, h should be taken as the full height of the form or the distance between horizontal construction joints when more than one placement of concrete is to be made. When working with mixtures using newly introduced admixtures that increase set time or increase slump characteristics, such as SCC, Eq. (1.1) should be used until the effect on formwork pressure is understood by measurements. It is important to note that the use of thixotropic concrete can increase the structural build-up at rest of the materials, whcih can decrease the extent of the lateral pressure and accelerate pressure decay (Khayat, et al., 2010).

## 1.3 Scope of work

The project is divided into two phases with specific objectives that are described below. Phase I is completed and is presented in this report. Phase II is work under way and will be reported elsewhere.

**Phase I: Design of Panel Material.** The UHPC was optimized by experimentally selecting appropriate material constituents, such as specialty cement, silica fume, fine quartz sand, fibers, and chemical admixtures. In this research, it is proposed to use high volumes of supplemental cementitious materials (SCMs) and fillers, as partial replacements for Portland cement. UHPC is incorporated with fibers to secure excellent performance in terms of cracking resistance, mechanical behavior, and durability. The mix design of this material is optimized using experimental design approach. The grading of the solid skeleton is investigated to obtain an optimum packing density, which is necessary to reduce viscosity. The composition of the cement paste/mortar is optimized to achieve suitable rheological properties and segregation resistance of solid particles during flow and thereafter until the onset of setting. Performance-based design was developed for the ultra-high performance fiber reinforced concrete (UHP-FRC). It is anticipated to produce a highly flowable material with mini-slump flow consistency of 260-300 mm, a 56-day compressive strength close to 150 MPa as well as 56-day splitting tensile and flexural strengths greater or equal to 10 MPa and 20 MPa, respectively. The selection of panel materials are illustrated in Figure 1.6.

This task also involves the optimization of the reinforcement systems for the UHPC panels. FRP grids are proposed to reinforce the panel elements to produce light-weight panels with minimum thickness that are not prone to corrosion. The bond between the concrete material and FRP grids was investigated by

innovative de-bonding tests in the laboratory. Detailing of the reinforcement will be optimized using FEA.
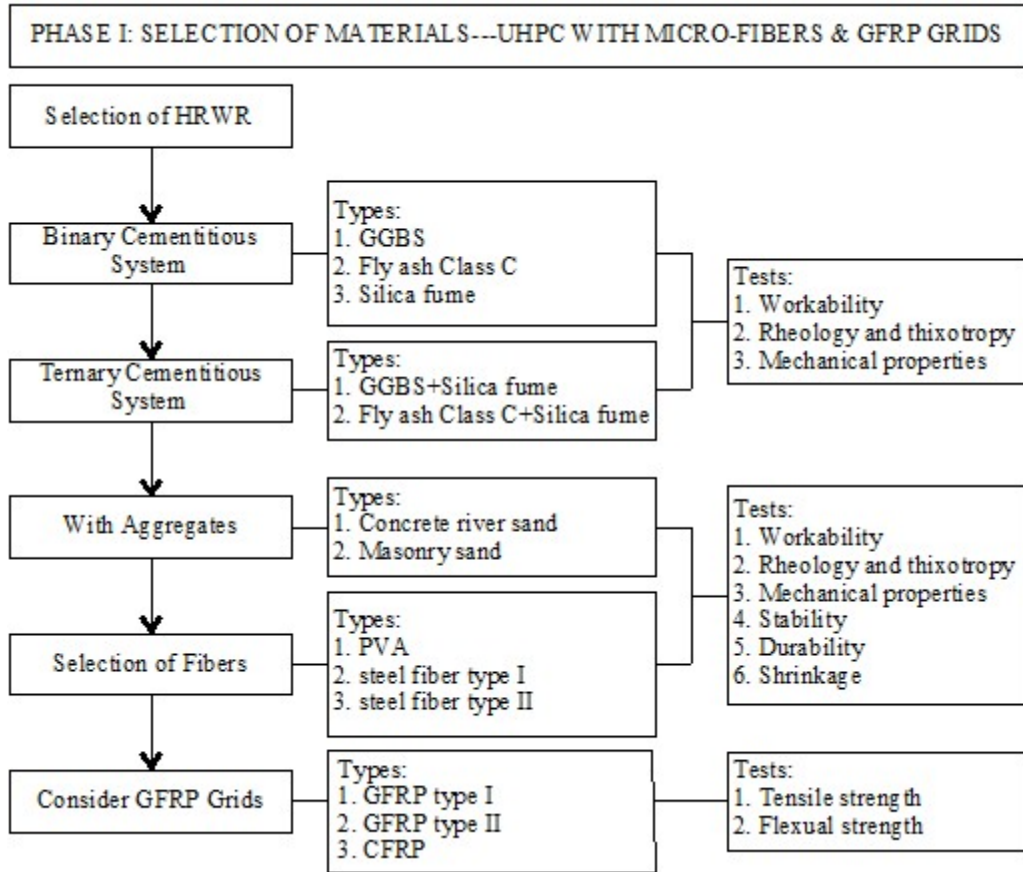
PHASE I: SELECTION OF MATERIALS---UHPC WITH MICRO-FIBERS & GFRP GRIDS

Selection of HRWR

Binary Cementitious System

Types:
1. GGBS
2. Fly ash Class C
3. Silica fume

Ternary Cementitious System

Types:
1. GGBS+Silica fume
2. Fly ash Class C+Silica fume

Tests:
1. Workability
2. Rheology and thixotropy
3. Mechanical properties

With Aggregates

Types:
1. Concrete river sand
2. Masonry sand

Selection of Fibers

Types:
1. PVA
2. steel fiber type I
3. steel fiber type II

Tests:
1. Workability
2. Rheology and thixotropy
3. Mechanical properties
4. Stability
5. Durability
6. Shrinkage

Consider GFRP Grids

Types:
1. GFRP type I
2. GFRP type II
3. CFRP

Tests:
1. Tensile strength
2. Flexural strength

Figure 1.6 Phase I: Selection of panel materials

**Phase II: Design of Panel System.** The configurations of the panel system will be designed and optimized by conducting FEA, including appropriate selection of element dimensions, innovative designs of joints, stiffeners, and anchorages. In the design, joints, shear keys, stiffeners, fibers, GFRP grids and GFRP rebar will be considered. Nonlinear behaviors due to the nonlinear material properties and the nonlinear boundary conditions will be considered. Detailed three-dimensional finite element models will be established and the nonlinear contact behavior between joints was taken into account. The precast panels will be designed to resist various loads including self-weight, construction loads, wind, and earthquake. As stated earlier, the mass of each panel should be limited to 25 kg. Considering the specific gravity for the UHPC material of 2500 kg/m$^3$, the dimension of the panel should be about 50 cm × 50 cm × 4 cm. Stiffeners will be designed, and their effect on the structure performance will be evaluated. Generally, stiffeners can involve the use of corrugated shaped panels on the inside faces of the panels or other forms that can promote greater moment of inertia and mechanical interlock shear resistance with the SCC

The proposed panels will be designed to be assembled as Lego-like for ease and speed of construction. The joint arrangement of the panels will be evaluated. Mechanical performance of mock-up panel elements will be also tested to validate the numerical model prediction. Testing involves the evaluation of the performance of reinforced UHPC panels tested in compression, tension, flexural, shear, and impact. According to the structural test results, as well as unit weight and economic considerations, the UHPC panel design is selected. The research will also involve the use of SCC for the construction and rhehabilittion of concrete elements that will be errected using the precast panel system. The joints along the panels must be grout-tight in order to prevent any leakage of the cement paste from the SCC that will

be cast in the formwork enclosure. Figure 1.7 shows the structural design of the formwork panels.

```
┌─────────────────────────────────────────────────────────┐
│       PHASE II: STRUCTURAL DESIGN OF FORMWORK PANEL       │
└─────────────────────────────────────────────────────────┘

┌──────────────────────┐   ┌──────────────────────────────┐
│  Connection regions  │───│ 1. Dimensions                │
│                      │   │ 2. Shapes and configurations │
└──────────────────────┘   └──────────────────────────────┘
           │
           ▼
┌──────────────────────┐   ┌──────────────────────────────┐
│     Stiffeners       │───│ 1. Directions                │
│                      │   │ 2. Spacing                   │
└──────────────────────┘   └──────────────────────────────┘
           │
           ▼
┌──────────────────────┐   ┌──────────────────────────────┐
│                      │   │ 1. Weight≤25kg               │
│ Dimensions of panel  │───│ 2. Thickness≤0.04m           │
│                      │   │ 3. Length×Width≤0.5m×0.5m    │
└──────────────────────┘   └──────────────────────────────┘
           │
           ▼
┌──────────────────────┐   ┌──────────────────────────────┐
│   Reinforcement      │───│ 1. Micro-fiber               │
│                      │   │ 2. GFRP grids                │
└──────────────────────┘   └──────────────────────────────┘
```
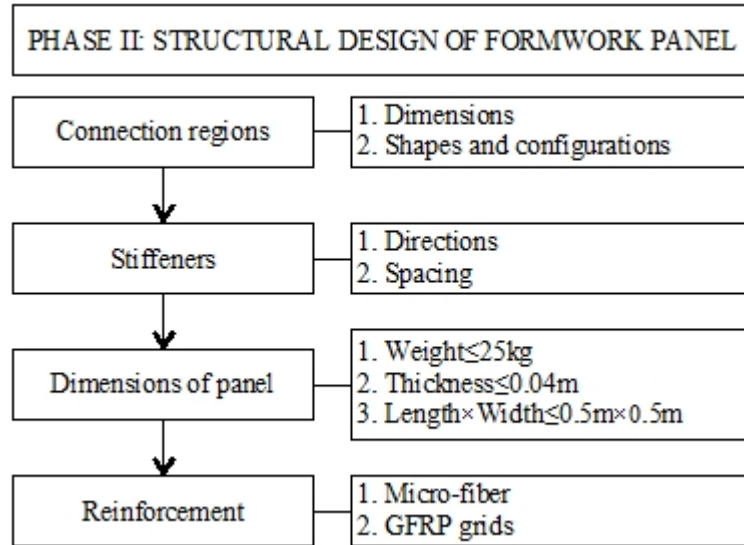
Figure 1.7 Phase II: Structural design of formwork panels

The overall structural performances of the assembled panel system with the cocnrete cast in the formwork enclosure will be evaluated by conducting axial, flexural, and combined axial and flexural loading tests. This involves the testing of structural responses of panel elements constructed with different panel materials and reinforcement configurations using an optimized SCC construction material. The UHPC formwork system, consisting of concrete panels, will be precast and assembled on-site layer by layer. The length of the panel will be optimized to reduce the need for joints and facilitate transportation and erection. The structural response of the elements fabricated by using the proposed formwork system will be evaluated by conducting pseudo static tests in the laboratory. The performance of composite/sections will be compared with similar sections that are cast monolithically.

Structural health monitoring (SHM) technologies will be implemented. The construction process will be monitored and controlled to guarantee the structural safety. Vibrating wire (VW) sensors will be used to measure strain and temperature variations throughout the precast panel mock-up sections during fabrication, transport, assembly, and subsequent testing. In addition, to understand the detailed strain distributions in the panel, distributed optical fiber sensing technique will be implemented to monitor the proposed formwork system.

# CHAPTER 2. MATERIALS, PRODUCTION, AND TEST METHODS

## 2.1 Constituent materials

UHPC formulations often consist of a combination of Portland cement, fine sand, silica fume, HRWR, fibers (usually steel), and water. Small sized coarse aggregates are sometimes used. Materials used in this project are listed in Table 2.1. In order to minimize porosity, it is important to achieve a high packing density of the solid materials.

In this project, the packing density of materials was evaluated using two approaches: a) packing density of the powder materials of cement, silica fume, fly ash, and GGBS in cement paste; as well as b) packing density of the sand (0-2 mm and 0-5 mm grading).

Table 2.1 List of investigated material

| Materials | Types | |
|---|---|---|
| Portland Cement | Type III | |
| SCMs | micro silica | |
| | Micro fly ash (Class C) | |
| | Slag Cement | |
| Fine aggregates | Masonry Sand (0-2 mm) | |
| | Natural Sand (0-5 mm) | |
| Admixtures* | Polycarboxylate HRWR | |
| FRP Grids (Pictures can be found in Appendix)** | CFRP | 46 mm× 41 mm |
| | GFRP type I | 25 mm × 25 mm |
| | GFRP type II | 12.7 mm × 12.7 mm |
| Fibers (Pictures can be found in Appendix) | PVA (8 mm) and steel fiber type I (13 mm) | |
| | Steel fiber type II (13 mm) | |

**Cementitious materials**

Type III cement was employed for the preparation of the UHPC. Such cement is typically used for precast concrete manufacturing, where high 1-day strength allows fast turnover of molds. Such cement can also be used in repairs and construction of machine bases and gate installations. According to the cement manufactures; data sheet, this cement is similar to Type I, but ground finer. This gives the concrete using this type of cement a 3-day compressive strength equal to the 7-day compressive strength of Type I. Its 7-day compressive strength is almost equal to 28-day compressive strength of Type I cement. The 6-months compressive strength of Type III is the same or slightly less than that of Type I cement. Coal-fired electric and steam generating plants produce fly ash as a by-product. Class C fly ash (FAC) is generalyy derived from sub-bituminous coals and consists mostly of calcium alumino-sulfate glass, such as quartzand free lime. Class C ash sometimes is referred to as high-calsium fly ash because it contains as much as 20% CaO. The primary ingredient of the materials used is ground granulated blast-furnance slag (GGBS) that is ground to a fine powder. The Blaine fineness of the GGBS is 589 $m^2$/kg. The specific gravity is 2.9. Silica fume (SF) is an industrial by-product from ferro-silicium alloys production and has a typical diameter of 0.2 μm. It is an essential constituent for UHPC

The physical and chemical characteristics of the cementious materials are shown in Table 2.2.

Table 2.2 Chemical and physical properties of cementitious materials

|  | Type III cement | Class C fly ash | Silica fume | GGBS |
|---|---|---|---|---|
| $SiO_2$, % | 22 | 36.5 | 85 | 36.8 |
| $Al_2O_3$, % | 6 | 24.8 | 0.4 | 9.2 |
| $Fe_2O_3$, % | 3 | 5.2 | 0.5 | 0.76 |
| CaO, % | 65 | 28.1 | - | 37.1 |
| MgO, % | 3 | 5 | - | 9.5 |
| $SO_3$, % | 3.1 | 2.5 | - | 0.06 |
| $Na_2O$ eq., % | - | - | - | 0.34 |
| $C_3S$, % | 57 | - | - | - |
| $C_2S$, % | 19 | - | - | - |
| $C_3A$, % | 10 | - | - | - |
| $C_4AF$, % | 7 | - | - | - |
| Blaine surface area, $m^2/kg$ | 400 | 465 | - | 589 |
| B.E.T., $m^2/kg$ | - | - | 17500 | - |
| Specific gravity | 3.15 | 2.4 | 2.2 | 2.9 |

**Aggregates**

All the sands used for the investigated UHPC mixtures were from Missouri rivers. Table 2.4 shows the gradation of the two types of sands. The water absorption of the fine masonry sand the concrete sand are 0.06% and 0.14%, respectively. The specific gravities are 2.63 and 2.64 respectivily.

Table 2.4 Sand gradation

| Sieve # | Masonry sand (0-2 mm) | | | River sand (0-4.75 mm) | | |
|---|---|---|---|---|---|---|
|  | Weight Retained (g) | Cumulative Weight Retained (g) | % Passing (finer) | Weight Retained (g) | Cumulative Weight Retained (g) | % Passing (finer) |
| 3 | 0 | 0 | 100 | 0 | 0 | 100 |
| 4 | 7.4 | 7.4 | 99 | 0.8 | 0.8 | 100 |
| 8 | 39.3 | 46.7 | 92 | 15 | 15.8 | 98 |
| 16 | 73.1 | 119.8 | 78 | 3.2 | 19 | 97 |
| 30 | 172.9 | 292.7 | 47 | 59.1 | 78.1 | 88 |
| 50 | 217.2 | 509.9 | 7 | 298.5 | 376.6 | 41 |
| 100 | 40.8 | 550.7 | 0 | 251.5 | 628.1 | 2 |
| 120 | 0 | 550.7 | 0 | 13.8 | 641.9 | 0 |
| Pan | 0 | 550.7 | 0 | 1.4 | 643.3 | 0 |

**HRWR**

High-range water-reducing admixture or superplasticizer was used. The HRWR is a polycarboxylate-based superplasticizer with an extended workability rentention ability. The use of HRWR can lead to faster setting characteristics and improved early age strength. Table 2.3 shows the characteristic of the HRWR.

Table 2.3 Charateristics of HRWR

|  | Solid content (%) | Specific gravity |
|---|---|---|
| HRWR | 23 | 1.05 |

**Fibers**

As mentioned in Chapter 1, the excellent ductility and impact resistance of UHPC are attributed to the use of proper fibers. Table 2.5 shows the properties of the fibers used in UHPC. Steel fiber is used in the UHPC because of its superior tensile strength. The using of polyvinyl alcohol (PVA) fiber is due to its high resistance to corrosion as well as good performance in tensile behavior.

Table 2.5 Fibers properties

| Type | Filament diameter | Fiber Length | Specific Gravity | Tensile strength | Flexural strength |
|------|-------------------|--------------|------------------|------------------|-------------------|
| Steel fiber* | 0.2 mm | 13 mm | 7.8 | 1900 MPa | 203 GPa |
| PVA fiber* | 38 Microns | 8 mm | 1.3 | 1400 MPa | 30  Pa |

*The details were shown in Appendix A.

## 2.2 Mixing

### 2.2.1 Mixers

Proper production of UHPC requires high mixing energy input compared to conventional concrete. The increased energy input, in combination with the reduced or elimination of coarse aggregate that would normally help in shearing the material, the low water content, and the inclusion of fibers would necessitate the use of modified procedures to ensure that the UHPC does not overheat during mixing, and that the end product is homogenous and workable. High-energy mixer and the lowering of the temperature of constituent materials and partial or full replacment of the mixing water with ice can help overcome these difficulties.

In this research, a Hobart mixer (Figure 2.1(a)) was employed during the initial optimization of the cementitious materials in mixtures made without fibers and fine aggregates. A high-shear Omni mixer (Figure2.1 (b)) was used during the optimization of fibrous UHPC. A larger high-shear EIRICH mixer (Figure2. 1(c)) was used for the final mixture optimization.



(a) Hobart Mixer       (b) Omni high shear mixer       (c) EIRICH mixer

Figure 2.1 Different mixers used in this investigation

### 2.2.2 Mixing time

The mixing time for the UHPC ranged from 7 to 18 min, which is much longer than that of conventional

concrete. This impedes continuous production processes and reduces the capacity of concrete plants. Mixing time can be reduced by optimizing the particle size distribution, replacing cement by cementitious materials, matching the type of HRWR and cement, and increasing the speed of the mixer. In this project, mixing time was optimized initially for cement paste to select the binder composition and optimum dosage of the HRWR, then for the non-fibrous UHPC and finely for the fibrous UHPC. Table 2.6 summaizes the main characteristics of the three mixers that were used in this investigation.

Table 2.6 Summary of the mixers characteristics.

| Mixers | Tested materials | Output capacity (L) | Batch size (L) | Mixing speed | Optimum mixing time | Main character |
|---|---|---|---|---|---|---|
| Hobart | Paste and mortar without fibers | 12 | 5 | 1 to 2 (low-medium) | 15 min for paste; 17 min for mortar | Three speed and a stir mode |
| Omni | Low volume UHPC | 15 | 10 | 6 to 10 (medium to high) | 8 min | High energy shear mixer and 10 speed |
| EIRICH | High volume UHPC | 150 | 80 | 2 rpm to 6 rpm (low to medium) | 8 min | High energy shear mixer and custom adjusted speed |

## 2.3 Sampling

The method of sampling UHPC influences the orientation and dispersion of the fibers (Kim, et al., 2008). The fiber orientation seems to have limited effect on the first cracking load but can have a considerable effect up to 50% on the ultimate tensile strength in bending (Kim, et al., 2008). The highest strengths can be achieved when the UHPC is sampled in the direction of the measured tensile strength. Stiel et al. (2004) reported significant differences between horizontally and vertically cast beams when tested in three-point bending. The fibers in the vertically cast beams were aligned in layers normal to the casting direction. As a result, the splitting and flexural strengths were only 24% and 34% of the corresponding values for the horizontally cast beams (Stiel, et al., 2004). The orientation of the fibers did not have a significant effect on the compressive strength and modulus of elasticity.

The sampling of the tested cement paste, mortar and UHPC mixtures in this project was carried out immediately following the end of mixing. For all the samples cast in this project, the method of one layer casting with slightly external form vibrating was implemented.

## 2.4 Curing

All specimens tested in this project were covered with wet burlap and plastic sheet until the age of 1-day before demolding and curing in lime-water at 23ºC until 1 hour before testing.

## 2.5 Testing methods

The flow of UHPC is frequently measured using ASTM C1437—Standard Test Method for Flow of Hydraulic Cement Mortar (ASTM C1437, 2007). This test method is intended for use with mortars exhibiting plastic to flowable behavior, and thus it is frequently appropriate for fresh UHPC. In this test, both initial flow and dynamic flow are measured.

In this research project ASTM C109—Standard Test Method for Compressive Strength of Hydraulic Cement Mortars (Using 50 mm Cube Specimens) was applied to UHPC (ASTM C109, 2012). UHPC does not present any specific challenges or require any specific modifications to the standard ASTM C469 test method for static modulus of elasticity (ASTM International, 2010).

Prism flexure testing and split cylinder testing are both appropriate means of determining first cracking, but the specimen must be closely monitored to capture the load at first cracking, since the load may continue to increase thereafter without noticeable change in global specimen behavior. Monitoring of specimens can be done visually, audibly, or through the use of nondestructive testing equipment (Graybeal, 2006). The post-cracking tensile behavior of UHPC is one of the unique properties that differentiate it from conventional concrete. UHPC generally falls into the category of strain-hardening fiber-reinforced concrete, which means that the post-cracking strength provided by the fiber reinforcement bridging a crack is equal to or greater than the cracking strength of the cementitious matrix. This behavior is responsible for the multi-cracking response of UHPC components and allows for the potential inclusion of UHPC tensile strength and strain capacities in structural design calculations. In this project, ASTM C 1609 test method was implemented to evaluate the flexural performance of steel reinforced UHPC.

Other conventional concrete durability test methods can also be applied to UHPC specimens. Many of these tests can provide comparative results indicating the relative durability of UHPC in terms of conventional concrete. However, many of these tests use subjective, qualitative measures to assess performance. Since these measures have been developed for use with conventional concrete, UHPC may exceed the anticipated performance range, thus making comparisons between individual UHPCs difficult.

The task for this research of materials design focused on determining both the fresh and hardened properties of the fiber reinforced UHPC mixtures for the proposed permanent formwork. Table 2.7 details the specific property tests that were implemented. The objective of this task was to understand the effect of variable influence on both the mechanical and materials performance of the UHP-FRC materials investigated.

Table 2.7 Tests proposed for experimental program of materials

| Property | Test Method | Test Title/Description |
|---|---|---|
| Aggregate Characterization Tests | | |
| Density & Absorption | ASTM C 127 | Test Method for Density, Relative Density (Specific Gravity), and Absorption of Coarse Aggregate. |
| Fresh Properties | | |
| Unit Weight | ASTM C 138 | Test Method for Density (Unit Weight). |
| Air Content | ASTM C 231 | Test Method for Air Content of Freshly Mixed Concrete by the Pressure Method. |
| Mini slump | ASTM C1437 | Test Method for Mini-Slump of UHPC. |
| Fresh concrete temperature at 10 and 70 min | ASTM C 1064 | Test Method for fresh concrete temperature |
| Bleeding | Investigation of ASTM Paste and Mortar Bleeding Tests Volume 3, Issue 1 (July 1981) | Test Method for Bleeding of UHPC |
| Setting time | ASTM C403 | Test Method for Time of Setting of Concrete Mixtures by Penetration Resistance |
| Rheology | - | Mini-V funnel; Anton Paar; ConTech 5 |
| Hardened Properties | | |
| Compressive Strength (1 to 56 d) | ASTM C 109 | Test Method for Compressive Strength of Cubes Specimens. |
| Splitting Tensile Strength | ASTM C 496 | Test Method for Splitting Tensile Strength |

| Property | Test Method | Test Title/Description |
|---|---|---|
| (1 to 56 d) | | of Cylindrical Concrete Specimens. |
| Flexural Strength (28 and 56 d) | ASTM C 1609 | Test Method for Flexural Strength of Concrete. |
| Modulus of Elasticity and Poisson's ratio (28 day) | ASTM C 469 | Test Method for Static Modulus of Elasticity. |
| Drying shrinkage (after 7 d of moist curing) | ASTM C 157 | Test Method for Length Change of Hardened Hydraulic-Cement Mortar and Concrete |
| Autogeneous shrinkage | ASTM C1698 | Standard Test Method for Autogenous Strain of Cement Paste and Mortar |
| Bulk Resistivity (28, 56 d) | ASTMC 1760 | Standard Test Method for Bulk Electrical Conductivity of Hardened Concrete |

# CHAPTER 3. MIX DESIGN OF FIBER-REINFORCED UHPC

Given the superior mechanical properties and durability of UHPC, and long-term stability of the material, this project aims at using UHPC for the production of UHPC prefabricated panels for fast construction and repair of infrustructure elements. The work described in this chapter aims at the development of cost-effective UHPC mixtures. This chapter addresses the experimental and analytical methods used to determine the optimization mix design of UHPC for precast permanent formwork.

## 3.1 Optimization of cementious materials combinations using cement paste

This section describes the investigation undertaken to optimize the composition of the cementitious materials of the UHPC. The type and content of the supplementary cementitious materials (SCMs), such as fly ash, GGBS and SF, was varied to achieve high packing density of the powder materials. In this part, packing density of powder materials is defined in both the binary and ternary parts. It was understood that an increase in the spread value was achievable by changing the type of material within its class, and/or by changing the materials proportions, which demonstrates an improved particle packing while the amount of water is kept constant. Therefore, the amount of water, and thus the water-to-cementitious materials (w/cm), can be reduced, while maintaining workability, which leads to an increase in compressive strength.

### 3.1.1 Mixture proportioning of cement paste

The samples of the UHPC pastes were prepared to evaluate the effect of HRWR-binder combinations on flow characteristics. For the first step, the saturation point of the polycarboxylate HRWR was determined using the flow cone test (ASTM C939). The flow time testing was conducted on mortar mixtures with the 0-2 mm sand employed at a sand-to-cement ratio of 1.2.

For the second step, a total of 108 mixtures were investigated to evaluate the workability of the paste and 26 mixtures to evaluate the 28-day compressive strength. Table 3.1 describes the various mixtures that were evaluated. This investigation of workability was carried out to determine the minimum water content (MWC) and relative water demand (RWD) with varied w/cm. On the otherhand, a fixed w/cm of 0.23 was used to determin compressive strengths of the optimized mixtures with selected SCMs combinations. Test results are discussed in section 3.1.4 of this report.

Table 3.1 Mixture codifications for workability and compressive strength testing

| Type | Mixture codification | | | | | |
|---|---|---|---|---|---|---|
| FAC | FAC60 | FAC50 | FAC40 | FAC30 | | |
| SF | SF5 | SF8 | SF11 | SF14 | SF20 | SF25 |
| GGBS | G70 | G60 | G50 | G40 | | |
| FAC+SF | FAC40SF5 | FAC50SF5 | FAC50SF8 | FAC60SF5 | | |
| GGBS+SF | G60SF5 | G50SF5 | G40SF5 | G50SF8 | G50SF11 | |
| FAC+SF+GGBS | FAC40SF5G30 | FAC40SF5G20 | FAC40SF5G10 | | | |

    *Note: as an example, FAC 60 refers to a combination of cementitious materials using 60% class c fly ash, by volume, with 40% Type III cement, by volume.

Eight of the 26 mixtures were evaluated further to determine the rheological parameters of optimized mixtures. The Anton Paar MCR 302 rheometer was used to measure the rhological properties. The mixtures that were used to evaluate rheological properties are shown in Table 3.2.

Table 3.2 Optimzied mixtures used for rheology testing

| Mixture codification | | | |
|---|---|---|---|
| SF5 | FAC40 | FAC60 | G50 |
| G50SF5 | G50SF11 | FAC40SF5 | FAC40SF5G10 |

## 3.1.2 Mixing procedure for cement paste

Table 3.3 compares the slump flow determined using the mini-slump test for various mortar mixtures that received different mixing procedures. According to the mixing procedures (Figure 3.1) of workability test, 12 min of mixing was needed before each slump test. To obtain the relationship between MWC and RWD, at least five slump tests should be done. In order to obtain reliable and steady results of slump testing, mixing time was proposed to be optimized. Four different batches of cement paste were tested with different mixing times. The mixing time was increased for step 3 (Table 3.3) from 3 to 12 min. The result showed in Table 3.3 that 9 min mixing for the last step should be the optimized time, because the corresponding slump flow became steady (27 cm) thereafter.

Table 3.1.2.1 Optimization of mixing time

| Mixing procedure | HRWR/powder | w/cm | Test time (min) | Slump flow (mm) |
|---|---|---|---|---|
| Step 1: Dry materials for 3 min<br>Step 2: Add 90%+50% HRWR speed 1 for 3 min<br>Step 3:Add10%water + 50% HRWR speed 2 for various test time | 4% | 0.18 | 3 | 230 |
| | | | 6 | 250 |
| | | | 9 | 270 |
| | | | 12 | 270 |
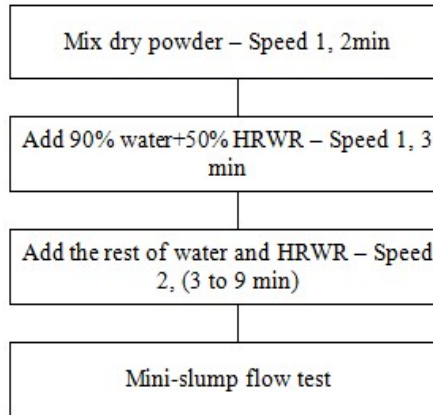


Figure 3.1 Mixing procedure for workablility test of cement paste

For the optimization of the rheological properties and compressive strength, the cement paste was mixed using the optimized procedure shown in Figure 3.2. The HRWR demand, retention of slump flow, rheological parameters, and visual static stability were determined. The paste mixtures tested with the rheometer had a controlled of 23℃. The time of water addition is defined as the reference time. Each batch had a total volume of 1.5 L. The initial mini slump flow was fixed to 350 mm to obtain similar yield stress values. The combination of SCMs that resulted in the lowest plastic viscosity was of interested in evaluation.
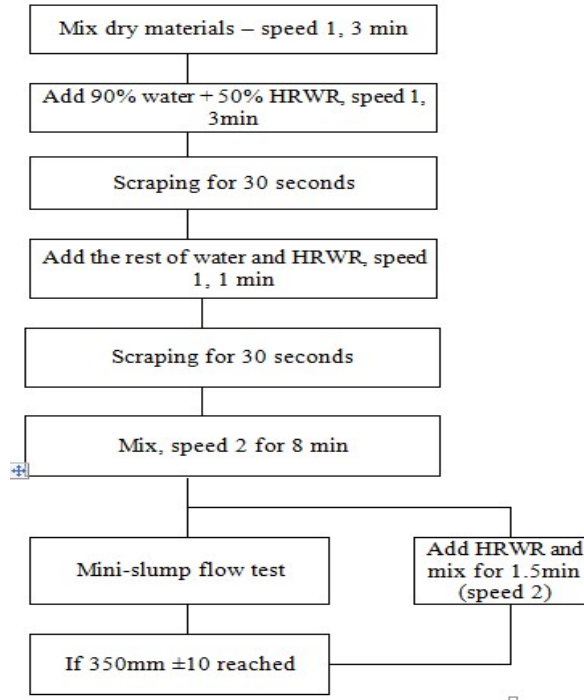
Figure 3.2 Mixing procedures for rheology testing of paste

### 3.1.3 Test methods of cement paste

**Saturation point of HRWR**

The saturation point of the HRWR was determined using flow cone test. Flow cone test method was used to determine the time of efflux of 1000 ml volume of mortar through a standardized flow cone with an opening of 19 mm. The mortar had a fixed w/cm of 0.23 and different dosage rates of HRWR to evaluate the saturation point. It should be noted that the saturation point is defined as HRWR dosage where increasing the amount of admixture does not cause any further reduction in the efflux time or spread value.



Figure 3.3 Flow cone used to determine saturation point of HRWR

**Test method for mini-slump spread**

Packing density is defined in both the binary and ternary parts. It was understood that an increase in the spread value was achievable by changing the type of material within its class, and/or by changing the material proportions, which demonstrates an improved particle packing while the amount of water is kept

constant. Therefore, the amount of water and thus the w/cm can be reduced while maintaining workability, which leads to an increase in compressive strength. Simply reducing the w/cm, while not having a higher packing density, leads to a decrease in workability and an increase in the amount of entrapped air, and thus, no enhancement in compressive strength.

As indicated in Figures 3.4 and 3.5, the mini-slump spread test consists of determining the variations of fluidity of a given mortar with changes in Wv/Pv whcih corresponds to the volume ratio of water-to-powder materials. The intercept of the curve with the ordinates axe (Wv/Pv) and the slope of the curve represents the minimum water content (MWC) to initiate flow and the relative water demand (RWD) to increase a given fluidity, respectively. The MWC corresponds to the minimum Wv/Pv needed to initiate flow, which is related to the packing density of the powder (Hwang, et al., 2006). The RWD reflects the robustness of the mixtures. A high RWD indicates that a given increase in Wv/Pv would result in limited impact on flow, thus a robust mixture (Hwang, et al., 2006). A minimum of five Wv/Pv values was used to evaluate two flow parameters for each mixture.

The mixing procedure was the same illustrated in Figure 3.2 expect omiting the last step, which can be found in section 3.1.2. In total, 108 mixtures were tested to determine the MWC and RWD. For the binary and ternary cementitious system testing, separate batches with different w/cm were tested. At the end of mixing, the paste was poured into the mini-slump cone to full capacity, in accordance with ASTM C 230/C 230M. The cone was then removed, allowing the paste to spread on the plate while the plate remained steady. After 30 seconds, when the flow had stopped, the spread was measured.
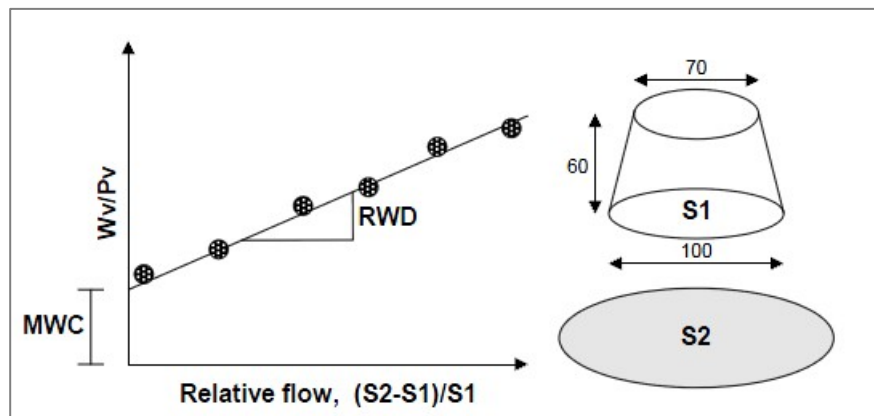


Figure 3.4 Definition of MWC and RWD parameters from flow test



Figure 3.5 Mini slump test

**Test method for rheology of cement paste**

The second phase of this study focused on the effect of HRWR-binder combinations on rheological characteristic of cement paste. The mixing of the paste was performed according to the procedure described in Figure 3.2 in section 3.1.2. The time of water addition is defined as the reference time. Each batch had a total volume of 1.5 L. The initial mini slump flow was fixed to 350 mm by adjusting the dosage of HRWR.

All mixing was performed at the lowest velocity of the Hobart mixer (140 rpm) to avoid splashing. The initial rheological test results were determined at the age of 20 min after water addition. The retention of rheological properties were measured determined at 30, 60, 90 min. of age.The first step in rheological testing involved the determination of the static yield stress using the shear growth approach. The paste was allowed to shear at a low rate of 0.01 per second for 60 seconds (Figure3.6).
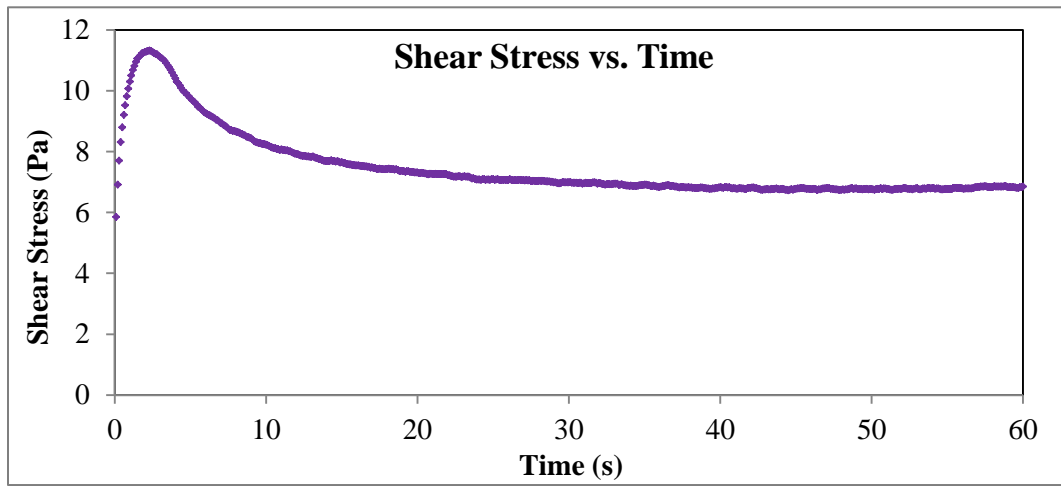


Figure 3.6 Static yield stress was measured by keeping the shear rate at 0.01 per second for 60 seconds

The paste was not re-mixed before each measurement. Therefore, the paste in the rheometer, has underwent a pre-shearing period for one minute at a high shear rate of 100 s$^{-1}$ before each test to minimize any effect of structural build-up of the paste at rest. Then, the shear rate was reduced by 10 s$^{-1}$ of 5 s intervals until the shear rate became zero. Figure 3.7 shows the time plot of torque of the C95SF5 mixtures. All these data were obtained in equilibrium conditions, so thixotropy did not influence the shear thickening behavior. It is important to note that the shearing time should be long enough to ensure that the flow of the paste has reached equilibrium; i.e., the material has achieved full break down.
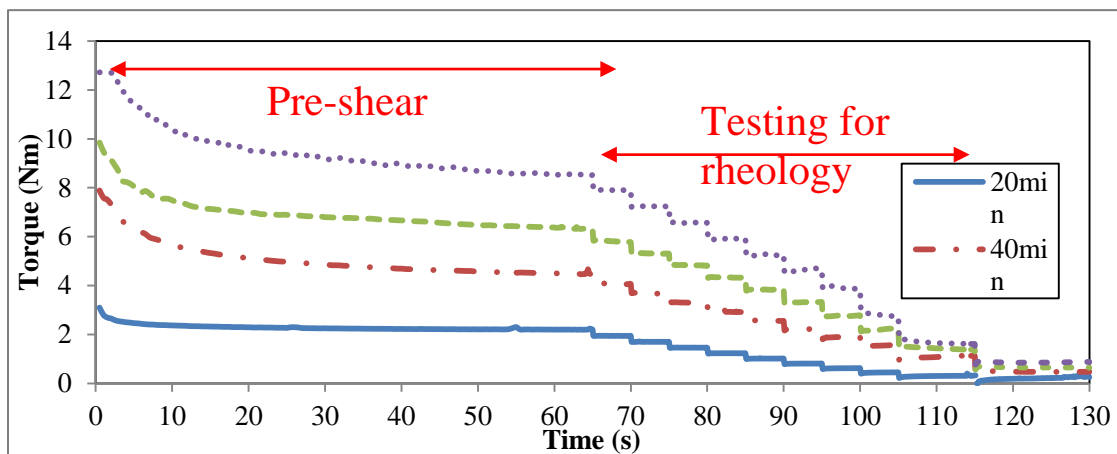


Figure 3.7 Torque values as a function of time for the G95SF5, tested at four different ages (dynamic rheological properties) *Note: one step of constant rotational velocity takes around 5 sec.*

26

Figure 3.8 shows the set-up for rheological properties testing.



Figure 3.8 Rheology test set up

**Test method for compressive strength of cement paste**

The compressive strength was tested according to ASTM C 39 at 1, 3 and 28-days using 50 mm cubes. All the samples were prepared at the conclusion of the workability testing, which was approximately 10 min of age. The paste was cast in a single layer without any tamping. Otherwise, the paste was cast in two layers and properly consolidated according to ASTM C 39. As previous stated, the samples were demolded after 1-day and stored in lime-saturated water until the time of testing. 50 mm cube test molds and the testing set up are shown in Figures 3.9 and 3.10, respectively.



Figure 3.9 Compressive strength test sampling       Figure 3.10 Compressive strength test set-up

3.1.4 Test results and discussion of cement paste

**Saturation point test**

The results indicate that the saturation point of the UHPC corresponds to approximately 4% of the mass of total cementitious material (Table 3.4 and Figure 3.11). It is important to note that this value corresponds to the powder/active content of the HRWR in the admixture solution.

Table 3.4 Saturation Point test results

| Test | Cement (kg/m$^3$) | Water (kg/m$^3$) | 0-2 mm sand (kg/m$^3$)(0-2mm) | Active HRWR/binder (%) |
|------|-------------------|------------------|-------------------------------|------------------------|
| 1 | | | | 1 |
| 2 | 809 | 188 | 1197 | 3 |
| 3 | | | | 4 |
| 4 | | | | 5 |



(a) Spread value versus HRWR content



(b) Flow time versus HRWR content

Figure 3.11 Results of saturation point testing
(a) spread value versus HRWR content (b) flow time versus HRWR content

**Results of mini-slump flow test of cement paste**

The cement content of UHPC is generally over 800–1000 kg/m$^3$. A high amount of cement not only increases the production costs, but also has negative effect on heat of hydration and may lead to shrinkage cracking. Replacing cement with a SCM is a feasible solution to these problems. Furthermore, incorporation of mineral admixtures may positively affect the durability of concrete. The aim of studying binary and ternary cementitious systemsis to decrease the cement and SF content of the UHPC using with FAC and/or GGBS.

Different types of SCMs were investigated to determine packing density and compressive strength at 1 and 28-days. Table 3.5 and Figure 3.12 compare the effect of the binder type and content on the MWC and RWD on different paste mixtures. For the binary system, the increase in FAC is shown to reduce MWC and increase RWD. The FAC60 mixture showed better performance than the other mixtures. For the

replacement of GGBS, the G50 mixture resulted in the best performance. For the silica fume mixtures, SF5 mixture showed the lowest MWC and highest RWD. Based on the binary results, the 60% FAC, 5% SF and 50% GGBS binary mixtures had higher RWD and lower MWC. This indicates that these combinations can achieve the higher packing density (low MWC) and a high robustness (high RWD).

The testing of the ternary systems results are shown in Figure 3.12. The G50SF5 mixture containing 5% SF and 50% GGBS replacement resulted in the highest RWD and lowest MWC.

In total, three quaternary systems were tested. The results show that the FAC40SF5G10 mixture with 40% FAC, 5% SF, and 10% GGBS can achieve high robustness and low water demand or high packing density.

Compared with all the mixtures, FAC 60 yielded the lowest MWC and the highest RWD. Further testing was carried out to evaluate compressive strength and rheological properties that are also needed for the optimization of the SCMs.

Table 3.5 Test results of workability evaluation

| Mixture Codification | RWD | MWC | $R^2$ | Mixture Codification | RWD | MWC | $R^2$ |
|---|---|---|---|---|---|---|---|
| Ref | 0.09 | 0.51 | 0.99 | FAC40SF5 | 0.13 | 0.23 | 1.00 |
| G70 | 0.10 | 0.38 | 0.99 | FAC50SF5 | 0.14 | 0.21 | 0.98 |
| G60 | 0.12 | 0.34 | 0.98 | FAC50SF8 | 0.14 | 0.22 | 0.98 |
| G50 | 0.14 | 0.26 | 0.98 | FAC60SF5 | 0.10 | 0.39 | 0.98 |
| G40 | 0.10 | 0.41 | 1.00 | G60SF5 | 0.13 | 0.30 | 0.99 |
| FAC60 | 0.20 | 0.12 | 0.97 | G50SF5 | 0.16 | 0.20 | 0.98 |
| FAC50 | 0.13 | 0.22 | 0.99 | G40SF5 | 0.10 | 0.38 | 0.99 |
| FAC40 | 0.11 | 0.22 | 0.98 | G50SF8 | 0.11 | 0.31 | 0.99 |
| FAC30 | 0.11 | 0.25 | 0.98 | G50SF11 | 0.11 | 0.31 | 0.99 |
| SF5 | 0.11 | 0.44 | 0.97 | FAC40SF5G30 | 0.14 | 0.25 | 1.00 |
| SF8 | 0.09 | 0.48 | 0.97 | FAC40SF5G20 | 0.12 | 0.24 | 0.99 |
| SF11 | 0.10 | 0.45 | 0.98 | FAC40SF5G10 | 0.15 | 0.15 | 0.99 |
| SF14 | 0.09 | 0.50 | 0.98 | | | | |
| SF20 | 0.10 | 0.48 | 0.97 | | | | |
| SF25 | 0.11 | 0.51 | 0.98 | | | | |
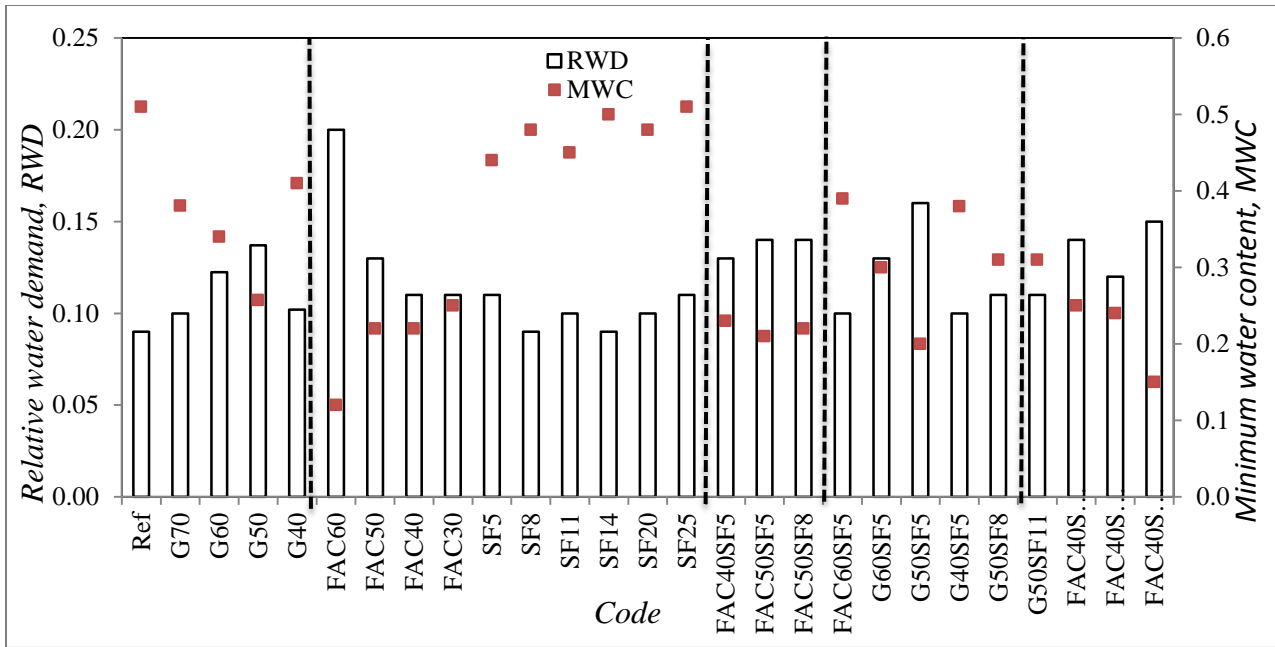
Figure 3.12 Effect of binder type on minimum water content and relative water demand

Figure 3.13 shows the 1-day compressive strength and mini-slump spread value, for 26 tested paste mixtures. As mentioned, all mixtures were prepared with a fixed w/cm of 0.23 and a fixed dosage of HRWR corresponding to 4% by active content component to binder mass. The early age strength is shown to improve with the addition silica fume. Based on the result, the SF5, SF8, and SF11 mixtures achieved the highest compressive strength at 1-day, but resulted in low spread values. Mixtures that achieved a minimum of 40 MPa 1-day compressive strength but resulted in relatively high mini-slump which are Ref, G50, FAC40, FAC40SF5, FAC50SF5 and FAC50SF8 mixtures,
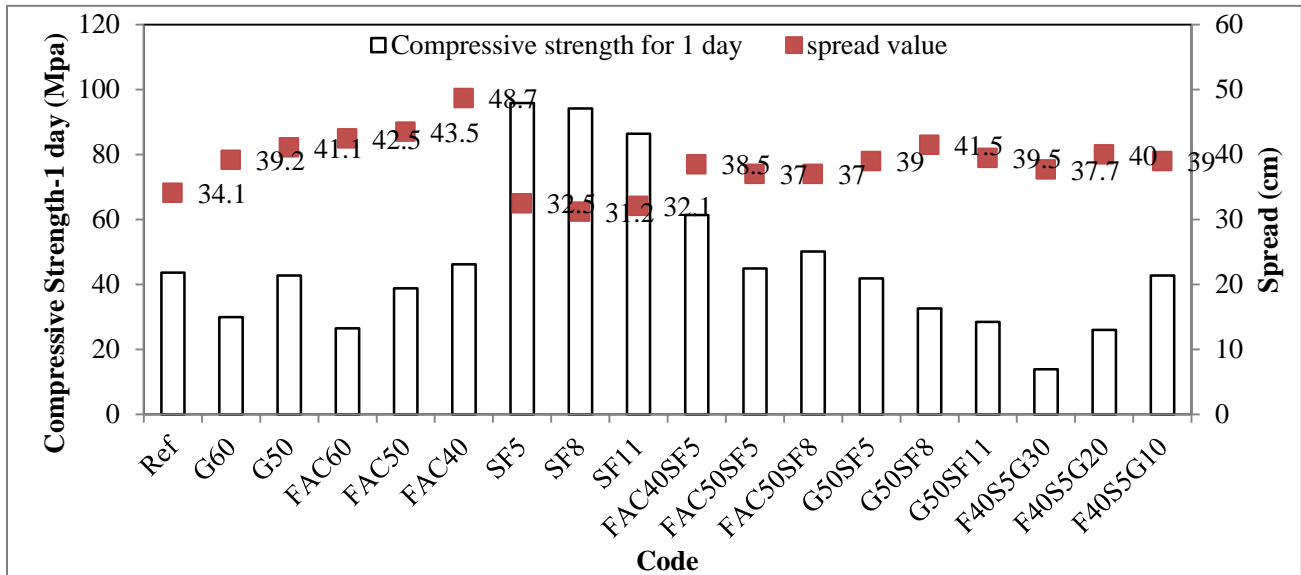


Figure 3.13 Compressive strengths for 1-day vs. spread values

The 28-day compressive strength is shown in Figure 3.14. All the mixtures gained more than twice the strength compared to 1-day compressive strength, expect for the silica fume binary system. According to Figure 3.14, the G50SF5 grout achieved compressive strength of 28-day greater than 140 MPa, G50

30

mixture was close to 140 MPa. This means that the binder with 50% GGBS had greater 28-day compressive strength than other content of GGBS or other type of binder materials. In addition to the G50 and G50SF5 mixtures, the FAC40SF5 mixture achieved 140 MPa strength. Furthermore, 1-day strength of FAC40SF5 was also the highest..
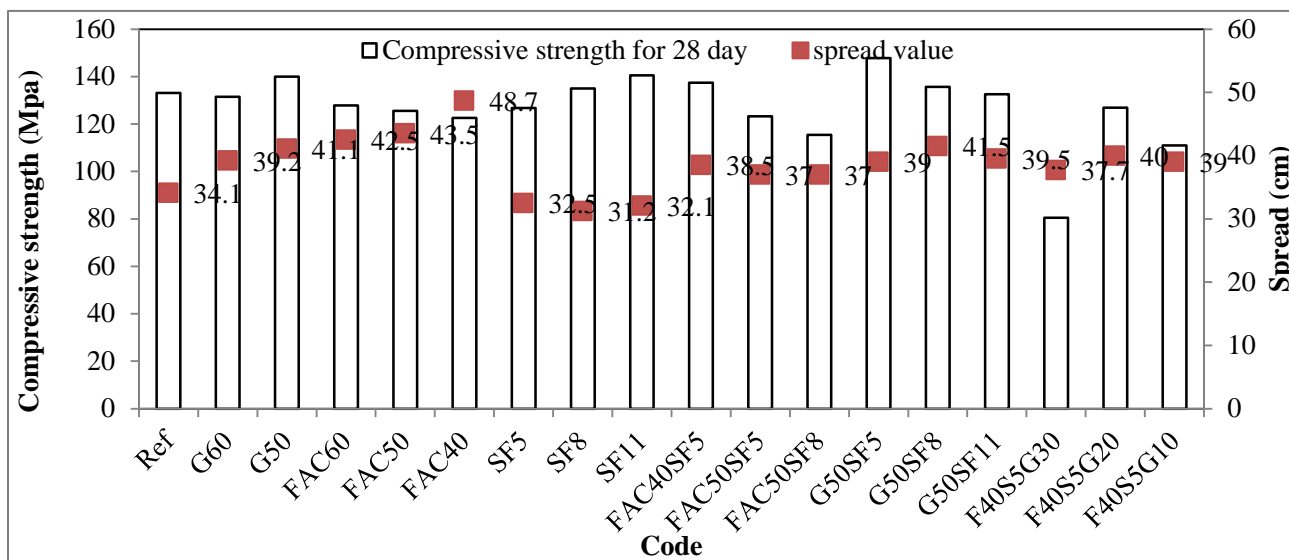


Figure 3.14 Compressive strengths for 28-day vs. spread values

In addition to the MWC and RWD, compressive strength of mixtures with w/cm of 0.23 was investigated and presented in Table 3.6. All mixtures had a fixed content of HRWR. As indicated in Table 3.6, mixtures with 5% SF and 50% GGBS obtained the highest compressive strength at 28-day, relatively high spread values, and low flow time. As a result, mixes with G50SF5 mixture can be a candidate for the optimum replacement percentage for considering both workability and compressive strength simultaneously. However, the performance of rheology should also be considered.

Table 3.6 Summary of test results

| Code | fc, 1day (MPa) | f'c, 28-day (MPa) | Unit weight (g/ml) | Flow cone (s) | Spread value (cm) | RWD | MWC |
|---|---|---|---|---|---|---|---|
| Ref | 43.7 | 133.1 | 2.220 | 47 | 34.1 | 0.09 | 0.51 |
| G60 | 29.9 | 131.4 | 2.114 | 34 | 39.2 | 0.12 | 0.34 |
| G50 | 42.7 | 139.9 | 2.121 | 44 | 41.1 | 0.14 | 0.26 |
| FAC60 | 26.5 | 127.9 | 2.154 | 16 | 42.5 | 0.20 | 0.12 |
| FAC50 | 38.8 | 125.6 | 2.175 | 17 | 43.5 | 0.13 | 0.22 |
| FAC40 | 46.2 | 122.6 | 2.168 | 13.22 | 48.7 | 0.11 | 0.22 |
| SF5 | 95.8 | 126.7 | 2.206 | 43 | 32.5 | 0.11 | 0.44 |
| SF8 | 94.2 | 135.0 | 2.185 | 49 | 31.2 | 0.09 | 0.48 |
| SF11 | 86.4 | 140.5 | 2.178 | 48 | 32.1 | 0.10 | 0.45 |
| FAC40SF5 | 61.4 | 137.5 | 2.152 | 33 | 38.5 | 0.13 | 0.23 |

| Code | fc, 1day (MPa) | f'c, 28-day (MPa) | Unit weight (g/ml) | Flow cone (s) | Spread value (cm) | RWD | MWC |
|---|---|---|---|---|---|---|---|
| FAC50SF5 | 44.9 | 123.3 | 2.144 | 31.34 | 37 | 0.14 | 0.21 |
| FAC50SF8 | 50.1 | 115.4 | 2.137 | 33.75 | 37 | 0.14 | 0.22 |
| G50SF5 | 41.9 | 147.8 | 2.140 | 35.47 | 39 | 0.16 | 0.20 |
| G50SF8 | 32.6 | 135.7 | 2.114 | 34.41 | 41.5 | 0.11 | 0.31 |
| G50SF11 | 28.5 | 132.6 | 2.102 | 36.81 | 39.5 | 0.11 | 0.31 |
| F40S5G30 | 13.9 | 80.5 | 2.103 | 32 | 37.7 | 0.14 | 0.25 |
| F40S5G20 | 26.0 | 126.9 | 2.119 | 28 | 40 | 0.12 | 0.24 |
| F40S5G10 | 42.8 | 111.0 | 2.147 | 31.54 | 39 | 0.15 | 0.15 |

**Test result of paste rheology**

In this part, different types of SCMs were investigated. Two systems were investigated. According to rheology test results, the relation between shear rate and the shear stress followed the non-linear curve. Therefore, the modified Bingham model, which can be expressed in Equations 3.1 to 3.4:

$$\tau = \tau_0 + \mu \cdot \dot{\gamma} + c \cdot \dot{\gamma}^2 \qquad \text{Equation (3.1)}$$

Where, $\mu$ - First order term, related to viscosity (Pa·s); $c$ - Second order term: modified Bingham model (Pa·$s^2$); $\dot{\gamma}$ - Shear rate ($s^{-1}$); $\tau_0$ -Yield stress (Pa); $\tau$ - Shear stress (Pa).

The transformation equations to obtain $\tau_0$ and $\mu$ from the G and H values are as follows:

$$\tau_0 = \frac{(\frac{1}{R_i^2} - \frac{1}{R_o^2})}{4\pi h \ln(\frac{R_o}{R_i})} G \qquad \text{Equation (3.2)}$$

$$\mu = \frac{(\frac{1}{R_i^2} - \frac{1}{R_o^2})}{8\pi^2 h} H \qquad \text{Equation (3.3)}$$

$$c = \frac{(\frac{1}{R_i^2} - \frac{1}{R_o^2})}{8\pi^3 h} \frac{(R_o - R_i)}{(R_o + R_i)} C \qquad \text{Equation (3.4)}$$

where: $R_i$ = Inner cylinder radius of coaxial cylinders rheometer (m); $R_o$ = Outer cylinder radius of coaxial cylinders rheometer (m); G = Intercept of curve in T-N graph with T-axis (Nm); H = First order term of second order curve in T-N graph: modified Bingham model (Nm s); C = Second order term of second order curve in T-N graph: modified Bingham model (Nm s); h = Height of the inner clinder submerged in concrete in coaxial cylinders rheometer (m).

In this phase, cement paste was considered to be similar to a concentrated suspension of cement particles in water. As such, the yield stress and plastic viscosity depend on the particle size distribution and concentration of the cement. For the rheology test, the initial w/cm was 0.23 (by mass), or 0.725 by volume , and the initial slump flow was adjusted using HRWR to secure a fixed mini-slump flow of 350 mm. Figure 3.15 shows the HRWR demand for each mixture. It can be observed that the FAC60 and G50SF5 mixtures required relatively low HRWR content to obtain 350 mm spread value. By using high volumes of GGBS and FAC, the HRWR demand can be decreased by more than 75% compared to the reference C100 and SF5 mixtures.
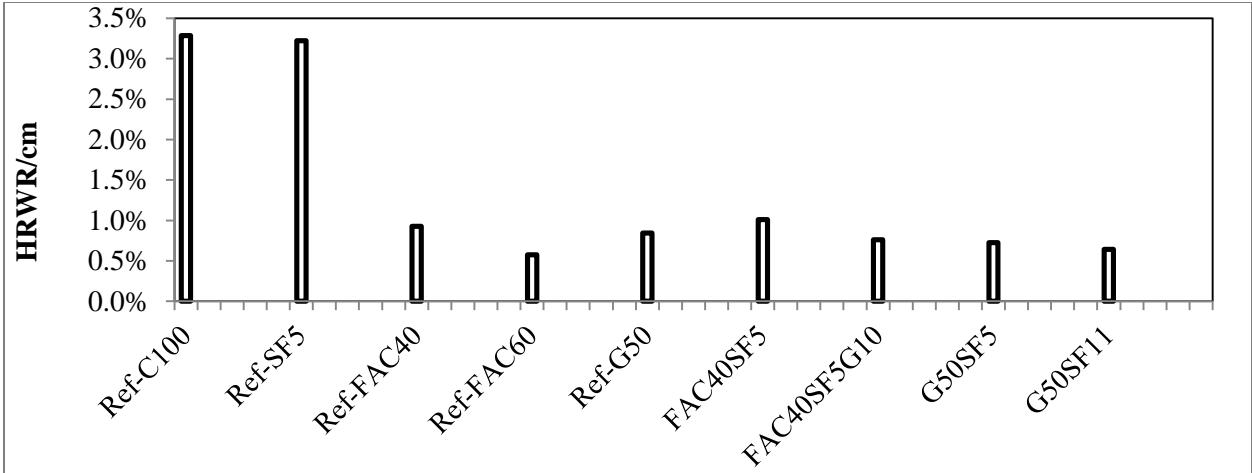
Figure 3.15 HRWR demand

Figures3.16 to 3.19 present the viscosity results measured from 20 min after adding water to 90 min. The low viscosity at 20 min was assumed as the indication of the mixture with high packing density. It is observed that the G50 mixture had the lowest viscosity, which is indicative of the highest packing density. However, the result are different than those of MWC flow test results, which concluded that the FAC60 mixture had the highest packing density. Future research should be carried out to find the appropriate indirect way of expressing packing density of cementitious materials.
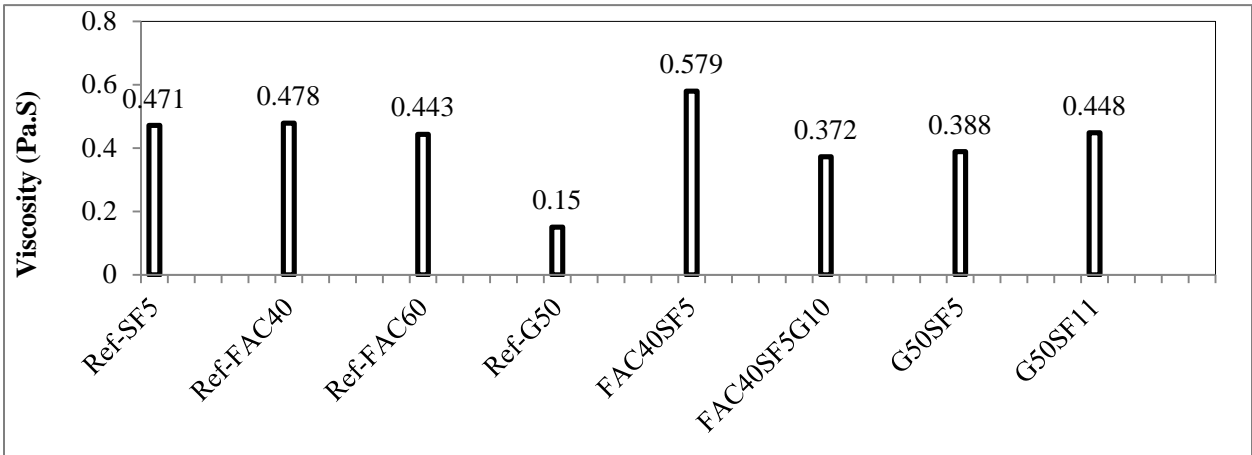


Figure 3.16 Viscosity at 20 min.

Figure3.17 indicates that the G50 mixture had the lowest viscosity at 40 min which was the same as at 20 min. However, the plastic viscosity of the SF5 and G50SF5 is decreased by 47% and 43%, respectively. This may be because the effect of the HRWR on the different binder combination in time.
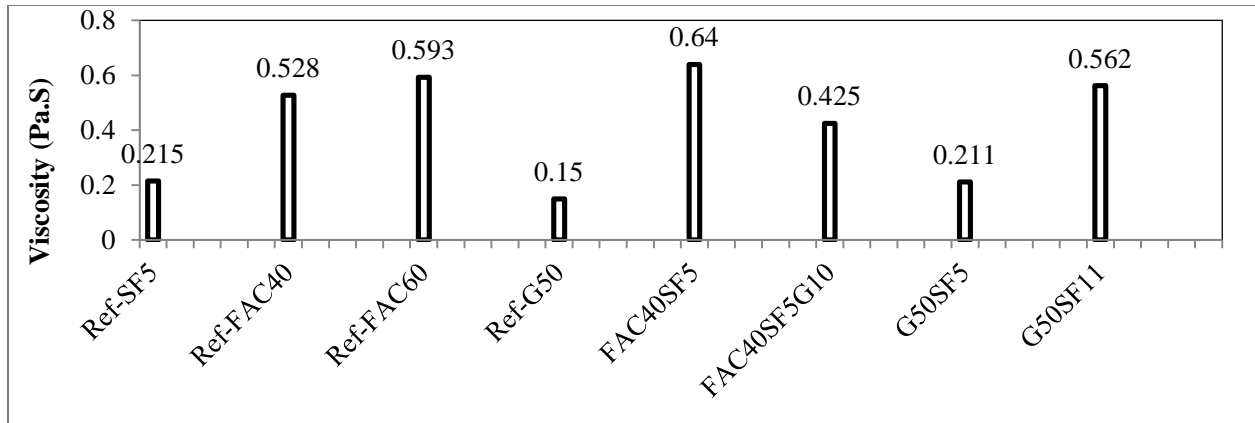
Figure 3.17 Viscosity at 40 min.

Figure3.18 shows the viscosity at 60 min that increased from the 20 min measurements except for the G50. It may because of the retarding effect of the HRWR on viscosity of a binder.
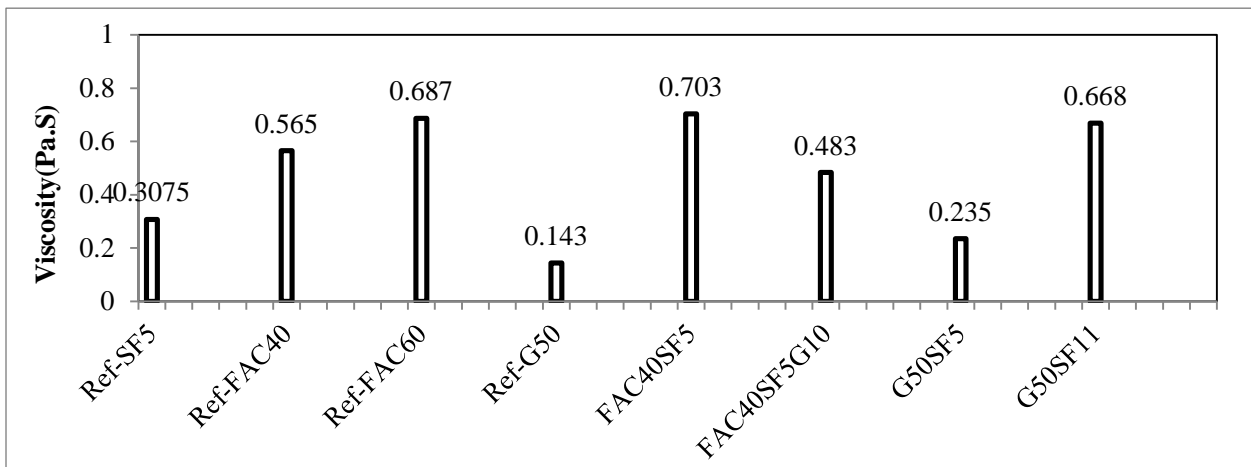


Figure 3.18 Viscosity at 60 min.

Figure3.19 shows the viscosity at 90 min. The viscosities at 90 min of the G50 is decreased and increased for the other mixtures, especially the G50SF11 grout that increased by 184% compared with the value of viscosity at 60 min. It concluded that after 60 min, more silica fume helped to enhance the early strength gaining by comparing the result of the G50SF5 and G50SF11 mixture. More details of the rheology test result are shown in Appendix B.
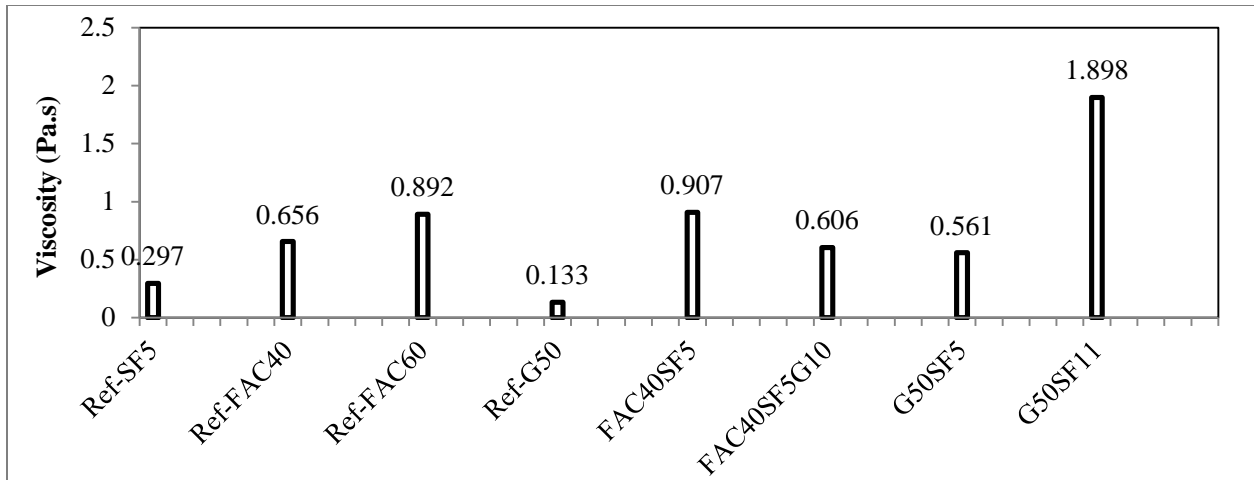
Figure 3.19 Viscosity at 90 min.

According to the results of of the mini-slump flow (see Figure 3.20), it can be observed that the C100, SF5, FAC40SF5G10, and FAC40 mixtures maintained mini-slump flow around 300 mm after 95 min,of age. The FAC60, FAC40SF5, and G50SF5 mixtures also maintained good workability with a mini-slump flow of approximately 250 mm.

According to Figure 3.20, the workability of the tested grouts up to 40 min was acceptable for all the mixtures HRWR/cementitious composite was fixed to 4%.
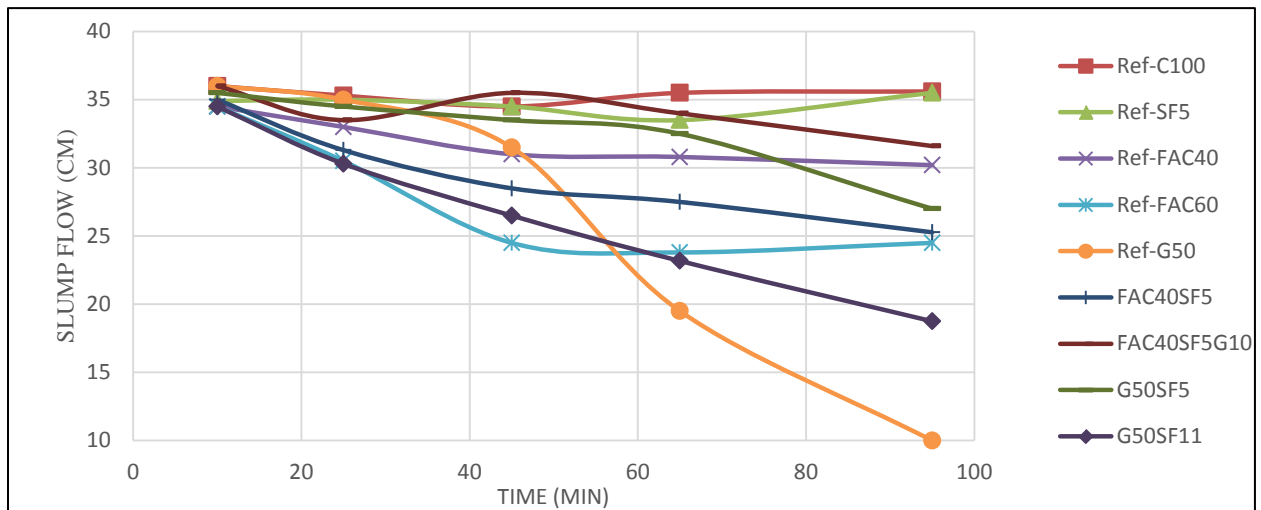


Figure 3.20 Loss of slump flow

3.1.5 Global analysis of paste test results

As mentioned before, considering only one or two property responses, such as workability, rheology and compressive strength, cannot easily point out the optimized binder combination. A star plot method was introduced to display multivariate data in the form of a two-dimensional chart of three or more quantitative variables represented on axes starting from the same point. It is a chart that consists of a sequence of equi-angular spokes, called radii, with each spoke representing one of the variables. The data length of a spoke is proportional to the magnitude of the variable for the data point relative to the maximum magnitude of the variable across all data points. A line is drawn connecting the data values for each spoke. When all the data is applied with weight, each spoke would have a specific area. The value of each area can be used to answer which observations are better, based on the bigger area of the corresponding spokes. Data in Tables 3.6 to

3.8 were analyzed using star plot method.

Table 3.7 Data set two for star plot analysis

| Code | Viscosity at 20 min (Pa.s) | Viscosity at 40 min (Pa.s) | Viscosity at 60 min (Pa.s) | Viscosity at 90 min (Pa.s) | Yield stress at 20 min (Pa) | Yield stress at 40 min (Pa.s) | Yield stress at 60 min (Pa.s) | Yield stress at 90 min (Pa.s) |
|------|------|------|------|------|------|------|------|------|
| Ref | 0.36 | 0.49 | 0.50 | 0.47 | 7.2 | 9.0 | 7.9 | 23.8 |
| G50 | 0.15 | 0.15 | 0.14 | 0.13 | 3.4 | 14.2 | 19.3 | 224 |
| FAC60 | 0.44 | 0.59 | 0.69 | 0.89 | 16.9 | 61.6 | 98.4 | 196.7 |
| FAC40 | 0.48 | 0.53 | 0.57 | 0.66 | 12.3 | 37.4 | 41.1 | 131.6 |
| SF5 | 0.47 | 0.22 | 0.31 | 0.30 | 26.0 | 10.2 | 10.3 | 30.3 |
| FAC40SF5 | 0.58 | 0.64 | 0.70 | 0.91 | 15.9 | 51.6 | 69.7 | 214.7 |
| G50SF5 | 0.39 | 0.21 | 0.24 | 0.56 | 70.0 | 19.3 | 26.2 | 438.2 |
| G50SF11 | 0.45 | 0.56 | 0.67 | 1.90 | 33.6 | 60.7 | 80.3 | 642.1 |
| F40S5G10 | 0.37 | 0.43 | 0.48 | 0.61 | 14.6 | 17.7 | 24.8 | 79.3 |

Table 3.8 Data set three for star plot analysis

| Code | Loss of slump flow at 25min (%) | Loss of slump flow at 45min (%) | Loss of slump flow at 65min (%) | Loss of slump flow at 95min (%) | HRWR/cm(%) |
|------|------|------|------|------|------|
| Ref | 1.94 | 4.16 | 1.38 | 1.11 | 3.28 |
| G50 | 2.77 | 12.5 | 45.83 | 72.22 | 0.84 |
| FAC60 | 11.59 | 28.98 | 31.01 | 28.98 | 0.57 |
| FAC40 | 4.34 | 10.14 | 10.72 | 12.46 | 0.93 |
| SF5 | -0.28 | 1.14 | 4.01 | -1.71 | 3.22 |
| FAC40SF5 | 10.57 | 18.57 | 21.42 | 27.78 | 1.01 |
| G50SF5 | 2.81 | 5.63 | 8.45 | 23.94 | 0.73 |
| G50SF11 | 12.17 | 23.18 | 32.82 | 45.65 | 0.64 |
| F40S5G10 | 6.94 | 1.38 | 5.55 | 12.22 | 0.79 |

Two sets of weights were applied to different sets of independent impact factors. For example, in this project, the plastic viscosity was measured using a rotational rheometer as a direct method, and flow cone flow time as an indirect method of characterizing of the fresh cement paste. Both of the methods are related to viscosity. It is not appropriate to put both the flow come flow time and plastic viscosity measured by rheometer in one chart to compare, since they were not independent. The same situation applies to spread value and yield stress measured by rheometer. Comparatively, the advantages of the indirect method are its simplicity and the portability of the device to mixing sites. The objective of using two measurements was to investigate whether the results correlates well between each method.

The determination of weight should be considered in the application. In this project, fresh properties such as spread value and flow cone flow time, plastic viscosity and yield stress before 60 min. and compressive strength at 28-day were taken for the key factors.

Table 3.9 shows the set of weights applied to each mixture listed in Table 3.4. To narrow down the number of mixtures for optimization, the results of workability tests and compressive strength tests for all mixtures were investigated. Based on the analysis, rheology properties measured by rheometer would be further investigated.

Table 3.9 First set of weighted factors

|  | fc, 1day | f'c, 28day | 1/(Flow cone) | Mini-slump spread value | RWD | 1/MWC |
|---|---|---|---|---|---|---|
| Weight 1 | 1 | 3 | 3 | 3 | 2 | 2 |

According to results showed in Figures 3.21 and 3.22 which considered the responses of workability and compressive strength, the high volume of FAC mixtures, especially FAC60 mixture, achieved highest area. To confirm this verdict, further test for rheology were carried out for a small number of mixtures selected with comparing star plot areas. The mixtures codification can be found in Table 3.4.
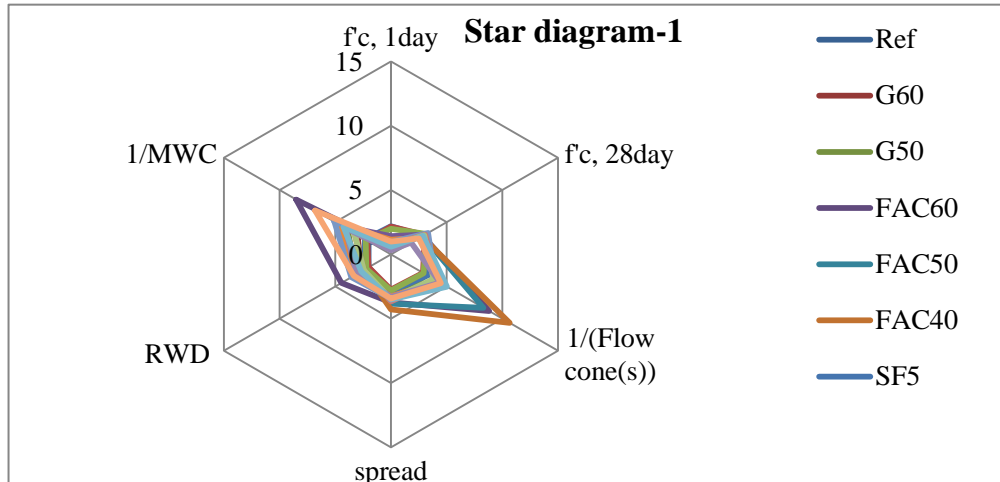


Figure3.21 Star diagram-1: taking into consideration workability and compressive strengths results
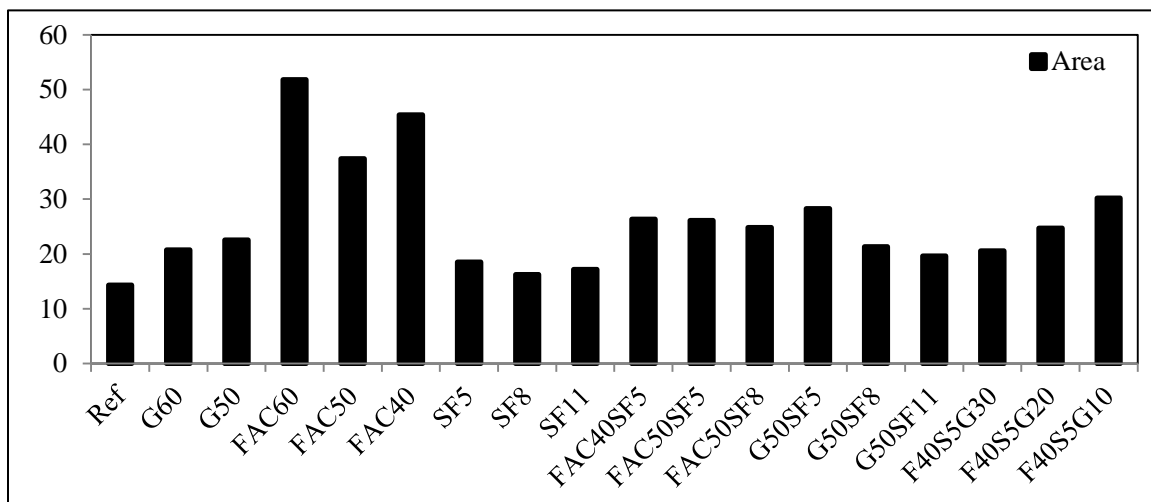


Figure 3.22 Area generated for star diagram-1

Another set of weighted factors is listed in Table 3.10 considers workability, compressive strengths, HRWR demand and mini-slump value at 60 min. The consideration of factor choosing was the same as weight 2.

Table 3.10 Second set of weighted factors

|  | f'c, 1-day | f'c, 28-day | 1/Flow cone | Mini-slump spread value | RWD | 1/MWC | Spread value at 60 min | 1/HRWR demand |
|---|---|---|---|---|---|---|---|---|
| Weight 3 | 1 | 3 | 3 | 3 | 2 | 2 | 2 | 3 |

The second set of weighted factors considered the time-dependent factor and the HRWR demand for each

mixture. By comparing the value of the area (Figure 3.23), FAC60 and G50SF11 should be the optimized mixture. And the secondary options can be G50, FAC40, FAC40SF5, G50SF5 and FAC40SF5G10.
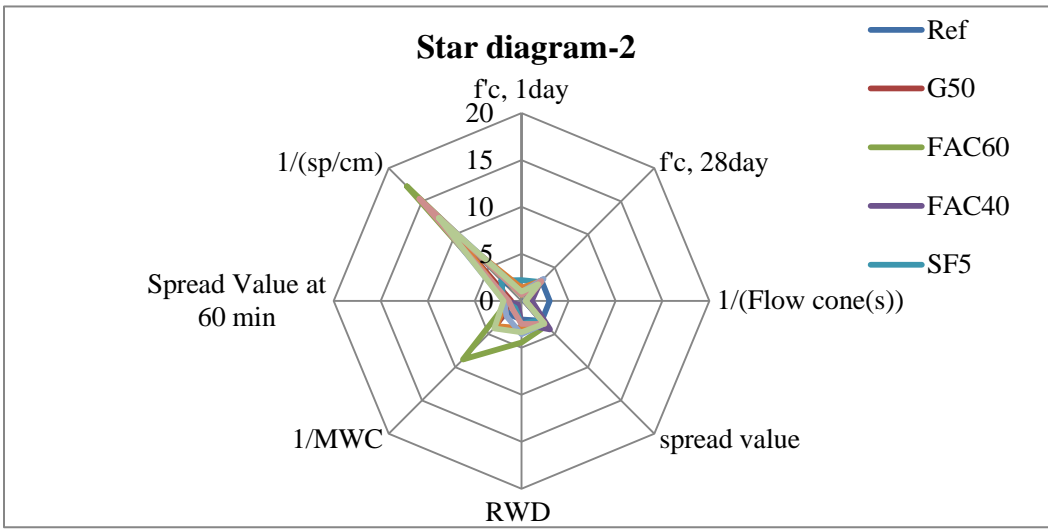


Figure 3.23 Star diagram
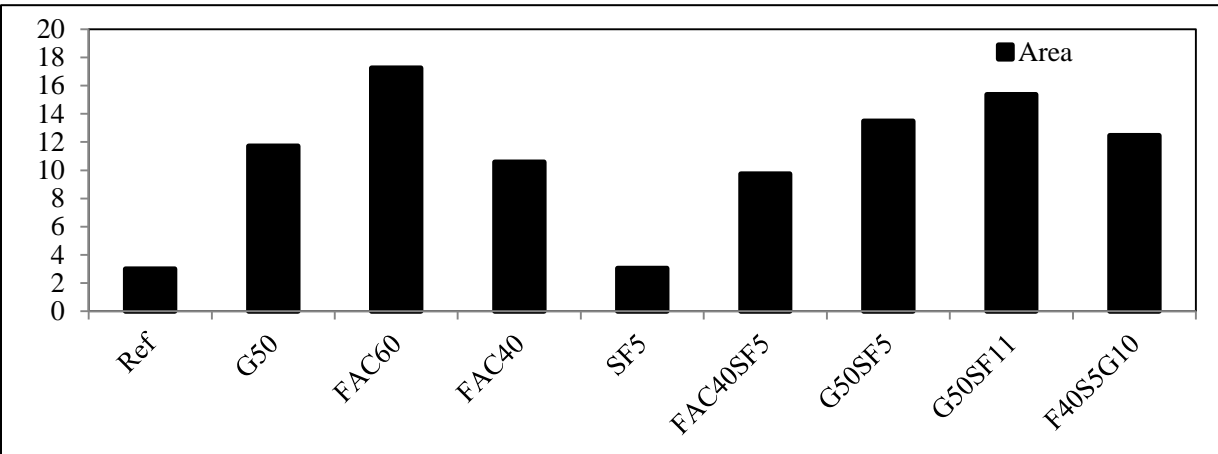


Figure 3.24 Area generated for star diagram-2

Based on the analysis of weight set 1 and 2 data, the interaction of optimum G50, FAC60, FAC40SF5, and G50SF5 mixtures was investigated further, which was addressed in section 3.4. The optimum mixture would be selected by comparingthe performance further on the concrete with other key material properties, such as shrinkage and durability.

## 3.2 Optimazation of fine aggregate

The packing density of aggregate particles has marked effect on performance. In this study, fine aggregates were applied to dry conditions was tested for packing density using the Gyratory compactor. When the combination of fine aggregate was found, wet packing method, which considers the effect of water, was implemented using ConTec viscometer 5 to measure rheology of the mortar. In this way, the relative packing density of each mixer could be found.

### 3.2.1 Mixture proportioning of mortar

Proportioning of the aggregate was optimized based on the result of workability, mechanical and rheology performance. Five mortar mixtures were evaluated, as shown in Table 3.11. The test results are discussed in

section 3.2.2. River sand (0-5 mm) and masonry sand (0-2 mm) were combined at varioius combinations. The aggregates were from rivers in Missouri.

Table 3.11 Mixtures for proportioning of aggregate

| | Mixture codification | | | | |
|---|---|---|---|---|---|
| agg/cm (by volume)[*] | 0.8 | 1 | 1.2 | 1.3 | 1.4 |

*agg/cm refers to the volume of fine aggregate over that of cementitious materials

## 3.2.2 Mixing procedure of mortar

A Hobart mixer with a maximum capacity of 12 liters was used. The volume of a batch for the rheology test was kept constant of 5 liters. Figure 3.25 shows the mixing procedure for the rheology test.
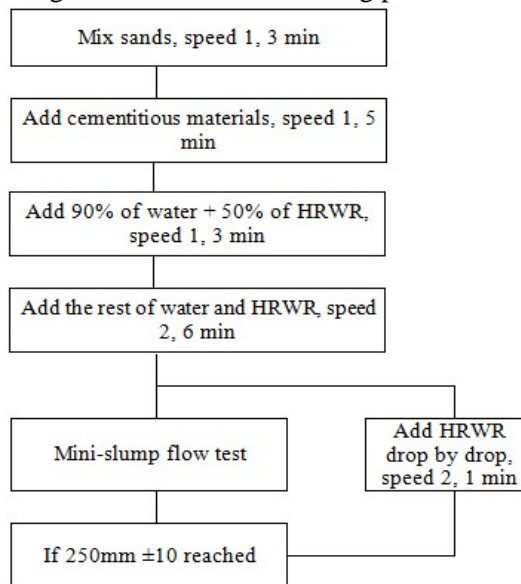
Figure 3.25 Mixing procedure for rheology test of mortar using Hobart Mixer-12 L

## 3.2.3 Test methods of mortar

**Test method for rheological properties of mortar**

In the present research study, the rheological properties of UHPC was performed by the ConTec Viscometer 5, as shown in Figure 3.26, which is a coaxial cylinder viscometer for coarse particle suspension that is suitable to measure the rheological properties of cement paste, mortar and concrete with 120 mm slump or higher.

Figure 3.26 ConTec Viscometer 5

The rheological properties are described by the fundamental parameters in the Bingham model. The values of G and H are transformed to obtain $\tau_0$ and $\mu$, respectively, as presented earlier. The calculation process also qualifies the tendency of the mixtures to segregate during the testing using the segregation factor (S), which can be considered as the change in viscosity during testing.

The specified performance range of the rheometer is 0.27 to 27 Nm for the torque, and 0.1 to 0.6 rps for the rotation velocity under normal testing conditions. The absolute range for both the velocity and torque can be optionally adjusted. An enhanced version has an extended performance range for rotation velocity of 0.0022 to 0.85 rps.

The mortar was prepared based on the aforementioned procedure. The mini slump flow was kept at $250 \pm 10$ mm by adjusting the HRWR dosage. The measurement setup parameters are tabulated in Table 3.12. The first measurement was performed once the target mini slump flow was obtained within 20 min. The measurement intervals were 20, 40 and 60 min of age.

Table 3.12 Measurement setup parameters (ConTec Viscometer 5)

| Run time parameters | |
|---|---|
| Max. rotation velocity (rps) | 0.5 |
| Min. rotation velocity (rps) | 0.025 |
| Number of T/N points | 10 |
| Transient interval (sec) | 1 |
| Sampling interval (sec) | 4 |
| Number of sampling points | 50 |
| Beater control | |
| Rotation velocity (rps) | 0.5 |
| Beater penetration time (sec) | 35 |
| Penetration speed, 0.1-1 | 1 |

**Test method for packing density of fine aggregate**

The highest packing density of the fine aggregates, the Gyratory compactor was used as shown in Figure 3.27.
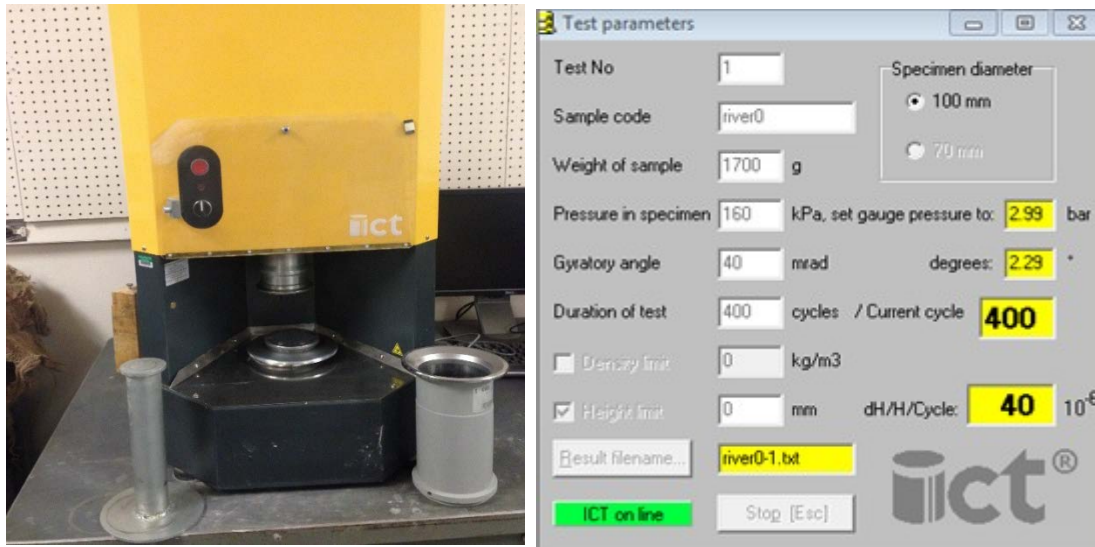


Figure 3.27 Gyratory compactor testing

In this machine, a sample of aggregate mass is compacted by a continuous kneading action consisting of axial pressure and shear. The compaction is given by the combination of two distinct and essential actions: pressure and shear movements. Shear movement under constant pressure allows particles to move closer to one another to reach a higher level of density. The constant vertical pressure, applied to a material in the machine, is obtained by compressing the mass in a test cylinder between the top and bottom plates. Gyratory movement of the cylinder during a test creates the required shear. Measurement setup parameters defined to the machine are tabulated in Table 3.13.

Table 3.13 Measurement setup parameters of Gyrator compactor testing

| | |
|---|---|
| Cylinder diameter | 100 mm |
| Sample height | 100 mm |
| Air pressure | 4 bar |
| Gyrator angle | 2° |
| Number of cycles | 200 |
| Working speed | 60 rpm |

Different percentages of the fine aggregate were combined using Hobart mixer then tested in the Gyrator compactor testing machine to optimize the packing density.

3.2.4 Test results and discussion

**(1) Grading of fine aggregate**

Table 3.14 shows the test results. The density of various combinations of the fine masonry sand and concrete river sand, as can be seen in Figure 3.28, a combination of 30% masonry sand with 70% river sand lead to a maximum density.

Table 3.14 Packing density of sands

| River sand % (by weight) | 0 | 10 | 50 | 60 | 70 | 80 | 90 | 100 |
|---|---|---|---|---|---|---|---|---|
| River sand (g) | 0 | 130 | 650 | 780 | 910 | 1040 | 1170 | 1300 |
| Masonry (g) | 1300 | 1170 | 650 | 520 | 390 | 260 | 130 | 0 |
| Density (kg/m3) | 1727.5 | 1754 | 1825 | 1850 | **1870** | 1855 | 1860 | 1857 |
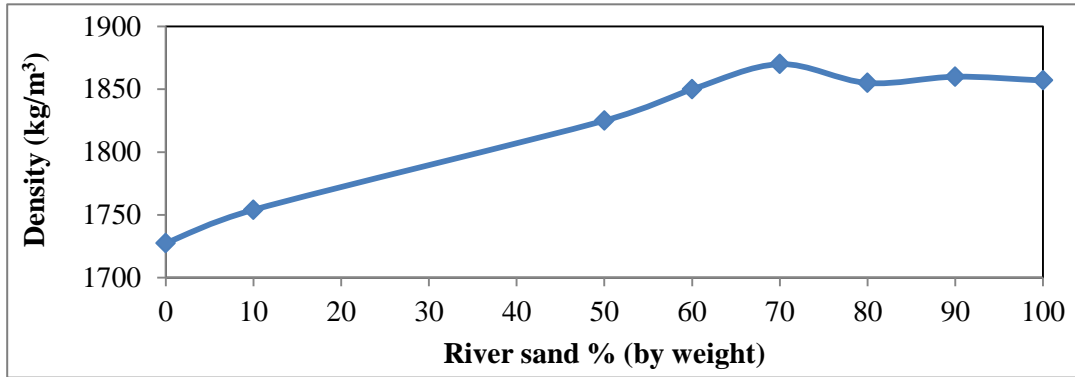


Figure 3.28 Packing density of various fine aggregate combinations

### (2) Determination of agg/cm

As stated before, the rheology or flow properties of concrete are important for precast concrete because concrete is usually put into place in complicated forms. Unfortunately, due to the complex composition of the material, no definite method for predicting the flow of UHPC from its components exists. The purpose of this part is to assess the measurement and analysis of the flow properties of mortars and determine the agg/cm ratio for the further work.

Table 3.15 shows some results related to the rheology, the time dependent viscosity and yield stress measured by the viscometer. To meet the same mini-slump spread value, the consumption of HRWR was different for different agg/cm.

Table 3.15 shows the flow properties and compressive strength for the three selected mixtures. The flow time was increased with the increasing of agg/cm ratio, which means the viscosity of mixtures decreased with the increasing of agg/cm. The compressive strength of 1-day was almost the same for each mixture. The 7 day compressive strength result shows that the lower agg/cm, the higher the strength. For the result of 28-day compressive strength, the agg/cm equal to 1 obtained the highest strength. The 1.2 and 1.4 had very close strength results.

Table 3.15 Test result of rheology

| agg/cm (% by volume) | Testing time | mini-slump (cm) | HRWR | HRWR/cm | Viscosity (Pa.s) | Yield stress (Pa) |
|---|---|---|---|---|---|---|
| 0.8 | 10 min | 24.60 | 51.9 | 0.01 | | |
| | 20 min | 15.00 | | | 12.04 | 23.8 |
| | 40 min | 10.73 | | | 16.5 | 25.2 |
| | 60 min | 10.00 | | | 15.9 | 28.0 |

| agg/cm (% by volume) | Testing time | mini-slump (cm) | HRWR | HRWR/ cm | Viscosity (Pa.s) | Yield stress (Pa) |
|---|---|---|---|---|---|---|
| 1.0 | 10 min | 25.10 | 36 | 0.008 | | |
| | 20 min | 21.25 | | | 6.3 | 30.5 |
| | 40 min | 14.25 | | | 8.7 | 26.2 |
| | 60 min | 10.88 | | | 12.2 | 25.3 |
| 1.2 | 10 min | 26.30 | 29.4 | 0.007 | | |
| | 20 min | 20.95 | | | 5.4 | 21.4 |
| | 40 min | 14.73 | | | 7.5 | 20.6 |
| | 60 min | 10.00 | | | 9.8 | 20.8 |
| 1.3 | 10 min | 24.48 | 22.3 | 0.005 | | |
| | 20 min | 19.38 | | | 7.5 | 26.2 |
| | 40 min | 17.23 | | | 9.4 | 23.8 |
| | 60 min | 13.38 | | | 11.2 | 23.2 |
| 1.4 | 10 min | 24.70 | 22.84 | 0.006 | | |
| | 20 min | 22.50 | | | 7.5 | 26.5 |
| | 40 min | 17.38 | | | 9 | 24.7 |
| | 60 min | 11.88 | | | 11.6 | 25.3 |

Table 3.16 Test result of flow properties and compressive strength

| agg/ cm | mini-slump (cm) | Flow time (s) | Compressive strength-1-day (MPa) | Compressive strength-7 day (MPa) | Compressive strength-28-day (MPa) |
|---|---|---|---|---|---|
| 1 | 33.25 | 64 | 42.4 | 88.4 | 123.2 |
| 1.2 | 32.25 | 104 | 43.2 | 87.5 | 111.3 |
| 1.4 | 30.13 | 129 | 43.6 | 83.3 | 115.6 |

Figure 3.29 shows the HRWR demand for each mixture to meet the mini-slump flow of 250 mm. It was observed that the demand of HRWR decreased when the volume fraction of agg/cm materials increased, up to agg/cm of 1.3. When the ratio was increased to 1.4, the HRWR demand was slightly increased by 0.1%.
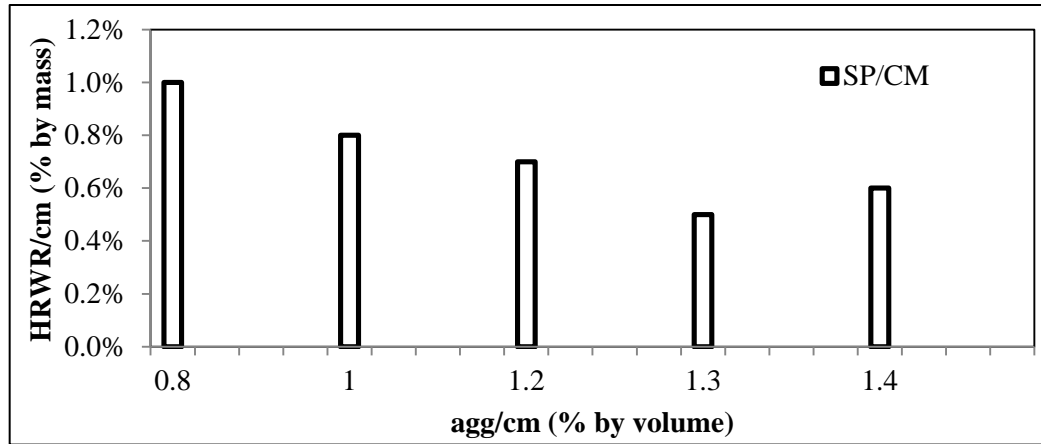
Figure 3.29 HRWR demand

The star plot method was implemented in optimizing the agg/cm. The key factors for star plot method for the first step - narrowed down the number of candidate mixtures.

Table 3.17 First set of weighted factors

|  | 1/SP/CM (HRWR demand) | 1/Plastic viscosity at 20 min (Pa.s) | 1/Plastic viscosity at 60 min (Pa.s) | 1/Statistic Yield stress at 20 min (Pa) | 1/Statistic Yield stress at 60 min (Pa) |
|---|---|---|---|---|---|
| Weight 1 | 3 | 3 | 2 | 3 | 2 |

According to results shown in Figures 3.30 and 3.31 which only considered the responses of rheology tests, agg/cm equal to 1.2 was observed as the optimum mixtures. To confirm this verdict, further tests for workability and compressive strength were carried out for agg/cm equals to 1, 1.2 and 1.4.
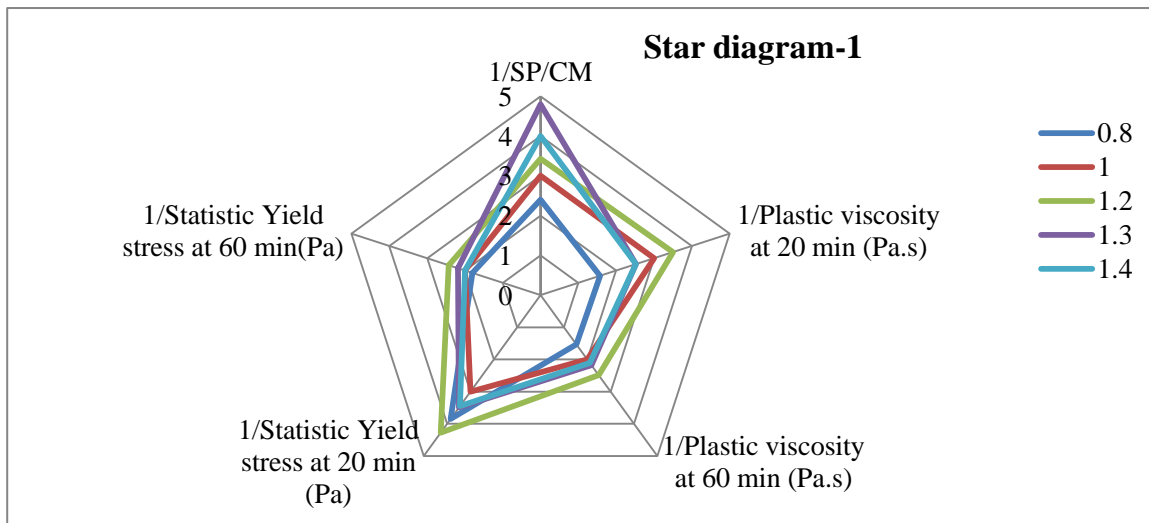


Figure 3.30 Star diagram-1for aggregate optimization
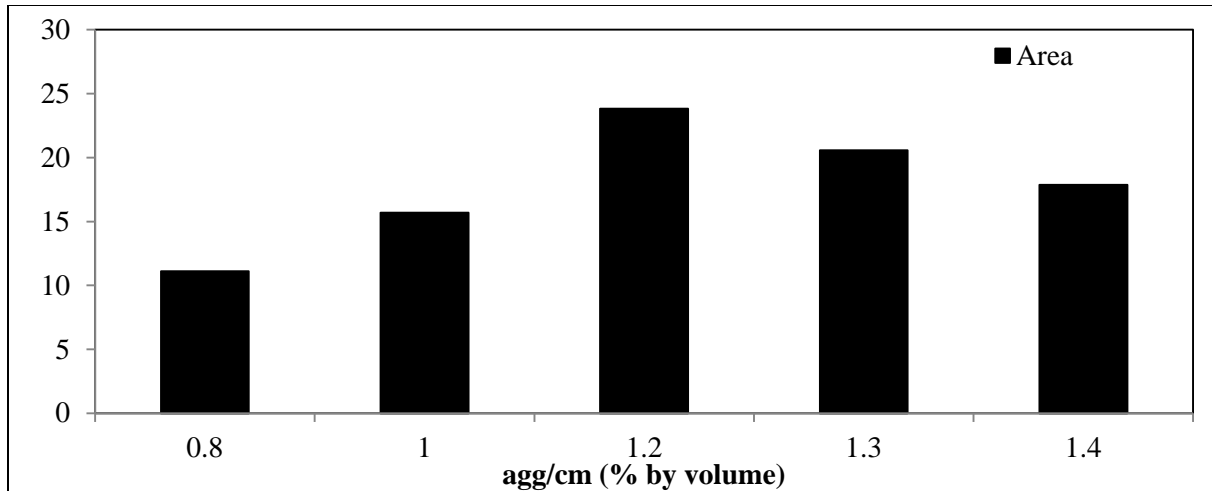
Figure 3.31 Area generated for star diagram-1 for aggregate optimization

The factors analyzed with the star plot method were listed in Table 3.18. In this analysis, HRWR demand, plastic viscosity and yield stress at 20 min. and compressive strength at 7 and 28 days were considered as the most significant factors. The dynamic yield stress and viscosity measured at 60 min. and compressive strength at 1-day were taken as the minor factors.

Table 3.18 Second set of weighted factors

|  | 1/SP/CM (HRWR demand) | 1/Plastic viscosity at 20 min (Pa.s) | 1/Plastic viscosity at 60 min (Pa.s) | 1/ Yield stress at 20 min (Pa) |
|---|---|---|---|---|
| Weight 2 | 3 | 3 | 2 | 3 |
|  | 1/ Yield stress at 60 min(Pa) | Compressive strength-1-day (MPa) | Compressive strength-7-day (MPa) | Compressive strength-28-day (MPa) |
| Weight 2 | 2 | 1 | 3 | 3 |

The results in Figure 3.32 and Figure 3.33 combined the effect of compressive strength. By comparing the area in Figure 3.33, the agg/cm equal to 1.2 can be the optimum mixture, which confirmed the conclusion obtained from the weight 1 set analysis.
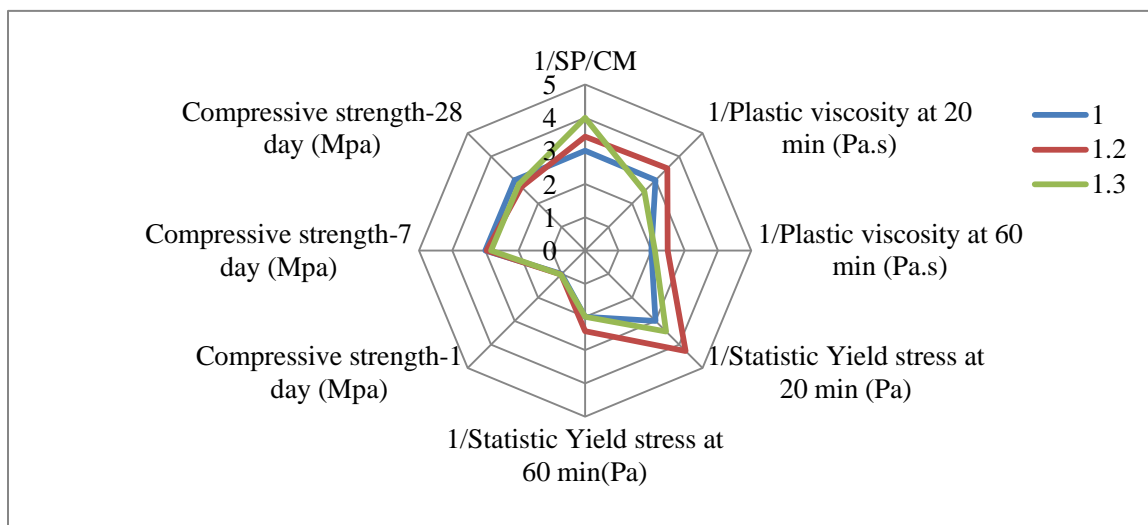


Figure 3.32 Star diagram-2 for aggregate optimization

45
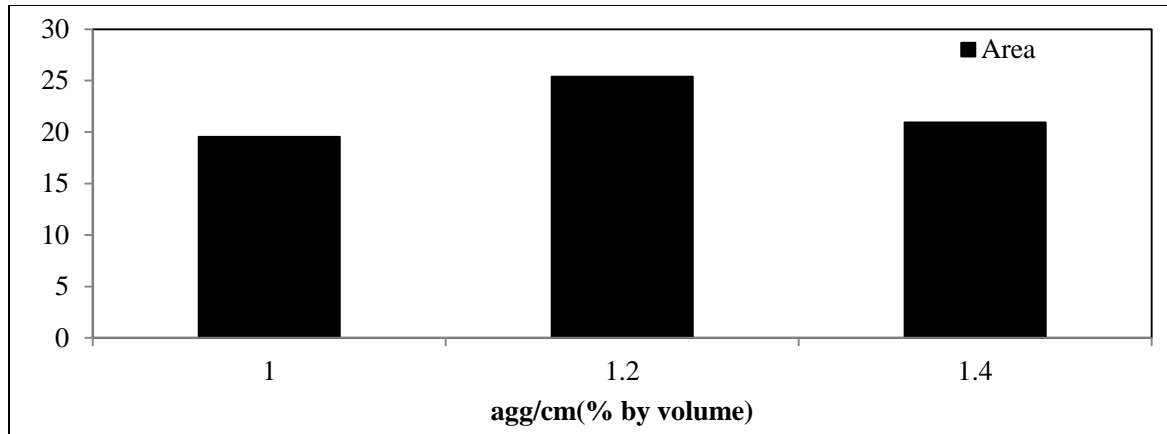
Figure 3.33 Area generated for star diagram-2 for aggregate optimization

The third set of weight was listed in Table 3.19. In this analysis, rheology properties related to spread value and flow cone flow time were measured. The consideration of factor choice was the same as weight 2.

Table 3.19 Third set of weighted factors

| | Compressive strength 1-day (MPa) | Compressive strength 7-day (MPa) | Compressive strength 28-day (MPa) | Slump (cm) | 1/Flow time | 1/SP/CM (HRWR demand) |
|---|---|---|---|---|---|---|
| Weight 3 | 1 | 3 | 3 | 3 | 3 | 3 |

When it was changed rheology related factors from viscosity and yield stress to spread value and flow cone flow time and spread value, the area of agg/cm of 1 is 7% bigger than that of 1.2. Compared all the analysis, in this project, agg/cm equal to 1.1 by volume was determined to the optimized ratio. Since the compressive strength is a key characteristic of UHPC and the result from the rheology test showed big difference between 1 and 1.2. On the other side, the the rheology properties show slightly difference. In the future design, the agg/cm will keep constant at 1.
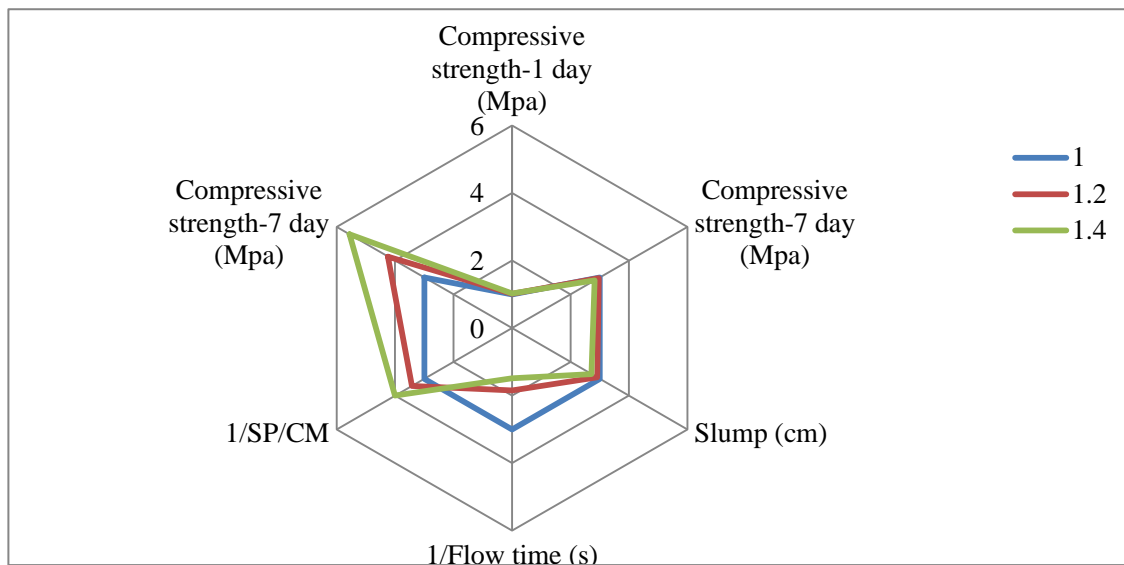


Figure 3.34 Star diagram-3 for aggregate optimization

46
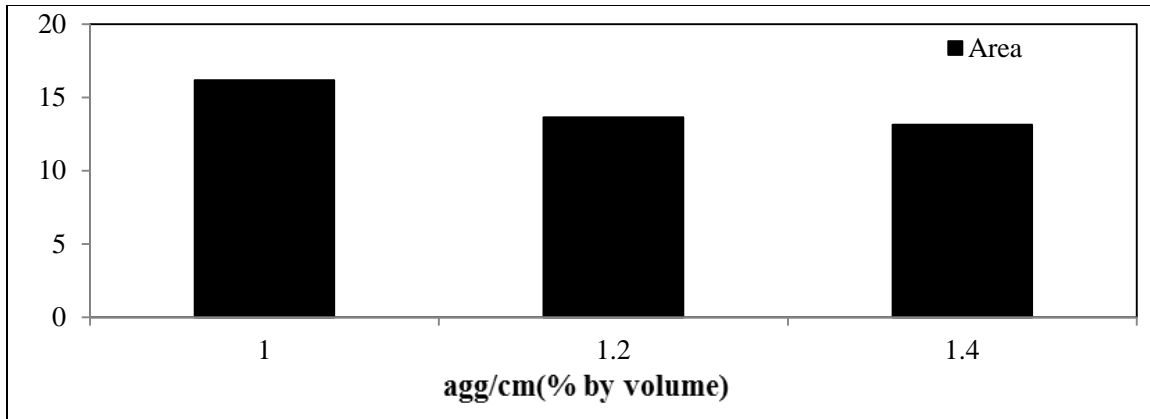
Figure 3.35 Area generated for star diagram-3 for aggregate optimization

## 3.3 Optimization of fibers in UHPC

Plain concrete has a low tensile strength and a low strain capacity at failure. As an alternative to conventional reinforcement, fibers have been used as reinforcement as well. Concrete materials produced with short, randomly distributed fibers may be superior to forms of reinforcing concrete using welded wire mesh or rebar. Both the tensile strength and toughness, especially the post-crack strength, can be improved (Bentur and Mindess, 1990). The small diameter of the individual fibers ensures a better and more uniform distribution of reinforcement. In addition, the high surface area offers significant bond capability. Because the fibers that bridge the matrix cracks are resilient and highly compliant, they can orient to carry the load across the crack faces.

This section addresses mechanical properties of fiber-reinforced UHPC prepared with different types and volumes of fibers, in addition to fresh properties. Furthermore, in order to achieve sufficient strain-hardening behavior, various volumes of steel fibers were incorporated. In this study, the fiber content was selected as the main test variable and was classified into groups corresponding to volume ratio, which was increased in increments of 0.5% from 0.5% to 2% of steel fibers.

### 3.3.1 Mixture proportioning of fiber optimization in UHPC

The experimental program consisted of three parts. The fresh viscosity and flowability of six fiber reinforced UHPC mixtures (with the same matrix but different HRWR content) were measured with the mini-V funnel and mini-slump test methods. In this part, steel fiber type I and PVA fiber were investigated. The properties of these two types of fibers are shown in Figure A-1 and Figure A-2 in Appendix A.

Second, complete flexural load-deformation curves, including the flexural capacity, first cracking strength and ultimate flexural strength were measured using 76.2 mm × 76.2 mm × 304.8 mm beams made from the same six mixtures and compressive strength for 28-day were tested using 50 mm cubes at the same time. Third, three mixtures with steel fiber type II were tested following the same procedure as last two steps,.

Table 3.20 Mixtures for proportioning of fibers

| Type | Mixture codification (% by volume) | | | |
|---|---|---|---|---|
| Steel fiber type I | 0.5% -0.21[*] | 1.0%-0.21 | 1.5%-0.21 | 2.0%-0.21 |
| Steel fiber type II | 1.5%-0.19[*] | 2.0%-0.19 | 2.0%-0.21 | |
| PVA fiber | 0.5%-0.21* | | | |

*0.5%-0.21: fibers/solid particles (by volume) = 0.5%, water/cm = 0.21 for this mixture.

*1.5%-0.19: fibers/solid particles (by volume) = 0.5%, water/cm = 0.19 for this mixture.

47

Table 3.21 Fibers properties

| Type | Filament diameter | Fiber Length | Specific Gravity | Tensile strength | Flexural strength |
|---|---|---|---|---|---|
| Steel fiber type I and II* | 0.2 mm | 13 mm | 7.8 | 1900 MPa | 203 GPa |
| PVA fiber* | 38 Microns | 8 mm | 1.3 | 1400 MPa | 31  Pa |

*Details in Appendix A.

## 3.3.2 Mixing procedure and sampling of fiber optimization in UHPC

The Omni mixer was used UHPC. First, the two 30% and 70% fine aggregate combination was mixed together using speed 6 (medium speed) for 1.5 min. Then cementitious materials were added and mixed for 1.5 min at speed 6. After that, 90% of the water and 50% of the HRWR were added, and mixing was resumed at speed 10 (high speed) to mix 3 min. The rest of the water and HRWR were added, and the mortar was mixed for 4 min. Finally, fibers were added gradually and mixed for 1 min. Figure 3.36 shows the mixing procedure.
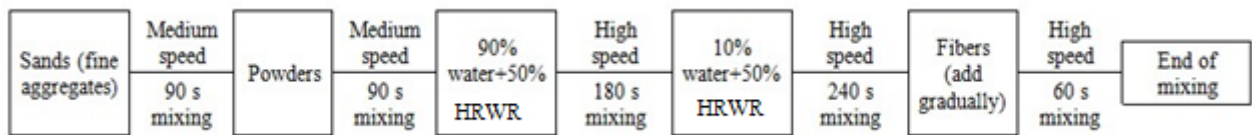


Figure 3.36 mixing procedure for UHPC using Omni mixer

The method of casting UHPC has an influence on the orientation and dispersion of the fibers.. During casting, special care was taken to ensure that the UHPC flowed from one end of the prism to the other for proper distribution and alignment of the fibers along the molds length. For this purpose, after mixing, the UHPC was placed on a 1 m long chute (pipe with 150 mm diameter) with an inclination of approximately 30 degrees (Figure 3.37). This helped the concrete to release part of the entrapped air. It also contributed to the alignment of the fibers. Figure 3.37 shows the procedure of casting schematically.
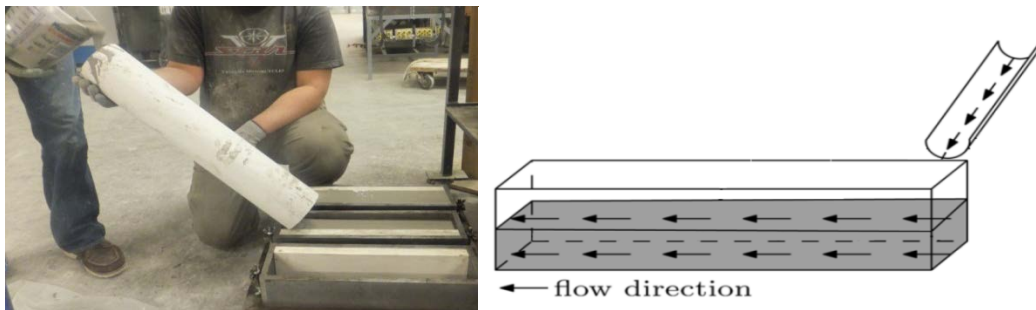


Figure 3.37 UHPC casting procedure with inclined chute

## 3.3.3 Test methods of fiber optimization in UHPC

### Flexural strength testing

Flexural performance of the UHPC was conducted using beams with third-point loading in accordance with ASTM C 1609. The beam specimens measure 304.8 mm (length) x 76.2 mm (width) x 76.2 mm (depth) with a bending span of 203.2 mm During the test, the load and deflection at mid-span of the prism were monitored, as shown in Figure 3.38. The obtained data were used to determine the cracking strength and post-cracking toughness of the concrete. For the test setup, a yoke similar to that shown in Figure 3.38 was used to measure the mid-span deflections. LVDTs were attached to the yoke on each side of the specimen at mid-span, and the yoke was attached to the specimen at mid-depth over the support points. The LVDTs bore

on a plate that was epoxied to the compression face and extended to hang over the sides of the prism. Figure 3.3.2.3 shows the deflection measurement setup for this three-point bending test.
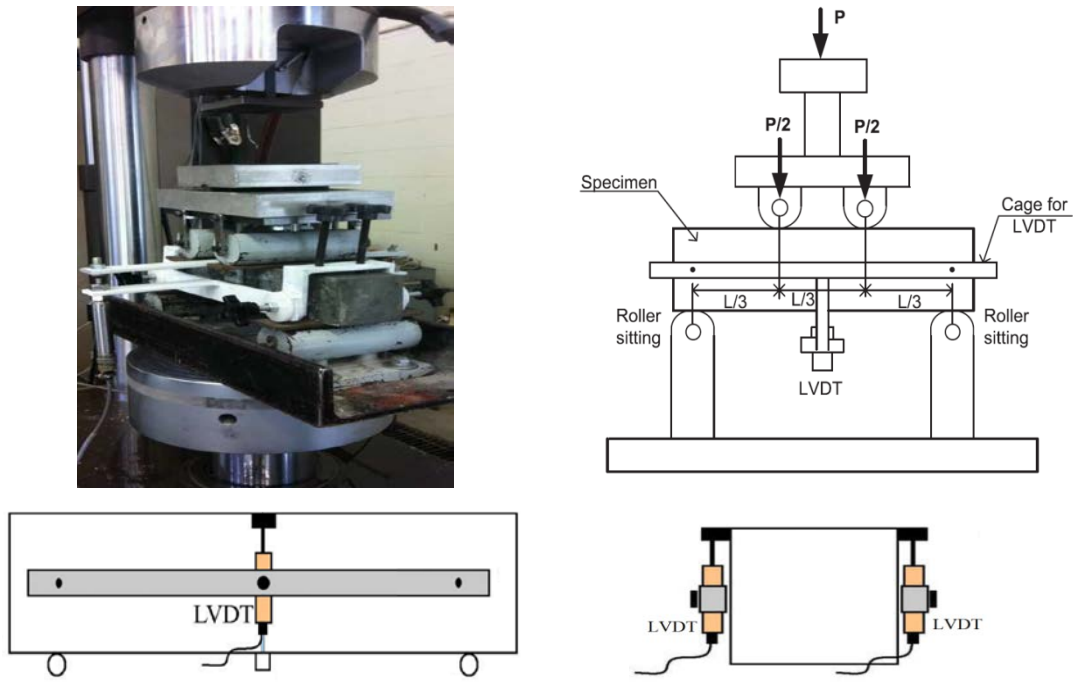


Figure 3.38 Test setup for flexural test (ASTM C 1609)

**Measure flow time**

In this section, mini-V funnel was used to measure the flow time in fresh state which was related to the viscosity of the mixture. As showed in Figure 3.39, this test consists of measuring the time required for a given volume of mortar (1 liter) to flow through the nozzle. This test is often used to measure the viscosity of the mortar, which may be related to properties such as cohesiveness, pumpability, and finishability.
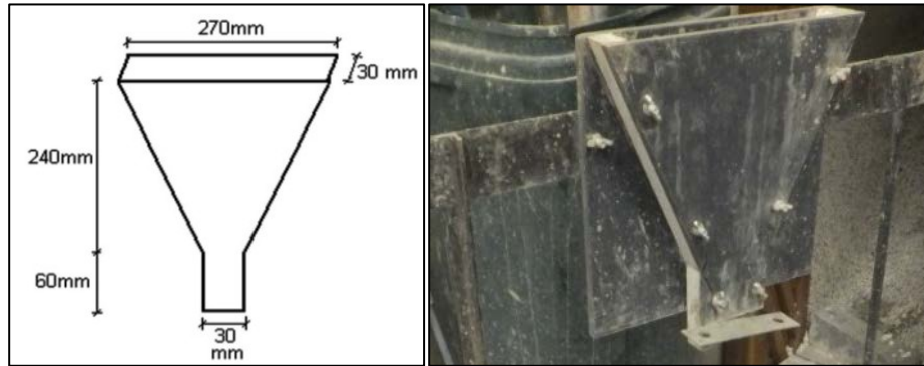


Figure 3.39 Mini-V funnel

**Other tests**

Mini-slump, compressive strength test and rheology test were also implemented to optimize fibers. The tests procedures were shown in sections 3.1 and 3.2.

### 3.3.4 Test results and discussion of fiber optimization in UHPC

Prior to start of the second measurement at 15 min, the mixture was completely mixed to avoid any segregation. It should also be noted that there was one control mixture without any fiber, four mixtures with different percentages of steel fibers, 0.5%, 1%, 1.5%, and 2%, as well as a mixture containing 0.5% PVA fiber but treated in two ways: PVA fibers and saturated with mixing water. The idea behind saturating the the PVA fibers with water was to investigate if it helps with good dispersion in the fibers. The saturating the PVA fibers before mixing does not affect yield stress.

**Test result for workability and compressive strength**

The optimized volume percentage of fibers for PVA and steel fibers was determined. The decision was made based on the test results of mini-slump, flow cone flow time, dynamic yield stress and flexural strength. Because the water adsorption capacity of the PVA was high, the maximum percentage of PVA that could be used was only 0.5% to meet the goal of spread value as much as 300 ± 10 mm.

The results of fresh and compressive strength tests are given in Table 3.22. From the test results, it can be concluded the relationship for steel fiber type I as shown in Figures 3.40 to 3.41. When w/cm is 0.21, for the volume fraction of steel fiber type I from 0% to 2.0% (the maximum fraction used for this project), to meet the target slump flow 300 mm ± 10 mm, the HRWR demand increased with the increasing of fibers volume fraction (Vf). Especially when Vf changed from 1.5% to 2.0%, the HRWR content increased by 0.3% which was ten times more than when Vf increased from 1.0% to 1.5%. In terms of 28-day compressive strength, the highest strength observed for Vf is 1.5%. When Vf increased from 1.5% to 2.0 %, the 28-day compressive strength decreased from 145.4 MPa to 141.9 MPa.

The performance of UHPC materials with steel fibers type I and II showed the same dimensions and lengths and properties. When tested, steel fiber type II (w/cm was 0.21) with 2% fibers was found to have a higher HRWR demand than that of steel fiber type I and the 28-day compressive strength was 149.6 MPa, which is higher than the steel fiber type reinforced concrete. It was concluded that steel fiber type II was more suitable to use in the case of pursuing higher compressive strength. When the w/cm was decreased to 0.19, the 28-day compressive strength of 2.0% was higher than 1.5% fiber. However, when the w/cm decreased to 0.19, the temperature of the UHPC at the end of mixing was closed to 35 ℃ given the higher viscosity of the material.

Table 3.22 workability and compressive strength test result of fibers

| Vf | HRWR/cm (by weight) | Slump flow - HRWR fixed to 1.20% (cm) | Slump flow (cm) | Flow time (s) | f'c (MPa) |
|---|---|---|---|---|---|
| Steel fibers type I – w/cm = 0.21 | | | | | |
| 0.0% | 1.20% | 30 | | 17.04 | 127.5 |
| 0.5% | 1.21% | 23 | 29.5 | 29.96 | 126.4 |
| 1.0% | 1.22% | 24.5 | 29.5 | 28.68 | 123.8 |
| 1.5% | 1.25% | 25 | 29 | 31.67 | 145.4 |
| 2.0% | 1.55% | 10 | 29.5 | 25.56 | 141.9 |
| Steel fiber type II – w/cm = 0.21 | | | | | |
| 2.0% | 1.65% | 20 | 29.7 | 19.56 | 149.6 |
| PVA – w/cm = 0.21 | | | | | |
| 0.50% | 2% | 10 | 28 | 13.49 | 120.7 |
| Steel fiber type II – w/cm = 0.19 | | | | | |
| 1.5% | 2.4% | 10 | 30 | 37.53 | 145.6 |
| 2.0% | 2.4% | 10 | 29.5 | 45.06 | 150.3 |

**Flexural strength results**

The flexural strength and toughness results and analysis were highly dependent on the correct identification of first cracking in each test. Plain concrete made without fibers and fiber reinforced UHPC may begin to behave nonlinear due primarily to internal microcracking before the first overall cracking of the prism. Therefore, determining first cracking can be somewhat subjective. The behavior of UHPC is such that the first cracking is tensile stress cracking on the bottom flange of the prism. Thus, first cracking – recorded by the data acquisition system and physically observed on the specimen – is usually quite clear.

Typical load-deflection curves obtain in this investigation for UHPC mixtures containing different type and combinations of fibers are presented in Figures 3.40 to 3.56. The average peak loads and corresponding deflections for fibrous UHPC with different types and combinations are presented in Table 3.23. The peak load and corresponding centre point deflection for mortars withour any fiber are also presented as references.

(1) Reference - non fibrous mixtures

Figures 3.40 and 3.41 show the results of load-deformation curves with respect to the control mixture made without any fibers. The load-deformation follows inear relationship and fails in a brittle moment. As the fracture failure happened suddenly, it is too brittle to be used as tensile resistant materials. The average peak load was 19.3 kN, while the maximum deformation was 0.099 mm.
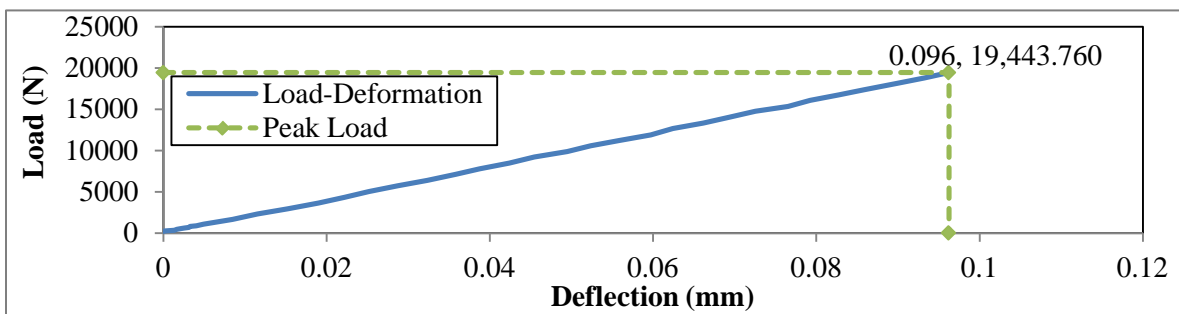


Figure 3.40 Load-Deflection: Reference-1 without fiber (w/cm=0.21)
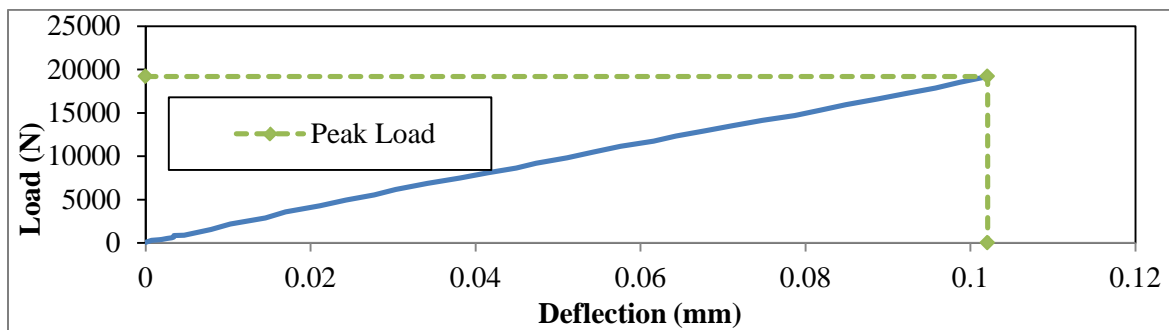


Figure 3.41 Load-Deflection: Reference-2 without fibers (w/cm = 0.21)

(2) PVA fibers (0.5%)

PVA fiber is commonly used in engineered composite concrete (ECC). ECC can enable the development of a strain hardening flexural behaviours when multiple cracking can occur given successive slip between the cement matrix and the fibers. However, the hydrophilic nature of PVA imposes a challenge in the composite design since the fibers are apt to adsorb free water from the cement paste, hence decreasing workability. In ECC applications, the fiber volume can be high reaching typically 3%. However, in this research with low w/cm for UHPC, the PVA volume ratio was limited to 0.5% given the impact of the fibers or water demand. When the fiber volume ratio exceeded 0.5%, for example, 1%, it was unable to increase the fluidity targeted

of 300 mm by adding n the HRWR.

The flexural test results of UHPC with 0.5% PVA fibers are shown in Figures 3.42 and 3.43. Mixtures incorporating PVA fiber showed performance similar to that of reference mixture where the specimens failed at first peak load, and there was not post cracking stage. Compared to the reference mixture, the average peak load of 0.5% PVA mixtures was 8% greater than that of the non-fibrous UHPC (reference), but the maximum deformation was 13% lower.
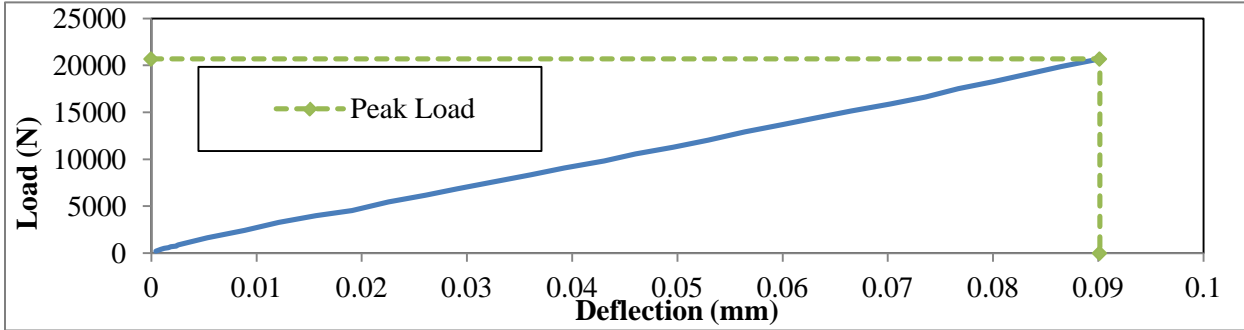


Figure 3.42 Load-Deflection: 0.5% PVA-1 fibers (w/cm=0.21)
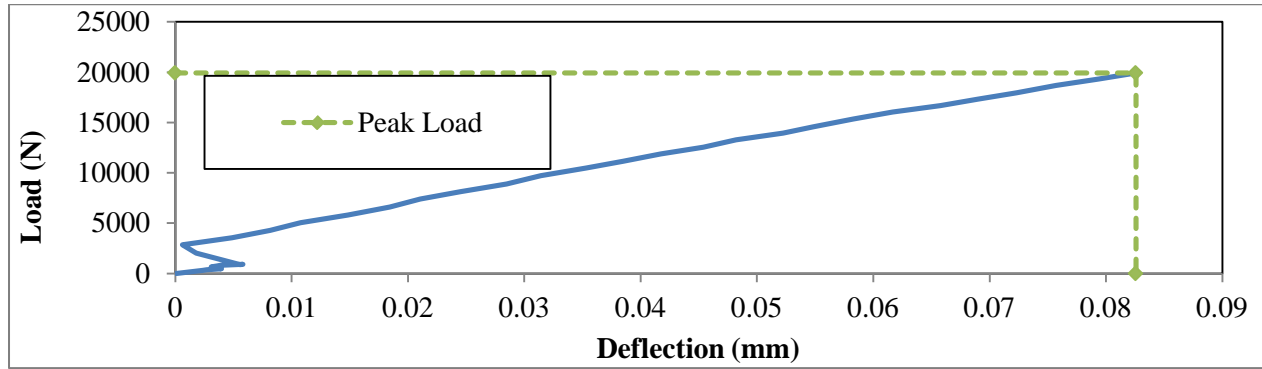


Figure 3.43 Load-Deflection: 0.5% PVA-2 fibers (w/cm = 0.21)

(3) Steel fibers type I

Figure 3.44 shows a typical failure configuration after 4-point bending test. After failure, one large crack existed, accompanying fibers, which plays an important role in bridging two crack faces. Due to the bridging mechanism of fibers, fiber reinforced UHPC can provide superior performance especially under tension as compared to the concrete without fibers.



Figure 3.44 Failure configuration after test

52

Figures 3.45 and 3.46 show the load-deformation curves of steel fibers type I with 0.5% volume ratio. The specimens showed better ductility compared with controlled and PVA reinforced beams (the centre-point deflection is increased by 25%), but no more ultimate strength was gained with this amount of steel fibers and no deformation-hardening behavior was observed. The flexural strength was 14.6 MPa, while the deflection at the peak load was 0.1 mm.
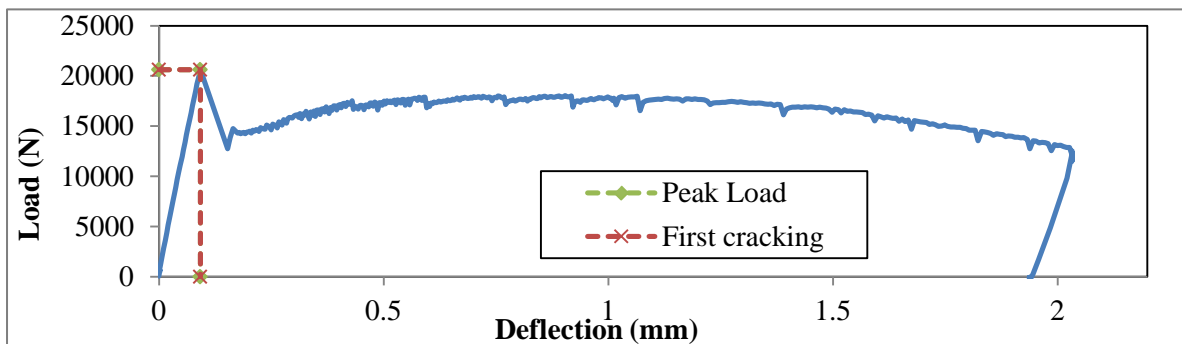


Figure 3.45 Load-Deflection: steel fiber type I 0.5% - 1 (w/cm=0.21)
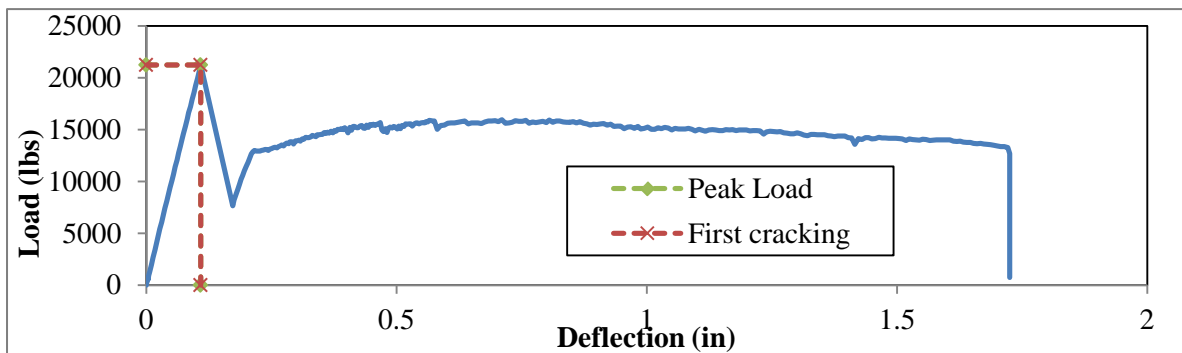


Figure 3.46 Load-Deflection: steel fiber type I 0.5% - 2 (w/cm=0.21)

When the fiber volume ratios reached and exceeded 1%, significant deformation-hardening can be seen and the corresponding flexural strength was increased significantly.

The steel fiber type I UHPC 1% fibers resulted in an average flexural strength of 18.0 MPa associated with a deflection value at peak load 0.558 mm. This was more than five times of the maximum deflection of the reference and PVA mixtures. Similar flexural strength 18.13 MPa and a slightly improved ductility (0.658 mm for the deflection at peak load) was obtained by using a 1.5% volume fraction of steel fibers type I (Figures 3.47 and 3.48).
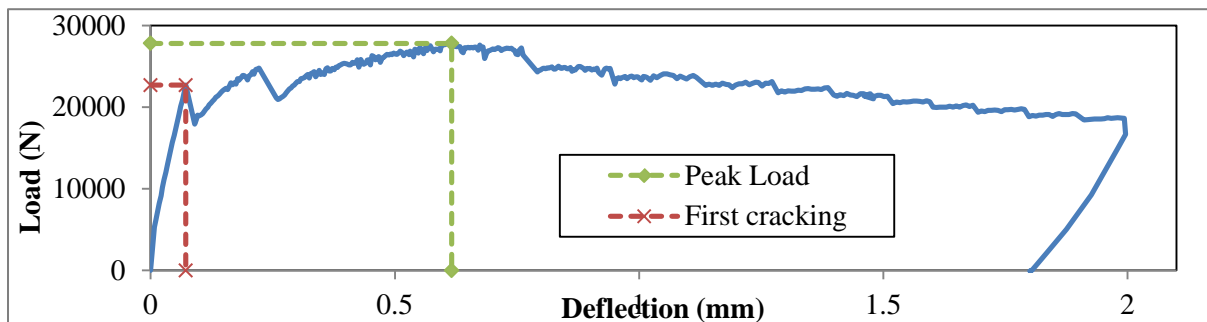


Figure 3.47 Load-Deflection: steel fiber type I 1% - 1(w/cm=0.21)
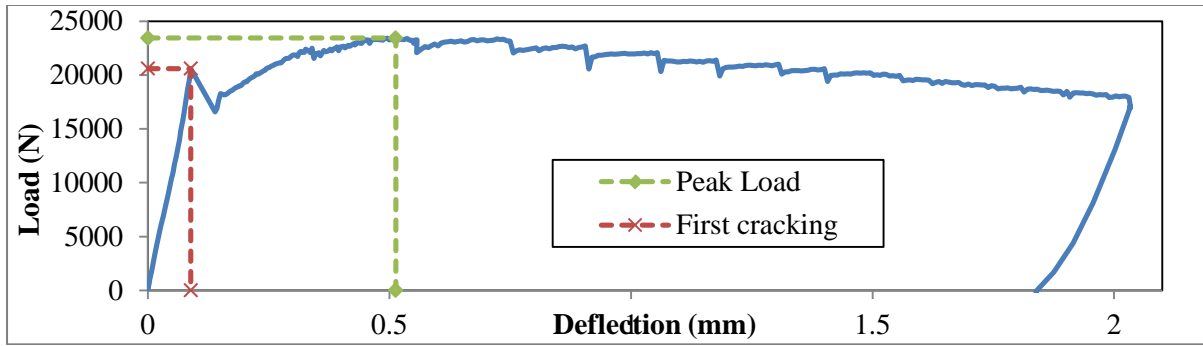
Figure 3.48 Load-Deflection: steel fiber type I 1% - 2 (w/cm=0.21)
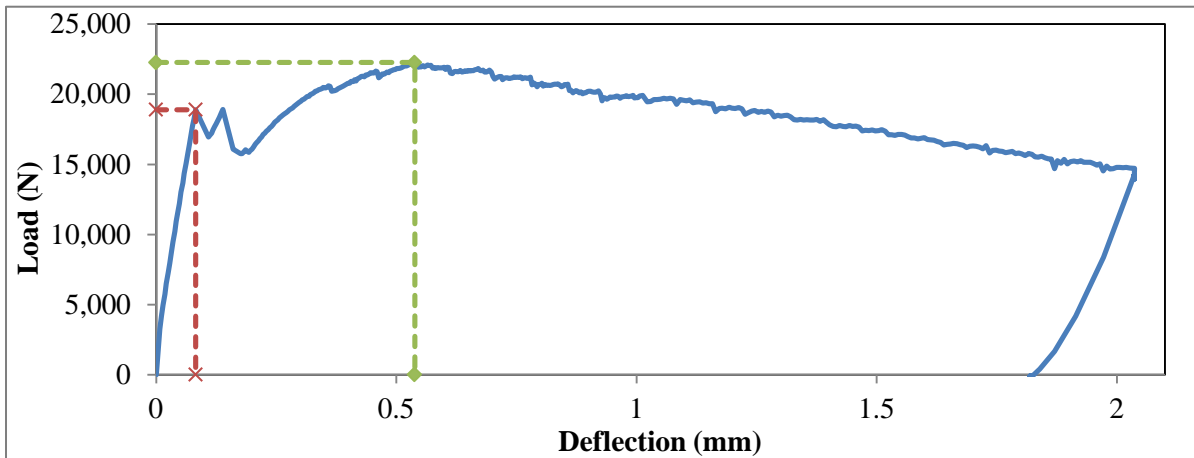


Figure 3.49 Load-Deflection: steel fiber type I 1.5% - 1 (w/cm=0.21)
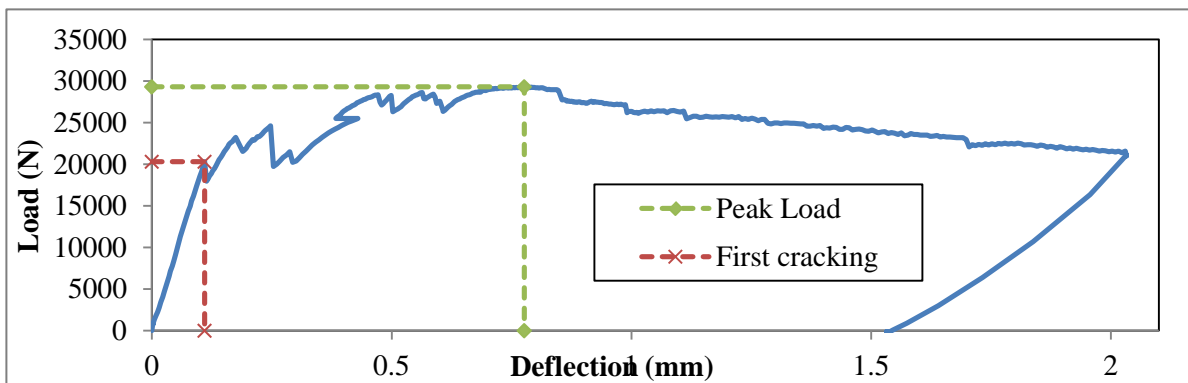


Figure 3.50 Load-Deflection: steel fiber type I 1.5% - 2 (w/cm = 0.21)

Although the specimens (Figures 3.47 to Figure 3.50) showed deflection-hardening behavior when the steel volume ratio exceeded 1%, the flexural strength did not increase much compared with the reference. However, large variations in deformation capacity and ultimate strength were found in steel fiber type I with the volume fraction of 2% (Figures 3.51 and 3.52). The use of 2% steel fibers developed a flexural strength of 41.2 MPa at a deflection of 1.05 mm. The results are the best overall for both strength and deflection capacity which were both twice the value of the other mixtures. Compared to the control, the specimens exhibited more consistent flexural behavior as well as improved deformation capacity with 300%.

In terms of energy absorption capacity, the toughness determined from the flexural testing (ASTM C 1609) was used. The results of the toughness values of the tested mixutres reported in Table 3.23. The T 150 index

is the area under the load versus net deflection curve calculated from 0 to L (span)/150. Higher toughness resulted in better performance in ductility. Toughness is shown to increase with the increase of the volume fraction of the steel fiber type I from 30 mm to 52 mm-kN.
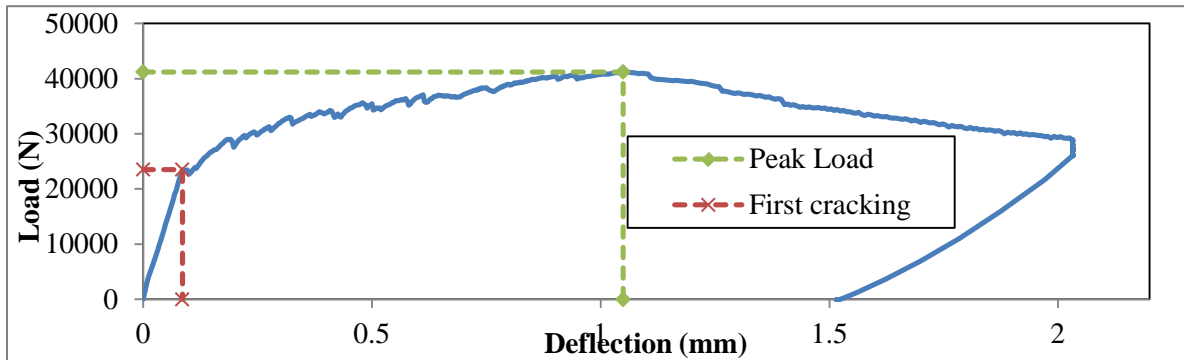


Figure 3.51 Load-Deflection: steel fiber type I 2% - 1(w/cm=0.21)
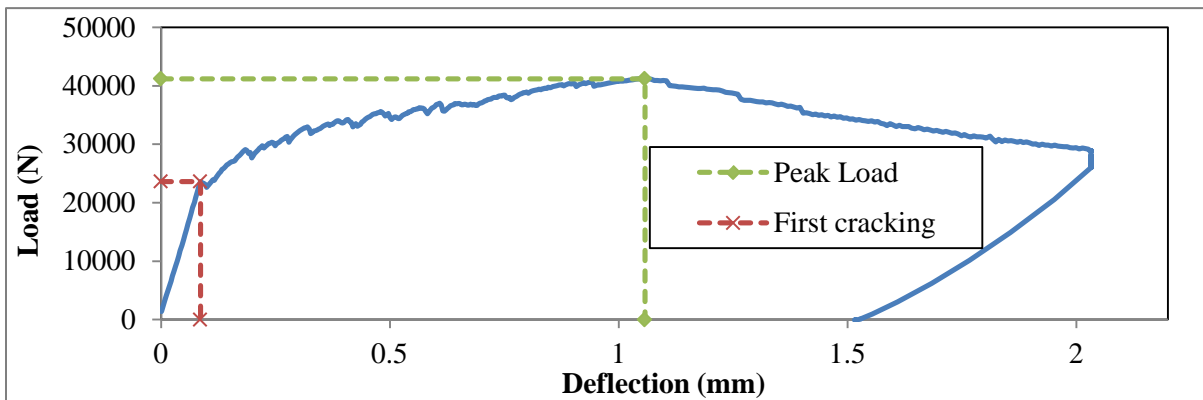


Figure 3.52 Load-Deflection: steel fiber type I 2% - 2 (w/cm=0.21)

(4) Steel fiber type II

From Figures 3.53 and 3.54 showed the load-deflection of the mixture with 2% steel fibers showed better deformation capacity and ultimate strength. These test results confirmed that mixes with 2% steel fibers have best hardened properties.

The performance of the mixtures tested using steel fiber type II is shown in Figures 3.53 to 3.56 and Table 3.23.
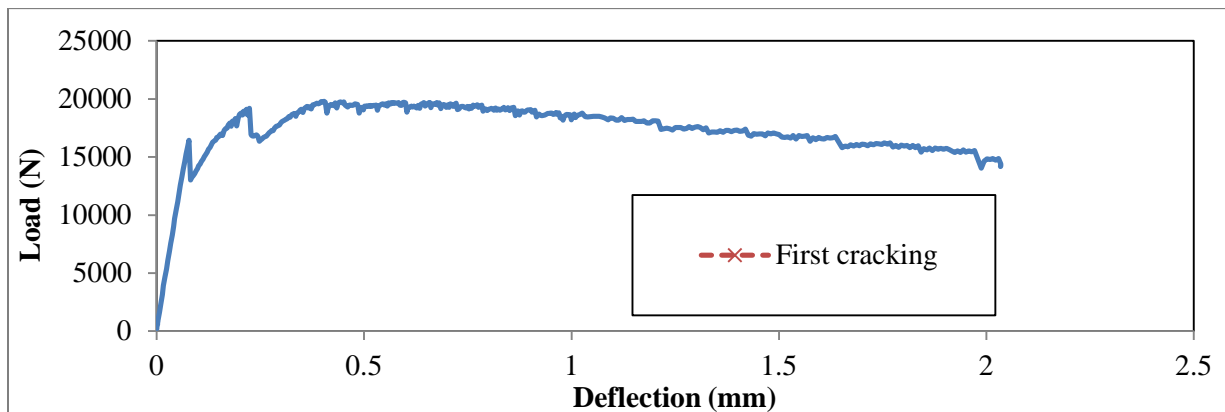


Figure 3.53 Load-Deflection: steel fiber type II 1.5% -1(w/cm=0.19)

55
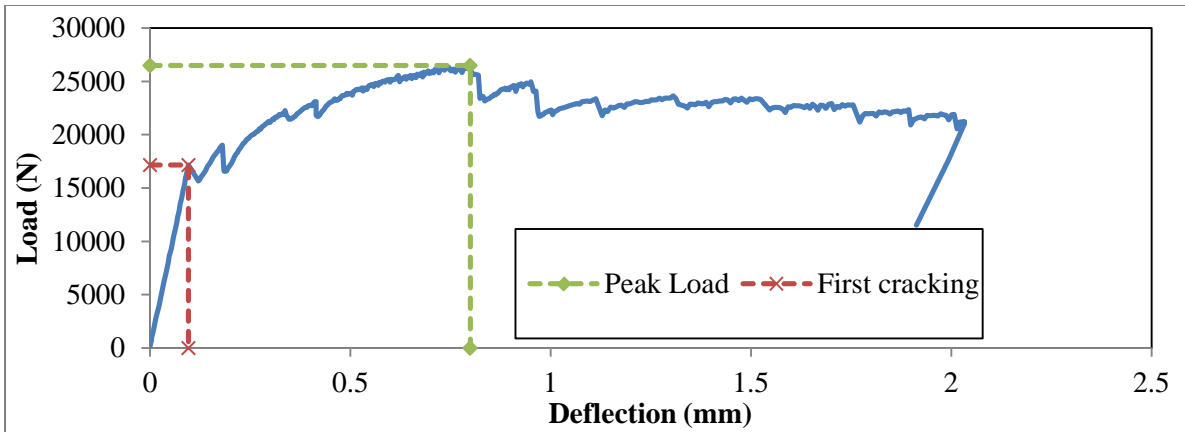
Figure 3.54 Load-Deflection: steel fiber type II 1.5% -2 (w/cm=0.19)

To further investigate the effect of w/cm on performance, fiber reinforced UHPC with lower w/cm of 0.19 (vs 0.21) was presented using steel fiber type II at 1.5% and 2%. However, both the flexural strength and peak load deflection decreased compared with the the UHPC with w/cm of 0.21. This means that decreased w/cm ratio decreases the tensile strength of UHPC. This can be attributed to with lower w/cm, the fibers can be difficult to disperse well in mortars, and thus result in clusters in the concrete mixtures.
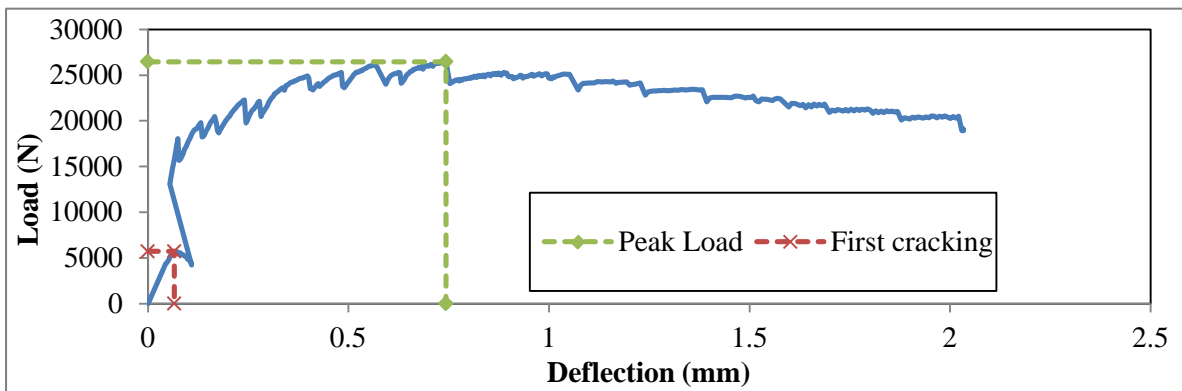


Figure 3.55 Load-Deflection: steel fiber type II 2% -1(w/cm=0.19)
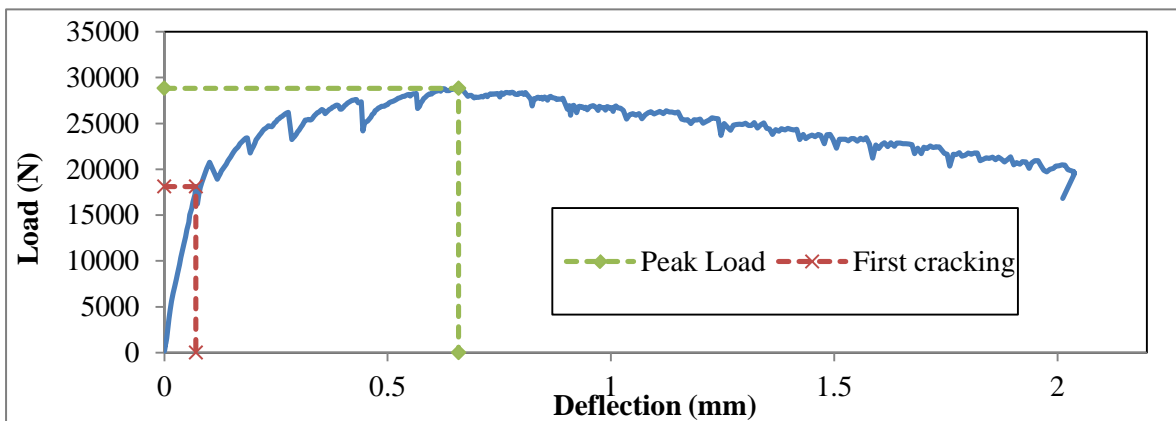


Figure 3.56 Load-Deflection: steel fiber type II 2% -2(w/cm=0.19)

Table 3.23 shows the final results for UHPC reinforced with steel fibers. The procedure implemented for the ASTM C 1609 prism flexure tests allowed for accurate recording of the flexural behavior of UHPC from initial elastic behavior, through tensile cracking, to tensile fiber pull out. Table 3.23 provides the results

56

from the prisms in each set. The first and most important result here is behavior at first cracking of the UHPC matrix. The first cracking (P1) is an indication of the tensile strength of the materials. The load, strength, and deflection at first cracking and peak load are listed in the table. The peak load values tended to be between 100% and 200% of the cracking load results. The equivalent flexural strength corresponding to peak load is based on equation (3.1) where it substitutes peak load for cracking load. This calculation is presented purely for comparative purposes, as this equivalent flexural strength has no physical meaning. At peak loading, the UHPC was exhibiting extensive cracking, and its midspan neutral axis no longer resides at mid-depth. Thus, the assumption of pure bending on a uniform, elastic cross section, which are inherent in this equation, is not met.

$$f_{ct,flexure} = \eta \frac{Pl}{bd^2}$$  Equation (3.1)

Concrete due to its brittle behavior has little ability to resis tensile stress and strain. Within concrete materials characterization testing, toughness is a term that provides some indication of the concrete's energy absorption capacity. Usually, toughness is quantified in terms of the area under a load-deflection response curve. Toughness values are specific to the testing procedure implemented. Table 3.23 presents the toughness results T 150 for the sets of prismatic flexural tests. As shows in the table, the steel fiber type I with 2% reached the highest T 150 of 56.7kN-mm, while the PVA and the reference reached the lowest T 150 of 1kN-mm. Steel fiber type II also resulted in 46.9 kN-mm, and can be increased by increasing w/cm. It can be concluded that, UHPC containing 2% steel fiber gave better performance than the other type and combinations.

Table 3.23 – Toughness values for different type and percentages of fibers

| Code | Depth (mm) | Span (mm) | P1* (kN) | f1* (MPa) | δ1* (mm) | PP* (kN) | fp* (MPa) | δp* (mm) | P600* (kN) | P150* (kN) | f600* (MPa) | f150* (MPa) | T150* (mm-kN) |
|---|---|---|---|---|---|---|---|---|---|---|---|---|---|
| Ref-0.21-1 | | | 19.9 | 13.7 | 0.100 | 19.9 | 13.70 | 0.100 | - | - | - | - | 1.0 |
| Ref-0.21-2 | | | 19.6 | 13.5 | 0.105 | 19.6 | 13.51 | 0.105 | - | - | - | - | 1.0 |
| PVA-0.5%-0.21-1 | | | 21.1 | 14.5 | 0.092 | 21.1 | 14.52 | 0.092 | - | - | - | - | 1.0 |
| PVA-0.5%-0.21-2 | | | 20.6 | 14.2 | 0.087 | 20.6 | 14.19 | 0.087 | - | - | - | - | 1.0 |
| steel #1-0.5%-0.21-1 | | | 20.6 | 14.49 | 0.092 | 20.6 | 14.49 | 0.092 | 17.4 | 11.3 | 11.96 | 7.78 | 32.7 |
| steel #1-0.5%-0.21-2 | | | 21.2 | 14.91 | 0.109 | 21.2 | 14.91 | 0.109 | 15.0 | 13.5 | 10.32 | 9.3 | 24.5 |
| steel #1-1%-0.21-1 | | | 22.7 | 15.97 | 0.072 | 27.8 | 19.55 | 0.616 | 23.2 | 15.4 | 16.01 | 10.61 | 38.4 |
| steel #1-1%-0.21-2 | 76.2 | 304.8 | 20.6 | 14.49 | 0.089 | 23.4 | 16.46 | 0.512 | 23.1 | 16.9 | 15.87 | 11.64 | 41.2 |
| steel #1-1.5%-0.21-1 | | | 18.9 | 13.29 | 0.082 | 22.3 | 15.65 | 0.538 | 21.0 | 13.4 | 14.49 | 9.23 | 35.5 |
| steel #1-1.5%-0.21-2 | | | 19.1 | 14.27 | 0.110 | 29.3 | 20.61 | 0.777 | 24.3 | 14.7 | 16.72 | 10.13 | 41.3 |
| steel #1-2%-0.21-1 | | | 23.5 | 16.53 | 0.086 | 41.2 | 28.98 | 1.049 | 29.6 | 16.2 | 20.35 | 11.14 | 44.6 |
| steel #1-2%-0.21-2 | | | 23.6 | 16.53 | 0.086 | 41.2 | 28.98 | 1.057 | 34.5 | 28.0 | 23.73 | 19.25 | 68.8 |
| steel #2 1.5%-0.19-1 | | | 16.3 | 11.25 | 0.108 | 19.6 | 13.51 | 0.404 | 19.2 | 14.6 | 13.21 | 10.07 | 34.8 |
| steel #2 1.5%-0.19-2 | | | 17.2 | 12.01 | 0.096 | 26.4 | 18.16 | 0.799 | 23.9 | 20.9 | 16.45 | 14.41 | 44.5 |
| steel #2 2%-0.19-1 | | | 5.72 | 4.02 | 0.066 | 26.3 | 18.13 | 0.743 | 24.4 | 18.5 | 16.83 | 12.72 | 45.1 |
| steel #2 2%-0.19-2 | | | 18.1 | 12.71 | 0.071 | 28.8 | 19.75 | 0.659 | 27.1 | 18.4 | 18.68 | 12.67 | 48.7 |

* First-peak load, P1 (kN); First-peak strength,f1 (MPa) ;First-peak deflection, δ1 (mm); Peak load , PP (kN); peak strength,fp (MPa); Peak deflection, δp (mm); L – Span length;

Residual loads, P600 (kN) – Residual load at net deflection of L/600 ;

Residual loads, P150 (kN) - Residual load at net deflection of L/150;

Residual strengths, f600 (MPa) - Residual strength at net deflection of L/600 ;

Residual strengths, f150 (MPa) - Residual strength at net deflection of L/150;

Toughnes,T150 (mm-kN) – Area under load vs. net deflection curve between 0 to L/150.

## 3.4 Optimazation of fiber-reinforced UHPC mix design

The stated goal of the UHPC materials characterization study is to determine the basic behaviors of UHPC with the intent of using UHPC in permanent formworks for bridge columns or walls. Many material behaviors are critical to the successful use of concrete in construction of the prefabricated panels to be used for permanent formwork. These behaviors include strength, durability, and long-term stability, which will be discussed in this section.

The curing applied to UHPC plays a critical factor. In most cases, standard steam treatment is applied to enhance performance of UHPC. However, water curing was used in this research instead of steam curing to evaluate the ability of producing UHPC. The material behavior obtained in this study will be further evaluated in a following project using steam curing or heat curing for 1 to 3 days.

### 3.4.1 Mixture proportioning of UHPC optimization

The candidate mix designs for the optimization of UHPC were selected in section 3.2. A mixture proportioning reproducing a commercially available UHPC is used for composition. In total, four mixtures were investigated in addition to the reference mixture. Table 3.24 shows the four mixtures with optimized cementitious matrix given the results of compressive strength, packing density, flowability, and rheology. The four optimized mixtures incorporated 2% steel fiber type II and had w/cm of 0.20. The mix design of reference UHPC is also given in Table 3.24. The targeted slump flow was fixed to 280 mm ± 10 mm by adjusting the HRWR dosage. The Mix-1 G50SF5 mixture required the largest of 69.5 $l/m^3$ HRWR, while the Mix-4 FAC 60 mixture required the lowest dosage of 24.5 $l/m^3$.

Table 3.24 Optimized UHPC mixture proportioning for optimization mix designs

| | Cement kg/m³ | SF kg/m³ | FAC kg/m³ | GGBS (0-2 mm) kg/m³ | River sand (0-5 mm) kg/m³ | Masonry sand kg/m³ | Ground quartz (0-0.6 mm) kg/m³ | Fine sand (0-0.6 mm) kg/m³ | HRWR l/m³ | Water kg/m³ | Steel fibers kg/m³ |
|---|---|---|---|---|---|---|---|---|---|---|---|
| **Mix-1 G50SF5** | 548 | 41.5 | - | 548 | 708 | 310 | - | - | 69.5 | 146.0 | 156 |
| **Mix-2 G50** | 593 | - | - | 546 | 704 | 298 | - | - | 54.2 | 173.7 | 156 |
| **Mix-3 FAC40SF5** | 663 | 42.1 | 367.4 | - | 717 | 314 | - | - | 51 | 151.1 | 156 |
| **Mix-4 FAC 60** | 486 | - | 555.6 | - | 722 | 306 | - | - | 23.8 | 179.8 | 156 |
| **Reference** | 712 | 231 | - | - | - | - | 211 | 1020 | 29.2 | 188.6 | 156 |

### 3.4.2 Mixing procedure and sampling of UHPC optimization

The EIRICH mixer was employed for the evaluated of the UHPC mix designs. The mixing speed and mixing time is illustrated below:
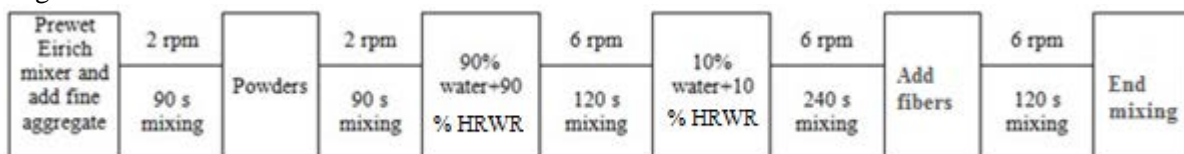


Figure 3.57 Mixing procedure of UHPC using the EIRICH mixer

As soon as mixing was completed, the casting of specimens and measurement of the fresh properties of the UHPC commenced. The casting of all specimens was completed within 20 minutes fromcompletion of mixing. All specimens were cast without any vibrating. In prism specimens for flexural and freeze-thaw tests, the UHPC was placed from one end of a chute and allowed to flow to the end of the molds to complete the filling of the molds, as was described in section 3.3 (Figure 3.37). The demolding of specimens was operated approximately 24 hours.

### 3.4.3 Fresh properties

Table 3.25 summarizes the results of the fresh material determind 5 mixtures after the end of casting. All mixtures were very fluid, stable, and appeared to self-consolidate. The mini-slump was $280 \pm 10$ mm. The SCMs type and content of mixtures were differed, whereas the agg/cm was the same. The mini-V funnel flow time varied from 12 to 46 seconds. The Mix-1, Mix-2, and Mix-3 mixtures were all acceptable, and results in homogeneous flow of the fibrous material, which was observed.

The air contents are given in Table 3.25. In the future study, the air reduced admixture can be introduced to reduce the air content.

An undesirable increase in air content can alter the fresh and hardened properties. Decreasing the air content can improve microstructure and will lead to greater strength. In this study, air was entrapped during the high shear mixing. Some air was released from the cast specimens with time. Further testing on hardened air content should be done to confirm this observation. Given viscosity of the mixtures are too high, the entrapped air may not easily escape from the fresh concrete.

Table 3.25 Test results: 5 mixtures in the fresh state

| | Unit weight | Air content (%) | Mini-slump value (mm) | Flow time (s) | Temperature at 10 min. (ºC) | Temperature at 40 min. (ºC) | Temperature at 70 min. (ºC) | Bleeding |
|---|---|---|---|---|---|---|---|---|
| **Reference** | 2.47 | 4.7 | 280 | 12 | 23 | 19 | 19 | Non |
| **Mix-1 G50SF5** | 2.45 | 5.0 | 270 | 37 | 24 | 23 | 22 | Non |
| **Mix-2G50** | 2.43 | 5.6 | 270 | 46 | 25 | 22 | 21 | Non |
| **Mix-3 FAC40SF5** | 2.44 | 4.5 | 280 | 39 | 21 | 19 | 19 | Non |
| **Mix-4 FAC60** | 2.41 | 3.5 | 270 | 30 | 20 | 19 | 19 | Non |

The rheological properties presented in Table 3.26, include the reference, FAC40SF5, and G50 SF5 mixtures only; G50 and FAC60 mixtures could not be tested given their highly cohesive nature. After performing the test with the viscometer it was checked whether equilibrium was obtained for at least one third of all data points. An analysis indicated that the steady state was achieved for all mixtures at the four lowest rotation speeds. These four points were used to calculate the yield value and the viscosity according to the "Modified-Bingham model" ($R^2$ was greater than 0.98 in all cases).

Table 3.26 Summary of rheology properties

| | Spread value (mm) | Yield value at 20 min (Pa) | Yield value at 40 min (Pa) | Yield value at 60 min (Pa) | Flow time (s) | Viscosity at 20 min (Pa·s) | Viscosity at 40 min (Pa·s) | Viscosity at 60 min (Pa·s) |
|---|---|---|---|---|---|---|---|---|
| **Reference** | 280 | 36 | 54 | 72 | 12 | 17 | 28 | 35 |
| **G50SF5** | 270 | 39 | 48 | 57 | 37 | 39 | 51 | 61 |
| **FAC40SF5** | 280 | 39 | 55 | 58 | 39 | 44 | 88 | 115 |

As shown in Table 3.26, the yield stress varied from 36 to 39 Pa. The mini-V funnel flow time at 20 minutes

increased with the increasing of viscosity.

## 3.4.4 Mechanical properties

The results of the mechanical properties of the investigated mixtures are discussed below.

**Compressive strength**

The compressive strength results of the five UHPC mixtures are presented in Table 3.27. The average 28-day compression strength of UHPC of the reference mixture was 135 MPa, which is maximum strength among the five mixtures. The Mix-4 FAC60 mixture is of the minimum strength which is 107 MPa.

These results, although quite high for concrete, are likely lower than would normally be observed with UHPC. Two factors that could influence the compressive strength are the environment that UHPC is kept in before any steam-based treatment and the steaming environmental conditions. It is well known that the reference mixture can achieve 200 MPa where subjected to steam curing at early age for 2 days.

Table. 3.27 Compressive strength test results

| | 1-day compressive strength (MPa) | C.O.V. (%)* | 28-day compressive strength (MPa) | C.O.V. (%)* |
|---|---|---|---|---|
| **Reference** | 53 | 9 | 135 | 2 |
| **Mix-1 G50SF5** | 52 | 10 | 125 | 2 |
| **Mix-2 G50** | 64 | 8 | 124 | 3 |
| **Mix-3 FAC40SF5** | 65 | 7 | 124 | 2 |
| **Mix-4 FAC60** | 69 | 5 | 107 | 2 |

*C.O.V .stands for coefficient of variation

With the exception of the G50SF5 mixture, the early strength (1-day compressive strength) for the other UHPC mixes was more than 10 MPa (22%) higher than the reference mixture (Figure 3.58). For 28-day compressive strength, the reference mixure had the highest value. However, the optimized mixture prepared with conventional concrete or masonry sands that is more cost-effective than that prepared with the quartz sands. The use of the finer quartz sand led to approximately 10% greater 28-day strength compared with Mix-1 to Mix-3 mixture, given changes in the micro-structure of the material, including that of the interfacial transition zone with the sand. The lowest strength corresponds to the FAC60 mixture, which had approximately 20% lower strength than that of the reference mixture.
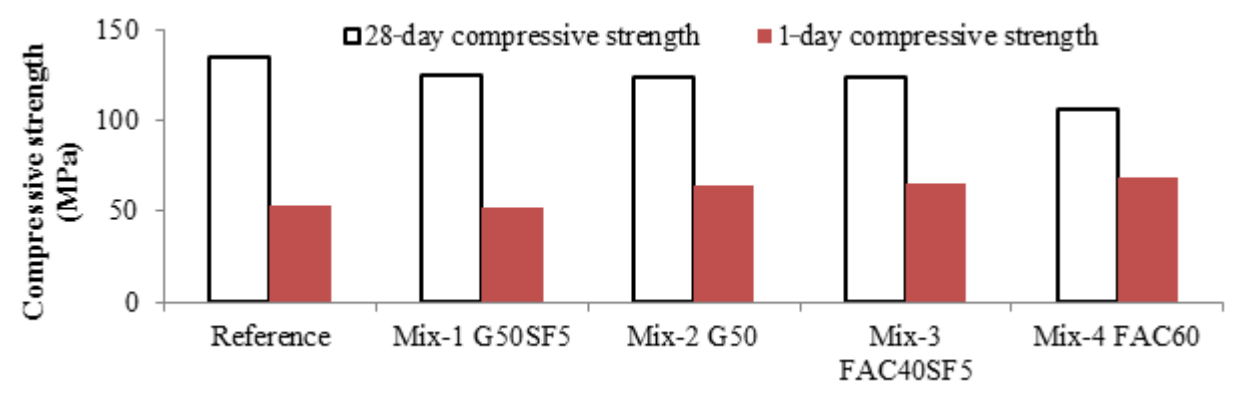


Figure 3.58 Comparsion of compressive strength results

**Splitting tensile strength**

The splitting tensile strength testing was carried out on cylindrical specimens of 100 mm diameter by 200 mm height at 28-days. The specimens were tested using a universal testing machine (UTM) of 1000 kN capacity. For each mix, three cylinders were tested at the age of 28-days and the mean value of the recorded data using equation 3.2 was reported:

Splitting tensile strength (ft) $= \frac{2P}{\pi DL}$ 　　　　　　　　　　　Equation (3.2)

Where, P= applied load; D = diameter of the specimen; L = length of the specimen

The results of the splitting tensile tests are shown in Table 3.28. There is a good enhancement between the Mix-1 mixture (G50SF5) and reference mixture. Mix-1, Mix-2, and Mix-4 mixture did not show good behavior in splitting tensile, especially Mix-4 mixture which had just 10 MPa of splitting tensile strength.

Table 3.28 Summary of splitting tensile strength

|  | Splitting tensile peak load (kN) | Splitting tensile strength (MPa) | C.O.V. (%) |
|---|---|---|---|
| **Reference** | 389.6 | 12 | 1 |
| **Mix-1 G50SF5** | 454.9 | 14 | 3 |
| **Mix-2 G50** | 331.1 | 11 | 1 |
| **Mix-3 FAC40SF5** | 389.2 | 12 | 2 |
| **Mix-4 FAC60** | 306.8 | 10 | 2 |

The tensile-to-compressivestrength values at 28-day are presented in Table 3.29. The strength ratio ranged from 8.5% to 11.4%, which is similar to published work (Grabeal, 2014).

Table 3.29 Splitting tensile strength normalized by 28-day compressive strength

|  | 28-day splitting tensile strength (MPa) | 28-day compressive strength (MPa) | Splitting to compressive strength (%) |
|---|---|---|---|
| **Reference** | 12 | 135 | 9.2 |
| **Mix-1 G50SF5** | 14 | 125 | 11.4 |
| **Mix-2 G50** | 11 | 124 | 8.5 |
| **Mix-3 FAC40SF5** | 12 | 124 | 10 |
| **Mix-4 FAC60** | 10 | 107 | 9.1 |

Figure 3.59 shows the failure modes of splitting tensile tests for each UHPC mixtures. It can be observed that the cracks at the failure were different for mixtures. The mixture with the highest splitting tensile strength, G50SF5, had a phenomenon of multiple cracking, compared to a major crack. This may due to the different bond strength between fibers and concrete matrix. Futher studies will be implemented to figure out the reason.



| (a) G50 | (b) G50SF5 | (c) FAC40SF5 | (d) FAC 60 |
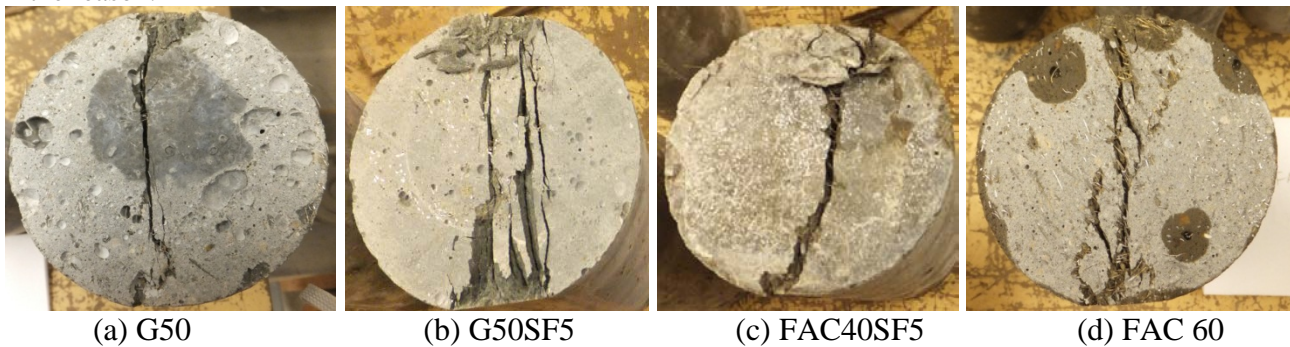
Figure 3.59 Failure mode of splitting tensile test for Mix-1 to Mix-4 mixtures

**Modulus of elasticity**

The modulus of elasticity was measured in compression in accordance with ASTM C469 at the age of 28-days. Reported values were the average value of three cylinders curing in lime-saturated water until the day of testing.

The test set-up included the specially designed axial deformation measuring device shown in Figure 3.60. The two parallel rings were both rigidly attached to the cylinder with a 50 mm gage length between attachment points. The upper ring holds three linear variable displacement transducers (LVDTs) whose ends bear on the lower ring. Thus, the axial deformation of the cylinder can be measured accurately from initiation of loading through 40% of the ultimate load.



Figure 3.60 Modulus ring attachment during testing

The modulus of elasticity results for the five mixtures is given in Table 3.60. The modulus of elasticity was calculated based on the average LVDT-based deformation measurements and the load reading. A best-fit linear approximation of the stress-strain results of each individual cylinder was used. The maximum modulus of elasticity is of the reference mixture, which is 52.7 GPa, while the minimum modulus of elasticity is of the FAC60 mixture, which is only 45.8 GPa. As for design of thin structural element, in this research, high modulus of elasticity is preferred.

Table. 3.30 Modulus of elasticity for each mixture at 28-day

|  | 28-day Modus of Elasticity (GPa) | C.O.V. (%) |
|---|---|---|
| **Reference** | 52.7 | 4 |
| **Mix-1 G50SF5** | 50.1 | 2 |
| **Mix-2 G50** | 49.5 | 3 |
| **Mix-3 FAC40SF5** | 51.6 | 2 |
| **Mix-4 FAC60** | 45.8 | 2 |

**Flexural properties**

The four point bending test was carried out in section 3.3, to evaluate flexural strength, Figures 3.61 to 3.65 present the load-deflection results for the different UHPC mixtures. All of mixtures developed good

ductility and high tensile strength. For most of the specimens, when the deflection was closed to 2 mm, the strength was as much as or more than 80% of the ultimate strength. Table 3.31 summarizes the crictial parameters of the flexural strength testing.

The actual tensile cracking strength of concrete is overestimated by the tensile cracking strength results of a small-scale flexural test. The overestimation is usually caused by the depth and strain gradient effects on the flexural cross section. The UHPC ahead of the crack front tends to microcrack, thus reducing stress concentrations (Chanvillard and Rigaud, 2003). The first crack tensile strength results, as modified by a correction factor, are provided in Table 3.31. Theresults related to peak load carried by each set of prisms are also given. The peak load values varied between 120% and 160% of the first cracking load. The equivalent flexural strength corresponding with the peak load is given.
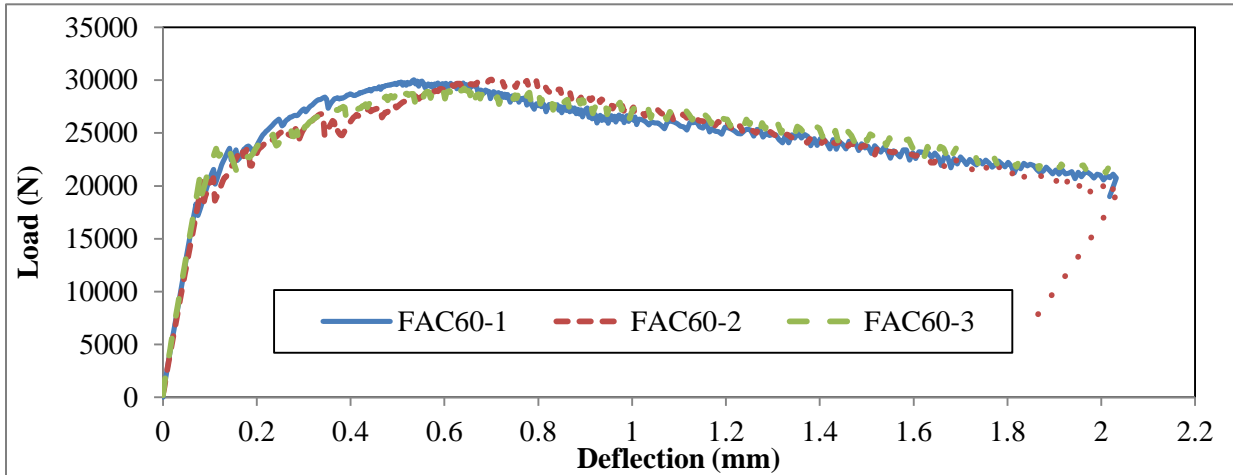


Figure 3.61 Load-deflection results of the FAC60 mixture
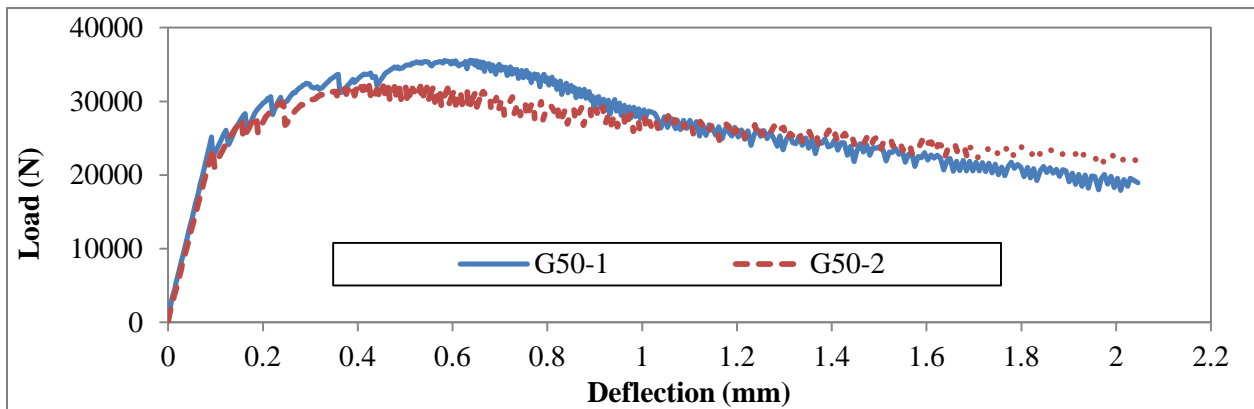


Figure 3.62 Load-deflection results of the G50 mixture
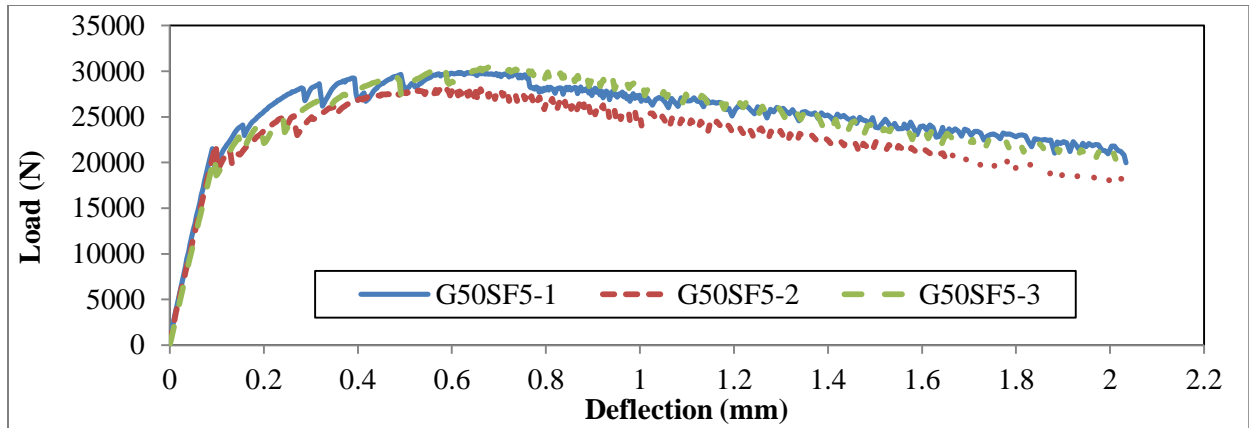
Figure 3.63 Load-deflection results of the G50SF5 mixture
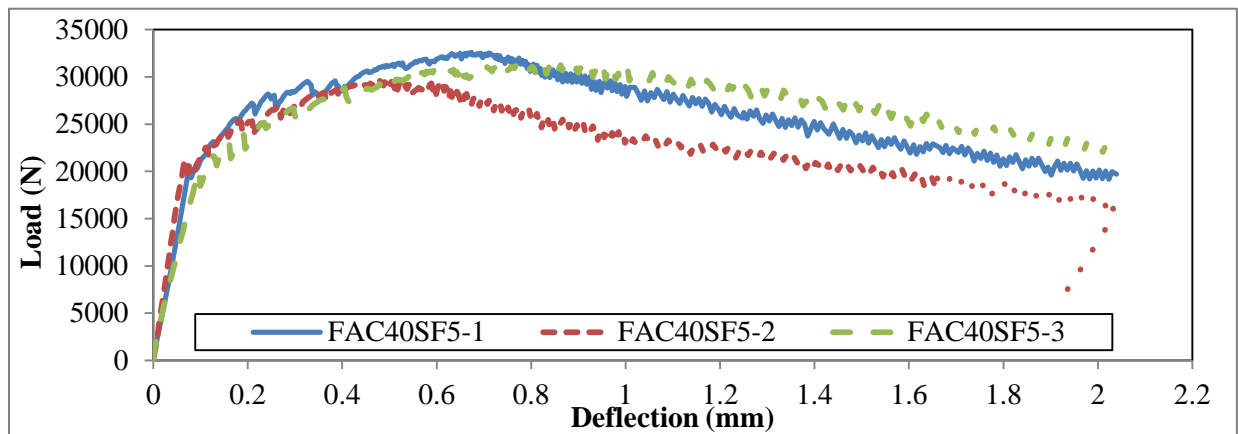


Figure 3.64 Load-deflection results of the FAC40SF5 mixture
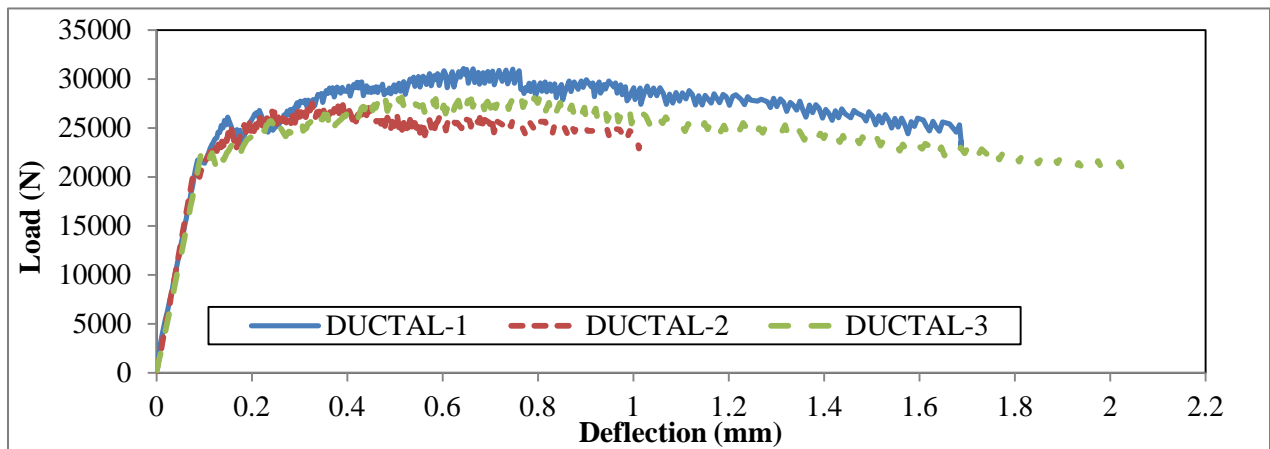


Figure 3.65 Load-deflection results of the reference mixture

Figures 3.66 and 3.67 compare the first cracking and peak load deflection, respectively. The results presented in Table 3.31. The analysis data was averaged by three specimens for each mix. The mixture with 50% GGBS performed well at the first cracking and showed higher first cracking than the other mixtures. However, for the peak load deflection corresponding to the maximum load, the mixtures containing fly ash (FAC 60 and FAC40SF5) performed better. Note that the peak load deflection for the FAC40SF5 mixture can be as much as 0.68 mm, which was 23% higher than that of the reference mixture.
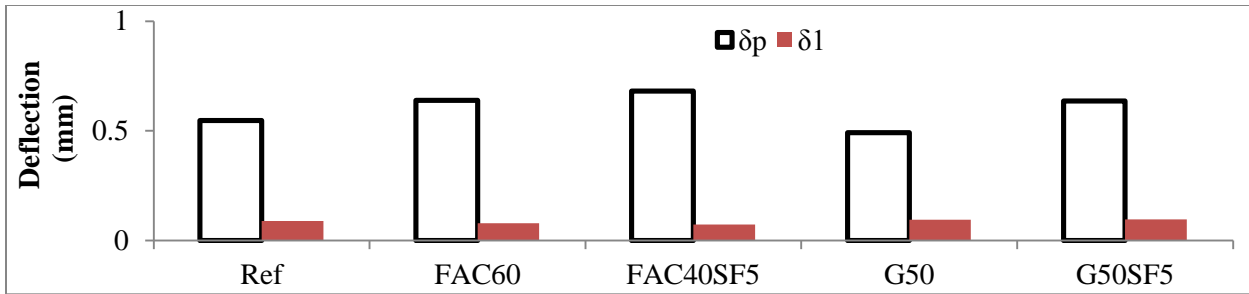
Figure 3.66 Comparison of first cracking and peak load deflection

From Figure 3.67, the peak strength for each mixture was clearly compared. For the first crack strength, which is related to the UHPC matrix strength itself, the G50 mixture showed slightly higher value. At the same time, the G50 mixture also showed the the highest flexural strength. All the specimens showed good performance at the point of flexural strength (peak strength); the best selection was not distinguished. In general, the maximum flexural strength is of Mix-2 G50 mixture, 22.8 MPa, while the minimum flextural strength is 19.7 MPa which is for reference mixture. For all of the mixtures, in fact, the flexural strengths are closed to 20 MPa.
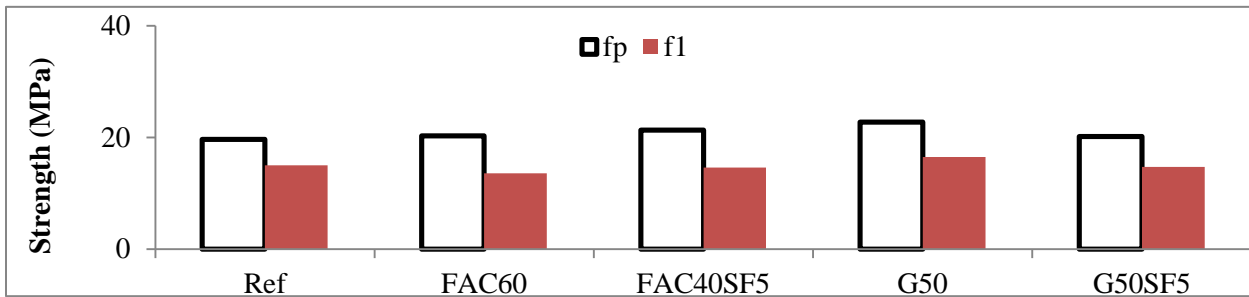


Figure 3.67 Comparison of peak strength and first cracking strength

T 150 toughness values show that the highest value was obtained for the G50 mixture (51.53 mm-kN), which was 34% higher than that of the reference mixture (38.43 mm-kN). The lowest value of T 150 was obtained for the reference mixture, which is 45 kN-mm. The results show that with high volume of SCMs (50% slag and higher than 40% fly ash), the flexural performance can be improved compared with the commercial reference mixture which was replaced with 25% silica fume by mass (the toughness increased by around 15%).

Table 3.31 – Toughness value for different UHPC mixtures

| Code | Depth (mm) | Span (mm) | P1 (kN) | f1 (MPa) | δ1 (mm) | PP (kN) | fp (MPa) | δp (mm) | P600 (kN) | P150 (kN) | f600 (MPa) | f150 (MPa) | T150 (mm-kN) |
|---|---|---|---|---|---|---|---|---|---|---|---|---|---|
| Ref-1 | | | 21.7 | 14.9 | 0.089 | 30.4 | 21.0 | 0.735 | 28.8 | 19.6 | 19.9 | 13.5 | 43.7 |
| Ref-2 | | | 21.1 | 14.6 | 0.082 | 27.4 | 18.9 | 0.393 | 24.5 | 20.0 | 16.9 | 13.7 | 23.6 |
| Ref-3 | | | 22.7 | 15.7 | 0.095 | 27.9 | 19.2 | 0.515 | 27.7 | 19.7 | 19.0 | 13.6 | 48.0 |
| FAC60-1 | | | 18.1 | 12.5 | 0.071 | 29.8 | 20.5 | 0.554 | 29.5 | 20.2 | 20.3 | 13.9 | 49.6 |
| FAC60-2 | | | 20.3 | 14.0 | 0.085 | 29.7 | 20.4 | 0.701 | 27.3 | 19.6 | 18.8 | 13.5 | 48.8 |
| FAC60-3 | | | 20.9 | 14.4 | 0.080 | 29.1 | 20.0 | 0.662 | 28.1 | 21.0 | 19.4 | 14.5 | 49.9 |
| FAC40SF5-1 | | | 20.5 | 14.1 | 0.080 | 32.4 | 22.3 | 0.712 | 31.1 | 19.8 | 21.4 | 13.6 | 51.6 |
| FAC40SF5-2 | | | 21.6 | 14.9 | 0.069 | 29.4 | 20.2 | 0.510 | 29.1 | 15.2 | 20.1 | 10.5 | 45.6 |
| FAC40SF5-3 | | | 21.6 | 14.9 | 0.069 | 31.2 | 21.5 | 0.820 | 29.5 | 21.8 | 20.3 | 15.0 | 53.3 |
| G50-1 | | | 25.4 | 17.5 | 0.093 | 35.6 | 24.5 | 0.653 | 34.8 | 19.5 | 23.9 | 13.4 | 53.9 |
| G50-2 | | | 23.7 | 16.3 | 0.096 | 32.1 | 22.1 | 0.425 | 30.1 | 19.2 | 20.7 | 13.2 | 52.6 |
| G50-3 | | | 22.9 | 15.8 | 0.095 | 31.6 | 21.8 | 0.398 | 31.3 | 17.8 | 21.6 | 12.2 | 48.1 |
| G50SF5-1 | | | 21.5 | 14.8 | 0.092 | 29.7 | 20.5 | 0.638 | 27.9 | 21.0 | 19.2 | 14.4 | 50.6 |
| G50SF5-2 | 76.2 | 304.8 | 21.6 | 14.9 | 0.098 | 27.8 | 19.2 | 0.580 | 27.5 | 18.0 | 18.9 | 12.4 | 45.9 |
| G50SF5-3 | | | 20.9 | 14.4 | 0.097 | 30.3 | 20.9 | 0.690 | 28.1 | 20.5 | 19.3 | 14.2 | 49.9 |

* First-peak load, P1 (kN); First-peak strength,f1 (MPa) ;First-peak deflection, δ1 (mm); Peak load , PP (kN); peak strength,fp (MPa); Peak deflection, δp (mm); L – Span length; Residual loads, P600 (kN) – Residual load at net deflection of L/600 ;  Residual loads, P150 (kN) - Residual load at net deflection of L/150;

Residual strengths, f600 (MPa) - Residual strength at net deflection of L/600 ;

Residual strengths, f150 (MPa) - Residual strength at net deflection of L/150;

Toughnes,T150 (mm-kN) – Area under load vs. net deflection curve 0 to L/150.

## 3.4.5 Electrical resistivity

Electrical resistivity testing was performed according to ASTM C 1760, a test covers the determination of the bulk electrical conductivity of saturated specimens. The electrical resistivity provides a rapid indication of the concrete's resistance to the penetration of chloride ions by diffusion. The process is affected by several parameters, mainly the porosity and pore structure of the materials. The pores of concrete can contain water with diluted salts in it, therefore making the concrete electrically conductive. This method measures the electrical current through a saturated specimen with a potential difference of 60 V dc current maintained across the ends of the specimen. The test specimens measure 100 mm in diameter and 200 mm in length. The specimens were tested at the age of 28-days. The data are given Table 3.32 .The test results of bulk resistivity and surface resistivity of the five UHPC mixes, in average.

Table 3.32 Electrical resistivity for five mixtures

| Code | Bulk resistivity - average (KΩcm) | Surface resistivity – average (KΩcm) |
|---|---|---|
| REF | 25 | 45 |
| G50SF5 | 11 | 20 |
| G50 | 13 | 22 |
| FAC40SF5 | 11 | 19 |
| FAC60 | 15 | 28 |

Figure 3.4compares the surface resistivity and bulk resistivity results. The reference mixture had the highest electrical resistivity, and the other mixtures had similar results, which are about one twice of the value of the reference UHPC. As far as the resistance to corrosion is concerned, the lower the electrical resistance of concrete, the greater is the probability of corrosion.For the surface conductivity ($\rho_c$), Broomfield in 2011 reported that:

$\rho_c > 20$ KΩcm        low risk of corrosion rate

$\rho_c = 10$ to 20 KΩcm        low to moderate corrosion risk rate

$\rho_c = 5$ to 10 KΩcm         high corrosion risk rate

$\rho_c < 5$ KΩcm        very high corrosion risk rate.

According to this scale, all the mixtures, except for the Mix-3 FAC40SF5 mixture, can exhibit  low risk of corrosion, while the FAC40SF5 mixture can develop low to moderate risk of corrosion rate.
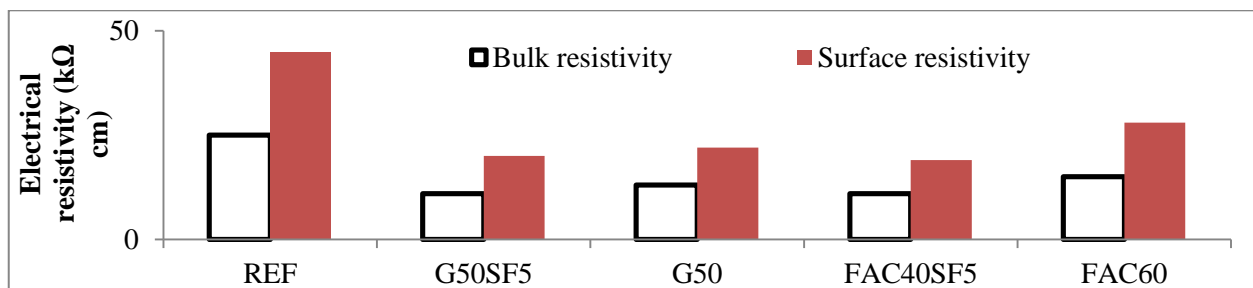


Figure 3.68 Comparison of electrical resistivity results

## 3.4.6 Shrinkage

Two types of shrinkage evaluations were determined. Drying shrinkage caused by loss of moisture from the

UHPC, and autogenous shrinkage is caused by a decrease in volume as the cementitious materials hydrate in the absence of any water loss. Autogenous shrinkage is responsible for a significant amount of the total shrinkage in UHPC. This shrinkage is dependent on the microstructure density and porosity, which are influenced by the materials in use and mixture proportioning. ASTM C 157 was employed measure drying shrinkage. The autogenous shrinkage was evaluated using ASTM C 1698.

Three prims measuring 25 ×25 ×85 mm were cast for measuring dry shrinkage. Tests were performed at the ages of 1, 2, 3, 4, 5, 6, 7, 14, 21, 28, 35, 42 and 56 days.

Two plastic tubes were cast for autogenous shrinkage (Figure 3.69 (c)) for each mixture. Autogenous shrinkage tests were carried out from the final setting that was determined for each UHPC,as well as at the age of 12 hours, 1, 2, 3, 4, 5, 6, 7, 14, 21, 28, 35, 42, and 56 days. For the autogeneous shrinkage, the maximum moisture loss at 42 days was only 0.2%. The prisms were demolded at 24 hours and immediately stored in a drying room at constant temperature of 24 ℃ and 55% RH. The maximum increase in temperature was 2 ℃. Standard ASTM C490 length change measurements were also recorded for verification purpose.



| (a) | (b) | (c) |
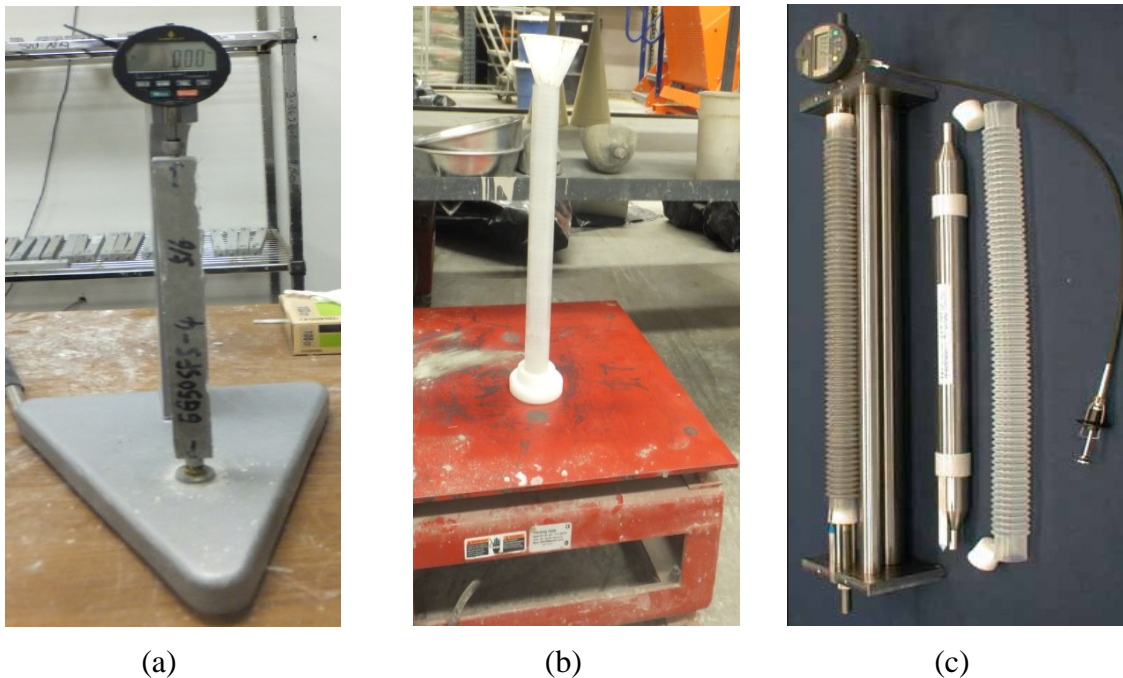
Figure 3.69 Shrinkage set-ups:
(a) set up for testing drying shrinkage; (b) vibration set up for casting autogenous tube;
(c) set up for testing autogenous shrinkage

Figure 3.70 shows the results of dry shrinkage from 1-day to 56 days. Due to heat of hydration, the dry shrinkage for reference exhibited rapidly occurring, large value, early age shrinkage. But this shrinkage dropped to a normal value at the third day after casting. The Mix-3 FAC40SF5 reached a total of 210 microstrains, which exhibited the highest drying shrinkage. The drying shrinkage of Mix-2 G50 was second highest, which was 166 microstrains. The minimum drying shrinkage is for Mix-4 FAC60 mixture, which is 144 microstrains. The total dry shrinkage for the other two mixes was close to each other, which was about 150 microstrain, and until the 56 days, the minus shrinkage around 3 microstrain was still observing.
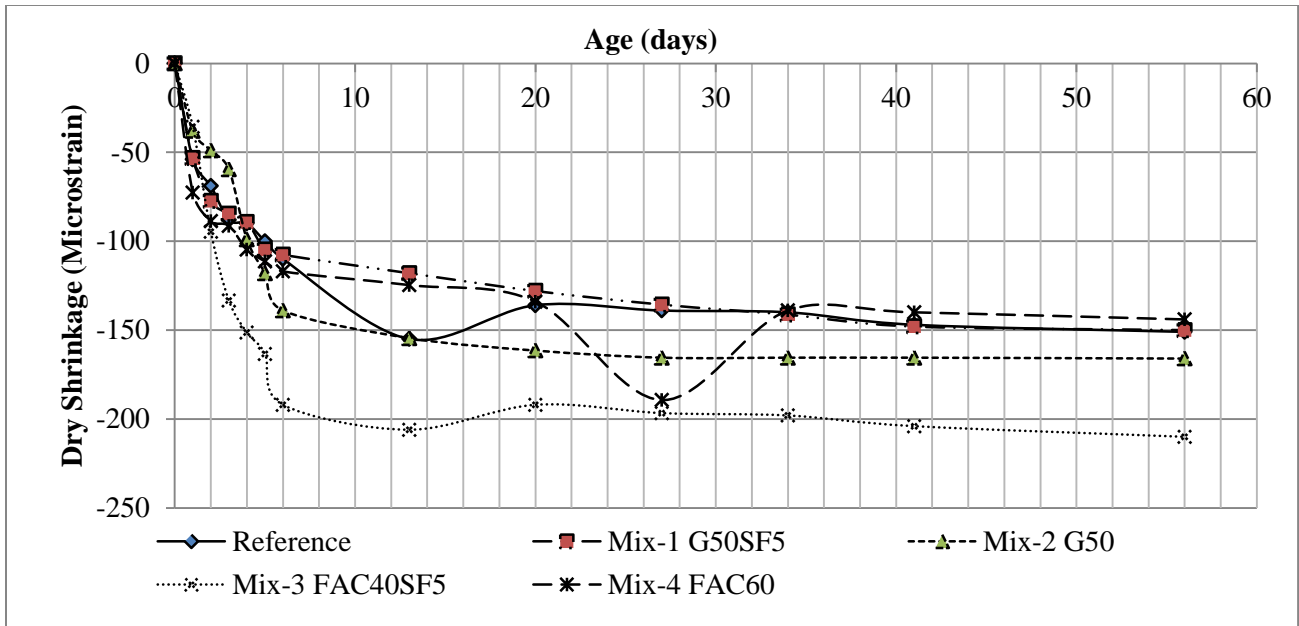
Figure 3.70 Dry shrinkage results starting at 24 hours (unsealed)

Figure 3.71 shows the results of autogenous shrinkage from final setting time to 56 days for each mix. The total autogenous shrinkage for the reference was highest, 293 microstrain. The autogenous shrinkage of Mix-2 G50 mixture is the lowest value with only 100 microstrains. This can be due higher pozolanic reactivity of slag which can produce the denser microstructure and reduce capillary porocity. The total autogenous shrinkage for the other three mixtures was close to each other, which was about 230 microstrains.

In general, the shrinkage behaviors of Mix-1 G50SF5 mixture and Mix-4 FAC 60 mixture are similar to each other. Mix-3 FAC40SF5 mixture had the highest dry shrinkage. Mix-2 G50 mixture had the lowest autogenous shrinkage.
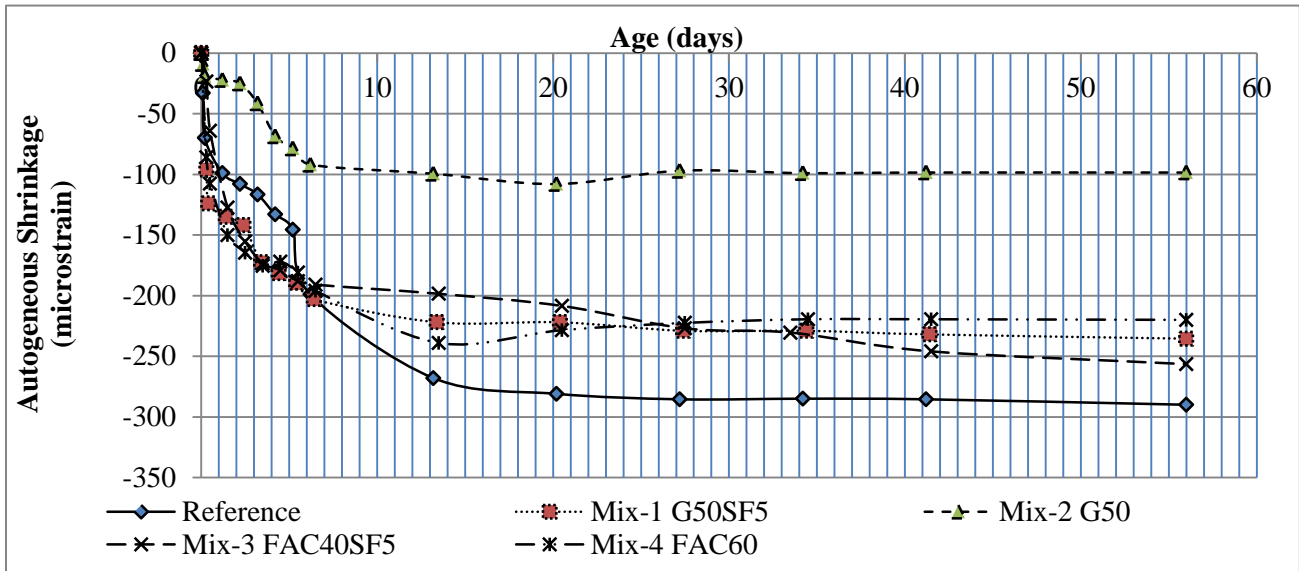


Figure 3.71 Autogenous shrinkage results starting at final setting time (sealed)

### 3.4.7 Rate of hydration at early age

The amount and kinetics of heat generated by cement hydration is an important parameter for predicting the temperature development and its distribution within a concrete member. The hydration of Portland cement is a highly exothermic chemical reaction (Neville, 1996). Usually, about one-half of the total heat of hydration is evolved between 1 and 3 days after mixing cement with water (Oluokun et al., 1990). At early-age, the rate and total heat of hydration are mainly influenced by the type, total content, and chemical composition of cement, the ambient temperature and the admixtures used (Khan, 1995). Generally, the total amount of heat liberated will depend on the pozzolanic activity and proportion of the added SCMs (Snelson et al., 2008). For example, adding silica fume can accelerate the hydration of cement, resulting in a higher rate of heat of hydration, while adding GGBS usually exhibit an opposite trend (Alshamsi, 1997).

The heat fluw generated by cement dydration was determined using small samples (about 100 grams) of UHPC. The differencesof heat of hydration between each mixture was observed. This was done using an induction calorimeter operating at a fixed temperature of 23℃.

Figure 3.72 shows the the heat flow per gram of each mixture for 40 hours of hydration. Based on the calorimetry test results, the cement hydration of different UHPC mixtures was analyzed. As expected, the substitution of cement by fly ash caused a dilution effect, due to the fact that most fly ashes are normally inert during the first few hours. The early rate peak height of G50 was the highest, while the FAC40SF5's was the lowest. Additionally, the time of reaching the main rate peak varies significantly with a change of SCM. The reference mix reached the earliest peak.  And it can be clearly noted that the dormant period for cement hydration in some samples were relatively long, such as FAC40SF5. This phenomenon should be attributed to the retarding influence of the HRWR. Due to a large amount of HRWR utilized to produce UHPC in this study, the cement hydration is significantly retarded, which can cause the poor mechanical properties of the samples at early age.
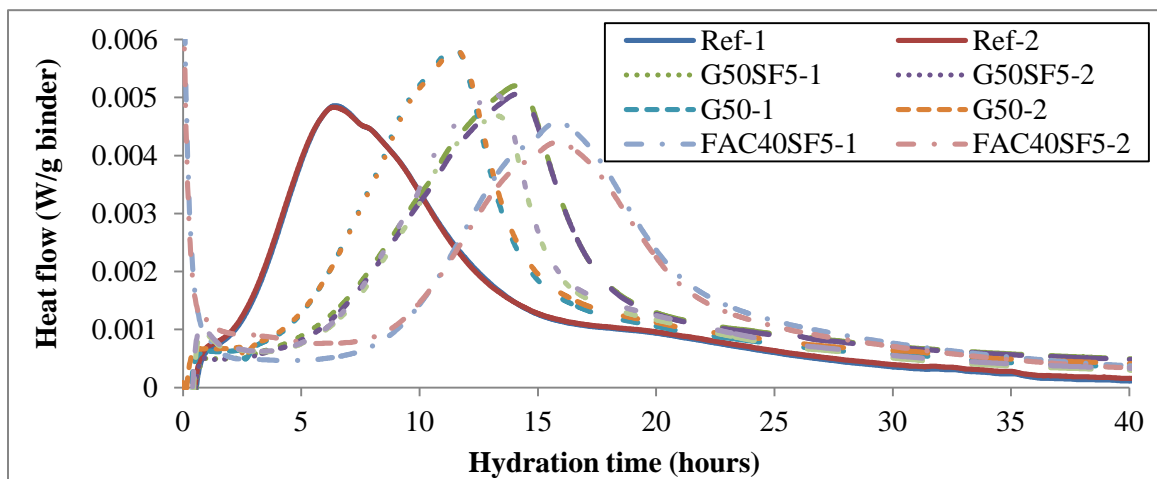


Figure 3.72 Hydration progress for five mixtures

### 3.5 Summary

UHPC is a new type of concrete that exhibits properties of enhanced strength, durability, and long-term dimensional stability. The objective of this chapter is to outline the design and evaluation of this novel material for potential use as a permanent stay-in-place formwork in aggressive environmental conditions. The following conclusions can be drawn based on the results presented in this chapter.

(1)  Using a SCM as a cement replacement can significantly improve the workability of binder.

(2)  The workability and rheological properties of cement paste and UHPC are influenced by the mixer

71

type, mixing energy, and mixing time. The mixing procedure should be adapted to provide proper dispersion. In this study, the optimized mixing involved the use of Omni and EIRICH high-shear mixers.

(3)  According to the result of the flow test, the FAC 60 mixture resulted in the lowest MWC, which corresponded to highest packing density. The mixture also exhibited the highest RWD, which corresponds to best level of robustness. From the results of the flow test, it can also be observed that for the ternary cementious composition, the G50SF5 mixture showed the lowest MWC and highest RWD.

(4)  By setting a target spread value, the HRWR demand for cementious compositions and UHPC mixes can be determined and compared.

(5)  The G50 mixture had the lowest viscosity determined using a co-axial rheometer at 20 to 90 minutes. The G50SF5 mixture also showed relatively low viscosity at of 40 min to 90 min after water addition.

(6)  A star plot method introduced in this study enable the display of multivariate data in the form of a two-dimensional chart of three or more quantitative variables. By applying this method, four cementitious compositions: G50 (powder portion of cement:GGBS of 1:1 by volume), G50SF5 (powder portion of cement: GGBS:silica fume of 0.45:0.5:0.05, by volume), FAC40SF5 (powder portion of cement:fly ash c:silica fume of 0.55:0.45:0.05, by volume), and FAC60 (powder portion of cement:FAC of 0.4:0.6, by volume), were selected as candidates of cementitious matrix to design UHPC panel product.

(7)  The intensive gyration testing was used to optimize the packing of fine aggregate.  In this study, the combination of 30% masonry sand with 70% river sand, by mass, was selected as the optimized sand combination.

(8)  Rheology testing was conducted with the ConTec Viscometer 5 to optimize agg/cm ratio, by mass. The lowest viscosity was combined with the results of flow properties and compressive strength. The optimum agg/cm ratio was determined to be 1.

(9)  The selection of fiber was based on the result of three point flexural testing. The addition of 2% of high strength steel fibers, by volume, led to a posted cracking flexural strength of 28 MPa, which is approximately twice that of concrete reinforced with 0.5% fibers. A deflection at peak load of 1.05 mm was obtained with the 2% fiber UHPC, which is more than 10 times that of the UHPC without any fibers.

(10) With high replacement volume of SCMs (50% slag and higher than 40% fly ash), the flexural performance can be improved, compared with the commercial reference mixture which was replaced with 25% silica fume by mass. The toughness increased by around 15%.

(11) No special treatment, such as heat curing, or pressure or vacuum mixing was used. Mechanical properties can be expected to enhace from some treatment, including steam curing at 80 - 90℃ for 2 - 3 days.

(12) For the optimization of UHPC mix design, a commercial product was cast for comparison purposes. According to the results, at the same w/cm, the reference was with the lowest viscosity while the UHPC matrix with 50% GGBS led to the highest viscosity. In terms of compressive strength, the reference UHPC had 135 MPa at 28-day which was the highest strength. The Mix-1 G50SF mixture achieved 125 MPa which wa 93% of the reference values. For the splitting tensile strength, the G50SF5 mixture also achieved the highest strength of 14 MPa, which is 16% higher than the reference mixture. Modulus of elasticity value for all mixtures was 45 to 53 GPa.

(13) In this study, all UHPC mixtures expect the FAC40SF5 mixture can achieve low risk of corrosion, based on electrical resistivity test results.

(14) According to drying shrinkage measurements, the G50SF5 and FAC60 mixtures are all within 150 microstrains for 56 days of testing, which performed better than the reference mixture (151 microstrain). For the autogenous shrinkage, the G50 mixture had100 microstrain of autogeneous shrinkage at 56 days, which was the lowest.

(15)  In this study, due to a large amount of HRWR utilized to produce UHPC, the hydration of cement was retarded.

(16) The final optimum mixtures will be determined by global analysis when all the durability tests, such as freeze-thaw test and water absorption are done.

# CHAPTER 4. CHARACTERIZATION OF UHPC ELEMENTS WITH EMBEDDED FRP GRIDS

UHPC elements with embedded FRP grids are tested to determine the tensile strength of individual FRP specimens, bonding strength of the interface between FRP grids and UHPC, as well as flexural strength of FRP reinforced UHPC panels.

## 4.1 Uniaxial tensile tests

Uniaxial tensile tests of three types of FRP grids were carried out to determine the tensile strength of each type of grid. The three types of grids are GFRP type I, GFRP type II, and CFRP. Table 4.1 shows the properties of the FRP grids investigated in this study.

Table 4.1 Description of FRP grids properties

| Name | Grid Size | Tensile strength (kN/m) | Modulus of elasticity (GPa) |
|------|-----------|-------------------------|------------------------------|
| GFRP type I | $25 \times 25$ mm | 45 | 72 |
| GFRP type II | $12.7 \times 12.7$ mm | 30 | 72 |
| CFRP | $46 \times 41$ mm | 97 | 234 |

### 4.1.1 Experimental setup

Single specimens were cut from the orthogonal grids and stretched by a load frame (Instron 5965), as shown in Figure 4.1. To ensure no slipping or debonding could occur at the grips, the two ends of each specimen were enhanced by steel plates that were filled with epoxy. When the epoxy hardened, the steel plates could be directly gripped by the load frame as shown in Figure 4.1 (b). The dimensions of the steel plates were $10 \times 30 \times 1$ mm. The tests conducted under displacement controlled mode, and the loading rate was set at 1 mm/min.



(a) Instron 5965                    (b) Set-up of tested specimen

Figure 4.1 Setup of the tensile tests

## 4.1.2 Test results and discussion

No debonding was observed due to the enhancement for the two ends. The break points were in between the ends of the tested specimens, as shown in Figure 4.2. A specimen of GFRP type I was broken at the middle, while a specimen of GFRP type II was broken at the bottom. The failure mode was brittle, the specimen was suddenly broken.



(a) GFRP type I       (b) GFRP type II     (c) CFRP
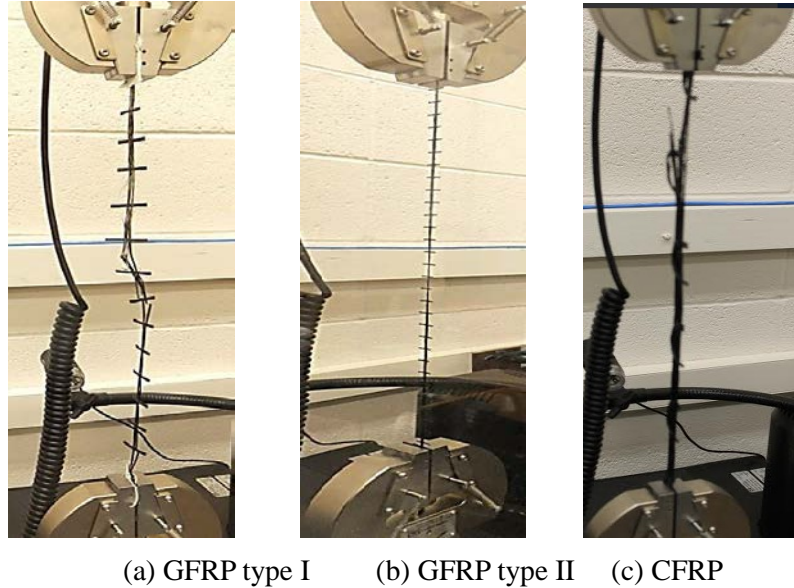
Figure 4.2 Failure mode

Given the initial length of each specimen, the force-strain relations were obtained. The relations for the two types of GFRP grids are compared in Figure 4.3. It was manifested that the GFRP type I grids demonstrated higher stiffness and tensile strength than the GFRP type II products. The curves were linear before the fracture. The slopes of the curves represent the tensile stiffness. For GFRP type I, the average slope of the three specimens was 57.6kN/ε; the average tensile strength was 1.20 N. For the GFRP type II, the average slope of the three specimens was 17.0 kN/ε; the average tensile strength was 0.24 N.
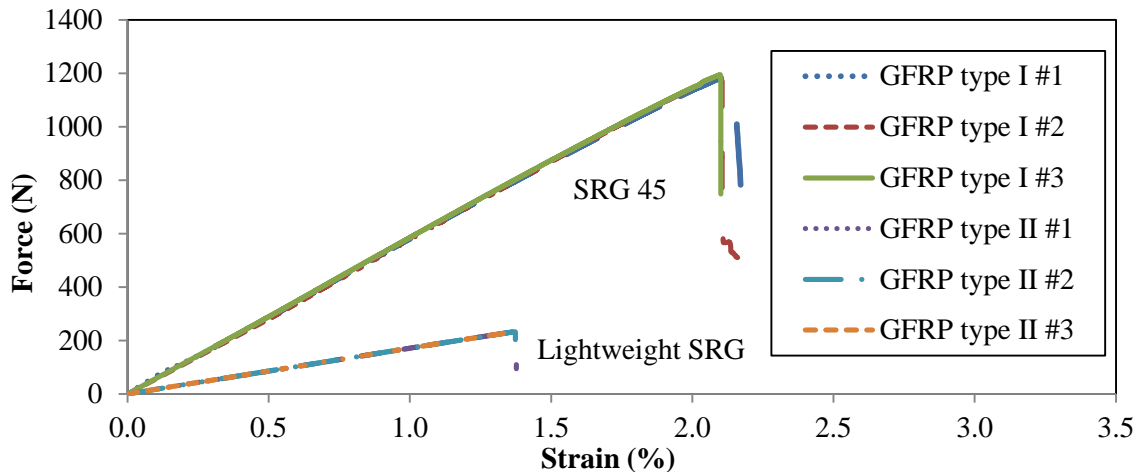


Figure 4.3 Force-strain relation of GFRP

The test results for the CFRP grids are shown in Figure 4.4 which indicates the average slope was 119.1 kN/ε and the average strength was 3.8 kN. It was manifested that the CFRP grids were of higher stiffness and strength than GFRP type I. However, the ductility of the GFRP grids was better than that of the CFRP.

75
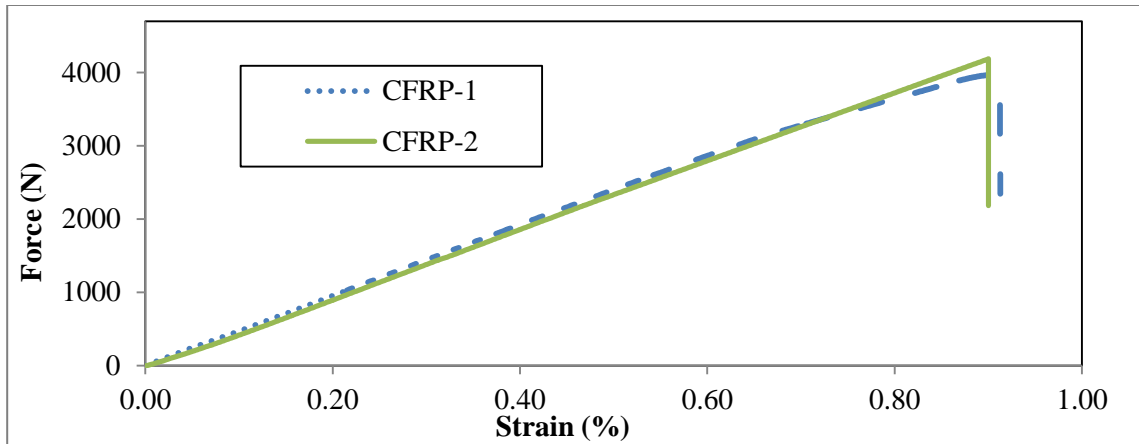
Figure 4.4 Force-strain relation of CFRP

## 4.2 Characterization of bonding conditions

In order to use FRP grids to enhance the UHPC panel performnace, there must be reliable bonding between the grids and concrete for strain transfer. To address this, the bonding condition was characterized by evaluating the strength of the cohesive interface between the FRP grids and UHPC. Pull-out tests were carried out, and the failure modes for different grid types and mixtures were observed. The effectiveness of two types of grids and four mix designs were evaluated. The optimized UHPC was used, in order to evaluate the ultimate strength and failure mode of the grid for delamination within the mortar.

### 4.2.1 Fabrication of specimens

A piece of FRP grid was installed in each brick that was of $250 \times 80 \times 120$ mm (length $\times$ thickness $\times$ height). Each piece of grid was bent into a 'U' shape. Each leg's length of the 'U' was around 400 -500 mm, of which a 25 cm portion was embedded in concrete. The thickness of the protective cover was about 8 mm. Since the stiffness of the GFRP type I is much higher than that of the GFRP type II, the GFRP type I was selected for this testing.

The four types of UHPC used in the fabrication of bricks are listed in Table 4.2.

Table 4.2 UHPC matrixes used for bonding test

|  | Cement kg/m$^3$ | SF kg/m$^3$ | FAC kg/m$^3$ | GGBS (0–2 mm) kg/m$^3$ | River sand (0–5 mm) kg/m$^3$ | Masonry sand kg/m$^3$ | HRWR l/m$^3$ | Water kg/m$^3$ | Steel fibers kg/m$^3$ |
|---|---|---|---|---|---|---|---|---|---|
| **Mix-1 G50SF5** | 548 | 41.5 | - | 548 | 708 | 310 | 69.5 | 146.0 | 156 |
| **Mix-2 G50** | 593 | - | - | 546 | 704 | 298 | 54.2 | 173.7 | 156 |
| **Mix-3 FAC40SF5** | 663 | 42.1 | 367.4 | - | 717 | 314 | 51 | 151.1 | 156 |
| **Mix-4 FAC 60** | 486 | - | 555.6 | - | 722 | 306 | 23.8 | 179.8 | 156 |

### 4.2.2 Experimental setup

A push-pull double lap test was carried out using a load frame (MTS 880, capacity: 250 kN) and a special test

rig, as indicated in Figures 4.5 and 4.6. The loading rate of this test was 1.3 mm/min (under displacement control).



Figure 4.5 Bricks with FRP grids embedded for pull-out test



(a) Testing scenario            (b) Dimensions of the setup
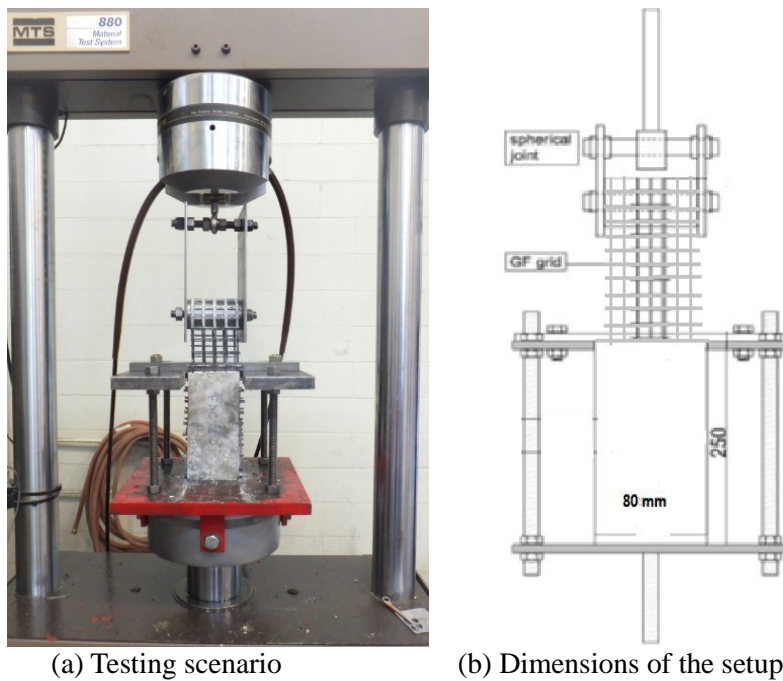
Figure 4.6 Experimental setup of debonding tests on single bricks

## 4.2.3 Test results and discussion

The specimens were loaded to failure. Force-deformation relations were obtained, as shown in Figure 4.7.

For specimens with GFRP type I, the cut-off cross section consisted of 20 specimens. Since the tensile strength of each specimen was 1.2 kN, as indicated in Figure 4.1.3, the total strength should be around 24 kN. However, the specimens were not tightly installed, so they were not stretched simultaneously. When one specimen started to be stretched, the others were still loose and free of stress. And it was observed in the testing that some specimens were loose at the onset of fracture of some specimens. Therefore, the specimens were not working together to resist the load and thus did not exhibit the expected stiffness and capacity. Two specimens

reinforced by CFRP grids were partially damaged by bending before the tests, due to the brittle nature of CFRP, as shown in Figure 4.7 (c) and (d).
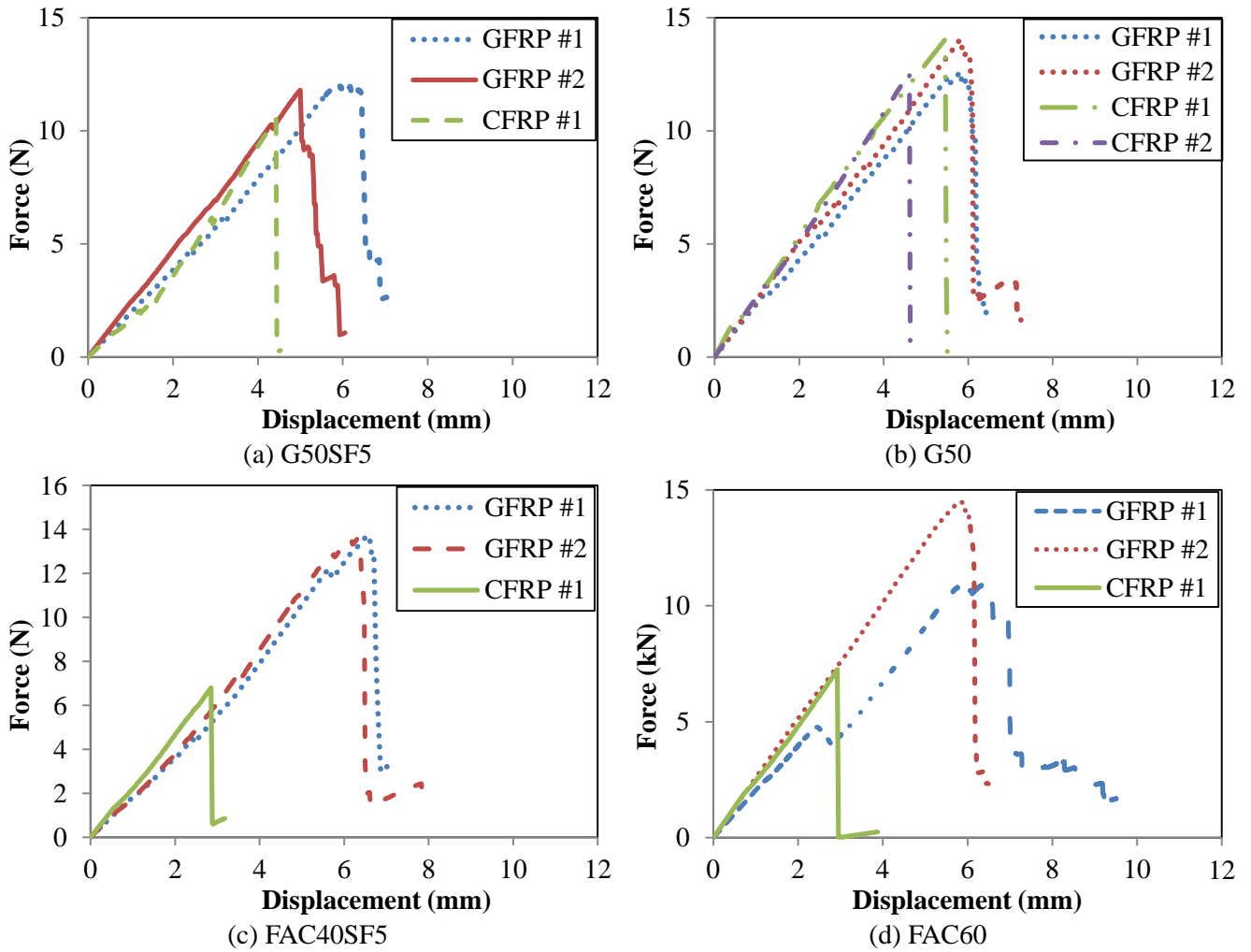


Figure 4.7 Failure mode for two layers of GFRP grids for bonding test

Even though the capacity was influenced by the fabrication method, the failure mode indicated that the bonding conditions were satisfied. The failure modes of specimens with GFRP or CFRP are shown in Figs. 4.8 and 4.9, respectively. All specimens failed due to rupture of the FRP specimens. No global slipping/debonding was observed, except for localized slipping at the break points, meaning debonding failure would not happen when the FRP grids were well embedded in UHPC.

Overall, the specimens with GFRP demonstrated progressive fracture of the specimens. Even though each GFRP fiber broke suddenly, since the specimens were not stretched to be tight simultaneously, the fibers were damaged one by one instead of at the same time. However, the CFRP grids fractured almost simultaneously and suddenly.

Figure 4.8 Failure mode of bricks with two layers of GFRP grids


Figure 4.9 Failure mode of bricks with one layer of CFRP grids

## 4.3 Flexual tests of panels

Flexural strengths of 18 panels were tested with a three-point bending test scenario. Of the eighten panels, nine panels did not contain steel fibers; the other nine panels had steel fibers. The panels were loaded to failure, and the force-deformation relations were obtained. The functions and effectiveness of steel fibers, GFRP grids, and CFRP grids were evaluated in this investigation.

### 4.3.1 Experimental setup

The experimental setup is illustrated in Figure 4.10. The tested panel was supported by two smooth steel rollers; a third roller connected to the fixture of the load frame was placed in the middle span for loading.



(a) 3D sketch          (b) Dimensions of setup
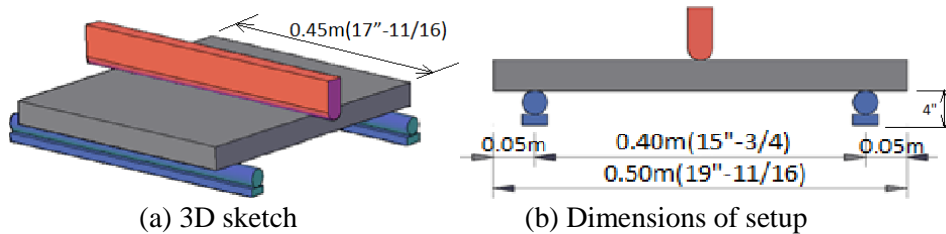
Figure 4.10 Illustration of the three-point bending scenario: (a) 3D sketch and (b) dimensions

### 4.3.2 Fabrication of panel specimens

The fabrication of the panel specimens is illustrated in Figure 4.11. The panels were cast in plywood formwork in a 'sandwich' way. The FRP grids were cut and fixed by wood specimens at the borders. The concrete was then cast into the preset cavity from the top face. To avoid swelling of the formwork due to internal pressure, the open width of the cavity was fixed to be $400 \pm 1$ mm. Figure 4.12 shows the casing of concrete in the fabrication. The panels were immersed in curing tanks for 28-days before the bending test.
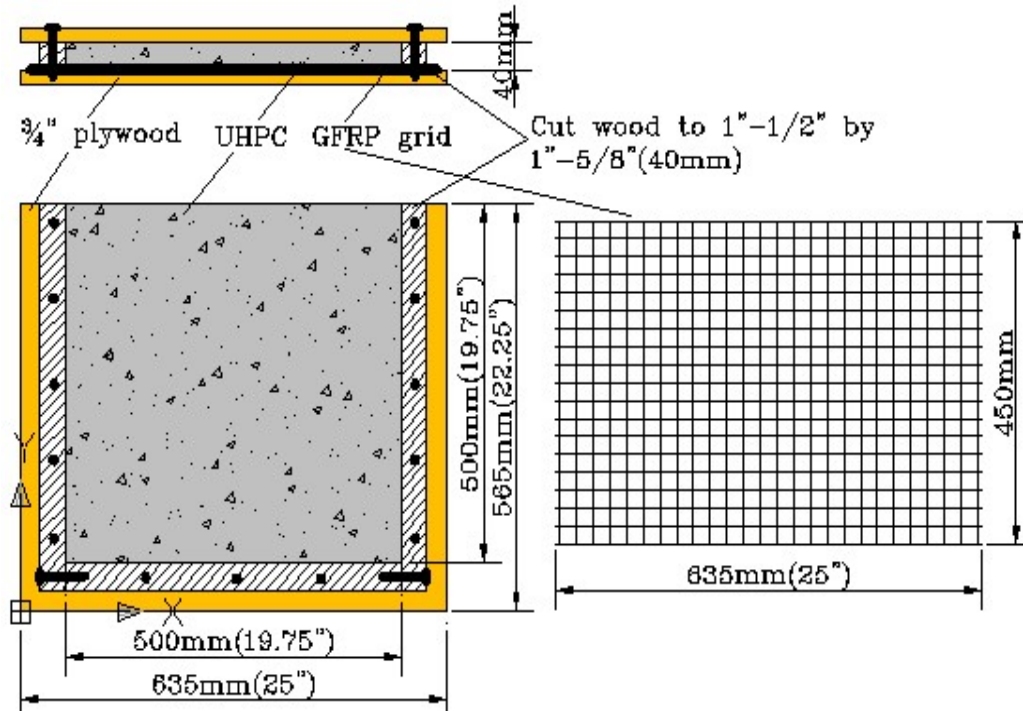


Figure 4.11 Design of the fabrication for UHPC panels reinforced by FRP grids
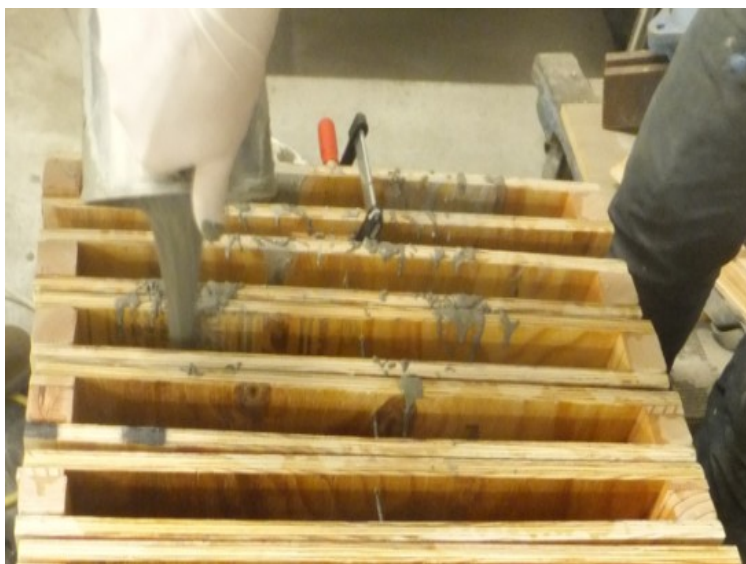


Figure 4.12 Fabrication of UHPC panels reinforced by FRP grids

### 4.3.3 Experiment matrixes

The UHPC containing 50% GGBS and 5% silica fume (by volume) was selected. The mix design of the UHPC is given in Table 4.3.

Table 4.3 UHPC matrix for three point bending test

| | Cement kg/m³ | SF kg/m³ | FAC kg/m³ | GGBS (0-2 mm) kg/m³ | River sand (0-5 mm) kg/m³ | Masonry sand kg/m³ | HRWR l/m³ | Water kg/m³ | Steel fibers kg/m³ |
|---|---|---|---|---|---|---|---|---|---|
| **Mix-1 G50SF5** | 548 | 41.5 | - | 548 | 708 | 310 | 69.5 | 146.0 | 156 |

Table 4.4 shows the three-point bending test specimens tested in this project. Two groups of tests were carried out. For the first group, the panels were made of mortars without steel fiber. In the second group, mixtures incorresponded 2% (by volume) of steel fibers. For each group, nine panels were cast and tested, including three panels without the FRP grid, three panels reinforced by GFRP grids, and three panels reinforced by CFRP grids. The three panels that did not contain any steel fiber or FRP grid were taken as the reference mixtures.

Table 4.3.2 Three-point bending test specimens

| Name | Panel Type | Amount | Description |
|---|---|---|---|
| Reference | Mortar without GFRP grid | 3 | Without fiber reinforcement |
| G-1 | Mortar with GFRP type I | 3 | |
| G-2 | Mortar with GFRP type II | 3 | |
| ST | UHPC without GFRP grid | 3 | With 2% micro-steel fibers |
| G-1-ST | UHPC with dual-layer GFRP type I | 3 | |
| C-ST | UHPC with single-layer CFRP girds | 3 | |

The codifications of specimens are listed in Table 4.5.

Table 4.5 Codification of mixtures for selection of FRP grids

| Mixture codification | | | |
|---|---|---|---|
| Reference panels | REF-1 | REF-2 | REF-3 |
| G-1 (GFRP type I) | G-1-1 | G-1-2 | G-1-3 |
| G-2 (GFRP type II) | G-2-1 | G-2-2 | G-2-3 |
| ST | ST -1 | ST -2 | ST -3 |
| G-1-ST (GFRP type I + 2% steel fibers) | G-1-ST-1 | G-1-ST-2 | G-1-ST-3 |
| C-ST (CFRP + 2% steel fibers) | C-ST-1 | C-ST-2 | C-ST-3 |

### 4.3.4 Test results

#### (1) Reference panels

The reference panel material was made of non-reinforced mortar. The panels exhibited brittle and sudden fracture failure, as shown in Figure 4.13. The panels were broken when the tensile strain at the bottom face exceeded the fracture limit at mid-span where the moment was the largest along the span. Once the cracking

was initiated, the crack developed quickly and propagated into the concrete section until collapse occurred.

The variations of load-deflection of the panel used for the reference material are shown in Figure 4.14. Fracture failure behavior was obtained. The maximum flexural load were 15.2, 17.4, and 17.6 kN. The max deflection at failure ranged between 1.0 mm and 1.5 mm.
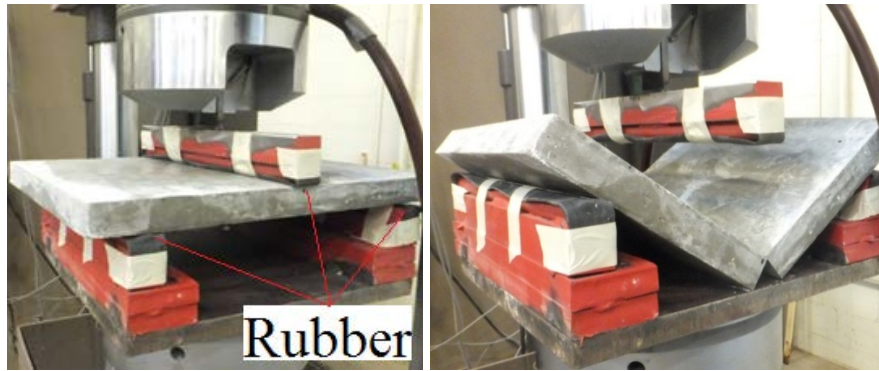


(a) Before failure          (b) After failure

Figure 4.14 Testing of reference panels
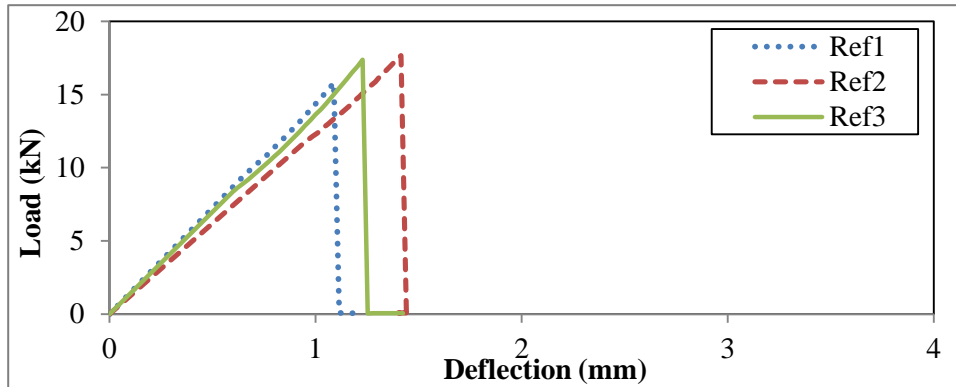


Figure 4.3.5 Force-deformation relations of panels without GFRP grid

**(2) Panels with GFRP type I grids**

Three panels that were solely reinforced by GFRP type I grids were tested. After the panels cracked, they could still stand and continue resisting load instead of sudden collapse, as shown in Figure 4.15. The panels cracked at the middle span of the bottom and the crack propagated through the panel. However, since the GFRP grids could hold the concrete, the widening of the crack was restrained, as indicated in Figure 4.16.
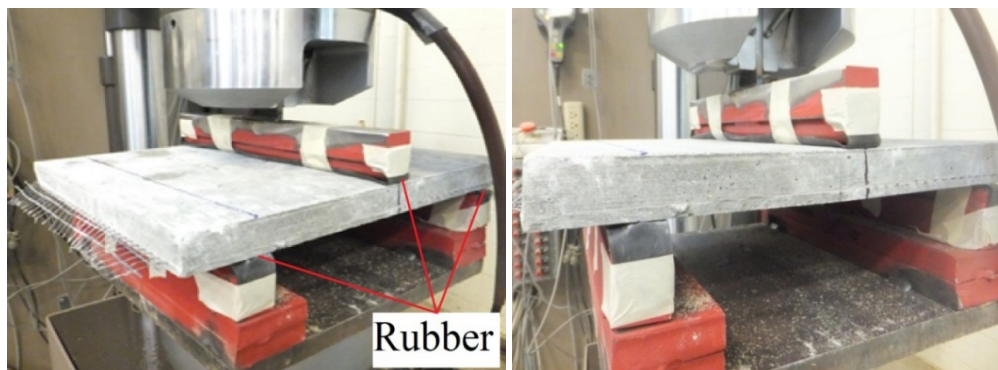


(a) Before failure          (b) After failure

Figure 4.15 Three-point bending test set-up of panels with GFRP type I grids

| (a) Onset of cracking | (b) Failure |
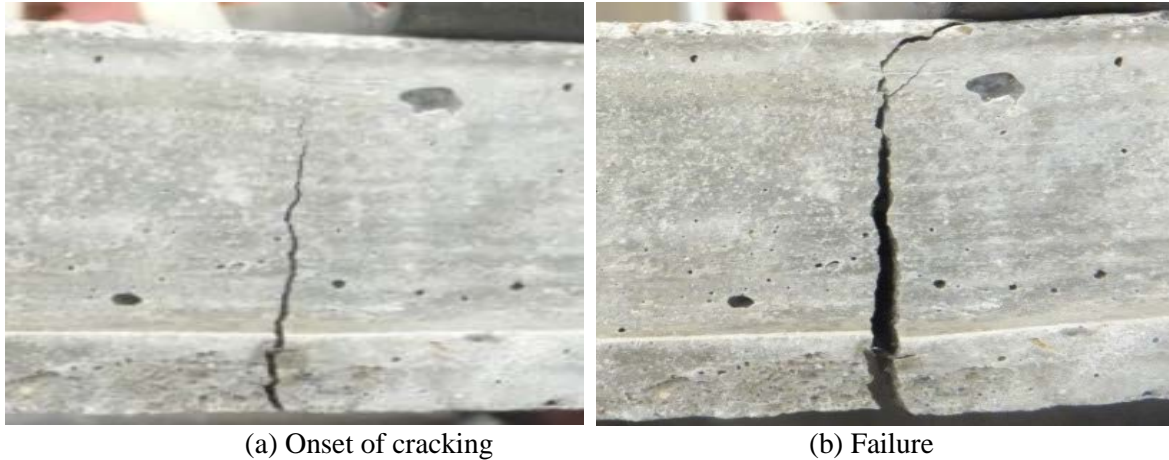
Figure 4.16 Crack propagation of panels with GFRP type I grids

The force-deformation relations are shown in Figure 4.17 where the fracture of concrete could be observed. The capacities were 14.1, 14.3, and 14.5 kN. The deflection corresponding to cracking was around 0.9 mm; however, after cracking the panels could still resist loading until deflecting of 3.5 mm, after which the test was interupted.
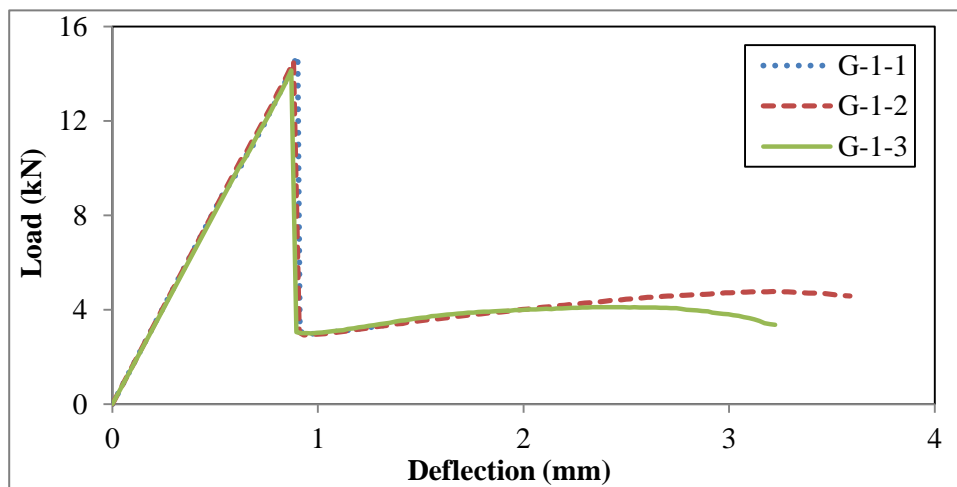


Figure 4.17 Force-deformation relations of panels with GFRP type I grid

### (3) Panels with GFRP type II grids

Three panels that were solely reinforced by GFRP type II grids were tested. After cracking, a residural strain can be observed after a sharp drop in load carrying capacity, as shown in Figure 4.18. The panels cracked at span in the the bottom section. Crack propagated through the panel. However, since the GFRP grids could hold the concrete, the widening of the crack was restrained.

The load-deflection relationship of the panels reinforced with GFRP type II grids are shown in Figure 4.19. The fracture of the concrete can be observed. The maximum flexural load were 12.2, 15.6, and 16.4 kN. The deflections corresponding to cracking were around 1.1 mm; however, after cracking the panels could still resist loads until about 3.5 mm deflection, after which the test was interupt..

Figure 4.18 Failure mode of panels with GFRP type II grids
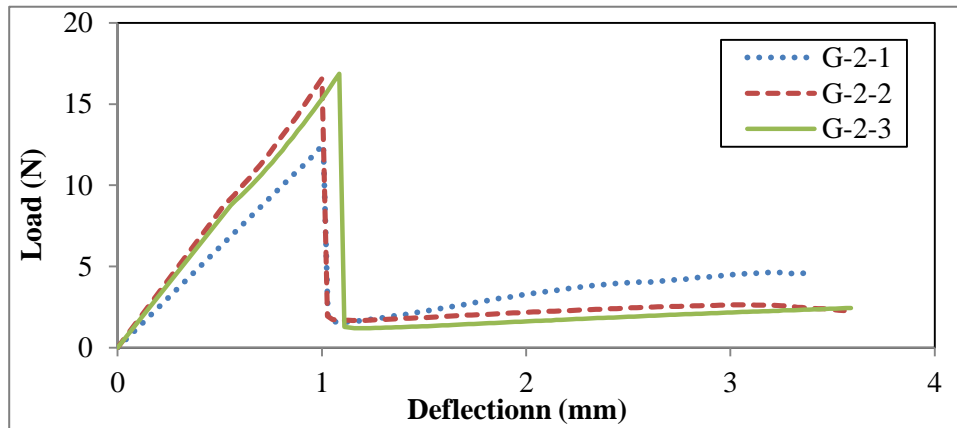

Figure 4.19 Force-deformation relations of panels with GFRP type II grids

**(4) UHPC panels with steel fiber**

Three UHPC panels reinforced by steel fibers were tested. The panels exhibited ductile failure, as shown in Figure 4.20. Multiple cracks formed at the bottom face near the mid-span. After cracks appeared, they gradually propagated through the concrete. Because the steel fibers should restrain the propagation of cracking, the panels exhibited a hardening stage after cracking, as indicated in the load-deflection relationship in Figure 4.21. After the peak load, the force dropped gradually to zero. The maximum loads were 18.2, 18.4, and 18.8 kN. The deflection corresponding to the first cracking was between 0.4 and 0.5 mm. However, the deflections corresponding to peak load ranged from 1.0 to 4.0mm. The ultimate deflection was 20 to 30 mm.


Figure 4.20 Testing of reference panels made with 2% steel microfiber
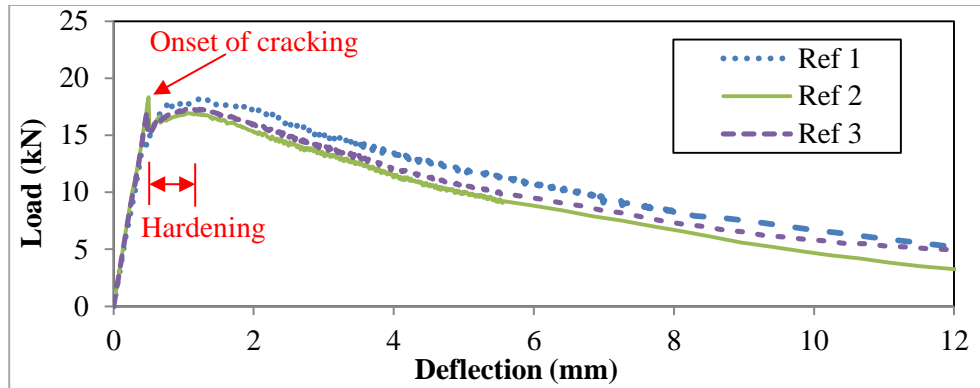
Figure 4.21 Load-deflection relationship of UHPC panels with steel fibers

**(5) UHPC panels with dual-layer GFRP type I grids**

Three UHPC panels reinforced by steel fibers and two layers of GFRP type I were tested. The panels exhibited ductile failure, as shown in Figure 4.22. Multiple cracks formed at the bottom face near the mid-span. After cracks appeared, they gradually propagated through the concrete.



(a) Before failure                    (b) After failure
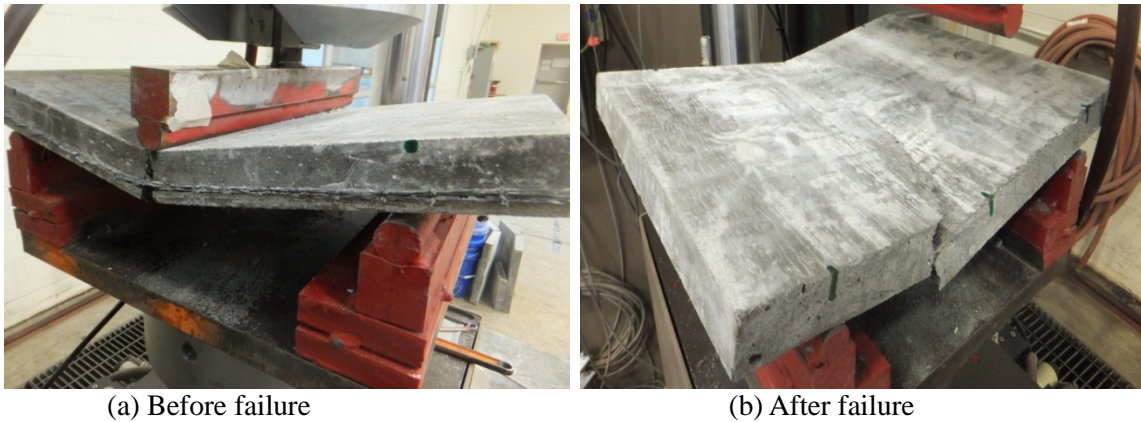
Figure 4.22 Three-point bending test set-up of UHPC panels reinforced with GFRP type I grids
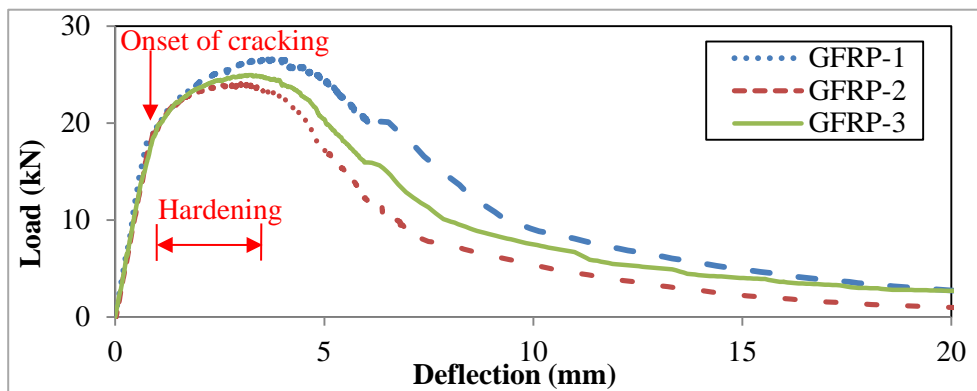


Figure 4.23 Load-deflection relationship of panels reinforced with GFRP type I grid

Since steel fibers would restrain the propagation of cracks, the panels could exhibit a hardening stage after cracking, as indicated in the load-deflection relationship in Figure 4.23. After the peak load, the flexural capacity decreased gradually. The maxium flexural load was 21.4, 24.7, and 26.5 kN. The deflections corresponding to the first cracks ranged between 0.6 to 0.8 mm. The deflection corresponding to the peak load ranged between 2.5 to 4.0 mm. The ultimate deflection was 20 to 30 mm.

85

**(6) UHPC panels with CFRP grids**

Three UHPC panels reinforced by 2% steel fibers and one layer of CFRP located at the bottom of the panel were tested. The panels exhibited ductile failure, as shown in Figure 4.24. Multiple cracks formed at the bottom face near the mid-span. After cracks appeared, they gradually propagated through the concrete.



(a)          (b)

(c)          (d)
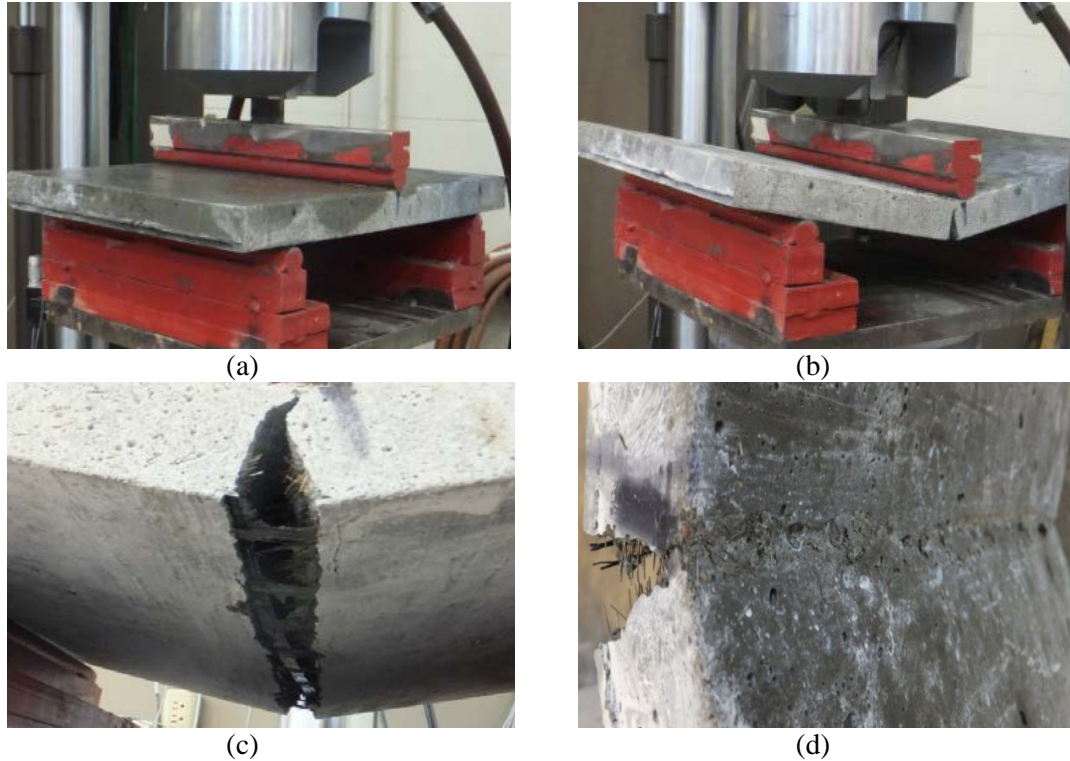
Figure 4.24 Failure mode of panels with CFRP grids

The panels exhibited a strain hardening stage after cracking, as indicated in the load-deflection relationship in Figure 4.25. After the peak load, the flexural capacity dropped gradually. The maximum loads were 21.0, 24.4, and 28.0 kN. The deflections corresponding to the first cracks ranged between 0.5 to 0.6 mm. The deflections corresponding to peak load were 2.0 to 4.0 mm. The ultimate deflection was 30 to 40 mm.
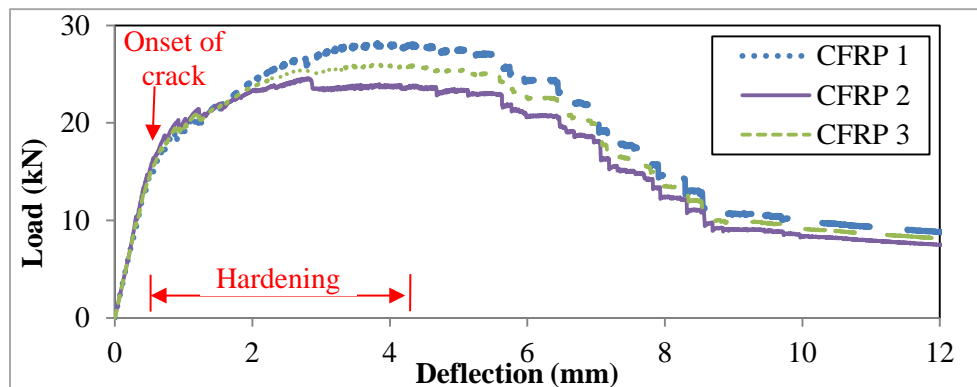


Figure 4.25 Load-deflection relationship of panels with CFRP grids

### 4.3.5 Analyses and discussions

Given the test results presented in this chapter, the function and effectiveness of different reinforcement configurations were evaluated by the comparisons of the panels' performance. Table 4.6 summarizes the main

structural characteristics of the tested panels. The capacity, deflection, and dissipated energy due to cracking are compared in Figure 4.26. The dissipated energy is related to the panel's ability to resist fracture, and is determined as the area under the load-deflection curve and the horizontal axis, and could be calculated by the numerical integration.

Table 4.6 Three-point bending test matrix

| Panel type No. | Steel fiber (volumn ratio) | Grids | Amount | Average capacity (kN) | Average deflection at peak load (mm) | Average dissipated energy (J) | Failure type |
|---|---|---|---|---|---|---|---|
| 1 | 0 | N.A. | 3 | 16.7 | 1.2 | 16.1 | Brittle |
| 2 | 0 | GFRP type I | 3 | 14.3 | 0.9 | 21.9 | Ductile |
| 3 | 0 | GFRP type II | 3 | 14.7 | 1.1 | 23.1 | Ductile |
| 4 | 2% | N.A. | 3 | 18.5 | 3.2 | 198 | Ductile |
| 5 | 2% | GFRP type I | 3 | 24.2 | 3.8 | 296 | Ductile |
| 6 | 2% | CFRP | 3 | 24.5 | 3.6 | 336 | Ductile |

In the absense of steel micro-fiber reinforcing in the mortar, once cracking initiated, it propagated quickly until collapse. Even if FRP grids were used as reinforcement, the maximum load was not significantly increased by the presence of the grid. The FRP grids could benefit concrete by improving the ductility. When concrete fractured, the grids could hold the panel pieces together, thus preventing sudden/instant collapse.

When steel fibers were incorpreated as reinforcement in the mortar, the performance of the panels was significantly improved in terms of load carrying capacity, deflection and dissipated energy. The effectiveness of the FRP grids was significantly improved given the ability of steel fibers to reduce cracks propagation and increase ductility. Interlock between the grids and fibers can benefite the panels by the full development of the grids' strength. However, the grids could not appreciably increase the cracking strain limit of concrete to postpone the onset of the cracking.

The main reason why the FRP grids could not significantly increase the stiffness, capacity, and the cracking strain limit was the tensile stiffness of the grids was relatively low compared with that of the UHPC; thus the grids could not take more tension than the concrete when they deformed together. However, when concrete cracked, the grids were stretched with much higher strain than concrete, so the grids could be beneficial after the concrete cracked.
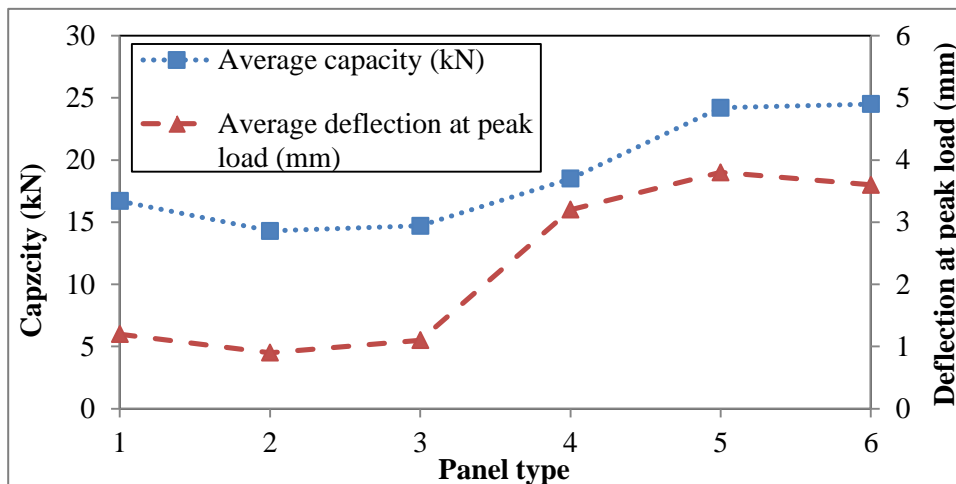


(a) Capacity and deflection corresponding to peak load
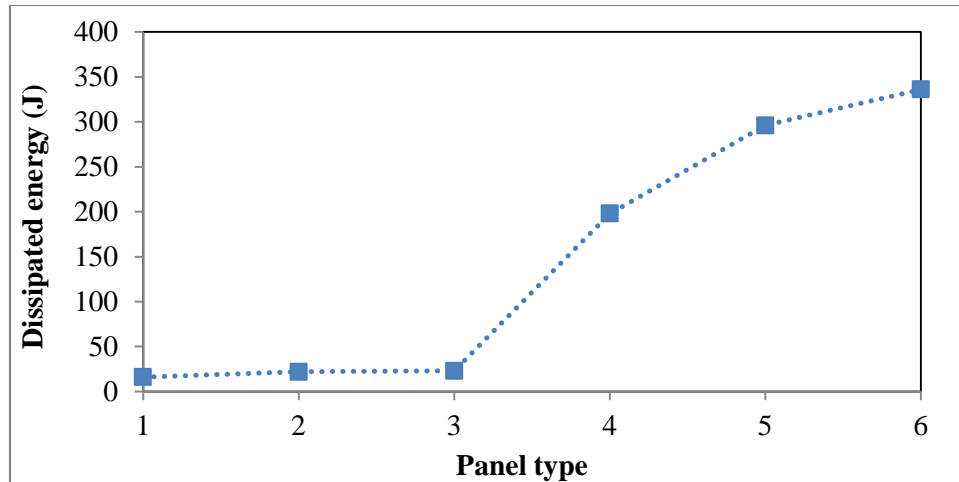
(b) Energy dissipated due to cracking

Figure 4.3.17 Comparisons of UHPC panels with various reinforcement configurations

## 4.4 Micro-structure

The micro-structure of UHPC and embedded GFRP and CFRP grids was observed. And the bonding conditions at the cohesive interfaces were evaluated. Optic microphotographs of GFRP and CFRP grids embedded in UHPC are shown in Figure 4.27 where the black specimens represent the GFRP and CFRP, respectively. Scanning electron microscope (SEM) photos are shown in Figure 4.28, demonstrating the bonding conditions of the GFRP and CFRP grids, the steel fibers, and the aggregates in the cementitious matrix.

It can be observed bond between the cementitiou paste and the various materials (sand and reinforcements) is good. There were cohesive interfaces grown surrounding the FRP grids, the steel fiber, and the fine aggregates. The thickness of the cohesive interface was at micrometer order. The interfaces transfer strain between the host matrix and the reinforcement or aggregates, and it could be damaged under loading. The bonding strength can be characterized by the strengths and distributions of the cohesive layers.



(a) 2 layers of GFRP
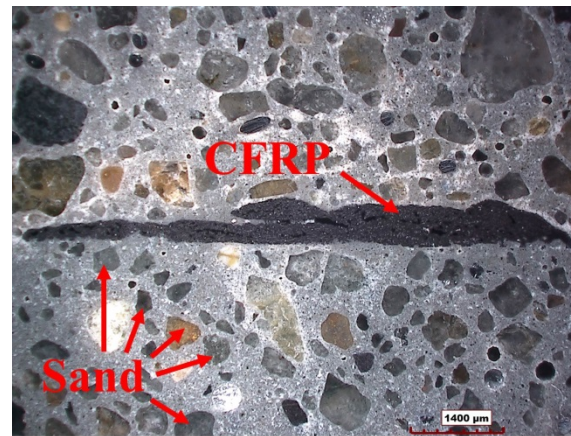
(b) Sigle layer of CFRP

Figure 4.27 Comparison of UHPC panels with 2 layers of GFRP type I and a single layer of CFRP grid

(a) GFRP

(b) CFRP

(c) Steel fiber

(d) Fine aggregates
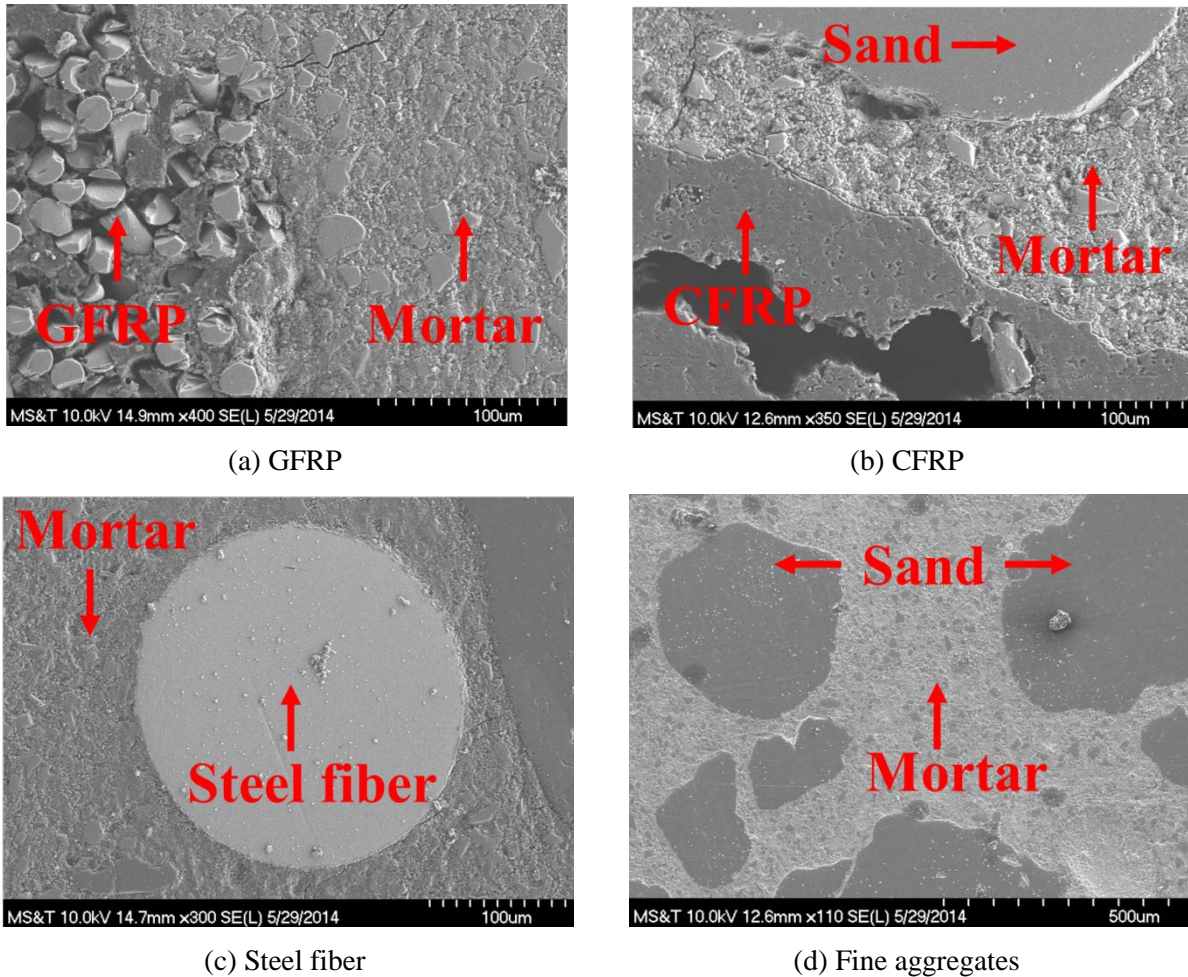
Figure 4.28 Comparison of interface between cement paste and GFRP, CFRP, steel fiber, and sand.

## 4.5 Summary

The characterizations of UHPC elements reinforced with internally installed FRP grids were evaluated. The tensile strength of individual FRP specimen, bond strength of the interface between FRP grids and UHPC, and flexural strength of FRP enhanced UHPC panels reinforced with CFRP and GFRP are also determined using three-point loading. The main findings are summarized below.

(1) Three types of FRP (GFRP type I, GFRP type II, and CFRP) grids were investigated. The strength and stiffness of individual CFRP specimens was the highest (119.1 kN/ε), which is 102% higher than that of GFRP type I; the strength and stiffness of individual GFRP type II specimens was the lowest (17.0 kN/ε); the performance of GFRP type I were in between the other types of grids (57.6 kN/ε).

(2) Bond between the FRP grid and UHPC matrix was investigated by evaluating the strength between the FRP grids and UHPC. Pull-out tests were carried out. Fracture of FRP grid was took place for the failure mode. No debonding/slipping at the interfaces was observed, meaning that the debonding would not happen when the grids are well embedded in UHPC with an embedment length of at least 250 mm.

(3) Flexural strength of panels with different reinforcement configurations was investigated. Three-point bending tests were carried out. When there was no steel fiber in the mortar, once cracking was initiated, it propagated quickly until the failure of the mortar. Even if FRP grids were used as reinforcement, the flexural capacity was not significantly increased. The FRP grids could benefit concrete by improving the ductility.

When concrete fractured, the grids could hold the panel sections, thus preventing sudden/instant collapse.

(4) When steel micro fibers were used as reinforcement in the mortar, the performance of the panels was significantly improved compared with the reference panel, in terms of flexural capacity (increased by 33%), deflection at peak load (increased by 166%), and dissipated energy was 11 times of the reference panel. The effectiveness of the FRP grids could be significantly improved by the inclusion of steel fibers that could restrain the cracking and increase the ductility. Compared panel 6 which reinforced with CFRP with panel 4, the dispatted energy is increased by 70%. Which means the interlock between the grids and fibers benefited the panels by the full development of the grids' strength. However, the grids could not appreciably increase the cracking strain limit of the UHPC to postpone the onset of the cracking according to the test results.

(5) The performance demonstrated by the dual-layer of GFRP reinforced UHPC panel was comparable to that of the single-layer CFRP reinforced UHPC panel.

# ONGOING AND FUTURE RESEARCH

The findings from this report suggest a number of potential topics for future research:

1. Develop the mixing procedures and curing methods to increase the compressive strength.
2. Develop a practical test to quantitatively determine the postcracking uniaxial tensile behavior of UHPC.
3. Fabricate the formwork panels with developed UHPC material, and test the structural responses.
4. The tests of durability such as freeze and thaw, deicing scaling and abrasion are still on going.
5. The design of stay-in-place permanent formwork using FEM is still on going.

# REFERENCES

**Aaleti, S., Sritharan, S., Bierwagen, D., and Wipf, T. (2011).** "Experimental Evaluation of Structural Behavior of Precast UHPC Waffle Bridge Deck Panels and Connections," Proceedings, Transportation Research Board Annual Meeting, Washington, DC.

**ACI 347-04. (2004). "Guide to Formwork for Concrete."** American Concrete Institute Farmington Hills, MI.

**American Concrete Institute American Concrete Institute （ACI）. (2004).** Guide test methods for fiberreinforced polymers (FRP) for reinforcing or strengthening concrete structures (ACI 440.3R–04), Detroit.

**ACI Committee 318. (2008).** "Building Code Requirements for Structural Concrete (ACI-I-08) and Commentary." American Concrete Institute (ACI), Farmington Hills, ACI Committee 355. (2007). Qualification of Post-Installed Mechanical Anchors in Concrete and Commentary (ACI 355.2-07) ." American Concrete Institute Farmington Hills, MI.

**AhlbornTM, SteinbergEP.** An Overview of UHPC Efforts through the North American Working Group. In:Proceedings of the 3rd International Symposium on UHPC and Nanotechnology for High Performance Construction Materials. Kassel, Germany: Kassel University Press GmbH. 2012.p.43-49.

**American Concrete Institute (ACI).(2002).** Guide for the design and construction of externally bonded FRP systems for strengthening concrete structures (ACI 440.2R–02), Detroit.

**American Concrete Institute (ACI).(2002).** Guide for the design and construction of concrete reinforced with FRP bars (ACI 440.1R–03), Detroit

**ASTM C109. (2012).** "Standard Test Method for Compressive Strength of Hydraulic Cement Mortars (Using 50 mmCube Specimens)", ASTM International, Volume 04.02, West Conshohocken, PA, 2012.

**ASTM C127 (2012),** "Standard Test Method for Density, Relative Density (Specific Gravity), and Absorption of Coarse Aggregate." ASTM International, PA, USA.

**ASTM C231 / C231M (2010),** "Standard Test Method for Air Content of Freshly Mixed Concrete by the Pressure Method." ASTM International, PA, USA.

**ASTM C1064 / C1064M (2012),** "Standard Test Method for Temperature of Freshly Mixed Hydraulic-Cement Concrete." ASTM International, PA, USA.

**ASTM A403 / A403M (2013),** "Standard Specification for Wrought Austenitic Stainless Steel Piping Fittings." ASTM International, PA, USA.

**ASTM C496 / C496M (2011),** "Standard Test Method for Splitting Tensile Strength of Cylindrical Concrete Specimens." ASTM International, PA, USA.

**ASTM C157 / C157M (2008),** "Standard Test Method for Length Change of Hardened Hydraulic-Cement Mortar and Concrete." ASTM International, PA, USA.

**ASTM C1698 (2009),** "Standard Test Method for Autogenous Strain of Cement Paste and Mortar." ASTM International, PA, USA.

**ASTM C1760 (2012),** "Standard Test Method for Bulk Electrical Conductivity of Hardened Concrete." ASTM International, PA, USA.

**ASTM International (2010),** "Standard Test Method for Electrical Indication of Concrete's Ability to Resist Chloride Ion Penetration," ASTM Standard C1202, West Conshohocken, PA.

**ASTM C1609-06, (2006),** Standard Test Method for Flexural Performance of Fiber-Reinforced Concrete (Using Beam with Third-Point Loading), ASTM International, PA, USA.

**ASTM International (2007).** "Standard Test Method for Flow of Hydraulic Cement Mortar," ASTM Standard C1437, West Conshohocken, PA.

**ASTM International (2010).** "Standard Test Method for Compressive Strength of Cylindrical Concrete Specimens," ASTM Standard C39, West Conshohocken, PA.

**ASTM International (2010).** "Standard Test Method for Static Modulus of Elasticity and Poisson's Ratio of Concrete in Compression," ASTM Standard C469, West Conshohocken, PA.

**ASTM C230. (2010).** "Standard Specification for Flow Table for Use in Tests of Hydraulic Cement," American Society for Testing and Materials Standard Practice C230, Philadelphia.

**Bakht, G. A., et al.(2000).** ''Canadian bridge design code provisions for fiber-reinforced structures.'' J. Compos. Constr., 3–15.

**Bakis, C. E., Nanni, A., Terosky, J. A., and Koehler, S. W. (2001).** ''Self-monitoring, pseudo-ductile, hybrid FRP reinforcement rods for concrete applications.'' Compos. Sci. Technol., 61- 67, 815–823.

**Bache HH.** Densified Cement/Ultrafine Particle-Based Materials.Second International Conference on Superplasticizers in Concrete,Ottawa, ON, Canada,1981,June 10-12.

**Bentur, A., and S. Mindess. (1990).** Fiber Reinforced Cementitious Composites. London: Elsevier.

**British Standards Institute (BSI). (1997).** ''Structural use of concrete. Code of practice for design and construction.'' BS 8110-1, London. Canadian Standards Association International (CSA). (2000). ''Canadian Highway bridge design code.'' CSA-S6-00, Toronto.

**Brühwiler, E., and Denarié, E. (2008).** "Rehabiltation of Concrete Structures Using Ultra-High Performance Fiber-Reinforced Concrete," Proceedings, The Second International Symposium on Ultra-High Performance Concrete, Kassel, Germany.

**Birchall JD, Howard AJ, Kendall K.** Flexural strength and porosity of cements. Nature1981;289(5796):388-390.

**Bjorn Taljsten and Thomas Blanksvard,(2007).** "Mineral-Based Bonding of Carbon FRP to Strengthen Concrete Structures", Journal of Composites for Construction, Vol.11, No. 2.

**Blaise, P.Y. and Couture, M.** "Precast, Prestressed Pedestrian Bridge—World's First Reactive Powder Concrete Structure," PCI Journal, Vol. 44, No. 5, September/October 1999, pp. 60–71.

**Buck JJ, McDowell DL, Zhou M.** Effect of microstructure on load-carrying and energy-dissipation capacities of UHPC. Cem Concr Res2013;43: 34-50.

**Cao Q. (2007).** "Development of pseudo-ductile permanent formwork with glass fiber reinforced plastics reinforcements." M.Phil. thesis, Hong Kong University of Science and Technology

**Canadian Standards Association International (CSA). (2002).** ''Design and construction of building components with fiber reinforced polymers.'' CSA-S8-06, Toronto.

**Chanvillard, G., and S. Rigaud. (2003).** "Complete Characterization of Tensile Properties of Ductal UHPFRC According to the French Recommendations," Proceedings of the 4th International RILEM Workshop on High Performance Fiber Reinforced Cement Composites (HPFRCC 4), 14 pp, Ann Arbor, MI..

**Chen, L., and Graybeal, B. (2010).** " Finite Element Analysis of Ultra-High Performance Concrete: Modeling Structural Performance of an AASHTO Type II Girder and a 2nd Generation Pi-Girder." Report No. PB2011-100864, National Technical Information Service, Springfield, VA.

**Cheng, L., and Karbhar. (2005).** Steel-Free Hybrid FRP Stiffened Panel-Concrete Deck System. Proceeding from ACI Special Publication SP-230-37 at the 7th International Symposium on Fiber Reinforced Polymer Reinforcement on Concrete Members(FRPRCS-7 . Kansas City, MO, USA. pp. 631-650.

**Christopher K. Y. Leung and  Qian Cao.(2010).** "Development of pseudo-ductile permanent formwork for durable concrete structures", Materials and Structures (2010) 43:993–1007.)

**Crane, C.K. (2010).** "Shear and Shear Friction of Ultra-High Performance Concrete Bridge Girders," Ph.D. Dissertation, Georgia Institute of Technology, Atlanta,

**Deskovic, N., Meier, U., and Triantafillou, T.(2005).** "Innovative Design of FRP Combined with Concrete: Long- Term Behavior." Journal of Structural Engineering , 121 (7): 1079-1089.

**Davalos, J. F., Qiao, P., and Barbero, E. J. (1996).** ''Multi objective material architecture optimization of pultruded FRP I beams.'' Compos. Struct., 271–281.Davalos, J. F., Qiao, P. Z., Xu, X. F., Robinson, J., and Barth, K. E.(2001). ''Modeling and characterization of fiber-reinforced plastic honeycomb sandwich panels for highway bridge applications.'' J. Compos. Constr., 52~3-4, 441–452.

**Davis, D., and Porter, M. L. (1999).** ''Glass fiber reinforced polymer dowel bars for transverse pavement joints.'' Proc., 4th Int. Symposium, Fiber Reinforced Polymer Reinforcement for Reinforced Concrete Structures, C. W. Dolan, S. H. Rizkalla, and A. Nanni, eds., SP-188, American Concrete Institute, Farmington Hills, Mich., 297– 304.

**De Larrard F, Sedran T.** Optimization of ultra-high-performance concrete by the use of a packing model. Cem Concr Res1994;24(6): 997-1009.

**Deitz, D. H., Harik, I. E., and Gesund, H. (1999).** ''One-way slabs reinforced with glass fiber reinforced polymer reinforcing bars.'' Proc., 4th Int.

**Degen, B. (2006).** "Shear Design and Behavior of Ultra-High Performance Concrete," Master's Thesis, Iowa State University, Ames, IA.

**DIN 18218:2010-01. (2010).** " Pressure of fresh concrete on vertical formwork—English translation of DIN 18218:2010-01."  Beuth Verlag.

**Donna S. M. Chen, Raafat El-Hacha. (2010).** "Flexural behavior of hybrid FRP-UHPC girders under static loading." Proceedings of 8th International Conference on Short and Medium Span Bridge Niagara Falls, Canada.

**El-Ghandour, Abdel Wahab, Pilakoutas, Kypros and Waldron, Peter. (2003).** "Punching Shear Behavior of Fiber Reinforced Polymers Reinforced Concrete Flat Slabs: Experimental Study," Journal of Composites for Construction, ASCE, v7, n3, pp. 258-265.

**Feylessoufi A, Crespin M, Dion P, et al.** Controlled rate thermal treatment of reactivepowder concretes. Adv Cement Based Mater 1997;6(1):21-27.

**Francesca Giulia Carozzi, Gabriele Milani, Carlo Poggi. (2014).** "Mechanical properties and numerical modeling of Fabric Reinforced Cementitious Matrix (FRCM) systems for strengthening of masonry structures", Composite Structures.

**Fujikake K., Senaga T., Ueda N., Ohno T., and Katagiri M. (2003).** "Effects of Strain Rate on Tensile Behavior of Reactive Powder Concrete", Journal of Advanced Concrete Technology, Vol. 4, No. 1, Feb

2005, pp 79-84.Future," Field Applications of FRP Reinforcement: Case Studies. Sami Rizkalla and Antonio Nanni (editors), American Concrete Institute, SP-215, pp. 3-20).

**Garcia, H. (2007).** "Analysis of an Ultra-High Performance Concrete Two-Way Ribbed Bridge Deck Slab", Report No. PB 2007-112112, National Technical Information Service, Springfield, VA.

**Gardner J, Keller L, Quattrociocchi R, Charitou G. (2012).** "Field Investigation of Formwork Pressures using Self Consolidating Concrete, Concrete International." Vol. 34, No. 1, pp 41–47

**Gardner NJ. (1985).** "Pressure of concrete on formwork: a review. In: Proceedings, American Concrete Institute." vol. 82, pp 744–753.

**Garas VY.** Multi-scale investigation of tensile creep of ultra-high performance concrete for bridge applications. Ph. D. Thesis, Georgia Institute of Technology,2009.

**Graybeal, B. (2006).** "Material Property Characterization of Ultra-High Performance Concrete." Report No. FHWA-HRT-06-103, Federal Highway Administration, McLean, VA.

**Graybeal, B. (2006).** "Practical Means for Determination of the Tensile Behavior of Ultra-High Performance Concrete," Journal of ASTM International, Vol. 3, No. 8, ASTM International, West Conshohocken, PA.

**Graybeal, B. (2006).** Structural Behavior of Ultra-High Performance Concrete Prestressed I-Girders, Report No. FHWA-HRT-06-115, Federal Highway Administration, McLean, VA.

**Graybeal, B. and Tanesi, J. (2007).** "Durability of an Ultrahigh-Performance Concrete," ASCE Journal of Materials in Civil Engineering, Vol. 19, No. 10, pp. 850–854, American Society of Civil Engineers, Reston, VA.

**Graybeal, B. (2007).** "Compressive Behavior of Ultra-High Performance Fiber-Reinforced Concrete," ACI Materials Journal, Vol. 104, No. 2, pp. 146–152, Farmington Hills, MI.

**Graybeal, B. (2008).** "Flexural Behavior of an Ultrahigh-Performance Concrete I-Girder," ASCE Journal

**Graybeal, B. and Davis, M. (2008).** "Cylinder or Cube: Strength Testing of 80 to 200 MPa (11.6 to 29 ksi)Ultra-High-Performance Fiber-Reinforced Concrete," ACI Materials Journal, Vol. 105, No. 6, pp. 603–609, American Concrete Institute, Farmington Hills, MI.

**Graybeal, B. (2009).** Structural Behavior of a Prototype Ultra-High Performance Concrete Pi-Girder, Report No. PB2009-115495, National Technical Information Service, Springfield, VA.

**Graybeal, B. (2010).** "Design, Fabrication, and Testing of a 2nd Generation Ultra-High Performance Concrete Pi-Girder," Proceedings, 3rd International fib Congress, Washington, DC.

**Graybeal, B.(2010).** "Behavior of Field-Cast Ultra-High Performance Concrete Bridge Deck Connections Under Cyclic and Static Structural Loading." Report No. PB2011-101995, National Technical Information Service, Springfield, VA.

**Graybeal, B. (2010).** "Simultaneous Structural and Environmental Loading of an Ultra-High Performance Concrete Component." Report No. PB2010-110331, National Technical Information Service, Springfield, VA.

**Graybeal, B.(2011),** "Construction of Field-Cast Ultra-High Performance Concrete Connections," *TechNote*, Federal Highway Administration, McLean, VA, FHWA-HRT-12-038, 2012. Graybeal, B., "Ultra-High Performance Concrete," *TechNote*, FHWA-HRT-11-038, Federal Highway Administration, McLean, VA.

**Graybeal B.** UHPC in the U.S. Highway Transportation System.In: Proceedings of the Second International Symposium on Ultra High Performance Concrete. Kassel, Germany: Kassel University Press GmbH. 2008.p.11.

**G.B. Kim, K. Pilakoutas , P. Waldron. (2008).** "Development of thin FRP reinforced GFRC permanent formwork systems". Construction and Building Materials 22 (2008) 2250–2259)

**Graubner CA, Boska E, Motzko C, Proske T, Dehn F. (2012).** "Formwork pressure induced by highly flowable concrete— design approach and transfer in practice." Structural concrete, journal of the fib. Ernst & Sohn Verlag, Berlin

**Green, B. (2010).** "An Investigation of UHPC/RPC Materials for Enhanced Penetration Resistance," Presented at the American Concrete Institute Fall Convention, Pittsburgh, PA.

**Harris, D. (2004).** "Characterization of the Punching Shear Capacity of Thin UHPC Plates," Master's Thesis, Virginia Polytechnic Institute and State University, Blacksburg, VA.

**Harries, K. A., Porter, M., and Busel, J. (2003).** "FRP materials and concrete—Research needs." Concr. Int., 25.10., 49–54.

**Habel K, Gauvreau P.** Response of ultra-high performance fiber reinforced concrete (UHPFRC)to impact and static loading. Cem Concr Res2008;30(10): 938-946.

**Honickman, H. (2008).** "Pultruded GFRP Sections as Stay-in-Place Structural Open Formwork for Concrete Slabs and Girders." M.Sc. Thesis. Queen's University, Department of Civil Engineering, Kingston, ON, Canada.

**Hajar, Z. et al**. "Design and Construction of the World First Ultra-High Performance Concrete Road Bridges," Proceedings of the International Symposium on Ultra High Performance Concrete, Ed., Schmidt, M., Fehling, E., and Geisenhanslüke, C., Kassel University Press, Kassel, Germany, 2004, pp. 39–48.

**Harik, I., et al. (1999).** ''Static testing on FRP bridge deck panels.'' Proc., 44th Int. SAMPE Symposium and Exhibition, Vol. 2, Society for the Advancement of Material and Process Engineering, Covina, Calif., 1643–1654.

**Heinz, D. and Ludwig, H.-M. (2004).** "Heat Treatment and the Risk of DEF Delayed Ettringite Formation in UHPC," Proceedings of the International Symposium on Ultra High Performance Concrete, Ed., Schmidt, M., Fehling, E., and Geisenhanslüke, C., Kassel University Press, Kassel, Germany, 2004, pp. 717–730.

**Institution of Structural Engineers (ISE).(1999).** ''Interim guidance on the design of reinforced concrete structures using fiber composite reinforcement.' Reference No. 319, London.

**Japan Concrete Institute (JCI). (1998).** ''Technical report on continuous fiber reinforced concrete.'' TC 952, Committee on Continuous Fiber Reinforced Concrete, Tokyo.

**Johansen, G. E., Wilson, R. J., Roll, F., and Gaudini, G. (1997).** ''Design and construction of long span FRP pedestrian bridges.'' Building to last, Proc., Structures Congress XV, L. Kempner and C. B. Brown, eds., ASCE, New York, 46–50.

**Jacobson, David A., Bank, Lawrence C., Oliva, Michael G., and Russell, Jeffrey S. (2004).** "Punching Shear in Fiber-Reinforced Polymer (FRP) Bi-layer Grid-Reinforced Concrete Bridge Decks," TRB 2004 Annual Meeting (on CD-ROM), 21 pp.

**Jensen BC et al. (1995).** "Connections in precast buildings using ultra high-strength fibre reinforced concrete." In: Nordic symposium on modern design of concrete structures, Aalborg University, Denmark.

**Joseph P. Hanus, Lawrence C. Bank, Michael G. Oliva. (2009).** "Combined loading of a bridge deck reinforced with a structural FRP stay-in-place form". Construction and Building Materials 23 1605–1619.

**Joseph Robert Yost, Charles H. Goodspeed, Edwin R. Schmeckpeper. (2002).** "Flexural Performance of Concrete Beams Reinforced with FRP Grids," Journal of Composites for Construction, Vol. 5, No. 1.

**J.-P. Korb, D. Petit, S. Philippot, H. Zanni, V. Marret, M. Cheyrezy, (1998).** "Nuclear relaxation of water confined in reactive powder concrete." in:P. Colombet, A.-R. Grimmer, H. Zanni, P. Sozzani (Eds.), Nuclear Magnetic Resonance Spectroscopy of Cement-Based Materials, Springer-Verlag, Berlin, pp. 333–343.

**Keller, T. (2005).** "All-FRP and Hybrid-FRP Load-Bearing Structures–Status and Future Prospects." 4th Middle East Symposium on Structural Composites for Infrastructure Application (MESC-4), Alexandria, Egypt. pp. 28-36.

**Kim, B.-S., Cho, J.-R., Park, S. Y., and Cho, K. (2006).** "Toward Hybrid Bridge Deck: An Innovative FRP-Concrete Composite Deck." Proceedings of International Joint Seminar of the KSCE and the JSCE: 2006 KSCE Annual.

**Kim, S.W. et al.(2008).** "Effect of Filling Method on Fibre Orientation & Dispersion and Mechanical Properties of UHPC," Proceedings of the Second International Symposium on Ultra High Performance Concrete, Ed., Fehling, E., Schmidt, M., and Stürwald. S., Kassel University Press, Kassel, Germany, 2008, pp. 185–192.).

**Khayat, KH, et al., (2010).** Inclined Plane Test Method to Determine Structural Build-Up at Rest of Self-Consolidating Concrete. ACI Materials Journal, V. 107, No. 5, pp. 515-522.

**Khayat KH, Omran AF. (2011).** "Field verification of formwork pressure prediction models." Concr Int 33(6):33–39.

**Khayat, K. H..(1999).** "Workability, Testing, and Performance of Self-Consolidating Concrete ," ACI Materials Journal, V. 96, No. 43, May.-June.1999, pp. 246-254.

**Khayat, K. H. (2000).** "Optimization and Performance of Air-Entrained, Self-Consolidating Concrete," ACI Materials Journal, V. 97, No. 61, pp. 526-535.

**Khayat, K. H.; Manai, K.; and Trudel, A. (1997).** "In-Situ Mechanical Properties of Wall Elements Cast Using Self-Consolidating Concrete," ACI Materials Journal, V. 94, No. 6, pp. 491-500.

**Kim GB, Pilakoutas K, Waldron P.(2005).** Bond characteristics of fiber reinforced polymers bars in glass fiber reinforced concrete. In: Third international conference on construction materials: performance, innovations and structural implications, August 22–24, Vancouver, Canada; 2005. p. 178. ISBN 0-88865-810-9 (10 pages in CD-Rom).

**Kim GB. (2006).** Development of thin FRP GFRC permanent formwork systems, PhD thesis, University of Sheffield,

**Lafarge. (2008).** Ductal ® Mechanical Performance. Lafarge Canada. Calgary, AB, Canada.

**Lankard DR, Newill JK.** Preparation of highly reinforced steel fiber reinforeed Conerete composites. ACIMater J1984;SP-81: 287-306.

**L.C. Bank. (2006).** "Composites for Construction: Structural Design with FRP Materials." John Wiley & Sons Ltd., Chichester.

**L.C. Bank, A.P. Malla, M.G. Oliva, & J.S. Russell, Bentur & A. Shapira. (2008)."**A Specification for thin FRP/FRC Forms for Bridge Deck Construction", Fourth International Conference on FRP Composites in Civil Engineering (CICE2008) 22-24July 2008, Zurich, Switzerland.

**Linning Ding & Hatem M. Seliem. (2010).** "Confinement of Concrete Piles with FRP", CICE 2010- the 5th international conference on FRP composites in civil engineering, September 27-29, Beijing, China.

**Lu, Z., Boothby, T. E., Bakis, C. E., and Nanni, A. (2000).** ''Transfer and development length of FRP prestressing tendons.,'' Precast Concrete Institute J., 45~2, 84–95.

**Ma J, Dietz J. (2002).** "Ultra high performance self compacting concrete." Lacer 7:33–42

**Max L. Porter, P.E., Hon.M.ASCE,Kent Harries, P.E., M.ASCE. (2000).** Future Directions for Research in FRP Composites in Concrete Construction, J. Compos. Constr. 11:252-257.

**Massidda L, Sanna U, Cocco E, Meloni P.** High pressure steam curing of reactive-powder mortars, ACI Mater J2001;SP200-27:447-464.

**Meade, T., and Graybeal, B. (2010).** "Flexural Response of Lightly Reinforced Ultra-HighPerformance Concrete Beams," Proceedings, 3rd International fib Congress, Washington, DC.

**Melcher Jindrich and Karmazinova Marcela. (2013).** "Experimental Verification and Design of Glass-FRP Composite Grids", Advanced Materials Research Vol. 664 pp 696-701.

**Matthys, S., and Taerwe, L. R. (2000).** ''Concrete slabs reinforced with FRP grids. I: One-way bending.'' J. Compos. Constr., 4(3), 145–153.

**Nanni, A., ed. (1993).** "Fiber-reinforced-plastic for concrete structures: Properties and applications." Elsevier Science, Amsterdam.

**Nanni, A., Bakis, C. E., O'Neil, E. F., and Dixon, T. O. (1996).** ''Performance of FRP tendon-anchor systems for prestressed concrete structures.'' PCI J., 41, 34–44.

**Precast/prestressed Concrete Institute. (2001).** "Concrete institute, recommended practice glass fiber reinforced concrete panels." PCI Committee on Glass Fiber Reinforced Concrete Panels.

**Proske T (2007).** "Formwork Pressure using Self- Compacting Concrete." Ph.D. Thesis), Technische Universita¨t Darmstadt, p 310.

**Ogawa A, Hitomi Y, Hoshiro H (2006).** "PVA-fiber reinforced high performance cement board." In: Fischer G, Li VC (eds) Proceedings of international RILEM workshop on HPFRCC in structural applications, pp 243–251.

**Qiao, P., Davalos, J. F., and Brown, B. (2000).** ''A systematic approach for analysis and design of single-span FRP deck/stringer bridges.'' Composites, Part B, 31~6-7, 593–610.

**Qingxu Jin , Christopher K. Y. Leung , Changli Yu.(2013).** "Effective joining method for pseudo-ductile permanent formwork", Materials and Structures,  46:345–360

**Rebentrost, M., and Wight, G. (2009).** "Investigation of UHPFRC Slabs Under Blast Loads," Proceedings, Ultra-High Performance Fiber Reinforced Concrete 2009, Marseille, France.

**Reda MM, Shrive NG, Gillott JE.** Microstructural investigation of innovative UHPC. Cem Concr Res1999;29(3): 323-329.

**Rebentrost M, Wight G.** Experience and applications of ultra-high performance concrete in Asia. In: Proceedings of the 2nd International Symposium on Ultra-High Performance Concrete. Kassel,Germany: Kassel University Press GmbH. 2008.p.19-30.

**Richard P, Cheyrezy M.** Reactive powder concretes with high ductility and 200-800 MPa compressive strength. ACI Mater J1994;144(3): 507-518.

**Robert L.Pearifoy, Garold D. Oberlender.(2007).** "Form Work For Concrete Structures", Fourth Edition, Copy right by The McGraw-Hill Companies, Inc..

**Rossi, P. et al.** "Bending and Compressive Behaviors of a New Cement Composite," Cement and Concrete Research, Vol. 35, No. 1, 2005, pp. 27–33.

**Schimidt M, Fehling E.** Ultra-High-Performance Concrete: Research, Development and Application in Europe. In: 7th International Symposium on the Utilization of High-Strength-and High-Performance-Concrete, ACI Washinton, 2005.SP.228-4, p.51-78.

**Spasojevic A.** Structural implications of ultra-high performance fiber reinforced concrete in bridge design. Ph.D. thesis, EPFL; 2008.

**Shioya T et al. (1997).** "Pre-cast concrete joint using steel fiber reinforced high strength mortar and/or H-beam." Proc Jpn Concr Inst 19(2):1305–1310

**Soo-Duck Hwang, Kamal H. Khayat, and Olivier Bonneau. (2006).** "Performance-Based Specifications of Self-Consolidating Concrete Used in Structural Applications," ACI Materials Journal, V. 103, No. 14, March.-April. pp. 121-129.

**Hwang, S.-D., Khayat, K.H.,** "Effect of Various Admixture-Binder Combinations on Workability of Ready-Mix Self-Consolidating Concrete", ACI-Special Publication 233, 2006, pp. 25-43.

**Stijn Matthys and Luc Taerwe. (2000).** "Concrete Slabs Reinforced with FRP Grids," Journal of Composites for Construction, Vol.4, No. 3.

**Staquet S., Rigot G., Detandt H., Espion B.. (2004).** "Innovative Composite Precast Precambered U-shaped Concrete Deck for Belgium's High Speed Railway Trains." PCI Journal, 49(6), 94-113.

**Swamy, R.N. and Mangat, P.S. (1974).** "Influence of fiber-aggregate interaction on some properties of steel-fiber reinforced concrete." Materials and Structures RILEM, 7 (41), 307-14.

**Tang, M.C..(2004).** " High Performance Concrete – Past, Present and Future," International Symposium on UHPC, Kassel, Germany, pp. 3-9.

**Tanaka, Y. et al.** "Innovation and Application of UFC Bridges in Japan," Proceedings of the International Workshop on Ultra High Performance Fibre Reinforced Concrete—Designing and Building with UHPFRC: State of the Art Development, 17–19 November 2009, Marseille, France, AFGC/fib, Paper 3.1.4.

**Teichmann, T. and Schmidt, M.** "Mix Design and Durability of Ultra High Performance Concrete (UHPC)," Proceedings of the 4th International Ph.D. Symposium in Civil Engineering, Munich, 2002, pp. 341–347.

**Tilo Proske, Kamal H. Khayat, Ahmed Omran, Olaf Leitzbach. (2014).** "Form pressure generated by fresh concrete: a review about practice in formwork design". Materials and Structures 47:1099–1113.

**Triantafillou, T. C., and Antonopoulos, C. P. (2000).** ''Design of concrete flexural members strengthened in shear with FRP.'' J. Compos. Constr., 4~4, 198–205.

**Washer, G., P. Fuchs, B. Graybeal, and J. Hartmann. (2004)**. "Ultrasonic Testing of Reactive Powder Concrete," IEEE Transactions on Ultrasonics, Ferroelectrics, and Frequency Control, Vol. 51, No. 2, IEEE Ultrasonics, Ferroelectrics, and Frequency Control Society, New York, NY.

**Wille, K., Naaman, A., and Parra-Montesinos, G. (2011).** "Ultra-High Performance Concrete with Compressive Strength Exceeding 150 MPa (22 ksi): A Simpler Way," ACI Materials Journal, Vol. 108, No. 1, pp. 46–54, American Concrete Institute, Farmington Hills, MI.

**Wille, K., Naaman, A.E., and El-Tawil, S.** "Optimizing Ultra-High-Performance Fiber-Reinforced Concrete," Concrete International, Vol. 33, No. 9, September 2011, pp. 35–41.

**Williams, E. et al.** "Laboratory Characterization of Cor-Tuf Concrete With and Without Steel Fibers," Technical Report No. ERDC/GSL TR-02-22, U.S. Army Corps of Engineers, Engineer Research and Development Center, Washington, DC, July 2009.

**Xian Gai, Antony Darby , Tim Ibell, Mark Evernden. (2013).** "Experimental investigation into a ductile FRP stay-in-place formwork system for concrete slabs". Construction and Building Materials 49 1013–1023.

**Yazici H.** The effect of curing conditions on compressive strength of ultra high strength concrete with high volume mineral admixtures. Build and environ2007;42(5): 2083-2089.

**Yazici H, Yardimci MY, Aydin S, Karabulut AS.** Mechanical properties of reactive powder concrete containing mineral admixtures under different curing regimes. Constr Build Mater 2009;23(3):1223-1231.

**YangSL, Millard SG, SoutsosMN, Barnett SJ, Le TT.** Influence of aggregate and curing regime on the mechanical propertiesof ultra-high performance fibre reinforced concrete (UHPFRC). Constr Build Mater2009;23(6): 2291-2298.

**Yunsheng Z, Wei S, Sifeng L, et al.** Preparation of C200 green reactive powder concrete and its static-dynamic behaviors. Cem Concr Compos2008; 30(9): 831-838.

**Zureick, A., and Steffen, R. (2000).** ''Behavior and design of concentrically loaded pultruded angle struts.'' J. Struct. Eng., 126(3), 406–416.

**Zhang YS, Sun W, Liu SF, Jiao CJ, Lai JZ.** Preparation of C200 green reactive powder concrete and its static-dyamic behaviors. Cem Concr Compos 2008, 30(9): 831-8.

# APPENDIX A MATERIAL PROPERTIES



| Filament Diameter | 0.008" (0.2 mm) |
|---|---|
| Fiber Length | 0.5" (13mm) |
| Specific Gravity | 7.8 |
| Tensile Strength | 285 ksi (1900 MPa) |
| Flexural Strength | 29,000 ksi (203 GPa) |
| Melting Point | 2760° F (1516° C) |
| Color | Copper |
| Water Absorption | Nil |
| Alkali Resistance | High |
| Corrosion Resistance | High |

Figure A.1 Physical properties of steel fibers type I and type II



| Filament Diameter | 8 Denier (38 Microns) |
|---|---|
| Fiber Length | 0.375" (8 mm) |
| Specific Gravity | 1.3 |
| Tensile Strength | 210 ksi (1400 MPa) |
| Flexural Strength | 4200 ksi (30 GPa) |
| Melting Point | 435° F (225° C) |
| Color | White |
| Water Absorption | <1% by Weight |
| Alkali Resistance | Excellent |
| Concrete Surface | Not Fuzzy |
| Corrosion Resistance | Excellent |

Figure A.2 Physical properties of PVA

## General Description

Knitting is a process in which three different yarn sources are used to form a fabric. There are warp (machine direction) yarns, weft (cross direction) yarns and a stitch yarn that is used to tie the warp and weft yarns together. The result is a high-strength fabric that is typically coated to provide further stability.

This process can be done with various input yarns and yarn spacing, and the addition of a substrate, if desired.

## Technical Data Sheet

### Properties

- Fabric is both mechanically and chemically bonded for added durability

- Offers impact resistance

- Wide range of input yarns and spacing

## Technical characteristics

| Property | Imperial | Metric | Testing |
|---|---|---|---|
| Construction: Warp | 255 lbs/inch | 45 kN/m | ASTM D-6637 |
| Construction: Weft | 255 lbs/inch | 45 kN/m | ASTM D-6337 |
| Elongation at Break (max): | < 3% | < 3% | |
| Mass / Unit Area (min): | 6.5 oz/yd$^2$ | 225 g/m$^2$ | ASTM D-5261 |
| Roll Length: | 50 yds | 45.7 m | |
| Roll Width: | 36" | 0.91m | |
| Grid Size: | 1.0 in x 1.0 in | 25mm x 25mm | |
| Coating: | Modified Acrylic Polymer | Modified Acrylic Polymer | |

*All values are minimum average roll values (MARV)

SRG products are manufactured at a Saint-Gobain ADFORS ISO 9001:2000 registered facility



Figure A.3 GFRP type I

## General Description

Knitting is a process in which three different yarn sources are used to form a fabric. There are warp (machine direction) yarns, weft (cross direction) yarns and a stitch yarn that is used to tie the warp and weft yarns together. The result is a high-strength fabric that is typically coated to provide further stability.

This process can be done with various input yarns and yarn spacing, and the addition of a substrate, if desired.

## Technical characteristics

| Property | Imperial | Metric | Testing |
|---|---|---|---|
| Tensile Strength: Warp | 170 lbs/inch | 30 kN/m | ASTM D-6637 |
| Tensile Strength: Weft | 170 lbs/inch | 30 kN/m | ASTM D-6337 |
| Elongation at Break (max): | < 3% | < 3% | |
| Mass / Unit Area (min): | 3.7 oz/yd$^2$ | 125.5 g/m$^2$ | ASTM D-5261 |
| Roll Length: | 27.3 yds | 25.0 m | |
| Roll Width: | 17.7" | 0.45m | |
| Grid Size: | 0.5 in x 0.5 in | 12.7mm x 12.7mm | |
| Coating: | Modified Acrylic Polymer | Modified Acrylic Polymer | |

*All values are minimum average roll values (MARV)

SRG products are manufactured at a Saint-Gobain ADFORS ISO 9001:2000 registered facility

## Technical Data Sheet

### Properties

- Fabric is both mechanically and chemically bonded for added durability

- Offers impact resistance

- Wide range of input yarns and spacing
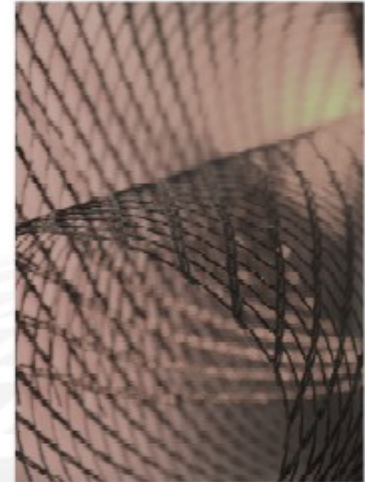


Figure A.4 GFRP type II

# APPENDIX B RHEOLOGY RESULT FOR CEMENTITOUS MATERIALS COMPOSITION USING ANTON PAAR MCR 302

**Shear Stress vs. Time**
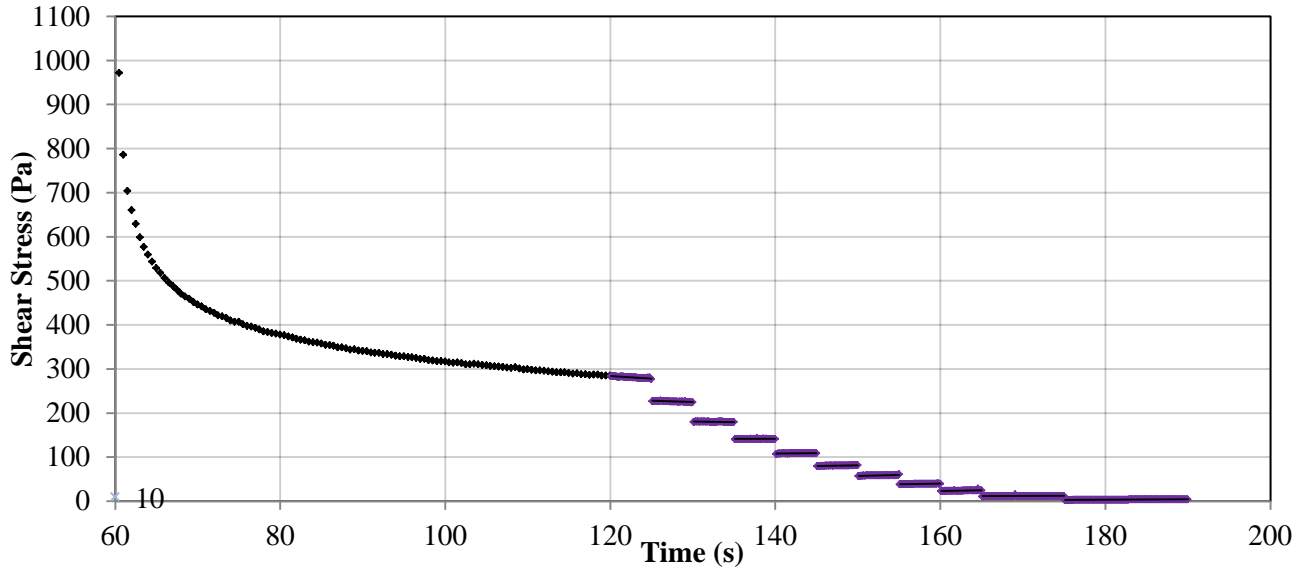
Figure B.1.1 SF5: Shear stress versus time at 20 min

**Shear Stress vs. Time**
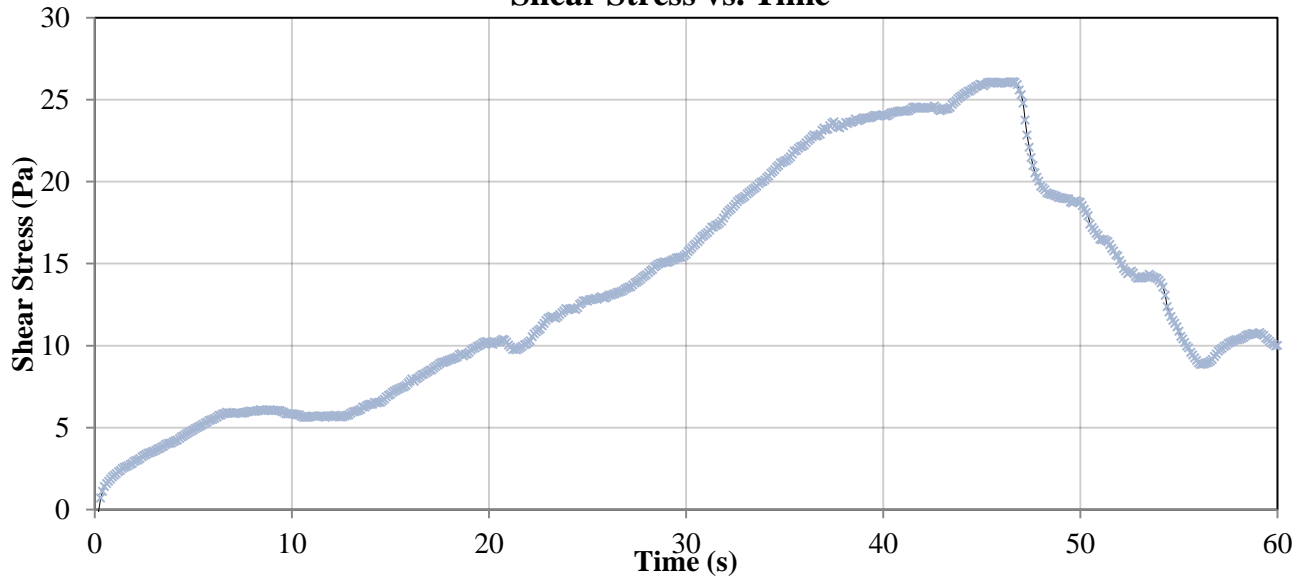
Figure B.1.2 SF5: Static yield stress at 20 min
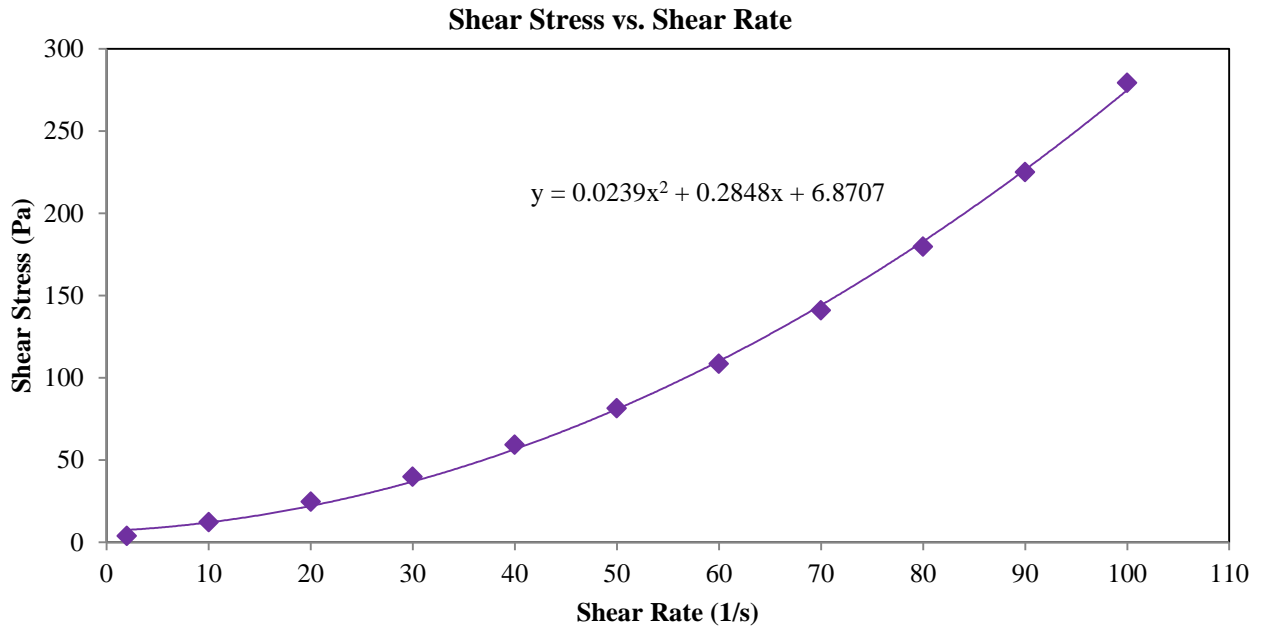
Figure B.1.3 SF5: Shear stress versus shear rate at 20 min

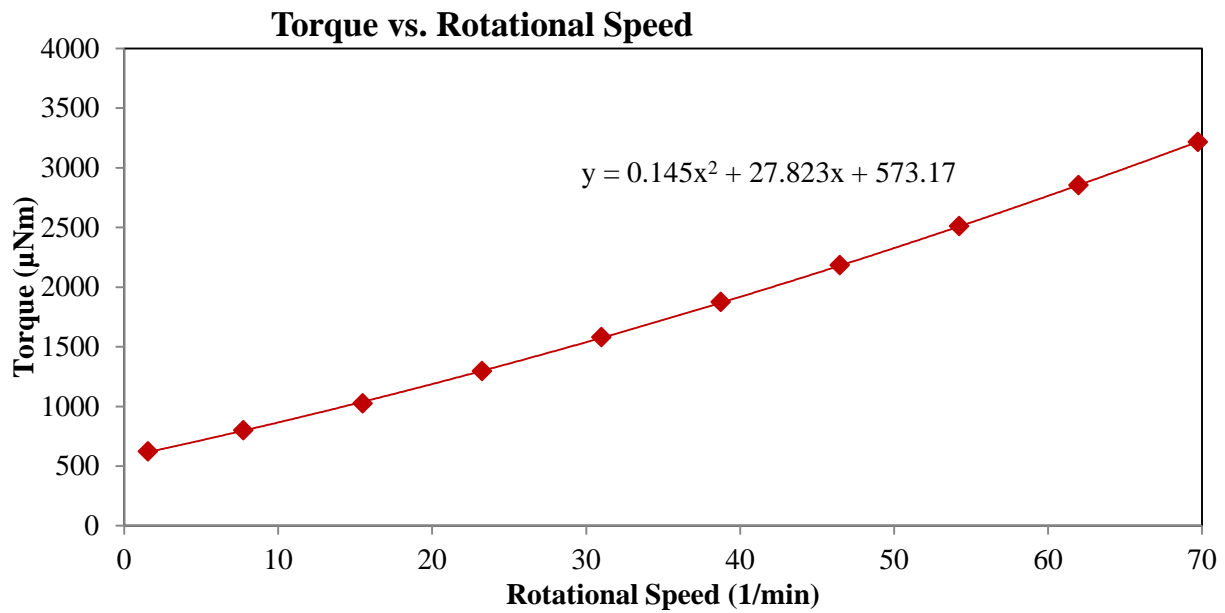$$y = 0.0239x^2 + 0.2848x + 6.8707$$
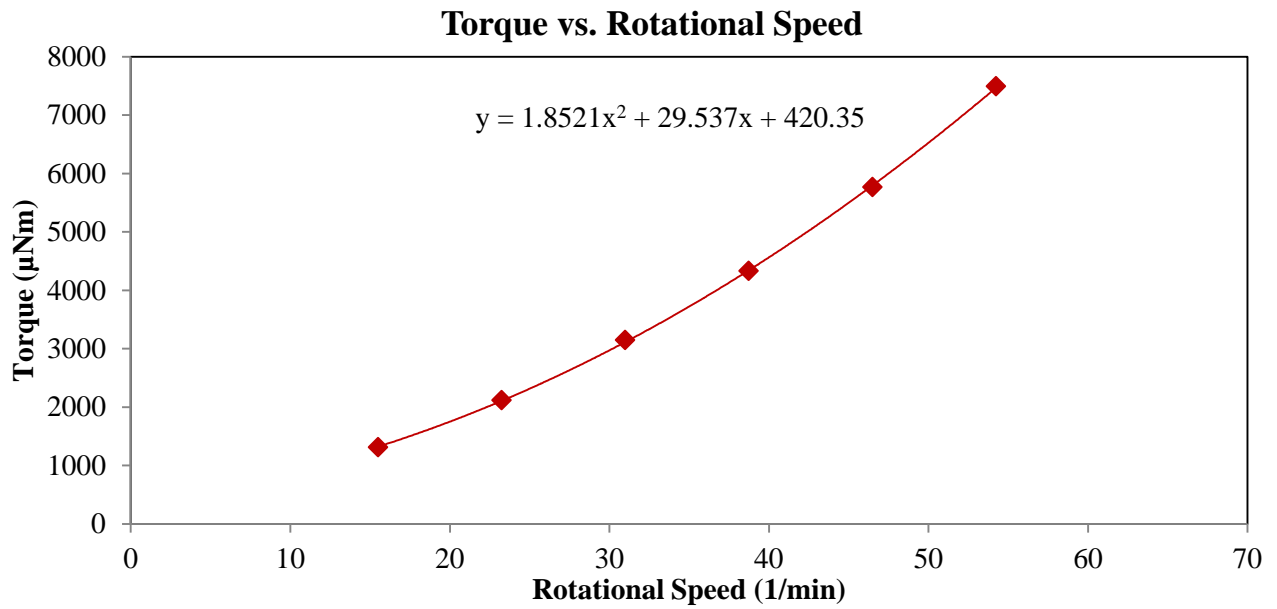


Figure B.1.4 SF5: Torque versus rotational speed at 20 min

$$y = 1.8521x^2 + 29.537x + 420.35$$
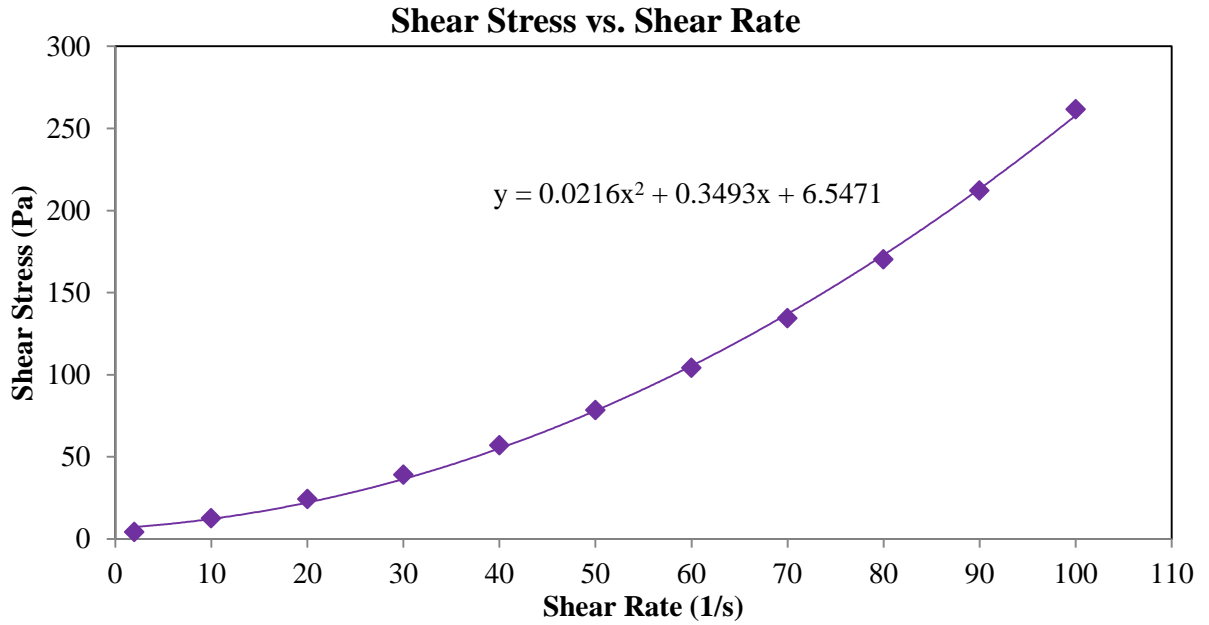
Figure B.1.5 SF5: Shear stress versus shear rate at 40 min

$$y = 0.0216x^2 + 0.3493x + 6.5471$$
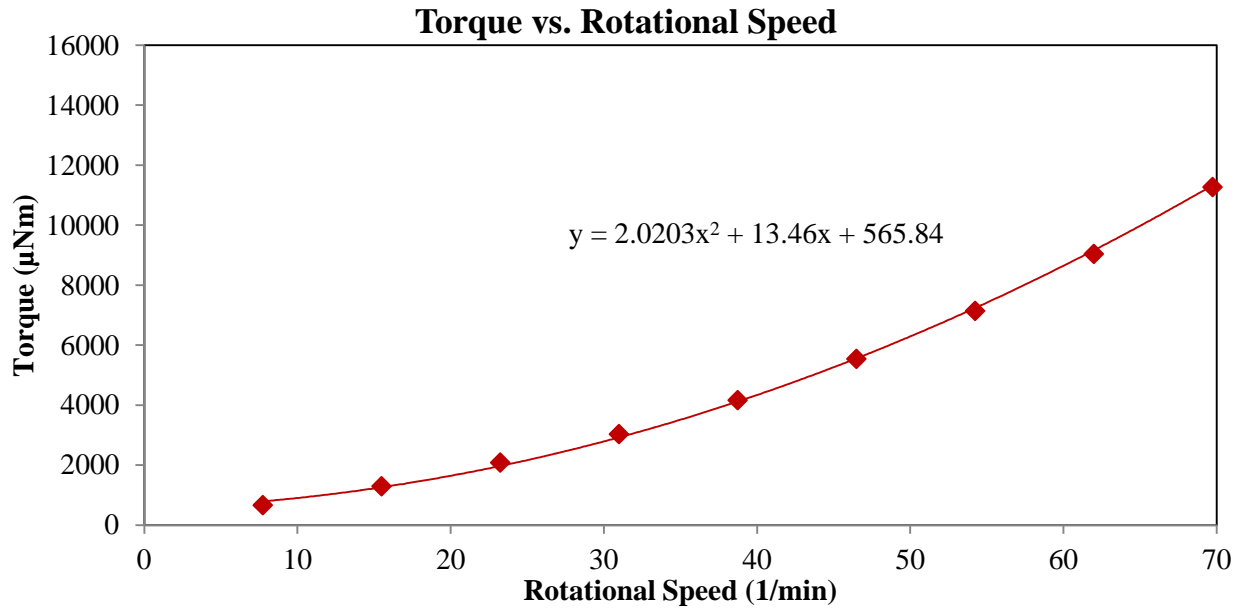


Figure B.1.6 SF5: Torque versus rotational speed at 40 min
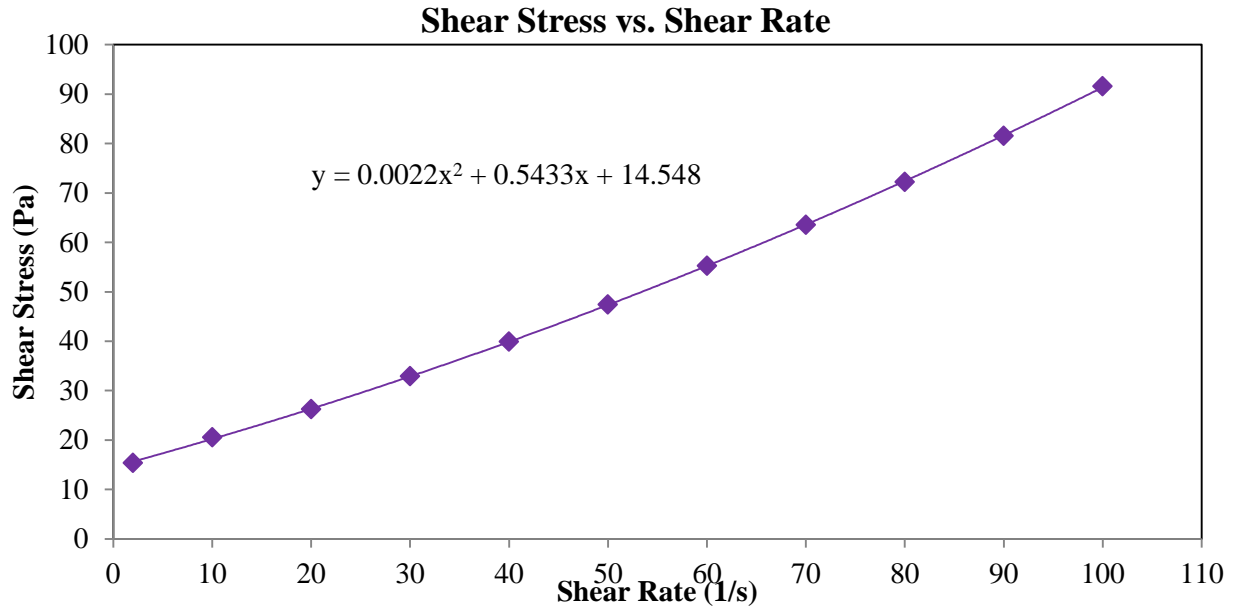
$$y = 2.0203x^2 + 13.46x + 565.84$$
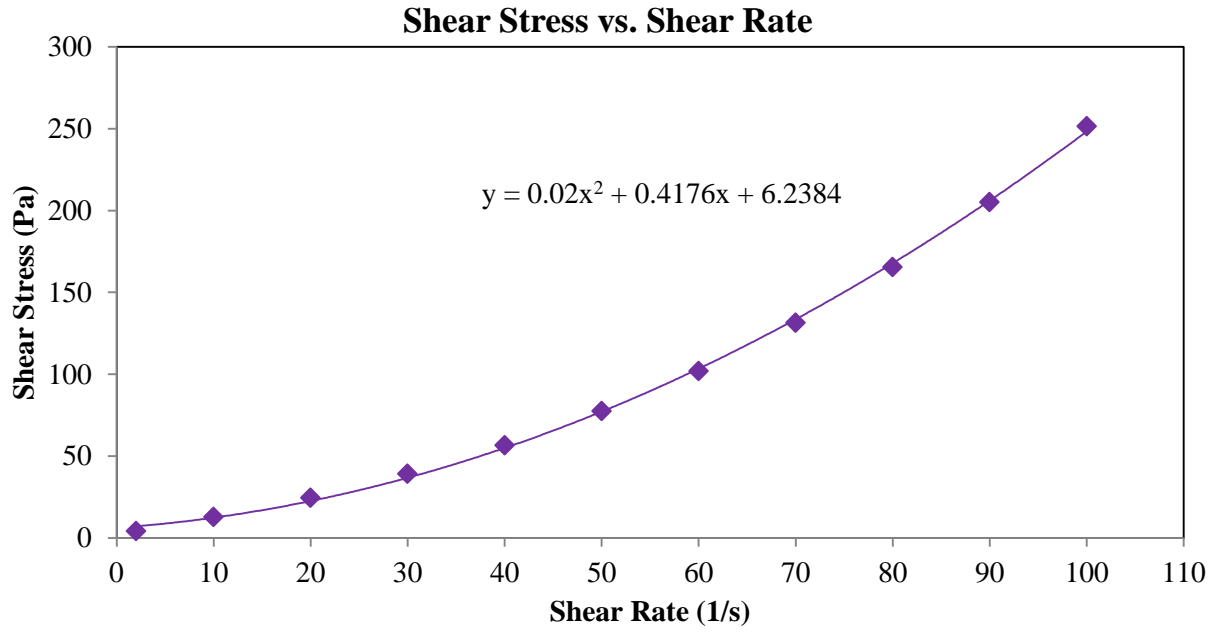
Figure B.1.7 SF5: Shear stress versus shear rate at 60 min
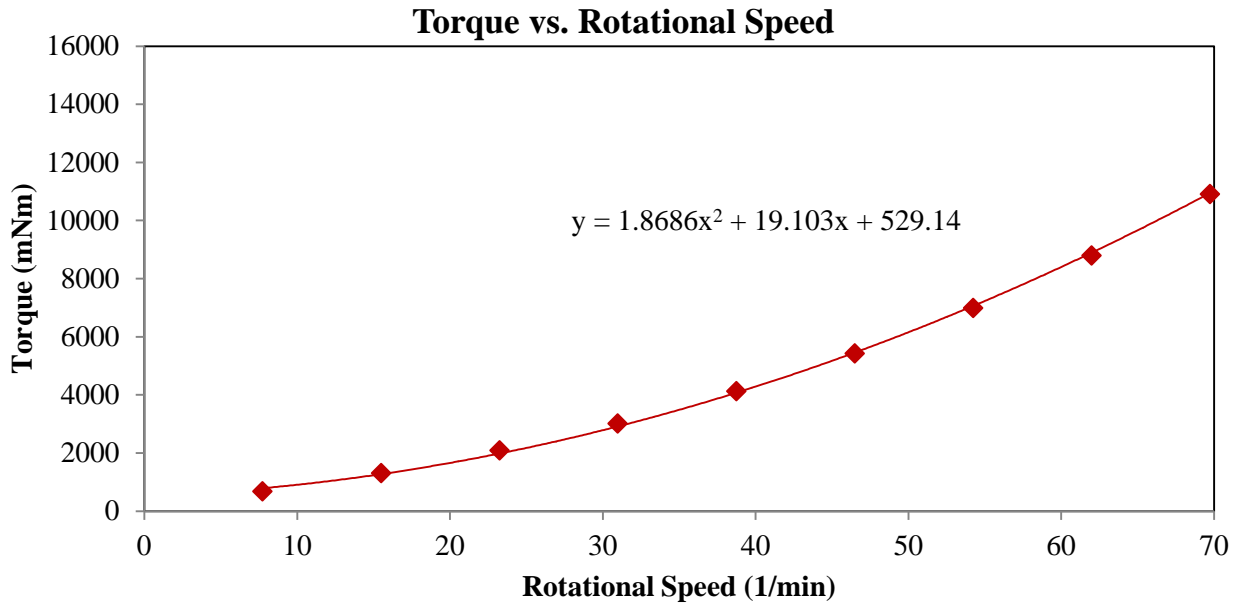


Figure B.1.8 SF5: Torque versus rotational speed at 60 min
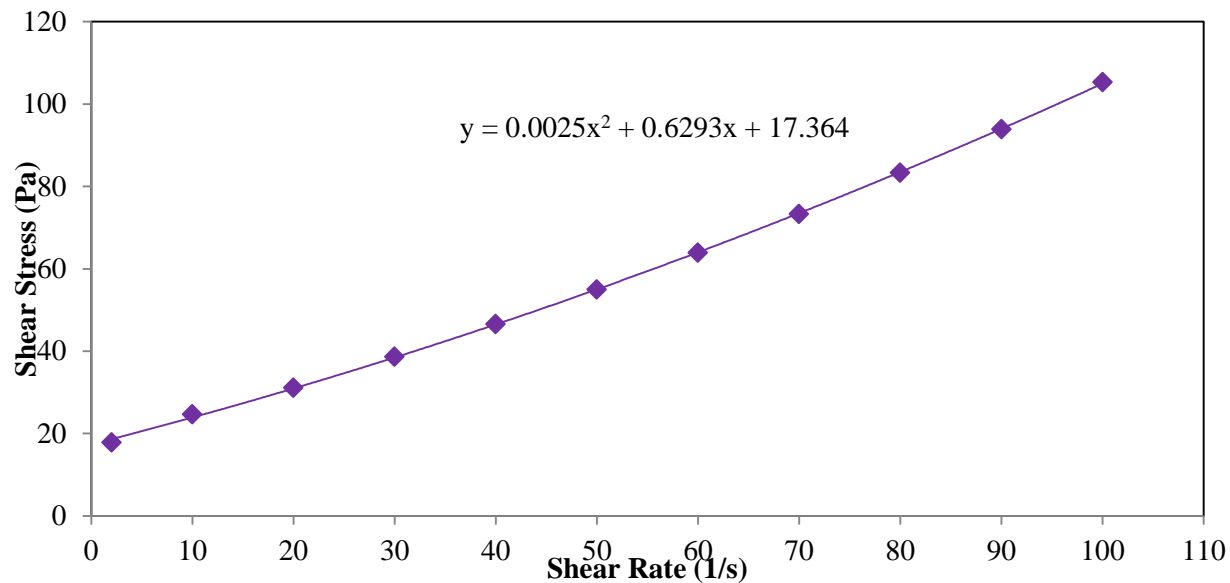
## Shear Stress vs. Shear Rate

$y = 0.022x^2 + 0.4183x + 6.7655$
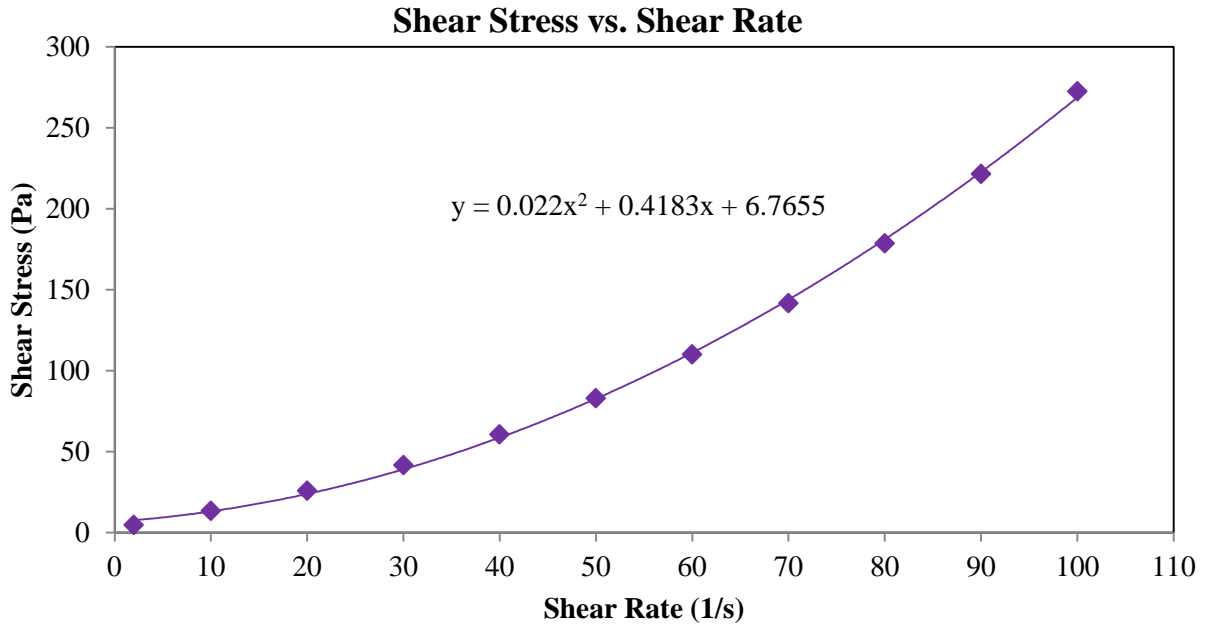
Figure B.1.9 SF5: Shear stress versus shear rate at 90 min

## Torque vs. Rotational Speed

$y = 2.0498x^2 + 18.618x + 568.36$
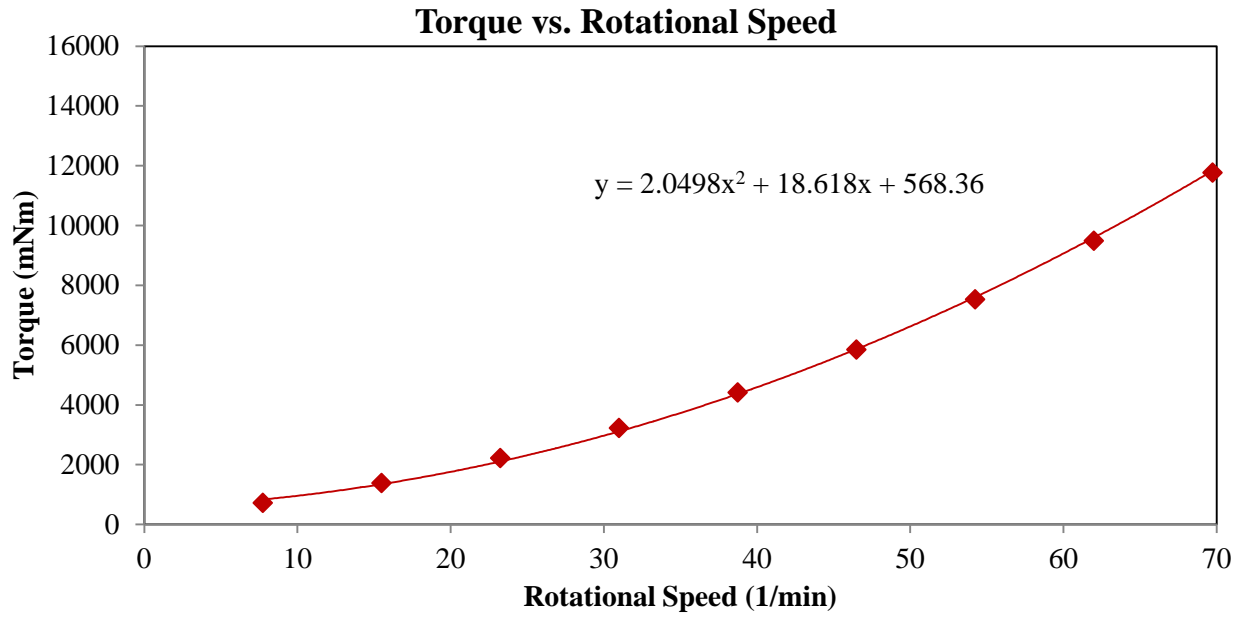
Figure B.1.10 SF5: Torque versus rotational speed at 90 min
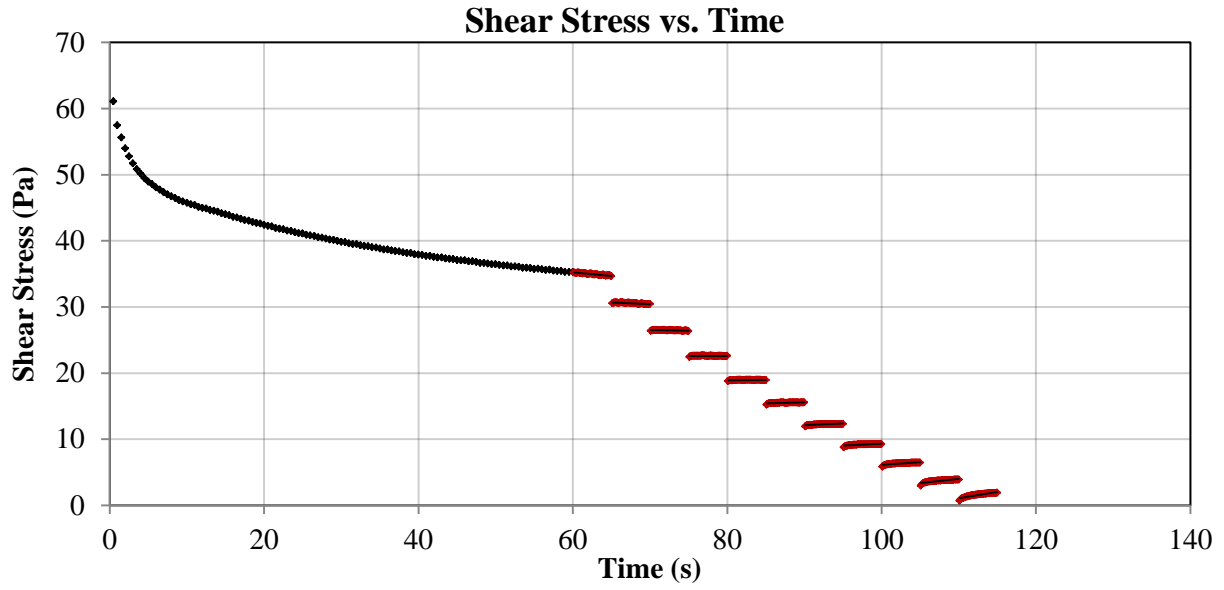
Figure B.2.1 C100: Shear stress versus time at 20 min
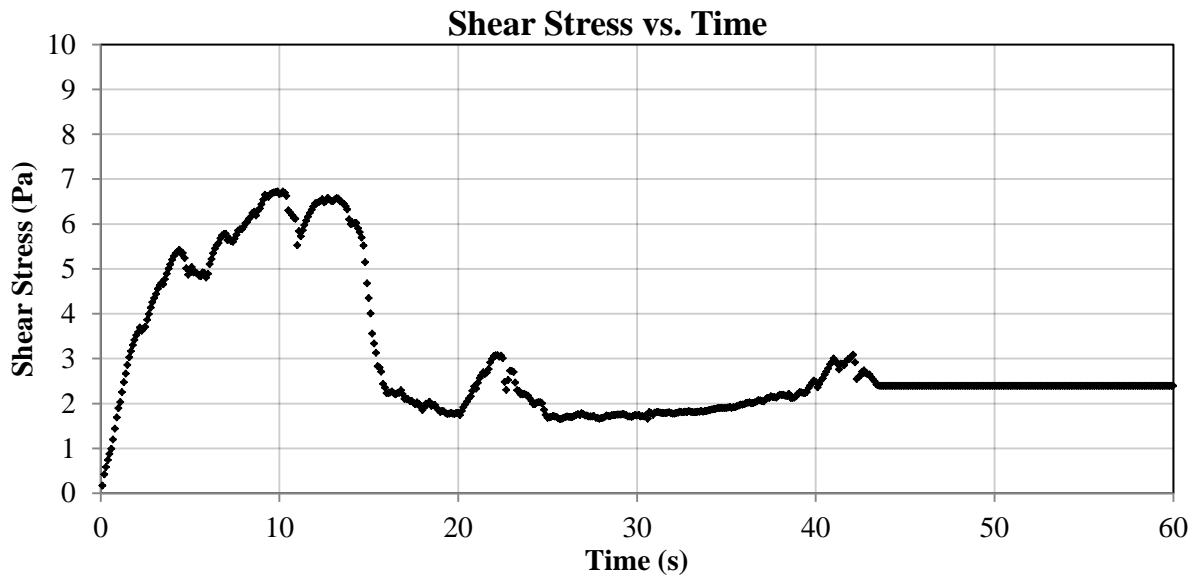

Figure B.2.2 C100: Static yield stress at 20 min

## Shear Stress vs. Shear Rate



$y = 0.0253x^2 + 0.0722x + 7.2012$
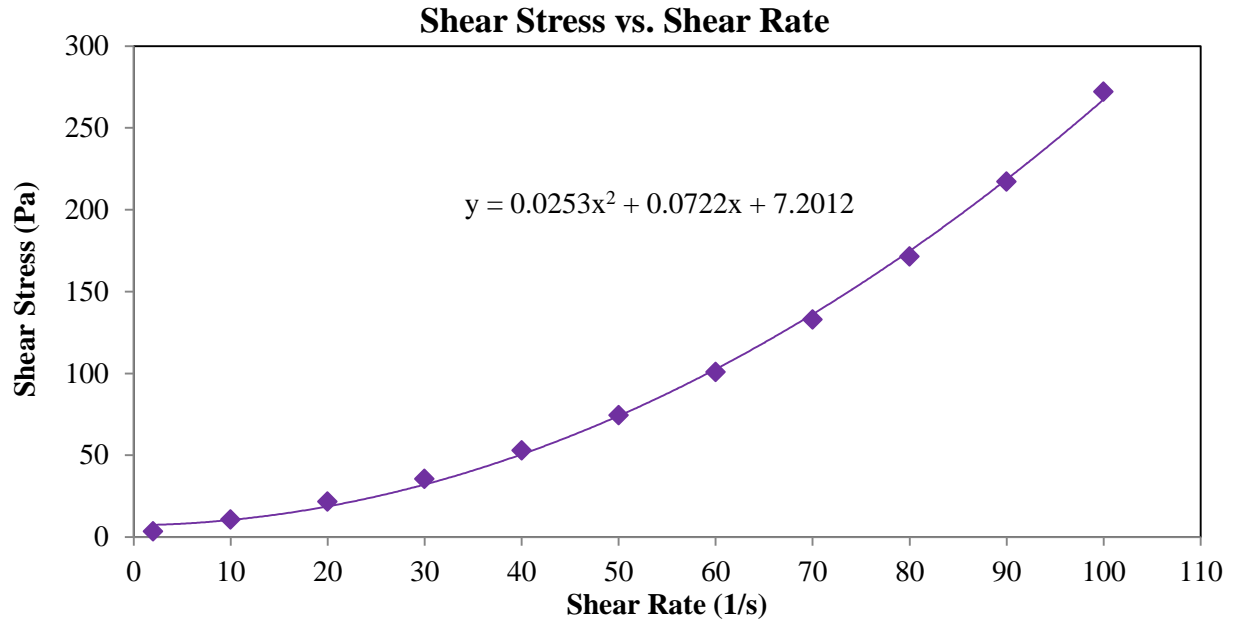
Figure B.2.3 C100: Shear stress versus shear rate at 20 min

## Torque vs. Rotational Speed



$y = 1.8171x^2 + 22.706x + 363.05$
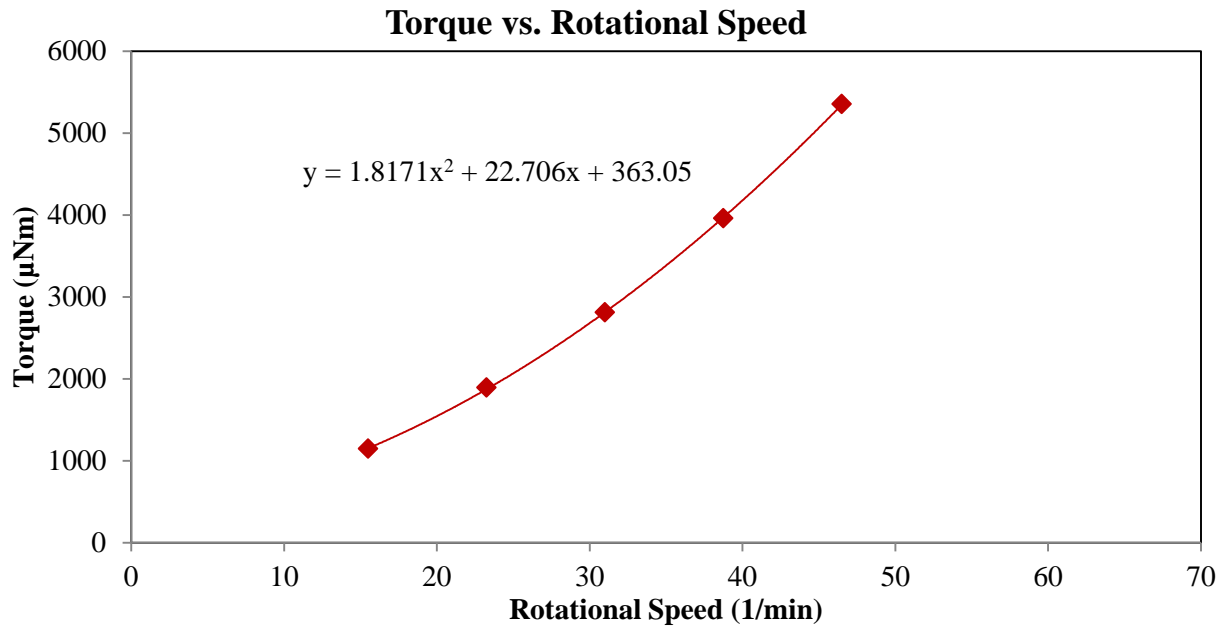
Figure B.2.4 C100: Torque versus rotational speed at 20 min

**Shear Stress vs. Shear Rate**

$y = 0.0223x^2 + 0.1773x + 6.9518$
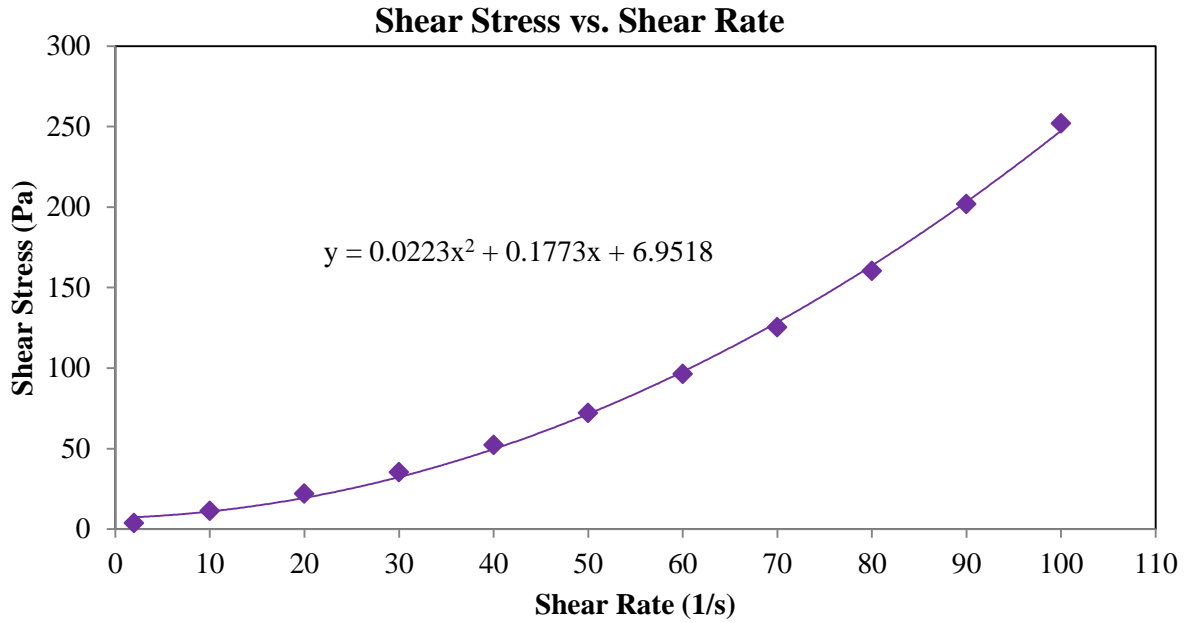
Figure B.2.5 C100: Shear stress versus shear rate at 40 min

**Torque vs. Rotational Speed**

$y = 1.5572x^2 + 30.477x + 321.27$
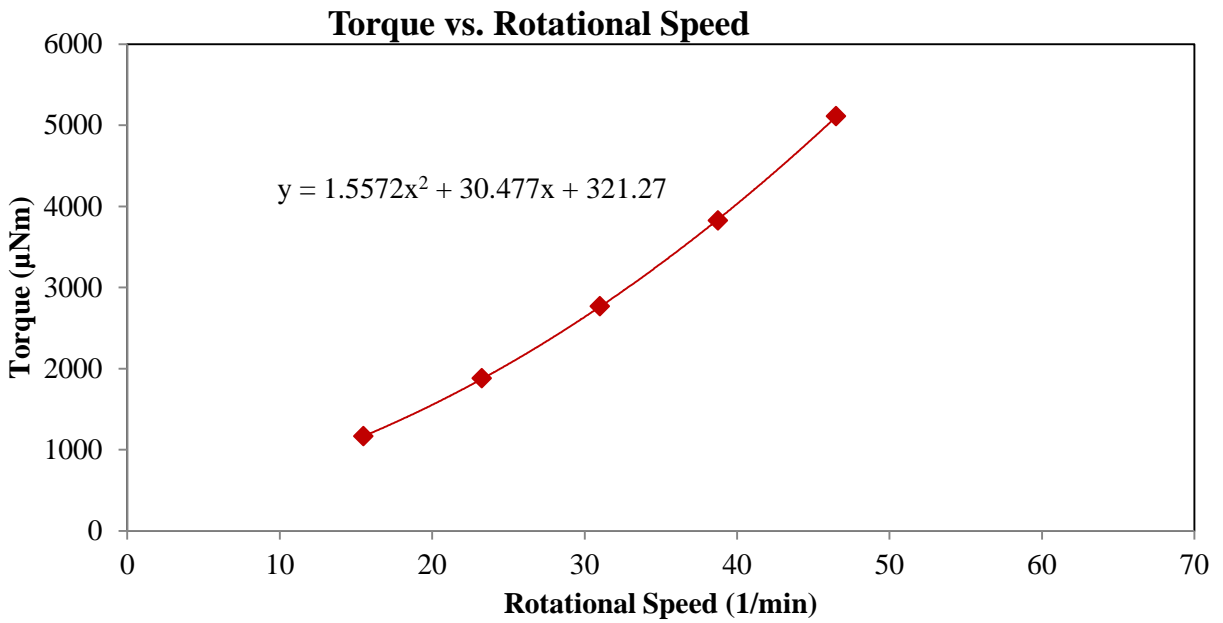
Figure B.2.6 C100: Torque versus rotational speed at 40 min

**Shear Stress vs. Shear Rate**

$y = 0.0239x^2 + 0.2848x + 6.8707$
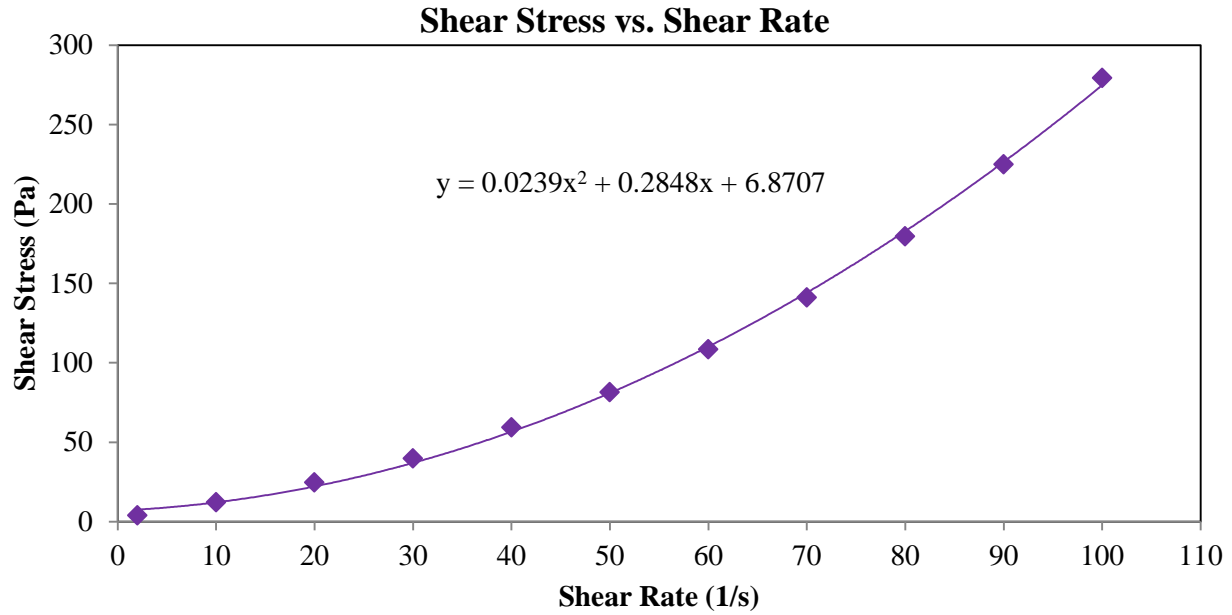
Figure B.2.7 C100: Shear stress versus shear rate at 60 min



**Torque vs. Rotational Speed**

$y = 1.4473x^2 + 31.057x + 343.84$
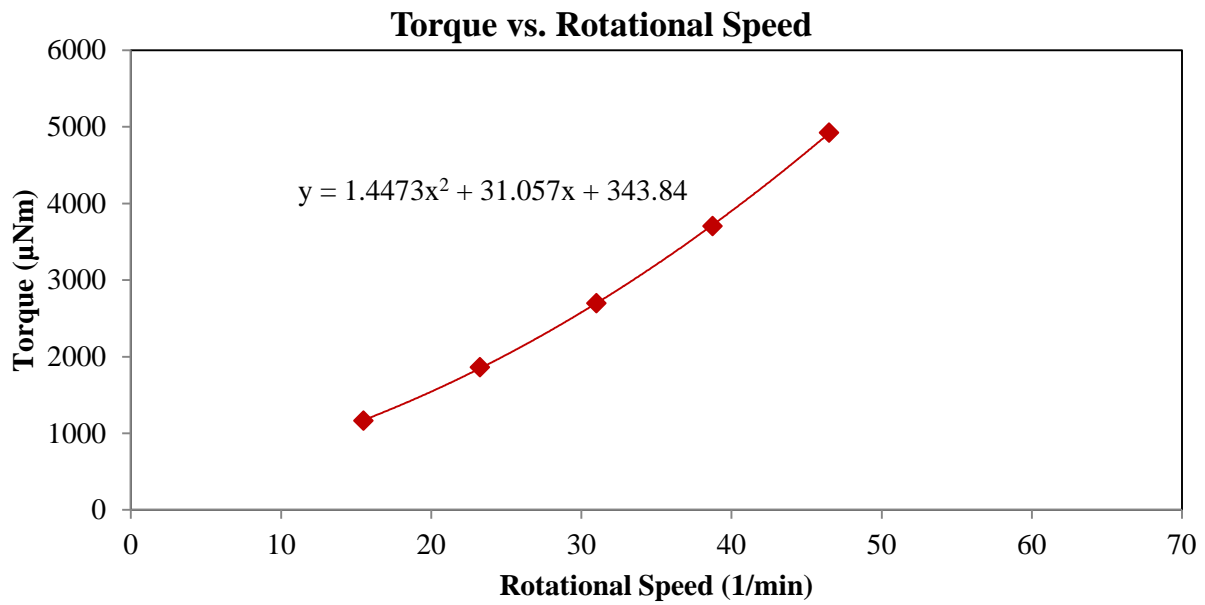
Figure B.2.8 C100: Torque versus rotational speed at 60 min

# Shear Stress vs. Shear Rate

$$y = 0.0239x^2 + 0.2848x + 6.8707$$
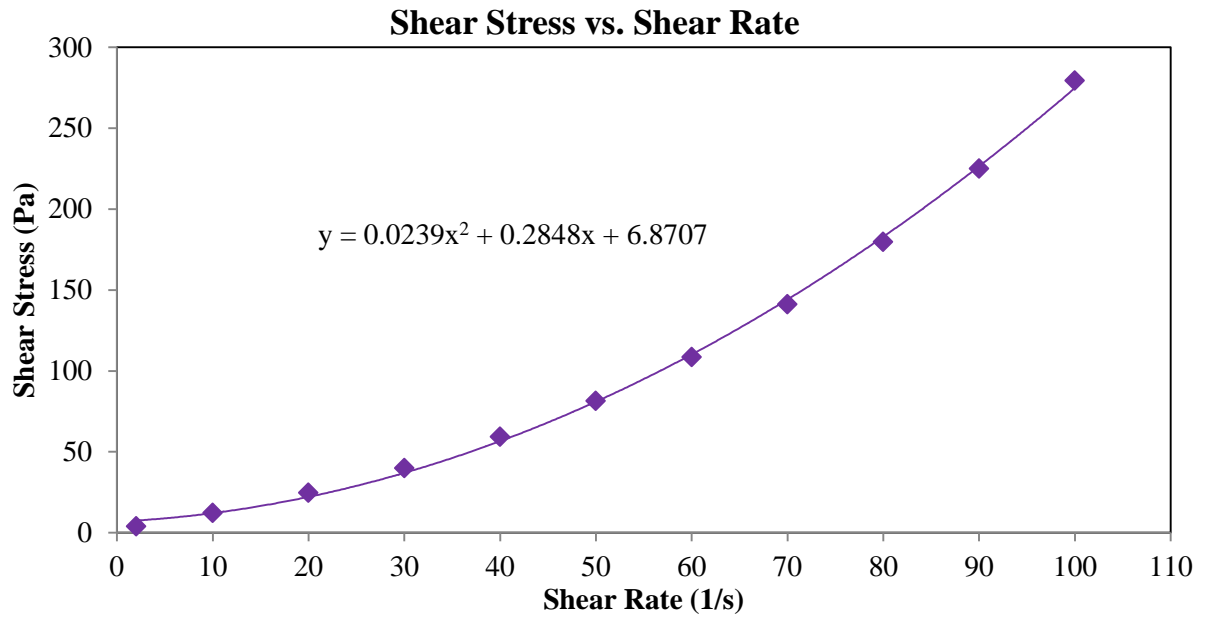
Figure B.2.9 C100: Shear stress versus shear rate at 90 min

# Torque vs. Rotational Speed

$$y = 0.0017x^2 + 0.0299x + 0.3899$$
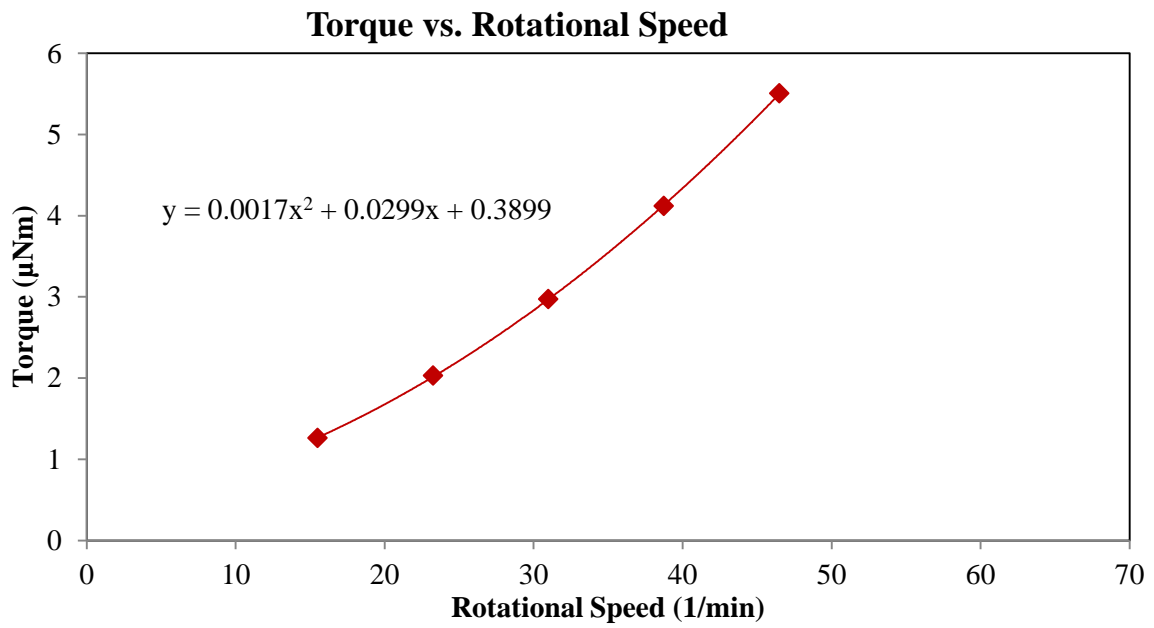
Figure B.2.10 C100: Torque versus rotational speed at 90 min

## Shear Stress vs. Time
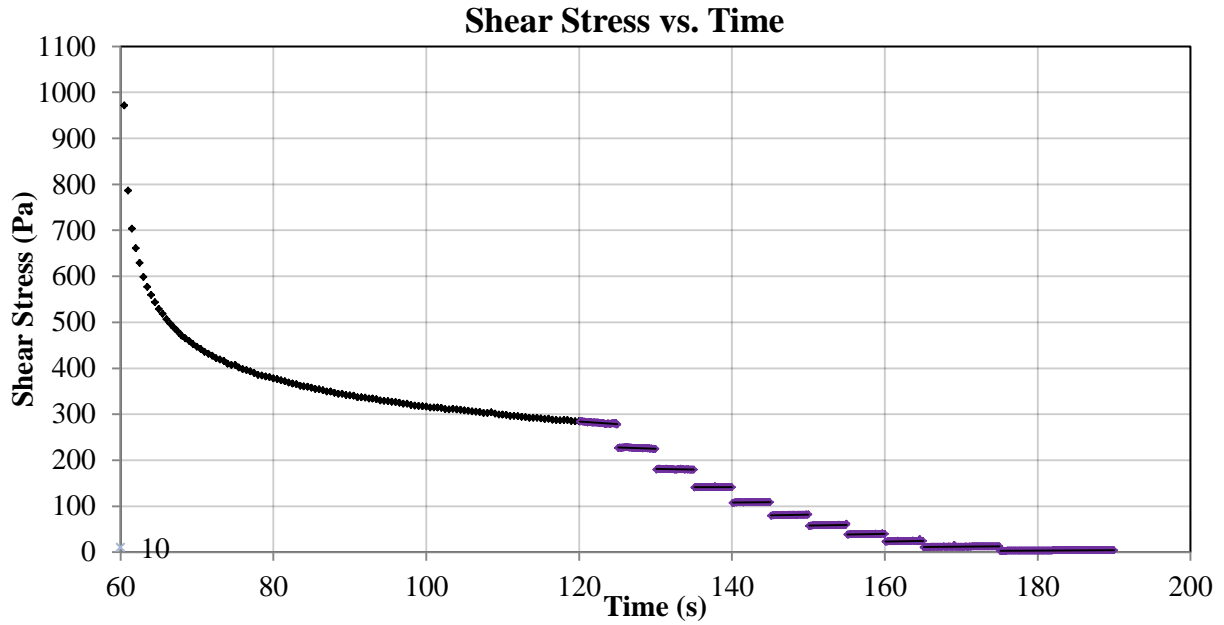


Figure B.3.1 G50SF11: Shear stress versus time at 20 min

## Shear Stress vs. Time
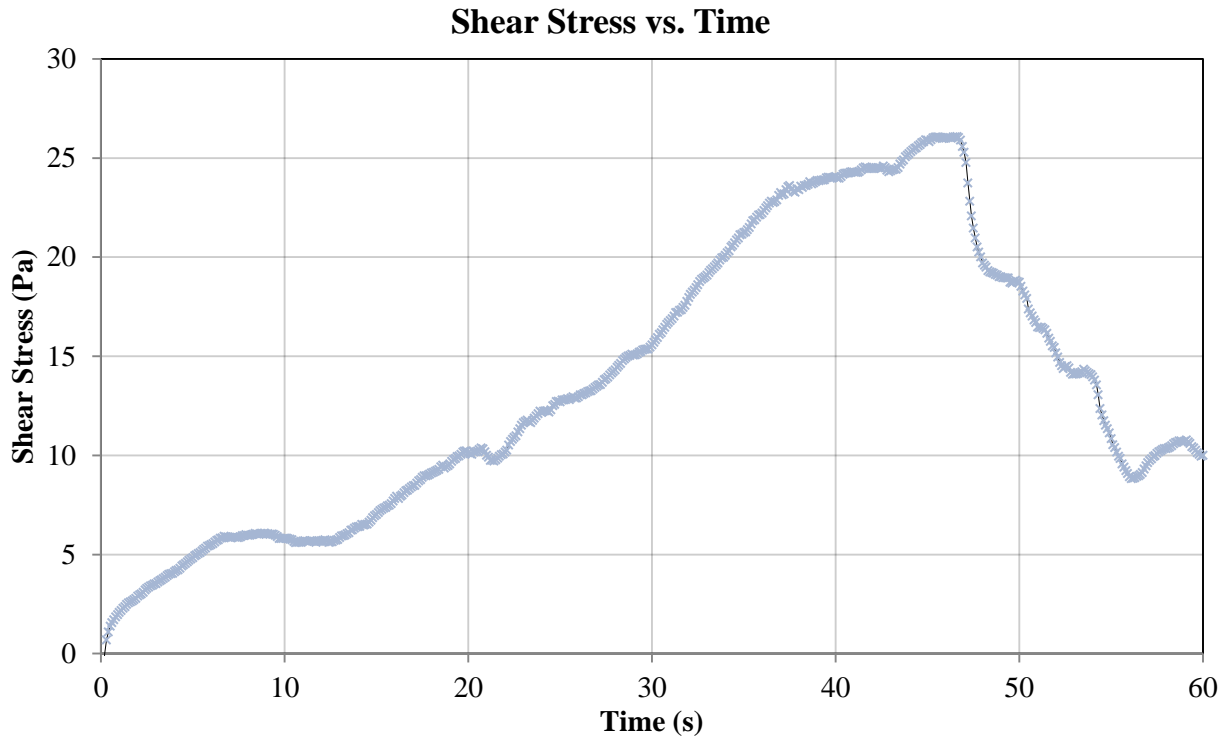


Figure B.3.2 G50SF11: Static yield stress at 20 min

114

## Shear Stress vs. Shear Rate

$y = 0.013x^2 + 0.4005x + 6.6564$
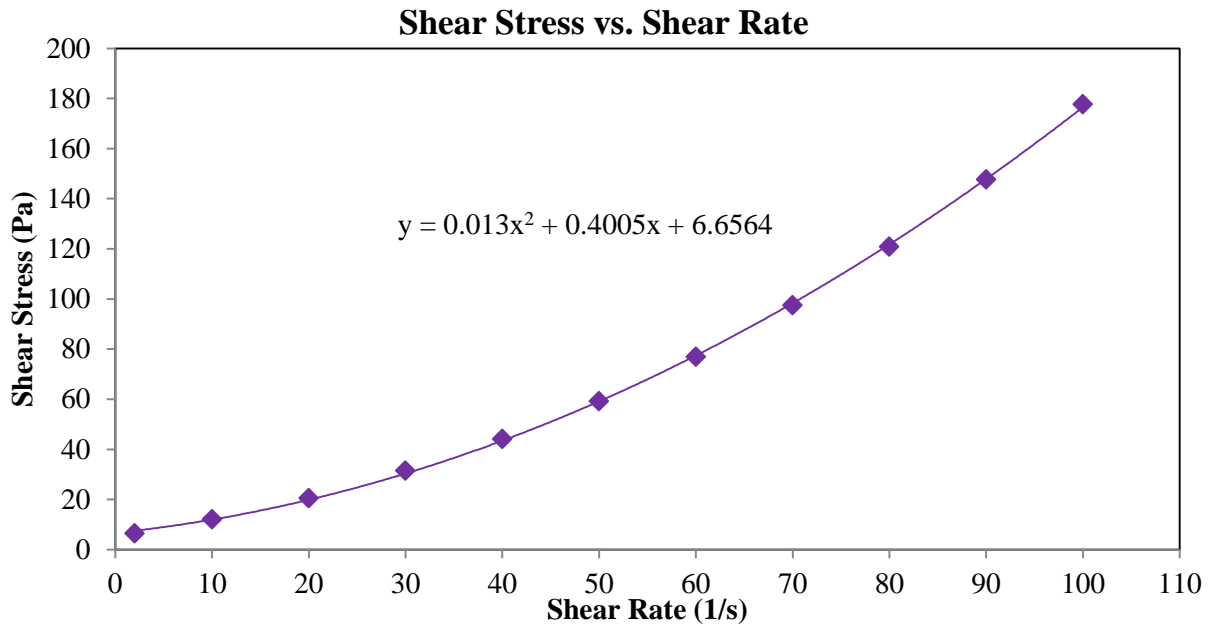
Figure B.3.3 G50SF11: Shear stress versus shear rate at 20 min

## Torque vs. Rotational Speed

$y = 1.1419x^2 + 28.118x + 346.9$
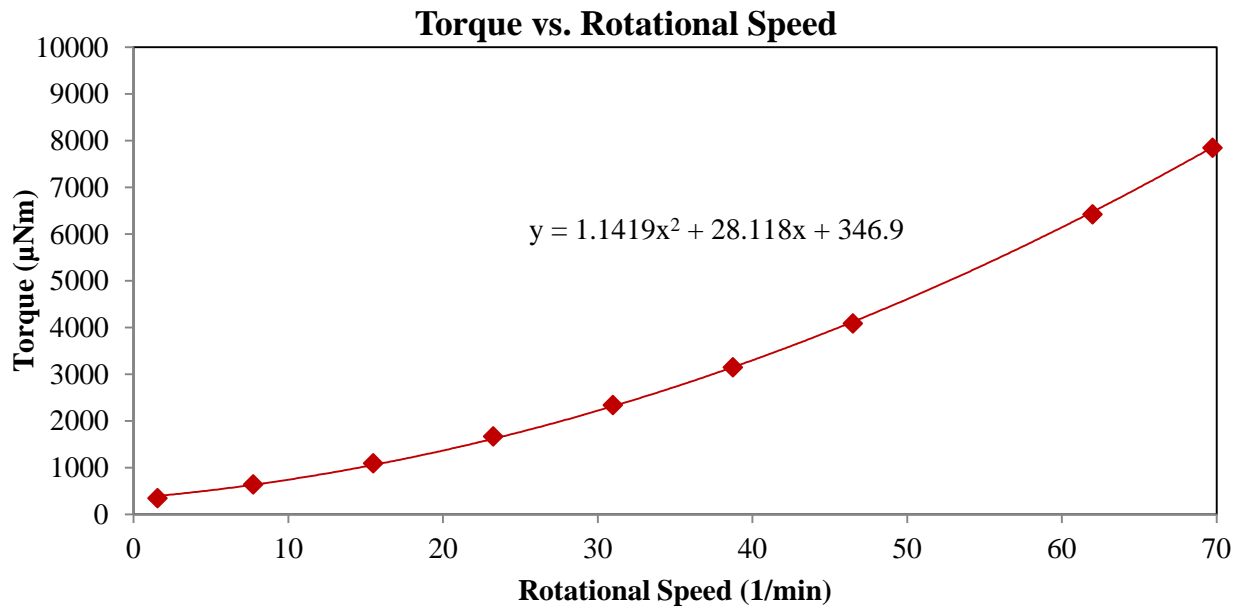
Figure B.3.4 G50SF11: Torque versus rotational speed at 20 min

## Shear Stress vs. Shear Rate

$$y = 0.0131x^2 + 0.5153x + 7.0252$$
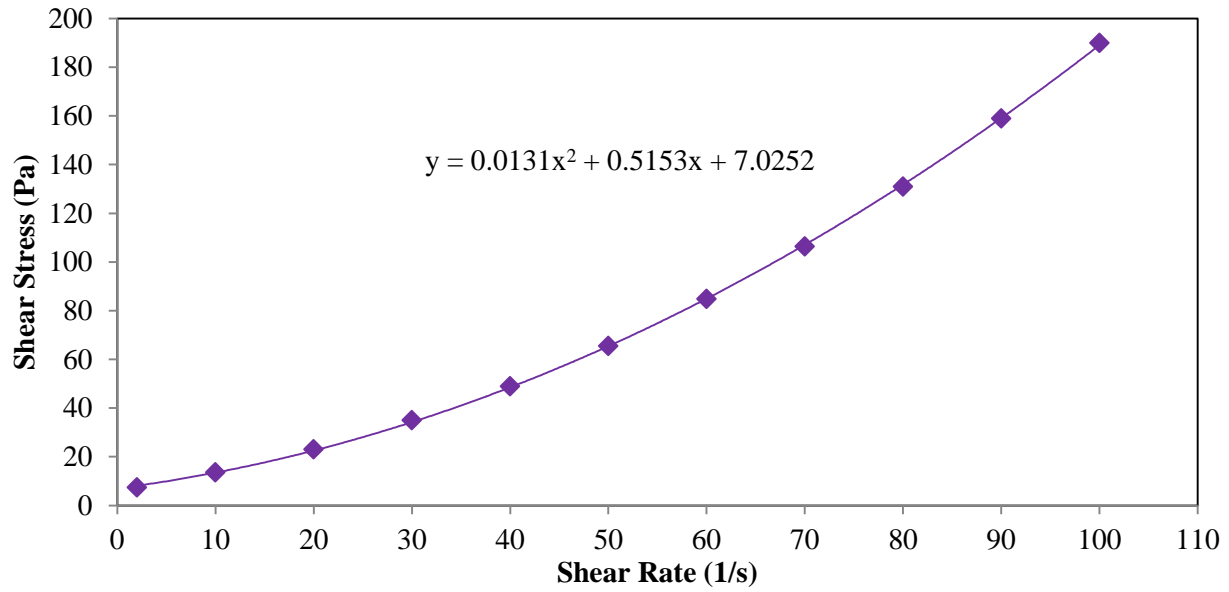
Figure B.3.5 G50SF11: Shear stress versus shear rate at 40 min

## Torque vs. Rotational Speed

$$y = 1.1547x^2 + 35.312x + 373.18$$
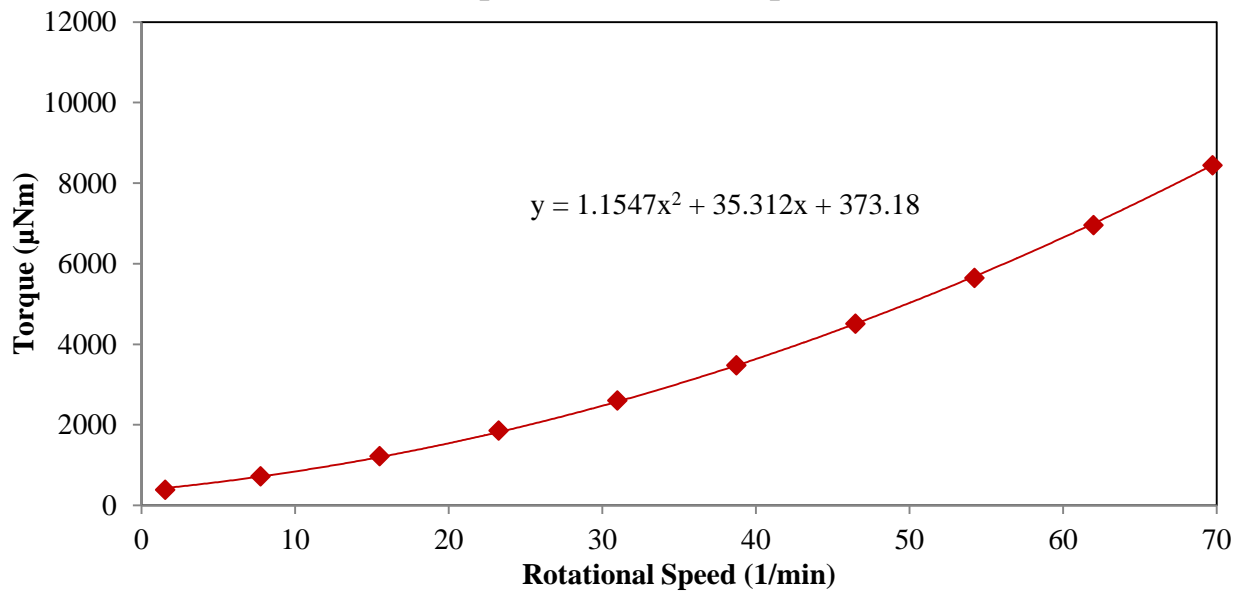
Figure B.3.6 G50SF11: Torque versus rotational speed at 40 min

**Shear Stress vs. Shear Rate**



$y = 0.0134x^2 + 0.6124x + 7.8824$
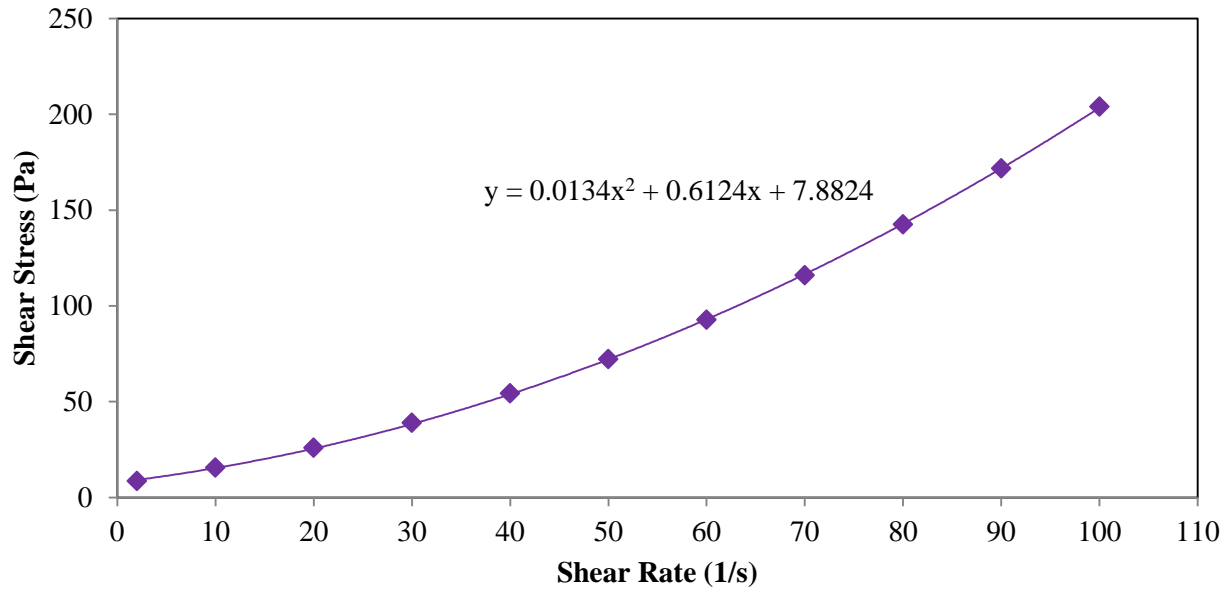
Figure B.3.7 G50SF11: Shear stress versus shear rate at 60 min

**Torque vs. Rotational Speed**



$y = 1.1885x^2 + 41.945x + 418.85$
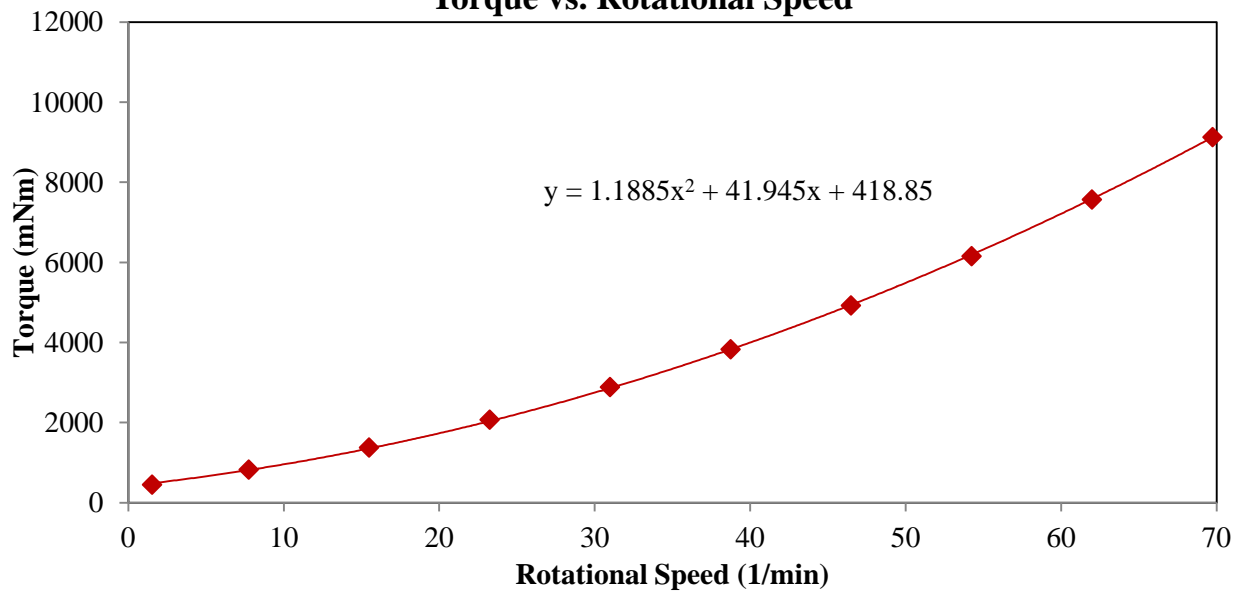
Figure B.3.8 G50SF11: Torque versus rotational speed at 60 min

**Shear Stress vs. Shear Rate**

$$y = 0.0175x^2 + 1.7398x + 13.056$$
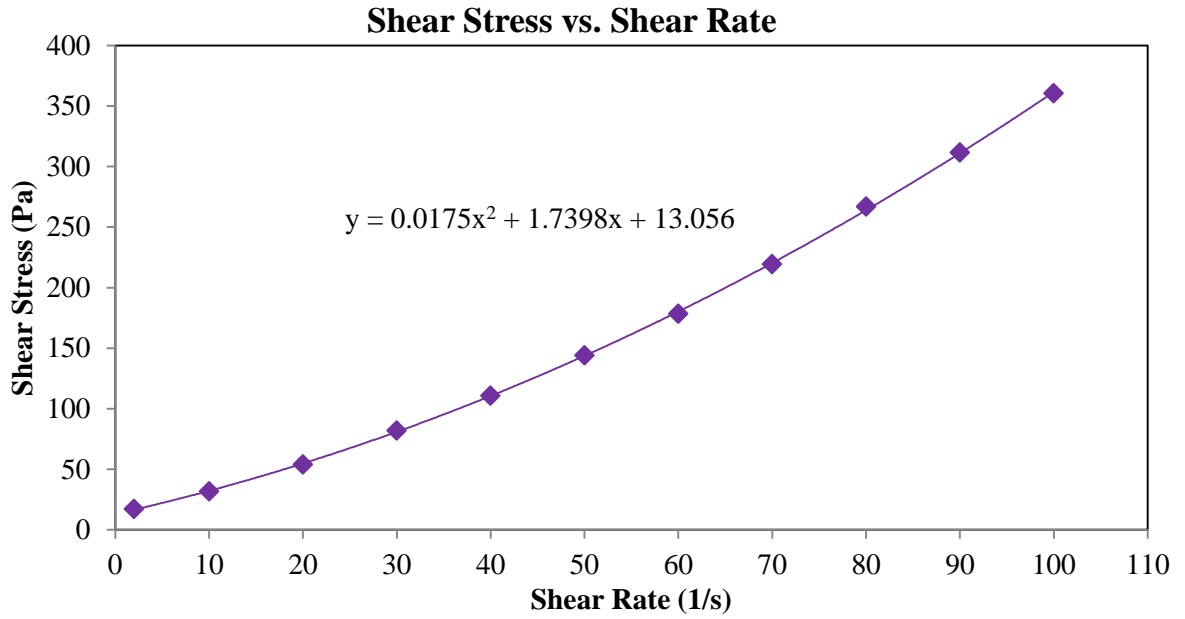
Figure B.3.9 G50SF11: Shear stress versus shear rate at 90 min

**Torque vs. Rotational Speed**

$$y = 1.5454x^2 + 119.19x + 693.89$$
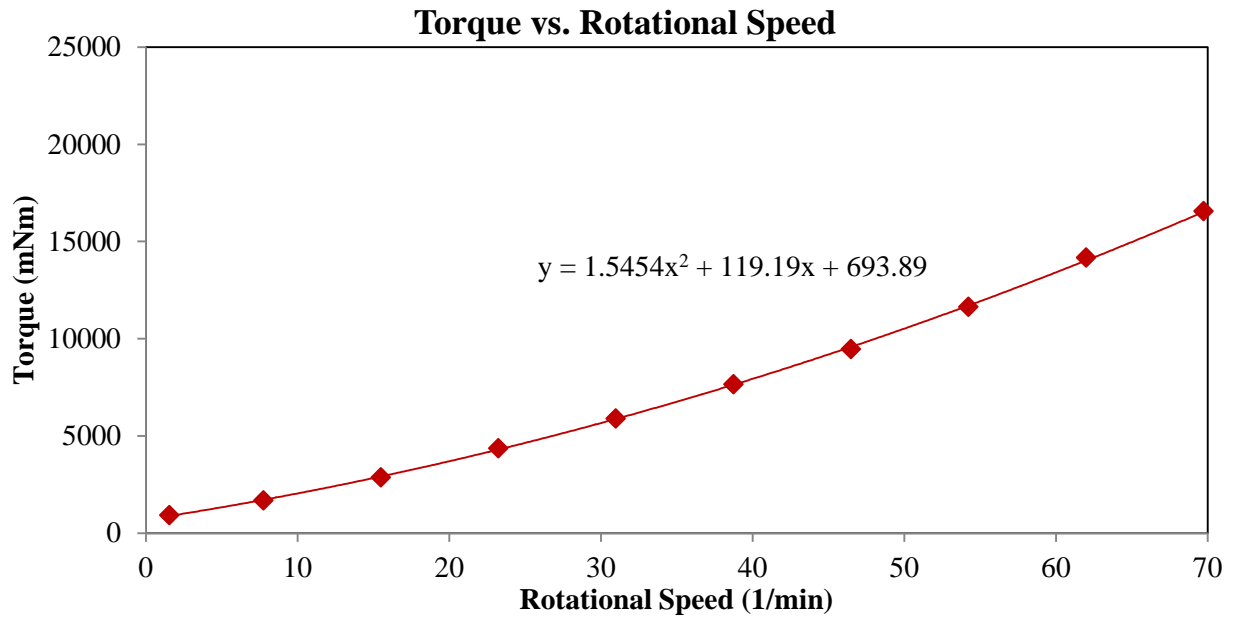
Figure B.3.10 G50SF11: Shear stress versus shear rate at 90 min

**Shear Stress vs. Time**

14.23
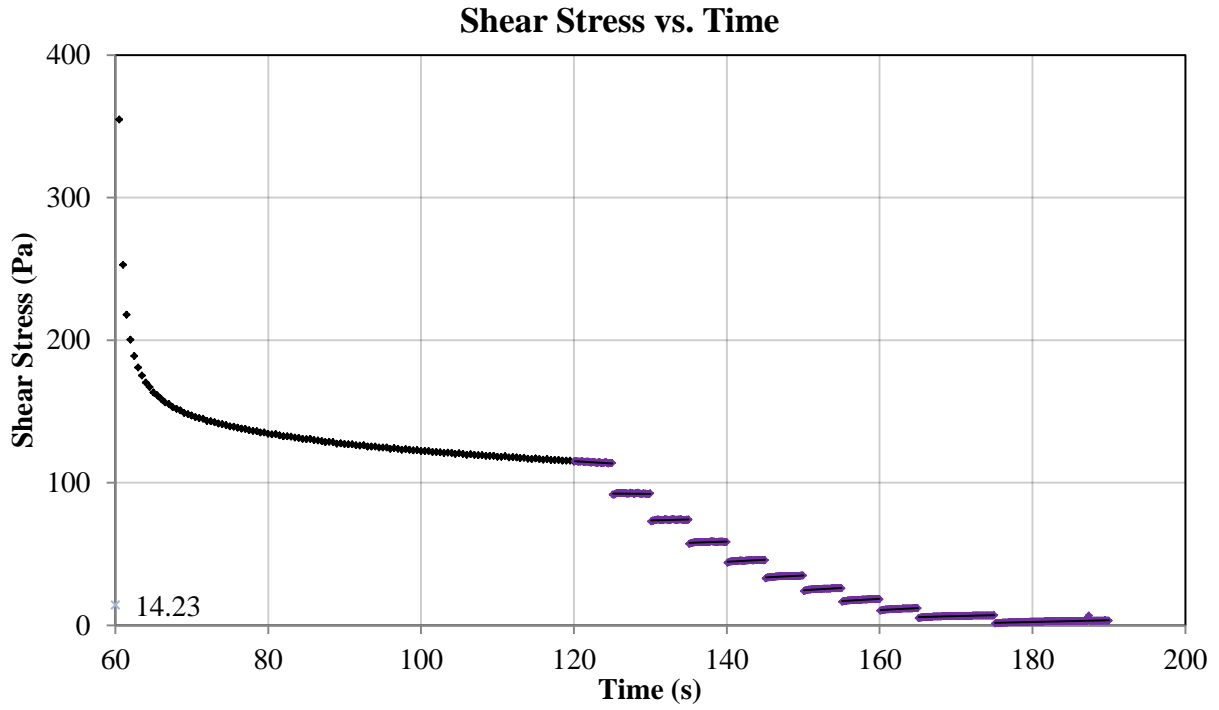
Figure B.4.1 G50SF5: Shear stress versus time at 40 min



**Shear Stress vs. Time**
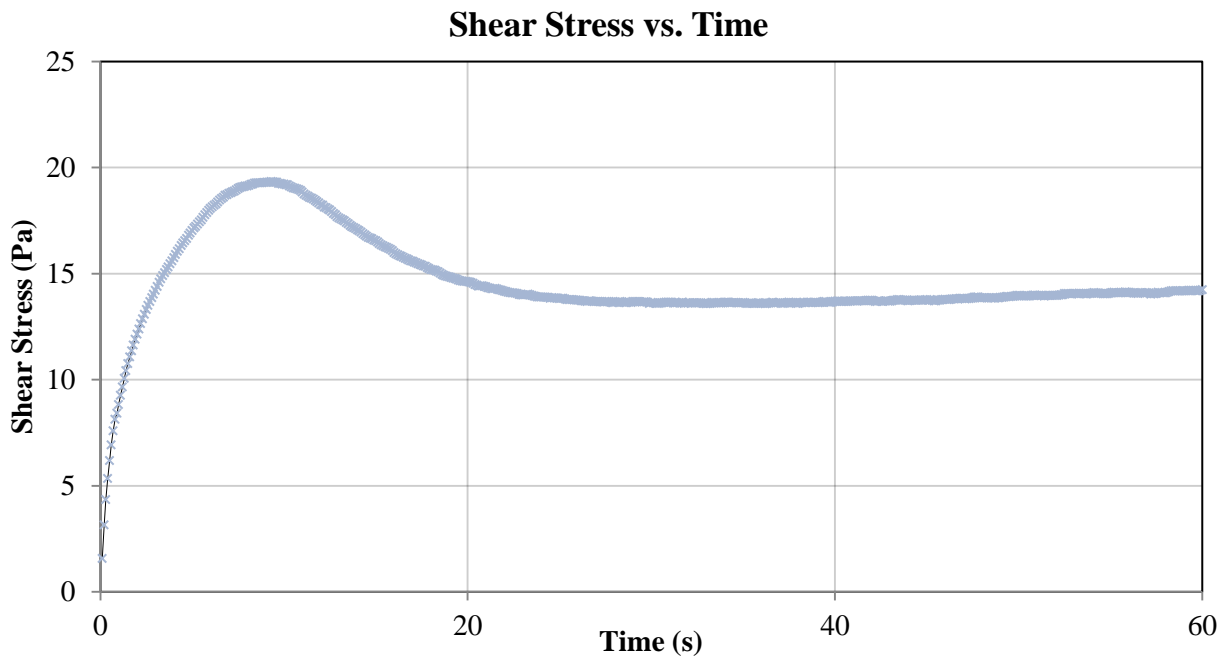
Figure B.4.2 G50SF5:Yield stress at 40 min

**Shear Stress vs. Shear Rate**

$$y = 0.0088x^2 + 0.2128x + 2.8202$$
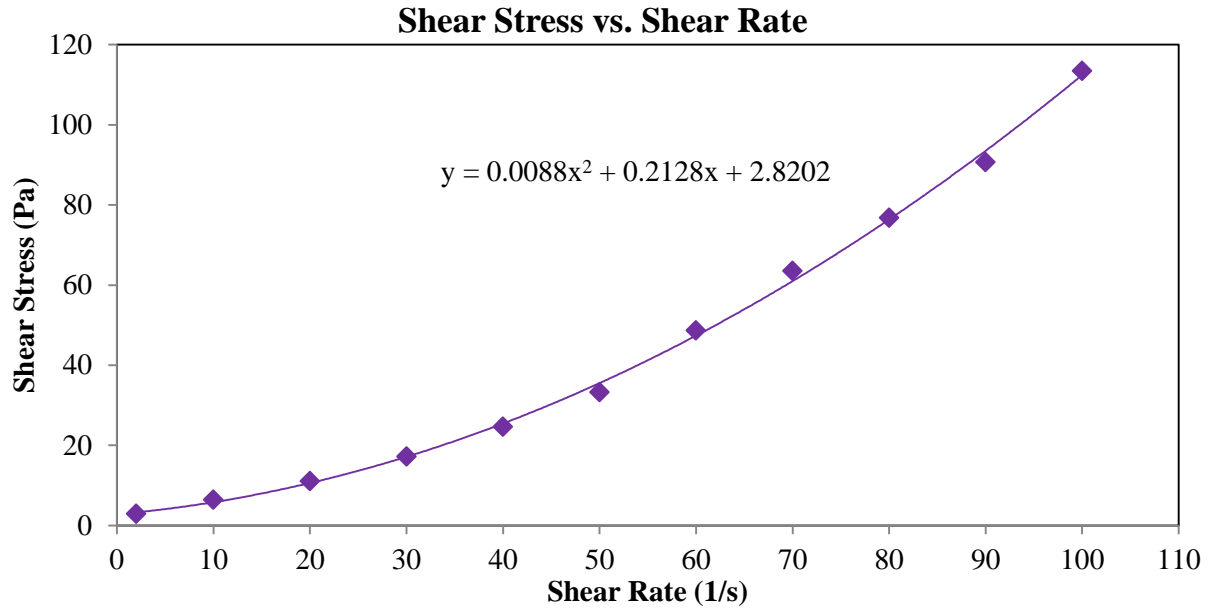
Figure B.4.3 G50SF5: Shear stress versus shear rate at 20 min



**Torque vs. Rotational Speed**

$$y = 1.8579x^2 + 29.244x + 423.53$$
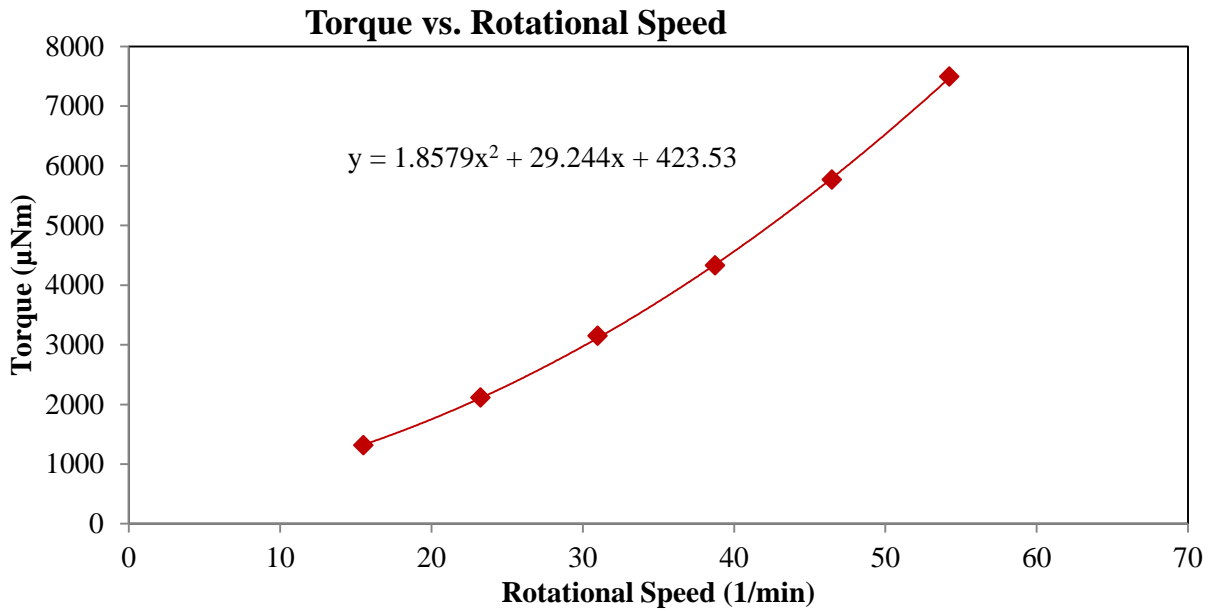
Figure B.4.4 G50SF5: Torque versus rotational speed at 20 min
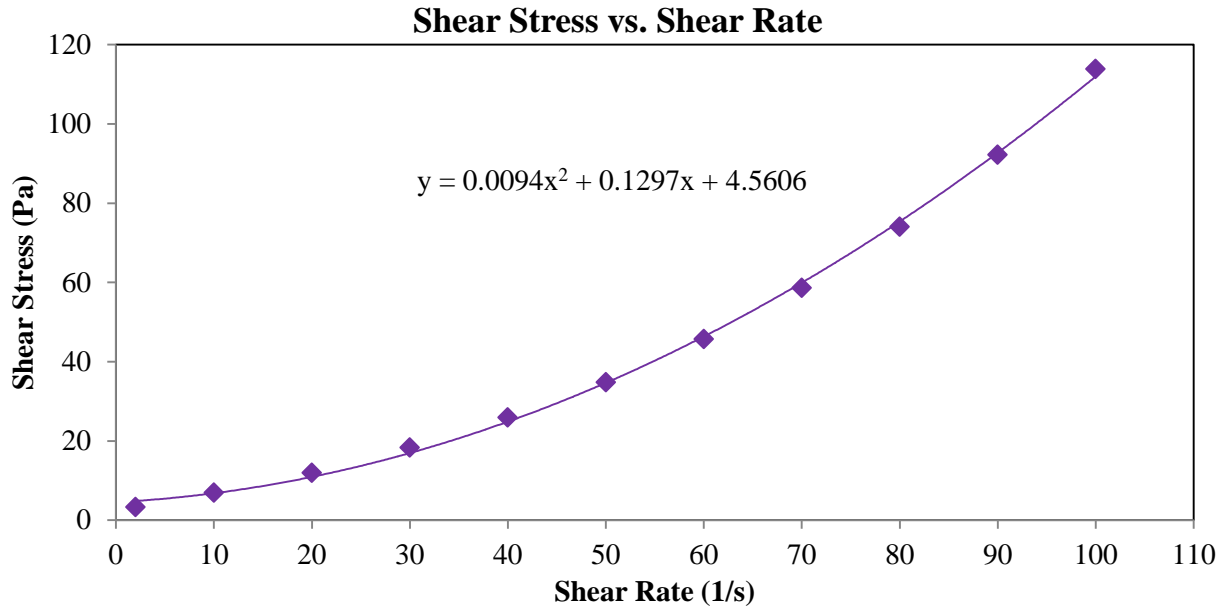
**Figure B.4.5 G50SF5: Shear stress versus shear rate at 40 min**

$$y = 0.0094x^2 + 0.1297x + 4.5606$$
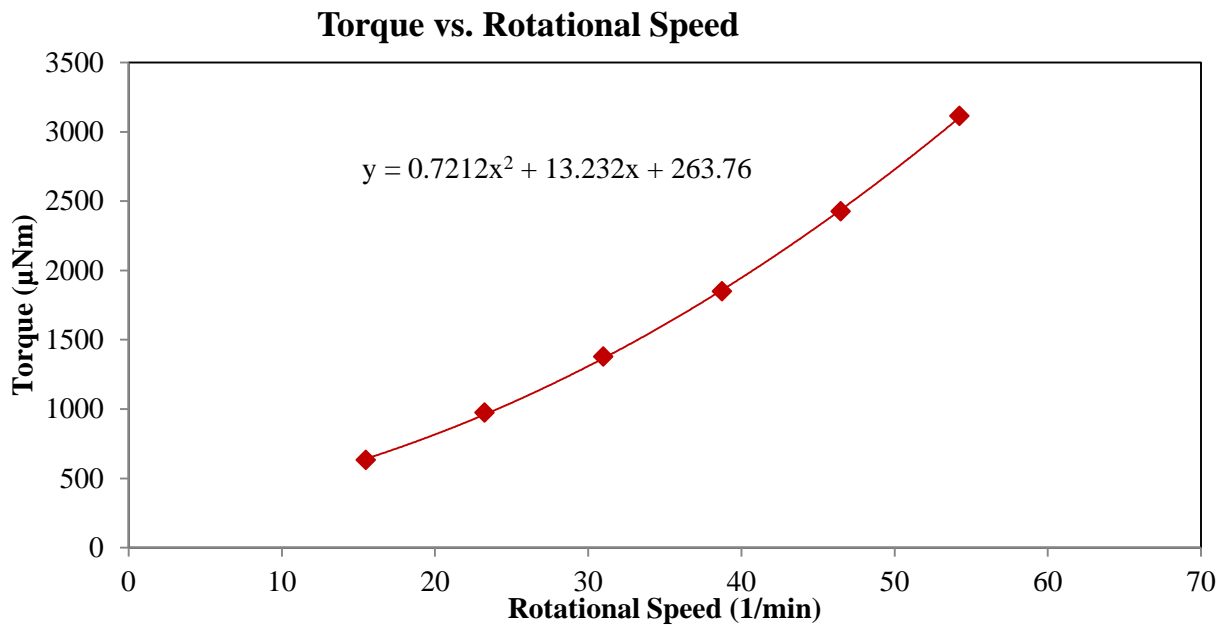


**Figure B.4.6 G50SF5: Torque versus rotational speed at 40 min**

$$y = 0.7212x^2 + 13.232x + 263.76$$
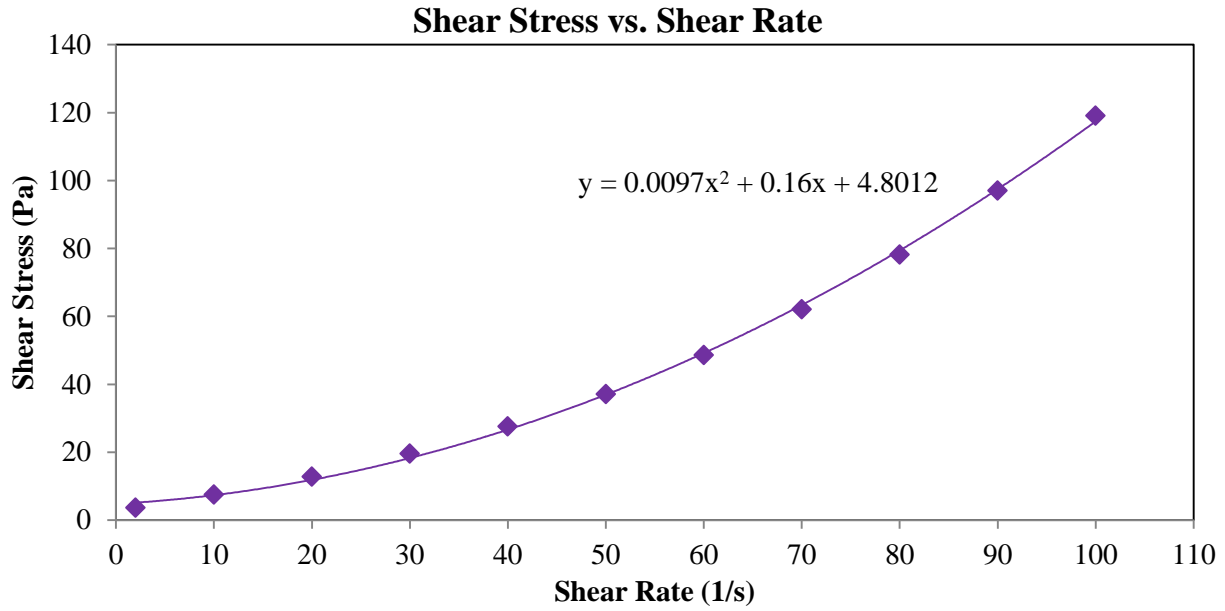
Figure B.4.7 G50SF5: Shear stress versus shear rate at 60 min

$$y = 0.0097x^2 + 0.16x + 4.8012$$
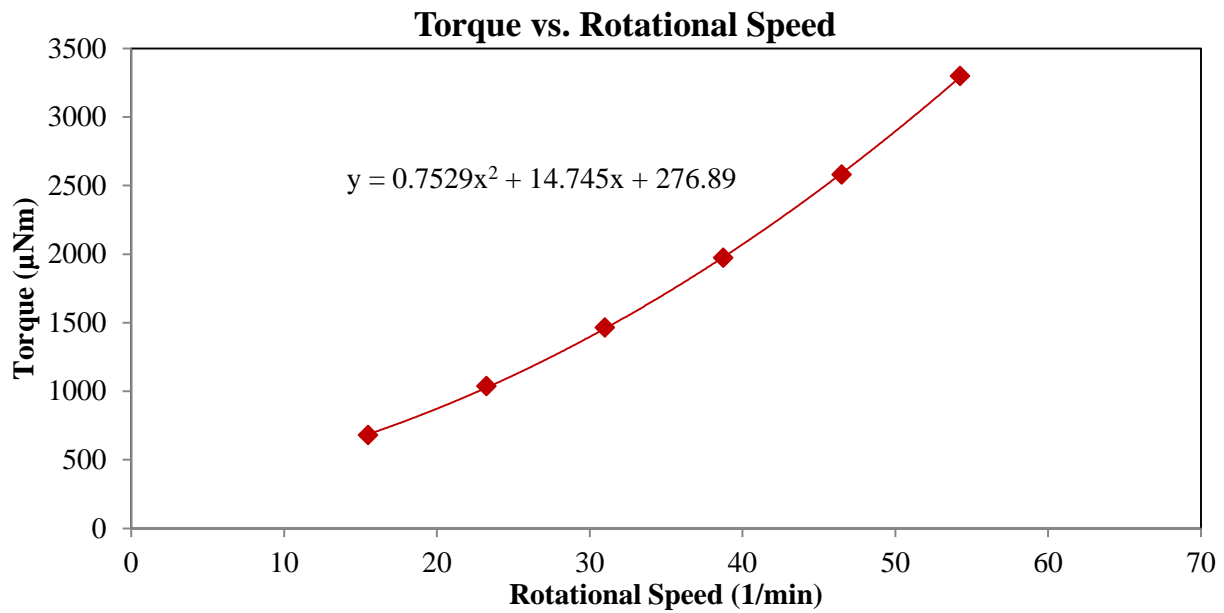


Figure B.4.8 G50SF5: Torque versus rotational speed at 60 min

$$y = 0.7529x^2 + 14.745x + 276.89$$
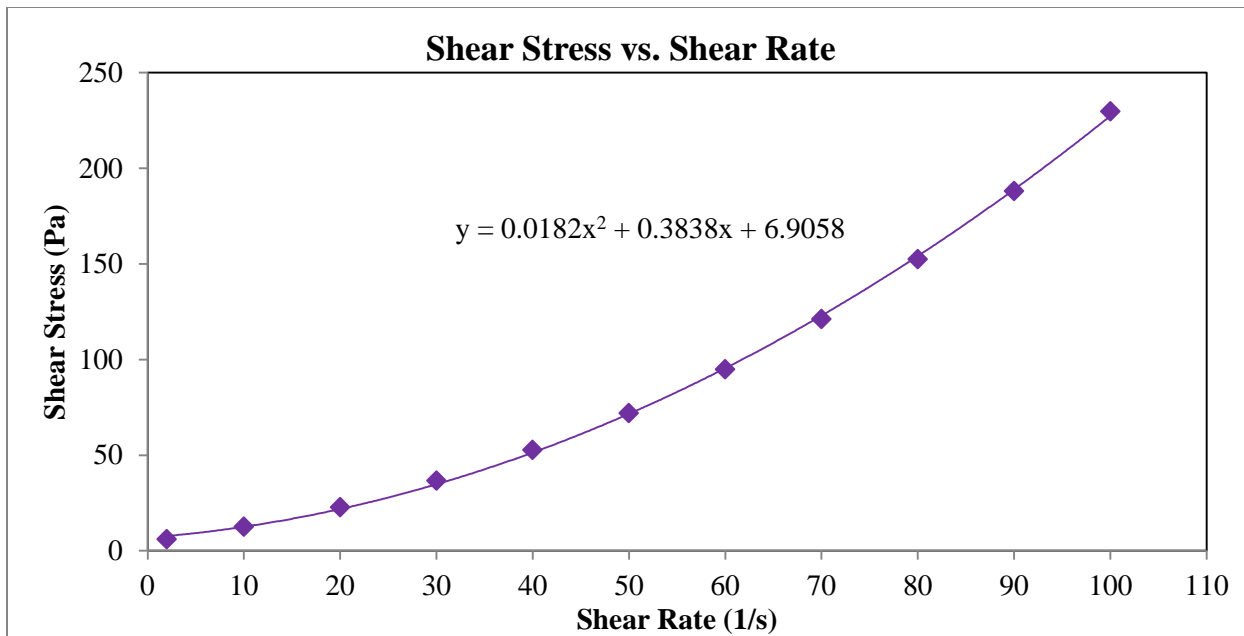
Figure B.4.9 G50SF5: Shear stress versus shear rate at 90 min
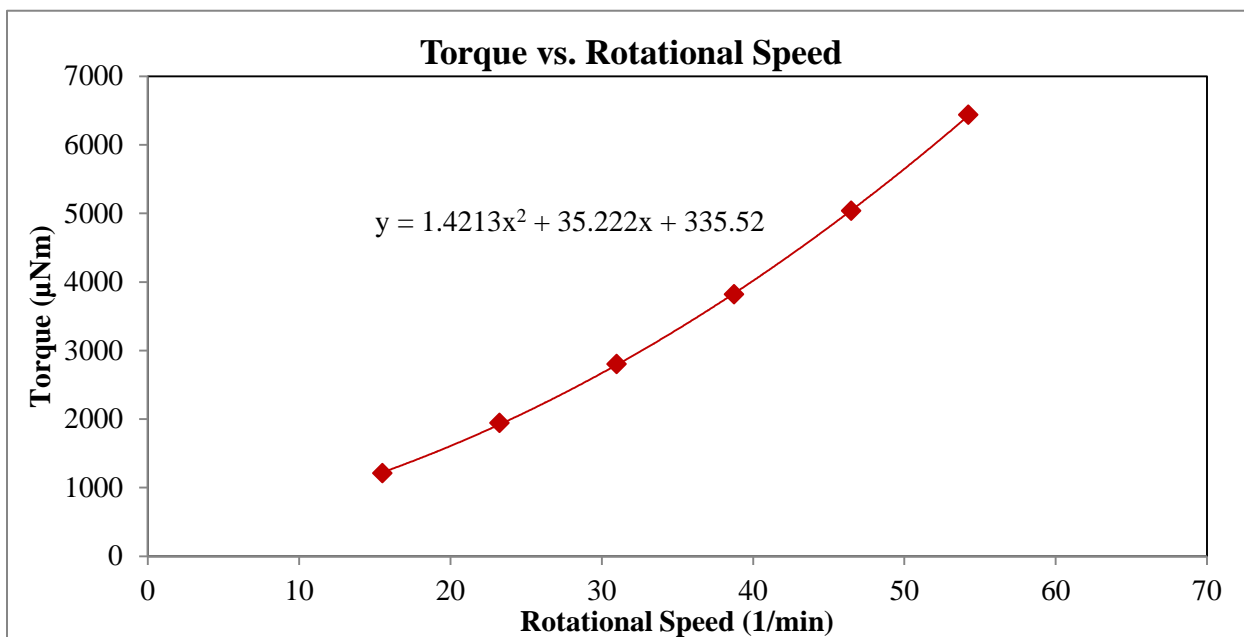


Figure B.4.10 G50SF5: Torque versus rotational speed at 90 min
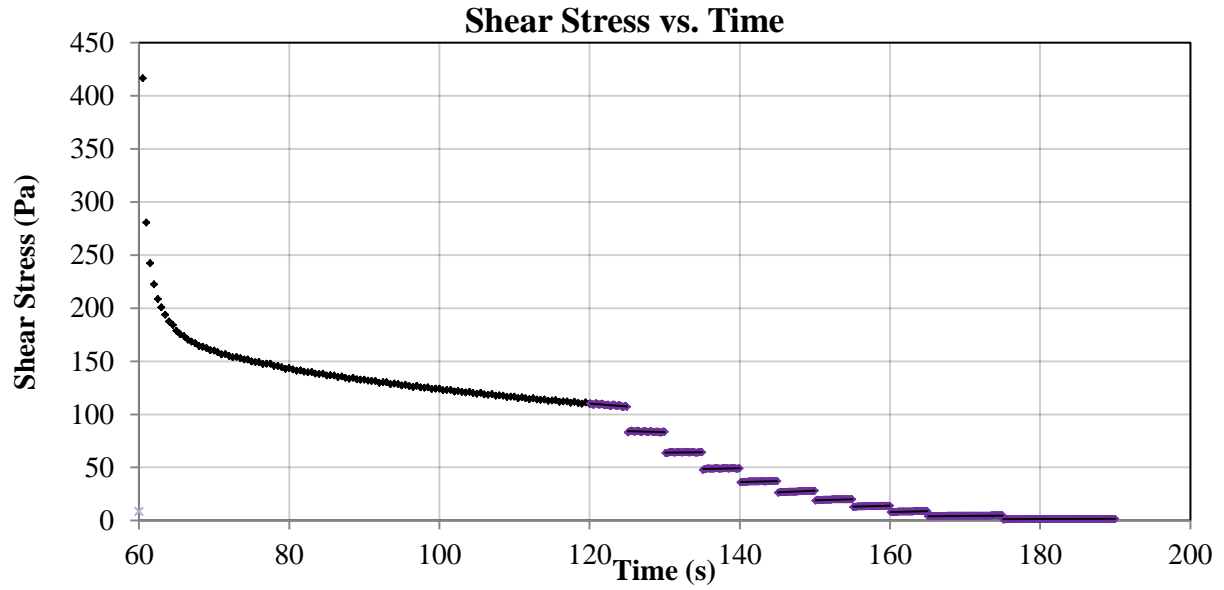
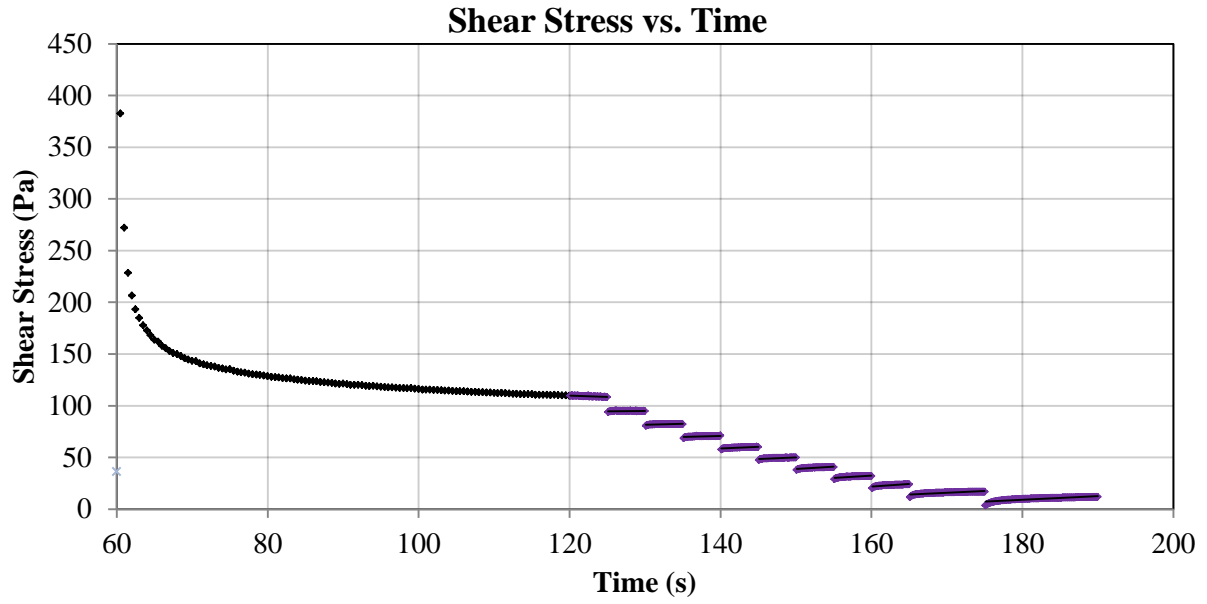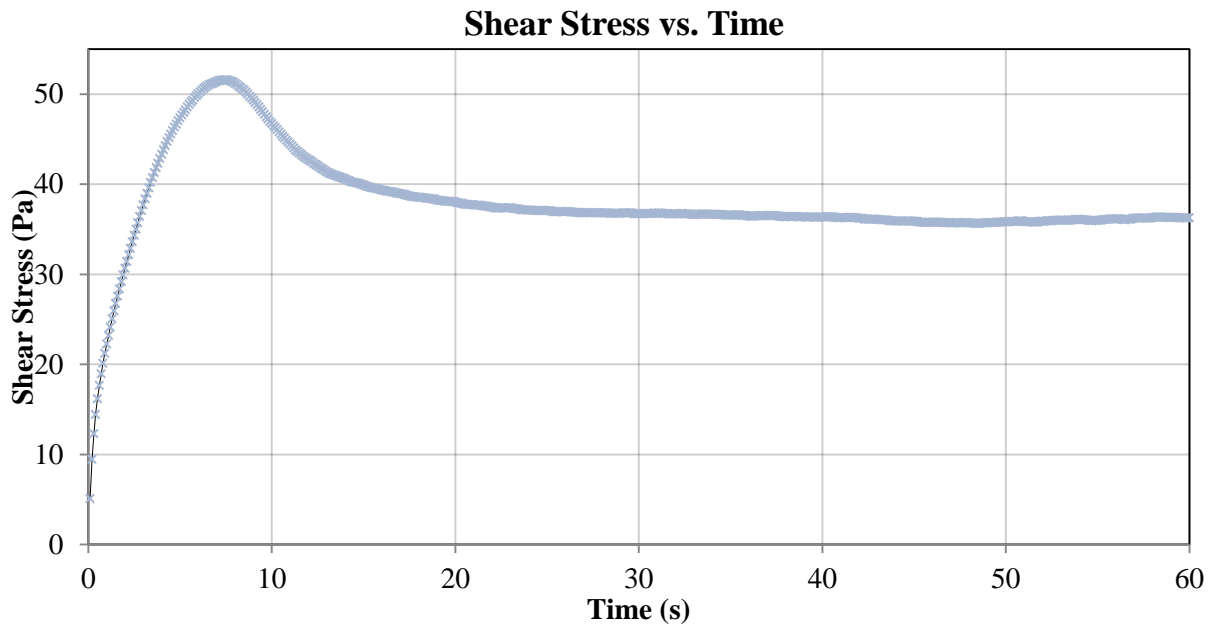Figure B.5.1 G50: Shear stress versus time at 40 min
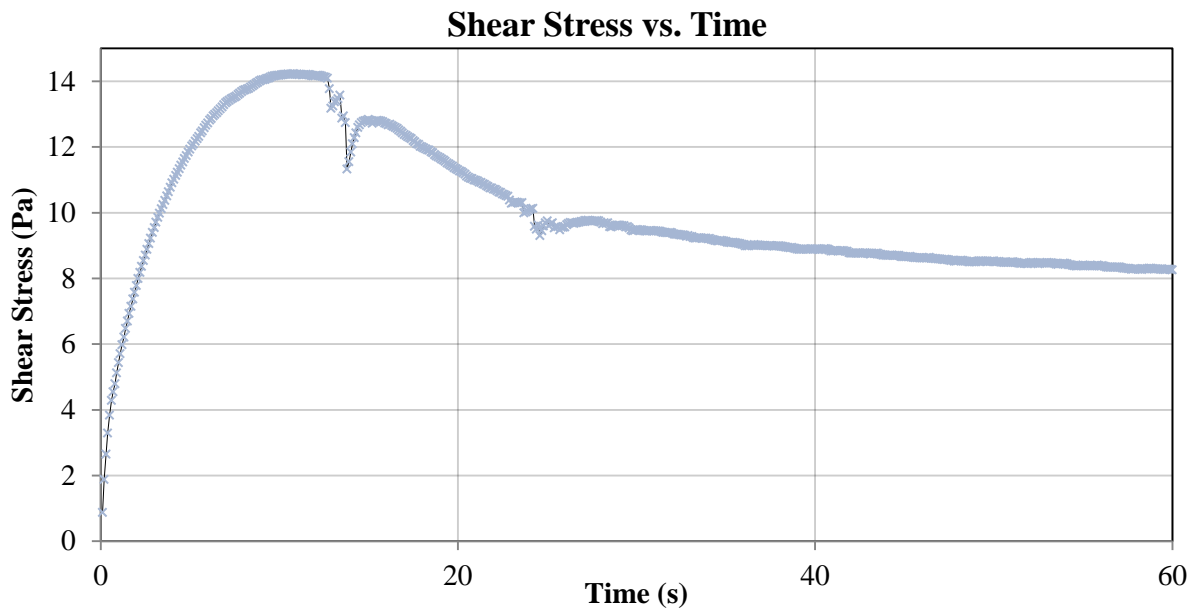


Figure B.5.2 G50: Static yield stress at 40 min

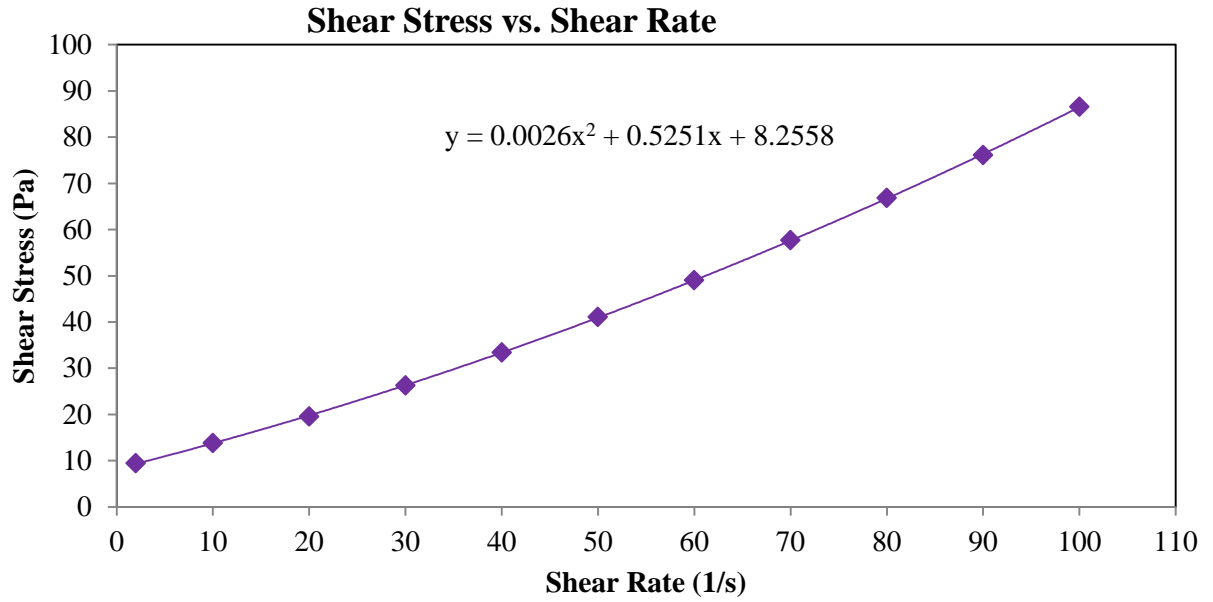**Shear Stress vs. Shear Rate**

$y = 0.0239x^2 + 0.2848x + 6.8707$
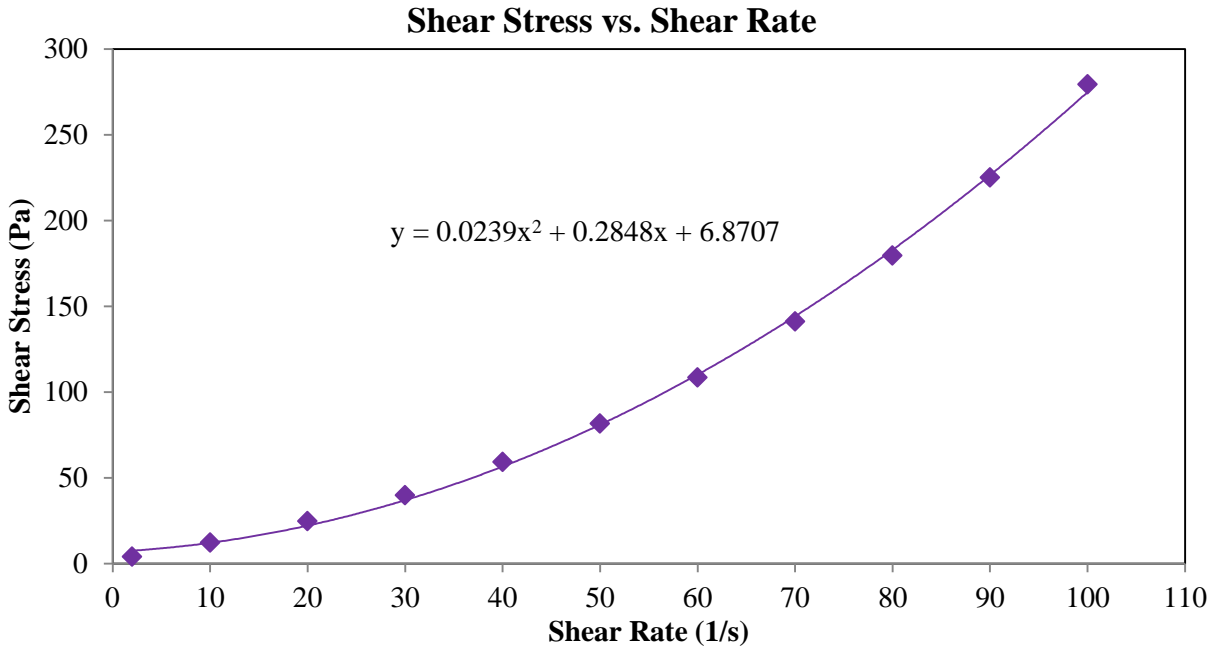
Figure B.5.3 G50: Shear stress versus shear rate at 20 min



**Torque vs. Rotational Speed**

$y = 0.7859x^2 + 9.8904x + 160.12$
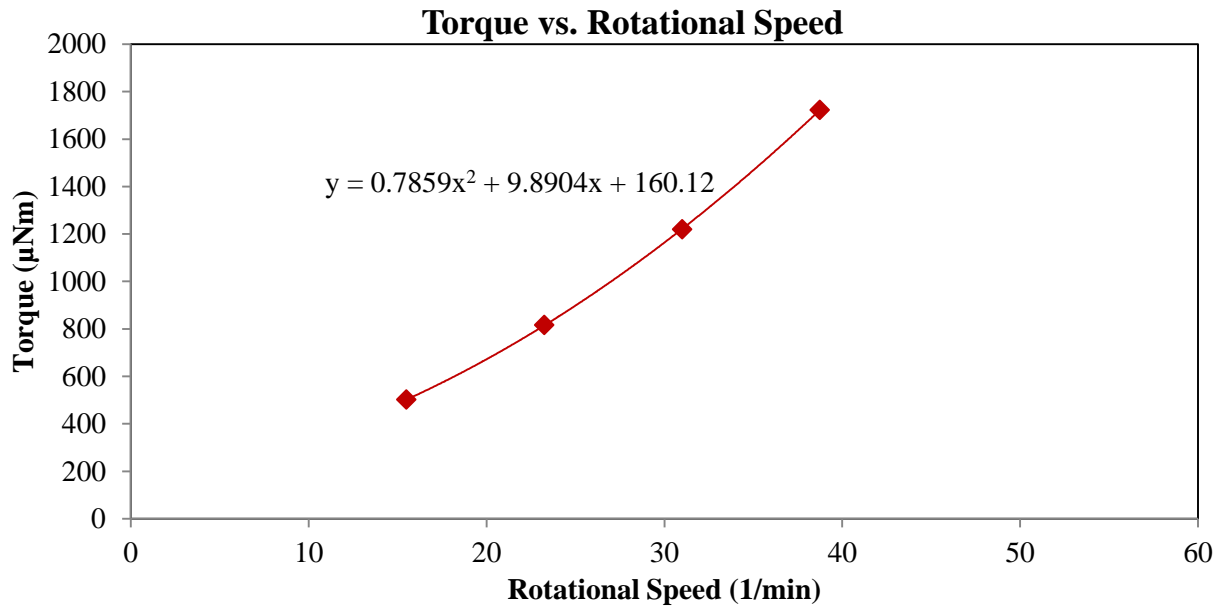
Figure B.5.4 G50: Torque versus rotational speed at 20 min

## Shear Stress vs. Shear Rate



$$y = 0.0108x^2 - 0.0883x + 4.3836$$
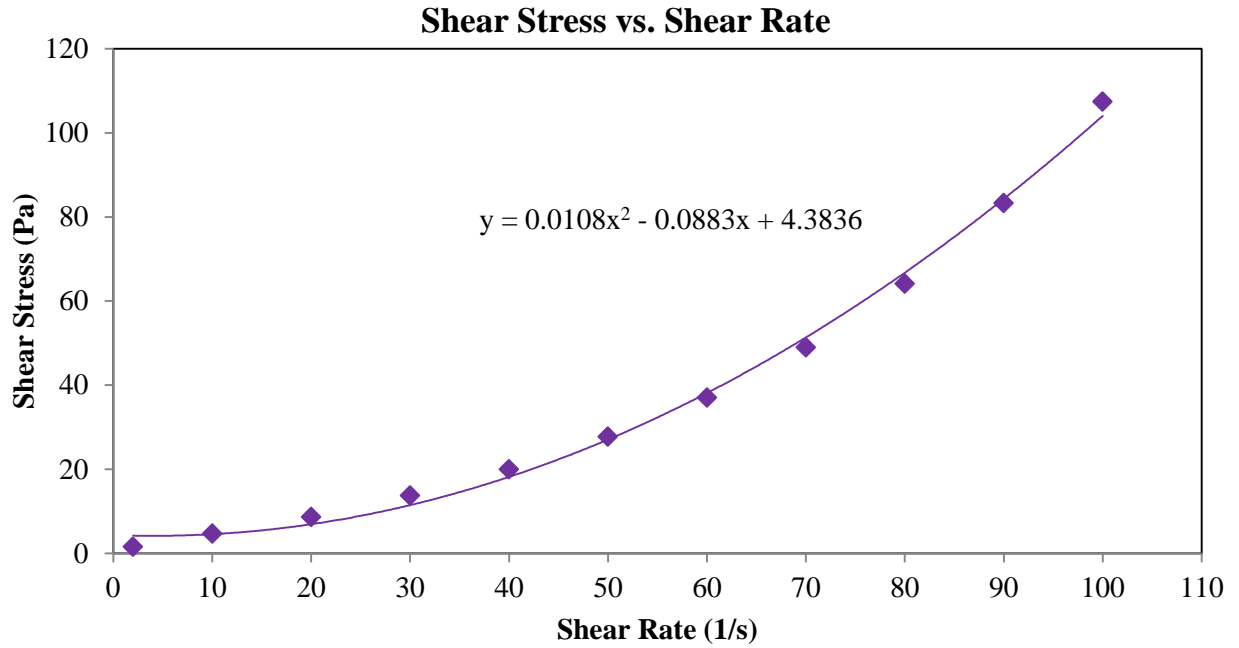
Figure B.5.5 G50: Shear stress versus shear rate at 40 min

## Torque vs. Rotational Speed



$$y = 0.6301x^2 + 9.4335x + 164.71$$
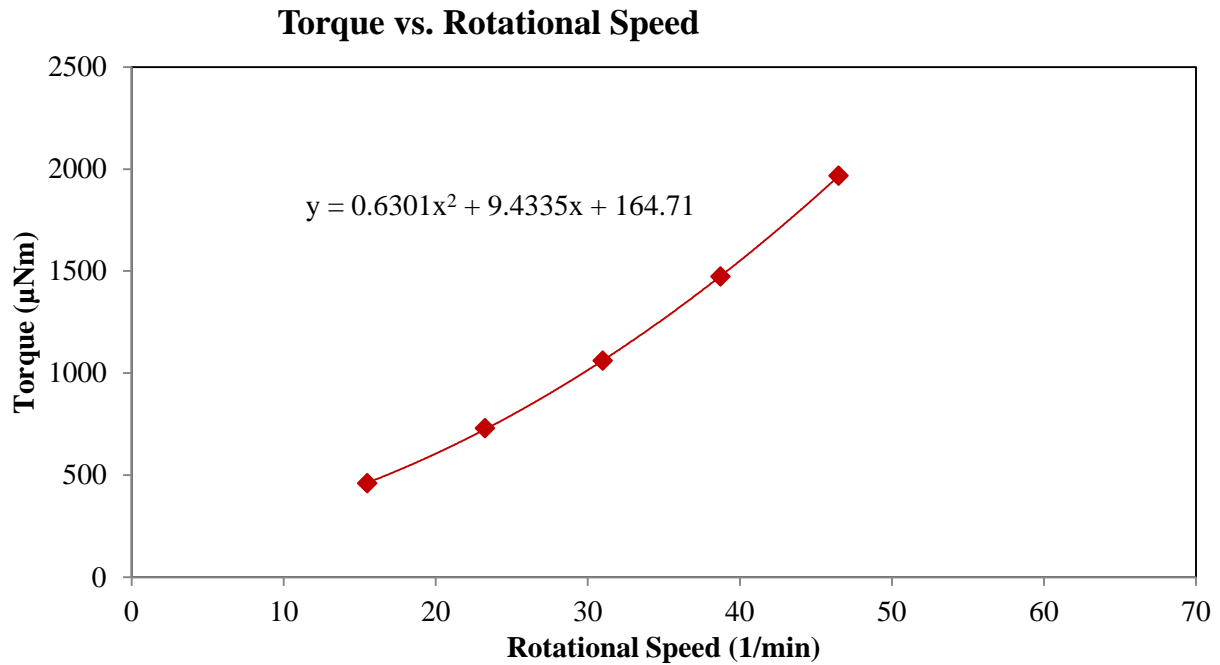
Figure B.5.6 G50: Torque versus rotational speed at 40 min

126

## Shear Stress vs. Shear Rate

$y = 0.0095x^2 - 0.0225x + 3.8721$
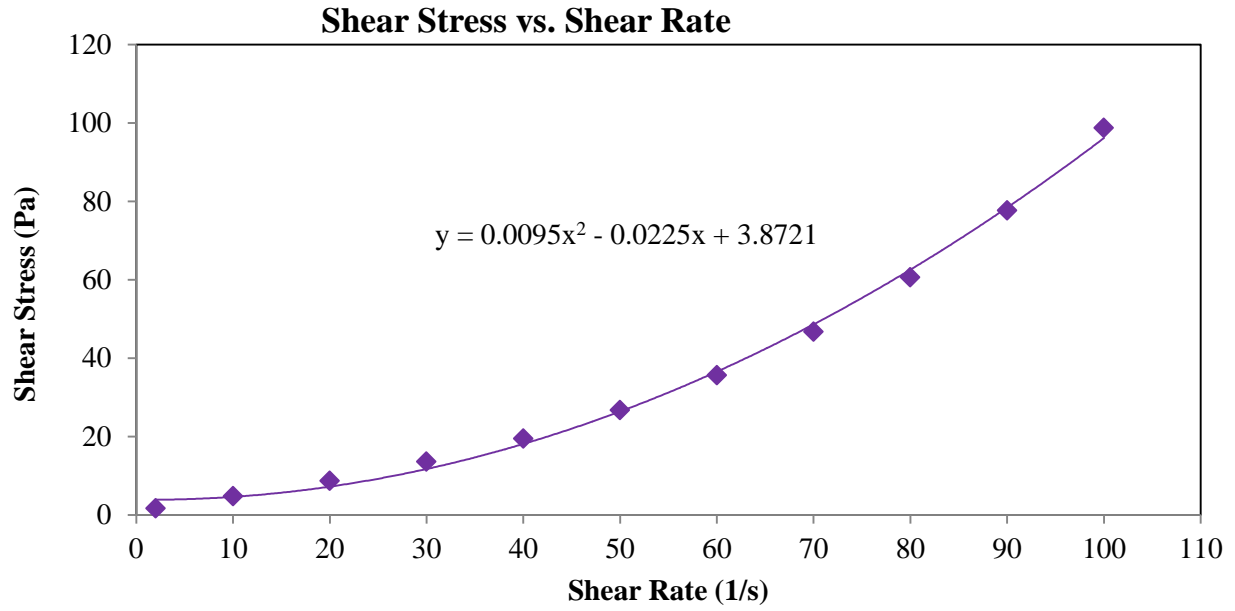
Figure B.5.7 G50: Shear stress versus shear rate at 60 min

## Torque vs. Rotational Speed

$y = 0.593x^2 + 9.2841x + 176.28$
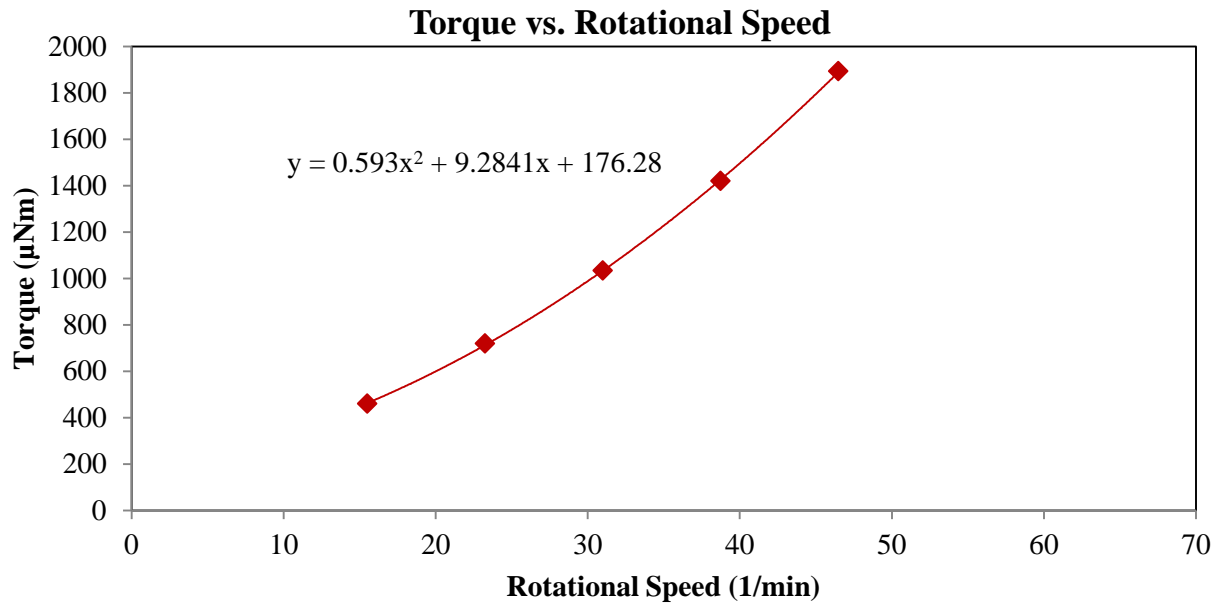
Figure B.5.8 G50: Torque versus rotational speed at 60 min

## Shear Stress vs. Shear Rate

$y = 0.0215x^2 - 0.2411x + 6.2198$
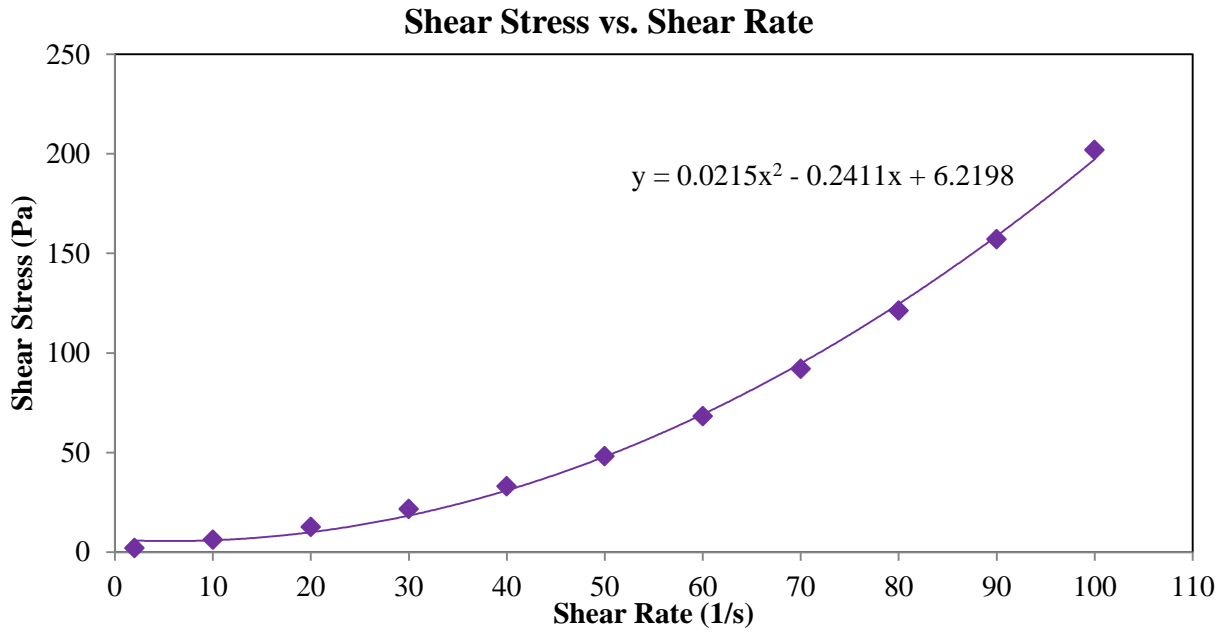
Figure B.5.9 G50: Shear stress versus shear rate at 90 min

## Torque vs. Rotational Speed

$y = 1.3367x^2 + 8.3457x + 220.17$
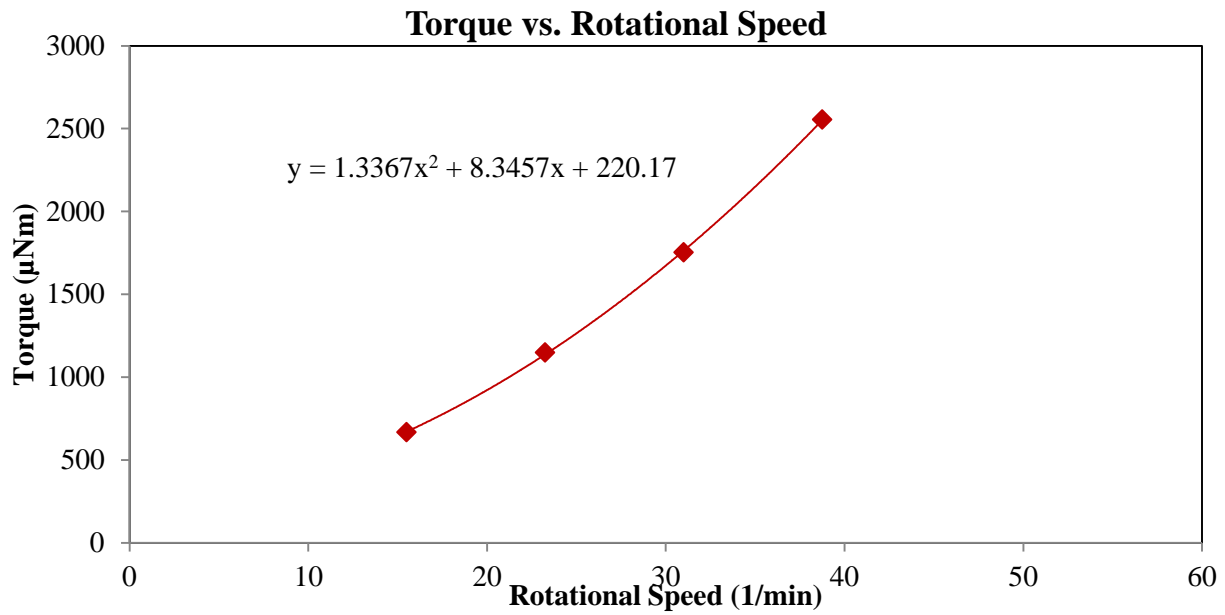
Figure B.5.10 G50: Torque versus rotational speed at 90 min
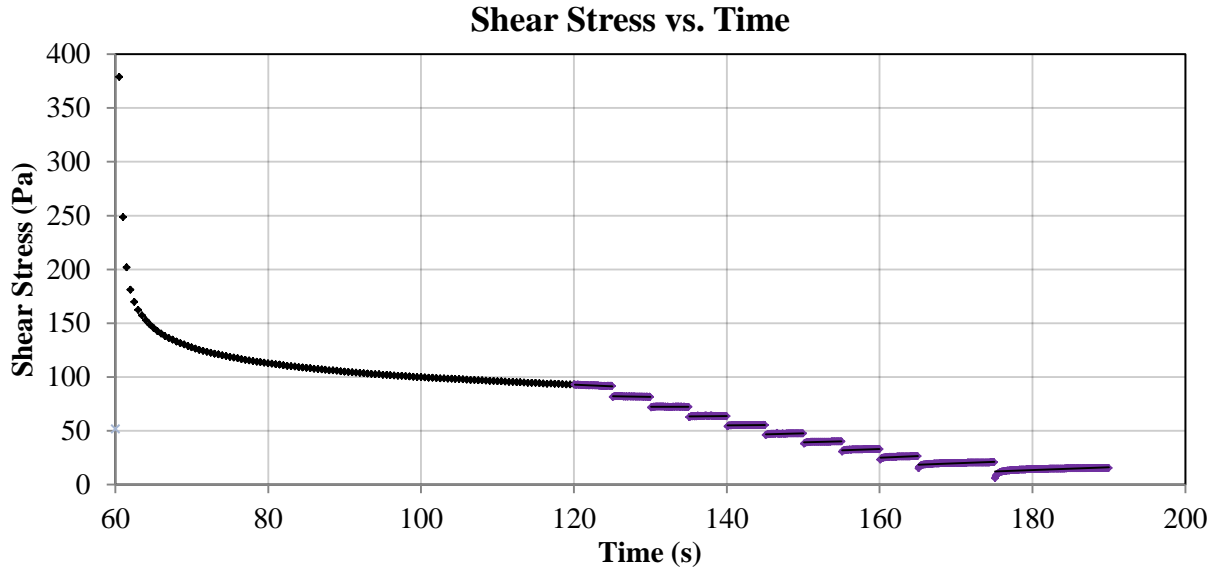
Figure B.6.1 FAC60: Shear stress versus time at 40 min
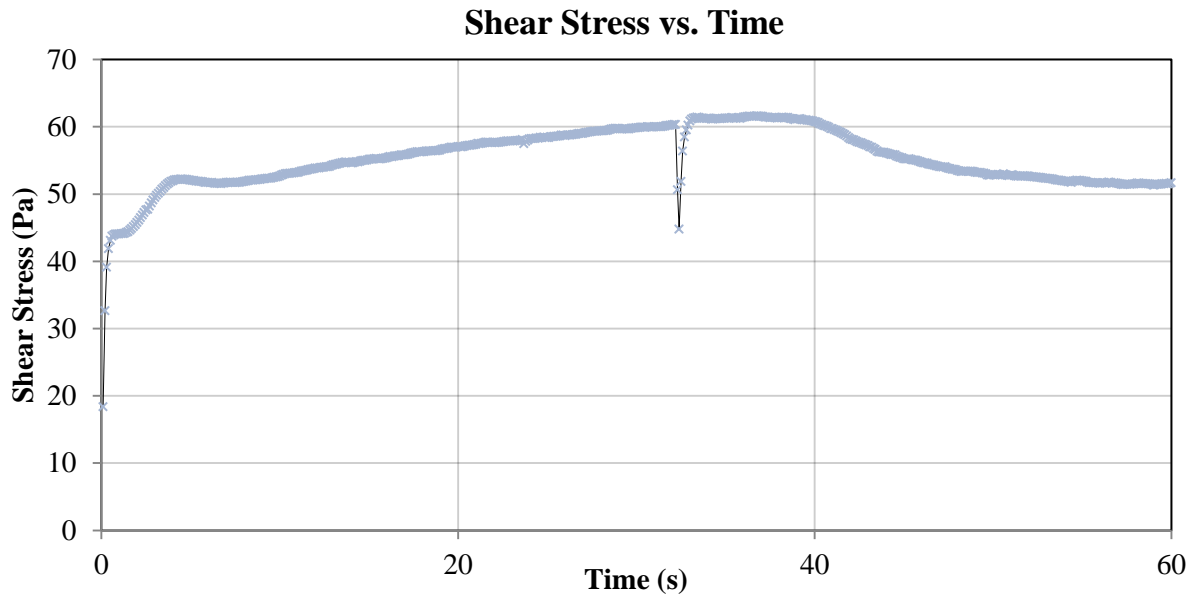


Figure B.6.2 FAC60: Static yield stress at 40 min

**Shear Stress vs. Shear Rate**

$y = 0.0016x^2 + 0.4059x + 10.79$
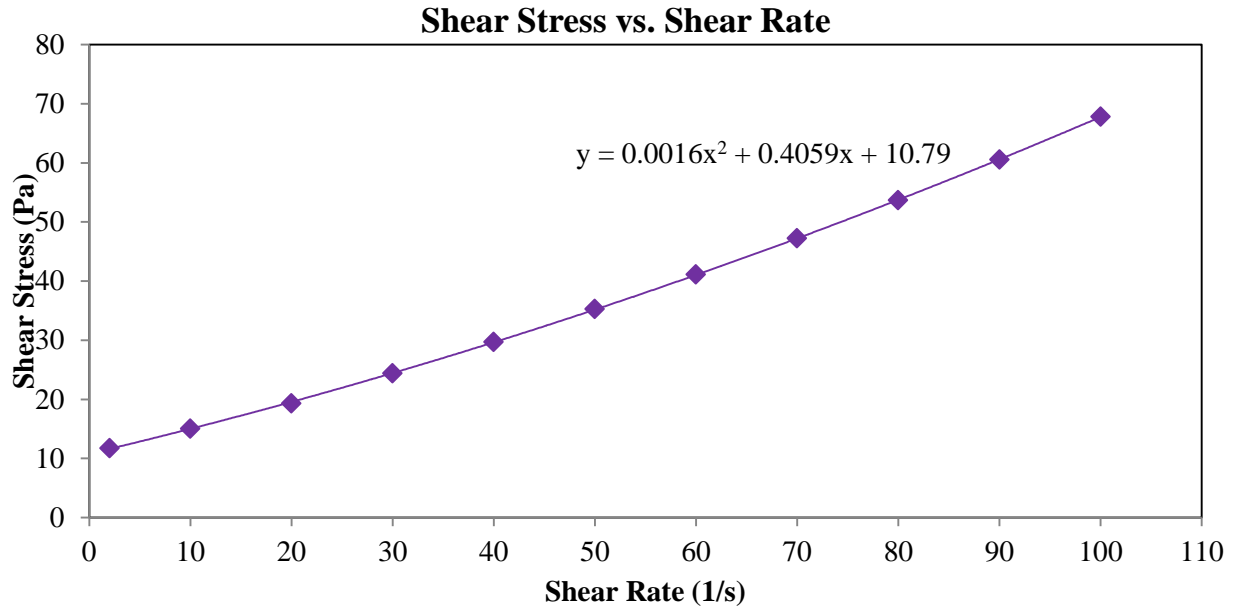
Figure B.6.3 FAC60: Shear stress versus shear rate at 20 min



**Torque vs. Rotational Speed**

$y = 0.145x^2 + 27.823x + 573.17$

Figure B.6.4 FAC60: Torque versus rotational speed at 20 min

**Shear Stress vs. Shear Rate**

$y = 0.0022x^2 + 0.5433x + 14.548$

Figure B.6.5 FAC60: Shear stress versus shear rate at 40 min



**Torque vs. Rotational Speed**

$y = 0.199x^2 + 37.245x + 772.62$
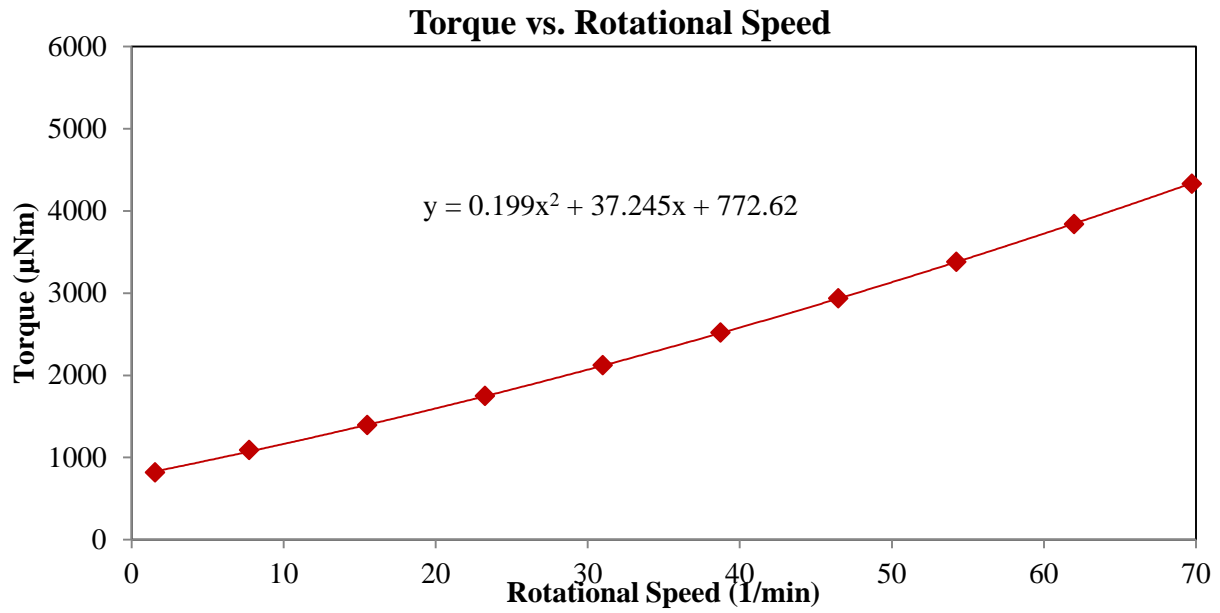
Figure B.6.6 FAC60: Torque versus rotational speed at 40 min

## Shear Stress vs. Shear Rate

$$y = 0.0025x^2 + 0.6293x + 17.364$$

Figure B.6.7 FAC60: Shear stress versus shear rate at 60 min

## Torque vs. Rotational Speed

$$y = 0.2182x^2 + 43.149x + 922.06$$
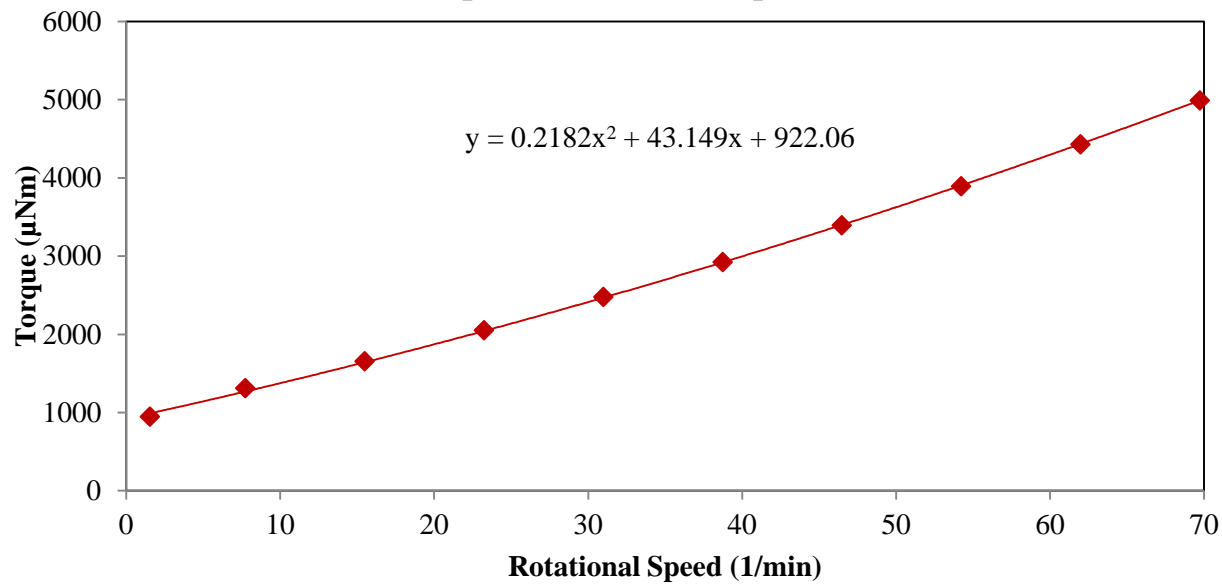
Figure  B.6.8 FAC60: Torque versus rotational speed at 60 min

## Shear Stress vs. Shear Rate

$$y = 0.0029x^2 + 0.8176x + 22.162$$
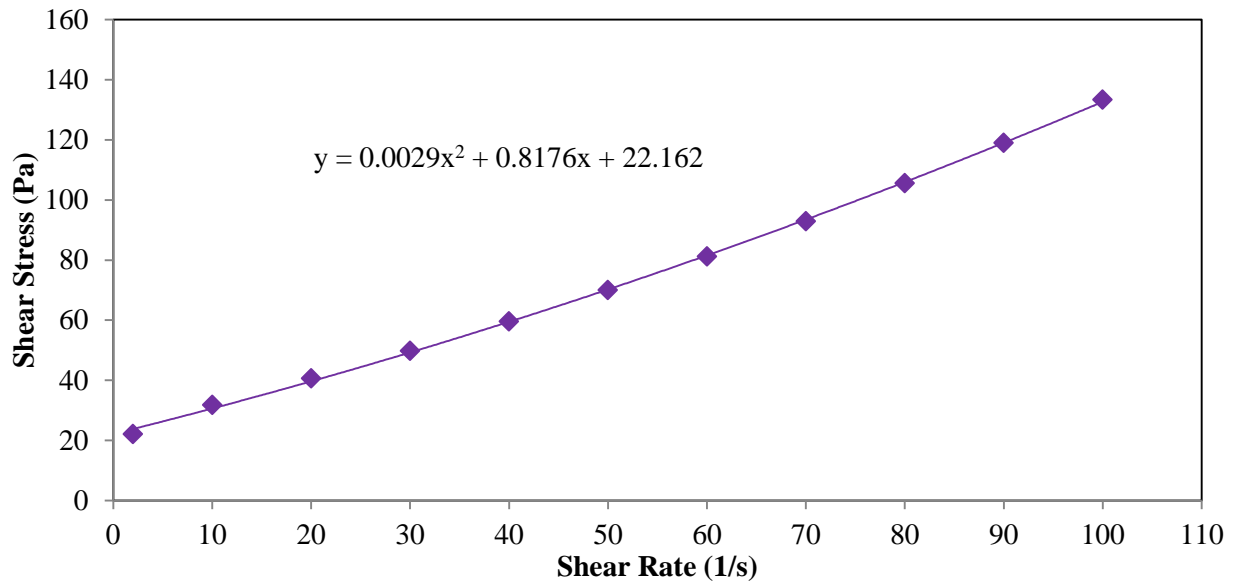
Figure B.6.9 FAC60: Shear stress versus shear rate at 90 min

## Torque vs. Rotational Speed

$$y = 0.2546x^2 + 56.031x + 1177.3$$
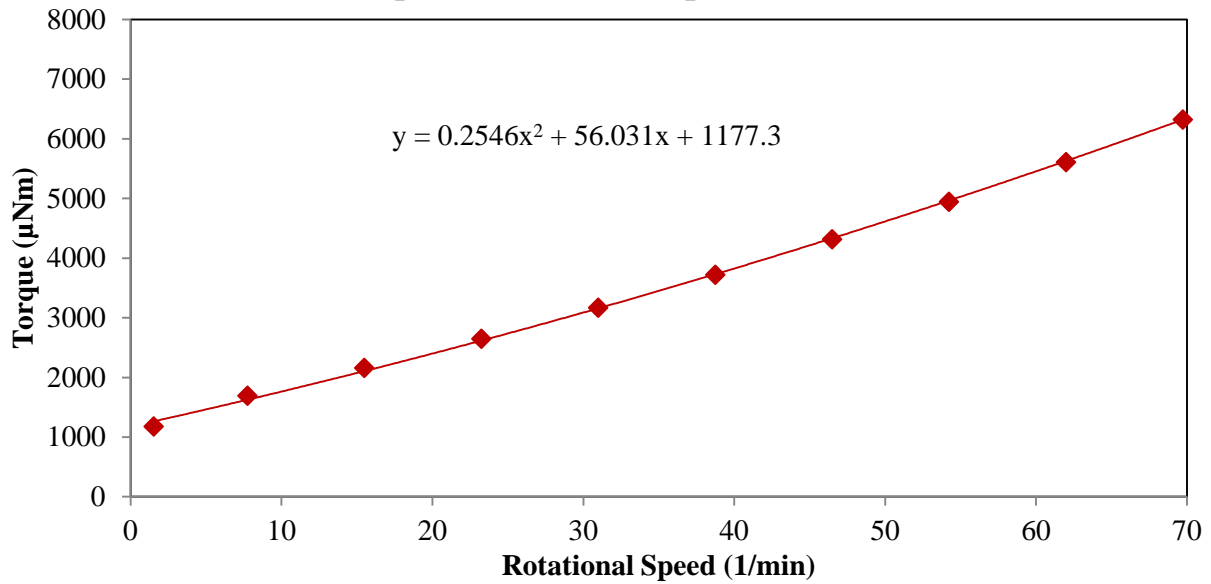
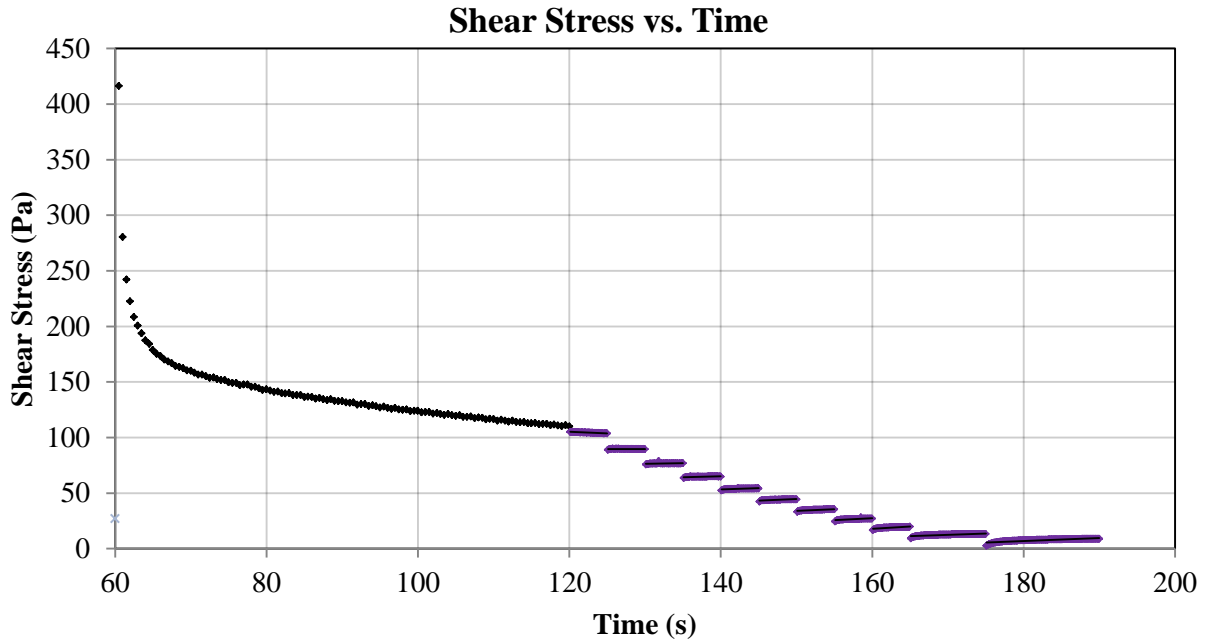Figure B.6.10 FAC60: Torque versus rotational speed at 90 min
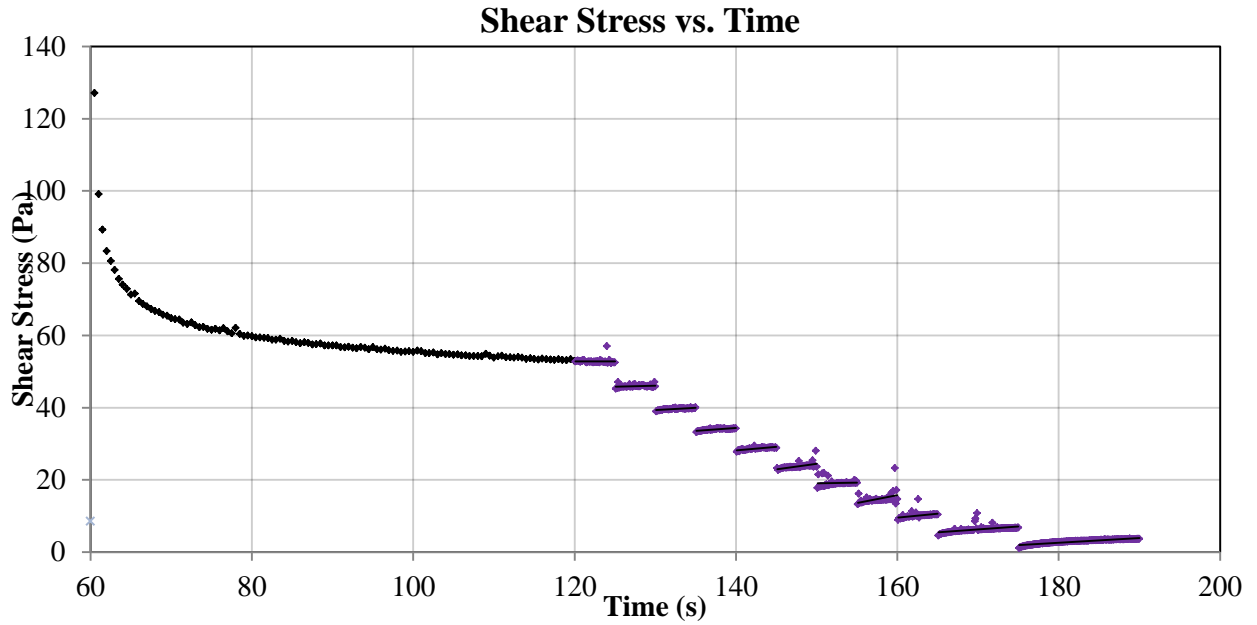
Figure B.7.1 FAC40SF5G10: Shear stress versus time at 20 min
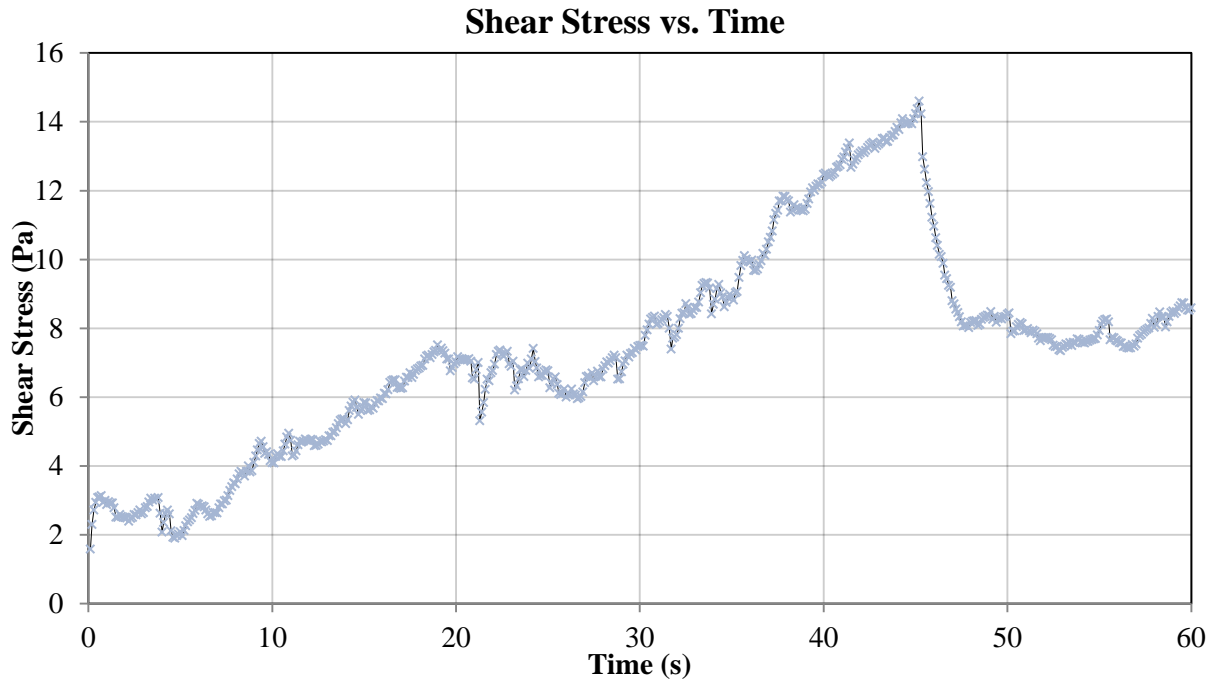


Figure B.7.2 FAC40SF5G10: Static yiled stress at 20 min
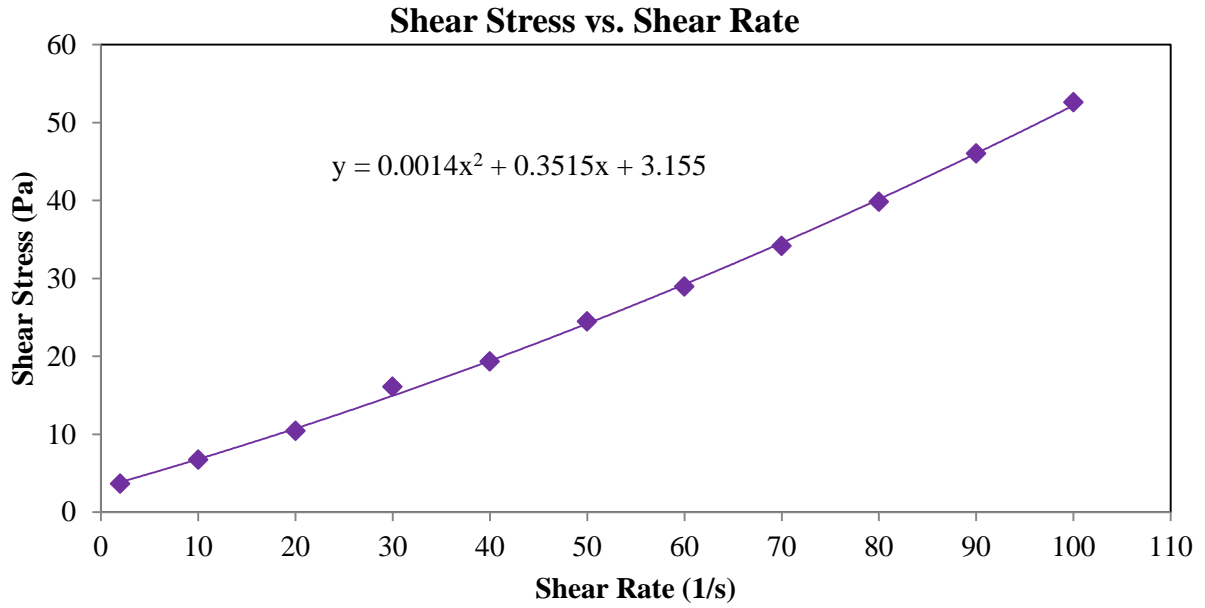
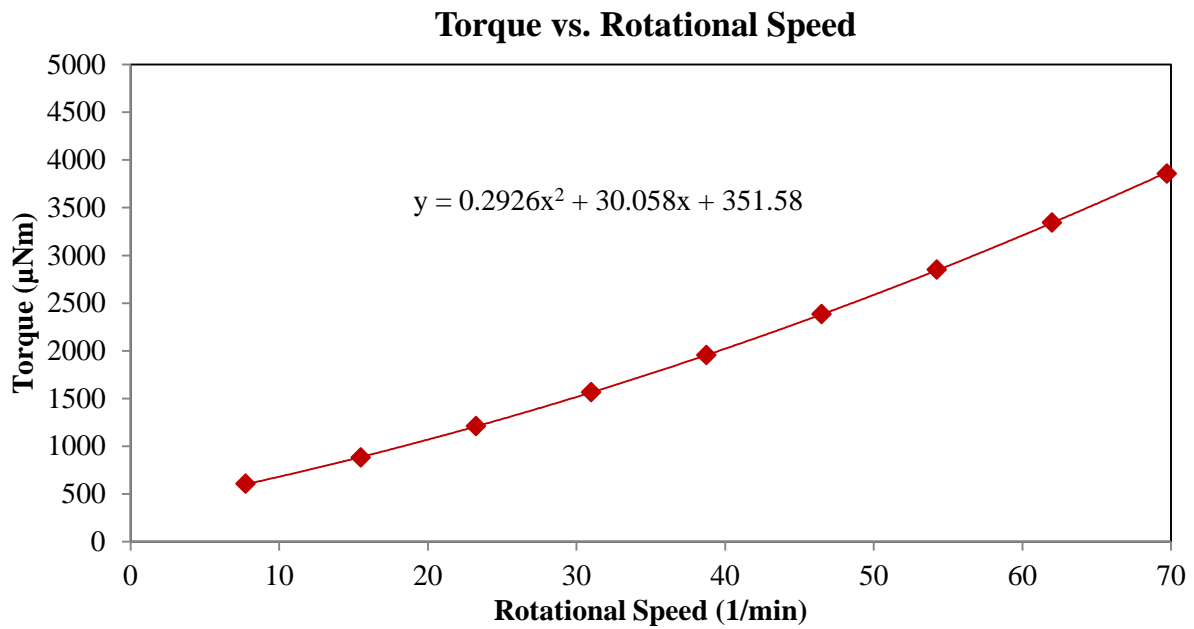**Figure B.7.3 FAC40SF5G10: Shear stress versus shear rate at 20 min**

The equation shown on the plot:
$$y = 0.0014x^2 + 0.3515x + 3.155$$
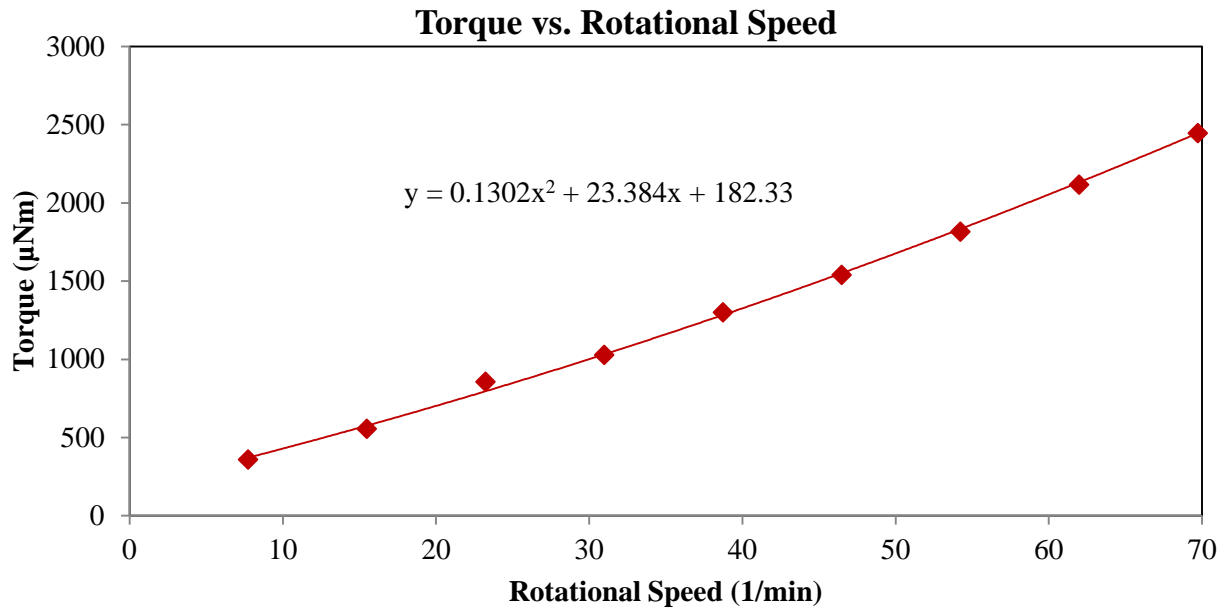


**Figure B.7.4 FAC40SF5G10: Torque versus rotational speed at 20 min**

The equation shown on the plot:
$$y = 0.1302x^2 + 23.384x + 182.33$$

**Shear Stress vs. Shear Rate**

$y = 0.0019x^2 + 0.3898x + 3.7375$
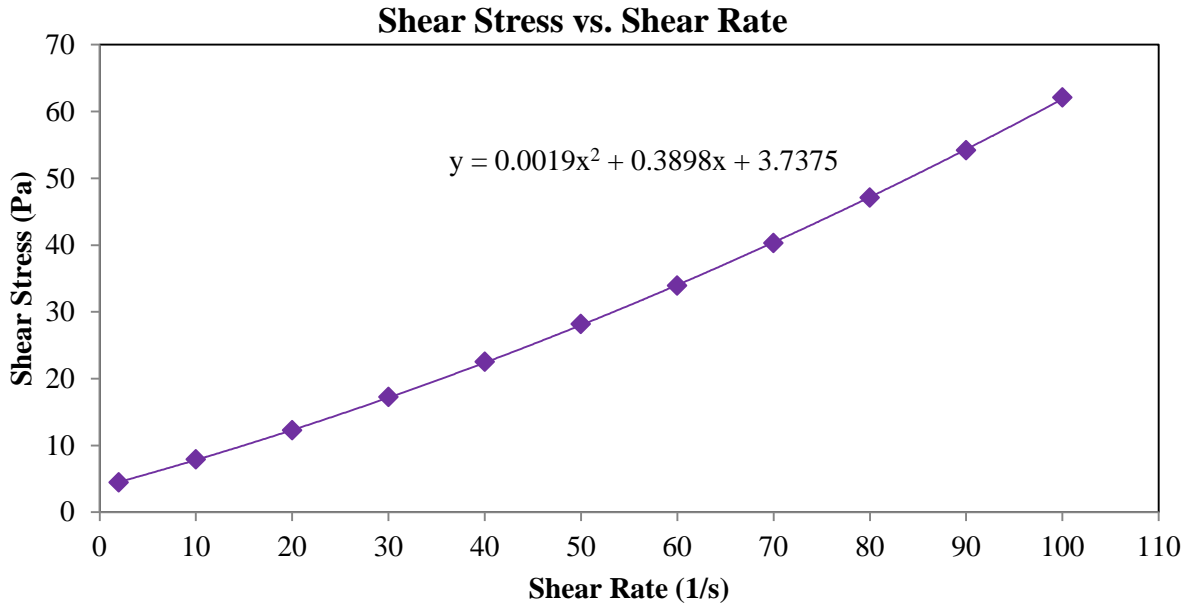
Figure B.7.5 FAC40SF5G10: Shear stress versus shear rate at 40 min



**Torque vs. Rotational Speed**

$y = 0.1694x^2 + 26.725x + 198.49$
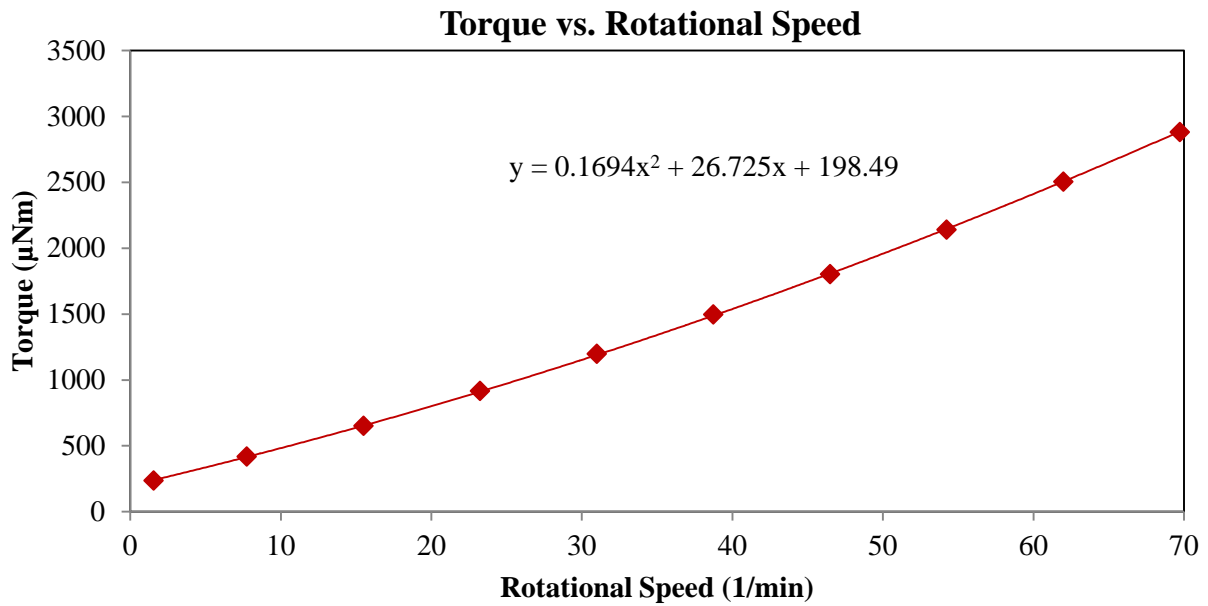
Figure B.7.6 FAC40SF5G10: Torque versus rotational speed at 40 min

## Shear Stress vs. Shear Rate

$$y = 0.0021x^2 + 0.4421x + 5.0698$$
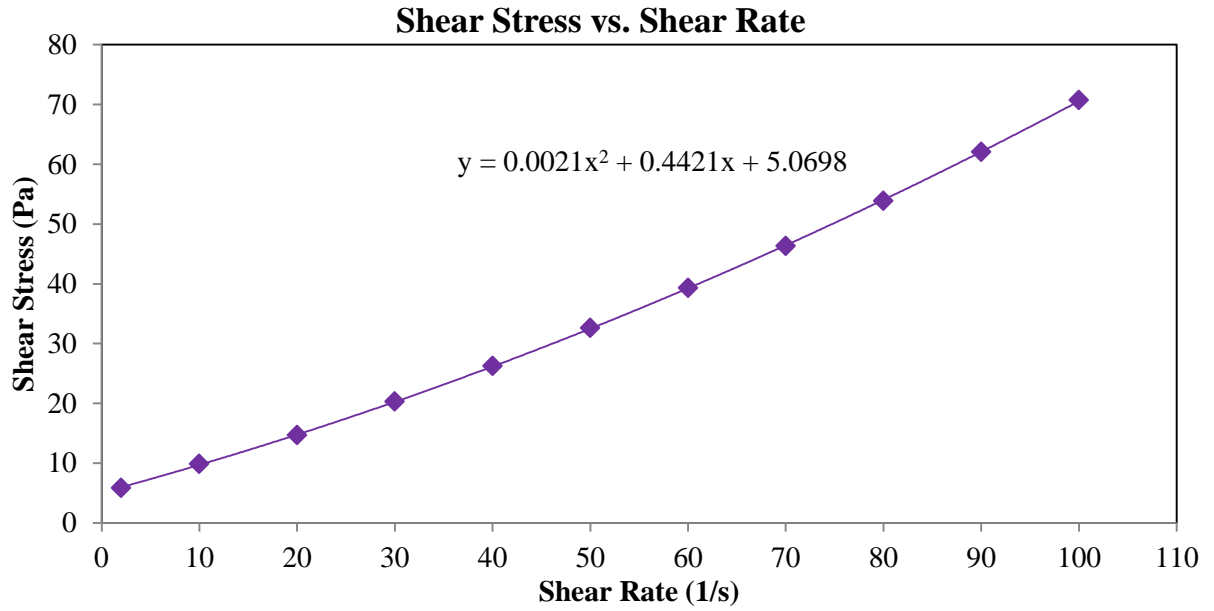
Figure B.7.7 FAC40SF5G10: Shear stress versus shear rate at 60 min

## Torque vs. Rotational Speed

$$y = 0.1882x^2 + 30.313x + 269.18$$
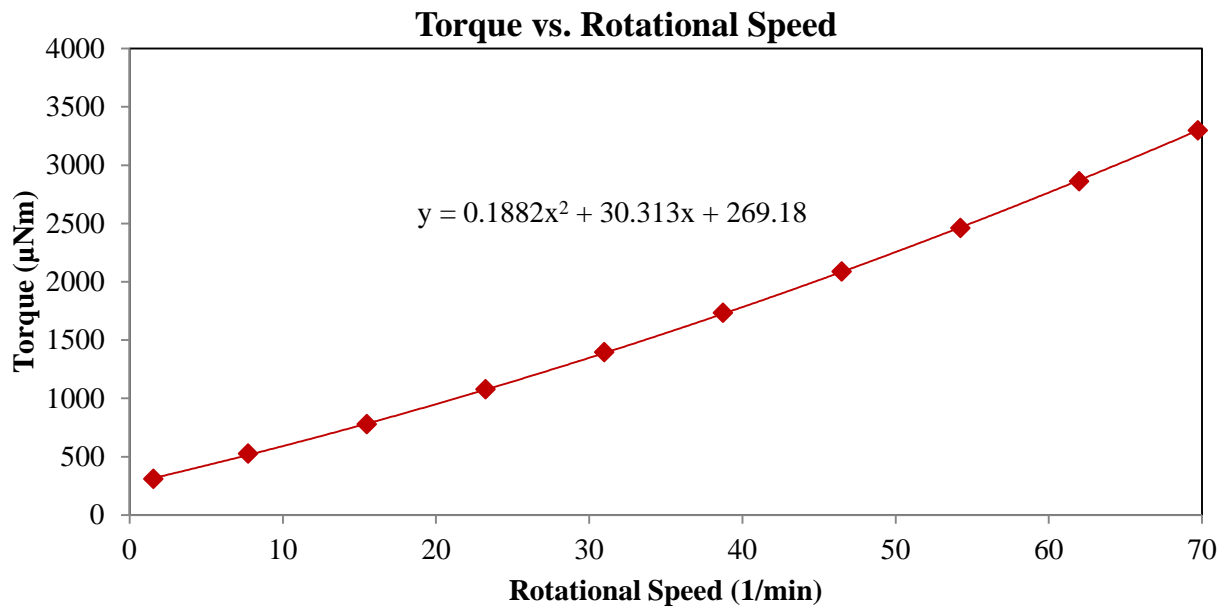
Figure B.7.8 FAC40SF5G10: Torque versus rotational speed at 60 min
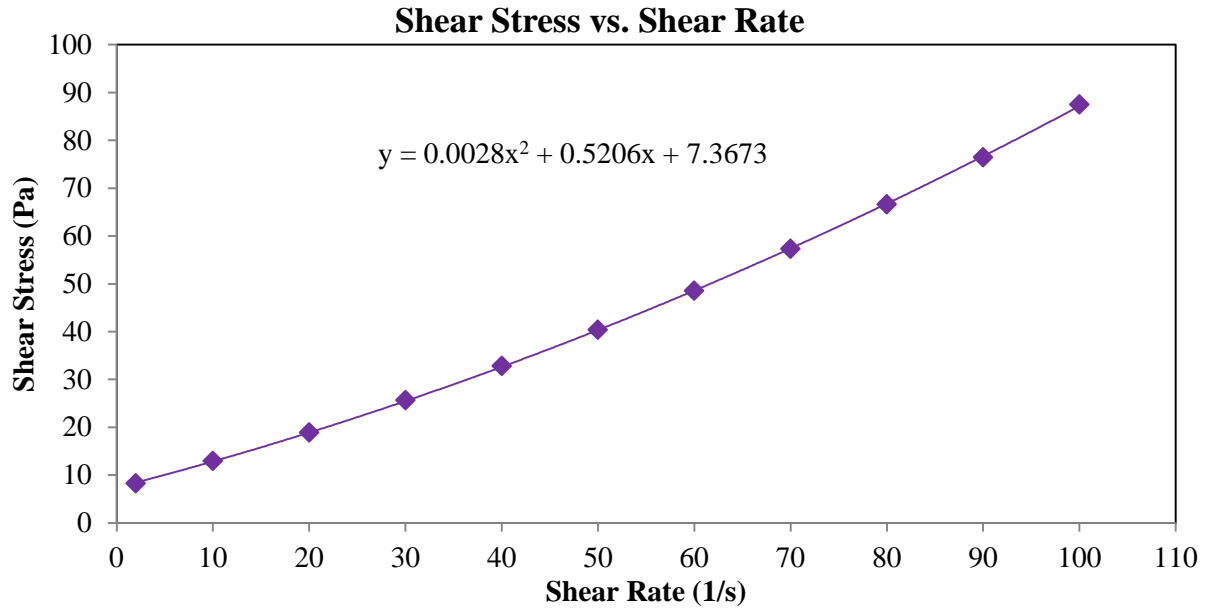
Figure B.7.9 FAC40SF5G10: Shear stress versus shear rate at 90 min

$$y = 0.0028x^2 + 0.5206x + 7.3673$$
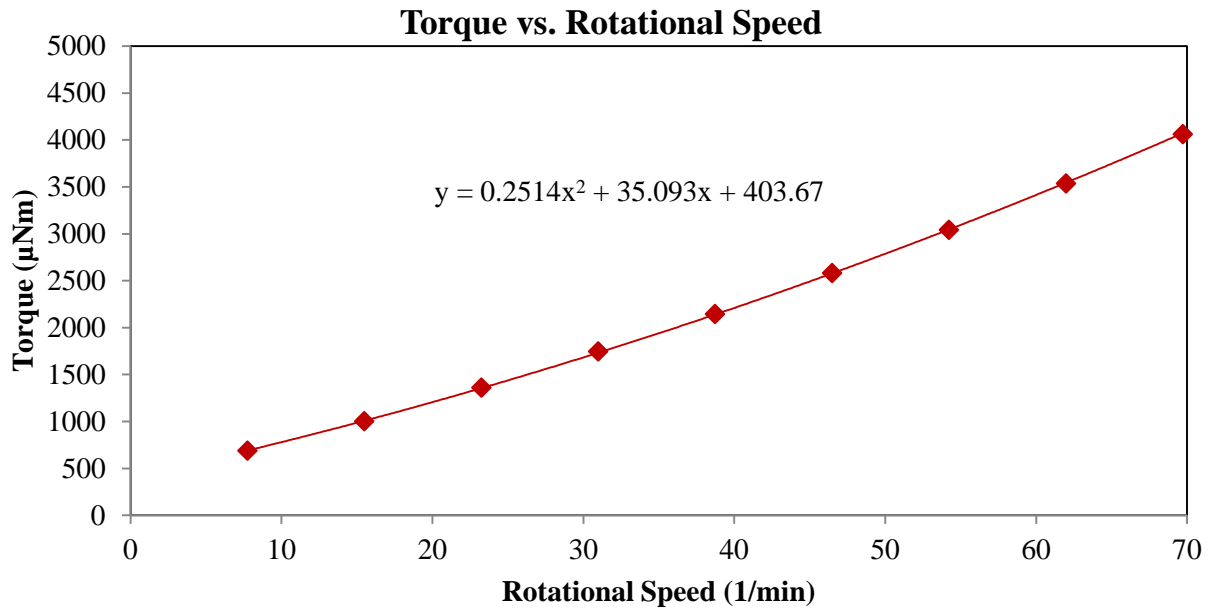


Figure B.7.10 FAC40SF5G10: Torque versus rotational speed at 90 min

$$y = 0.2514x^2 + 35.093x + 403.67$$

**Shear Stress vs. Time**



Figure B.8.1 FAC40SF5: Shear stress versus time at 40 min

**Shear Stress vs. Time**



Figure B.8.2 FAC40SF5: Static yield stress at 40 min

Figure B.8.3 FAC40SF5: Shear stress versus shear rate at 20 min
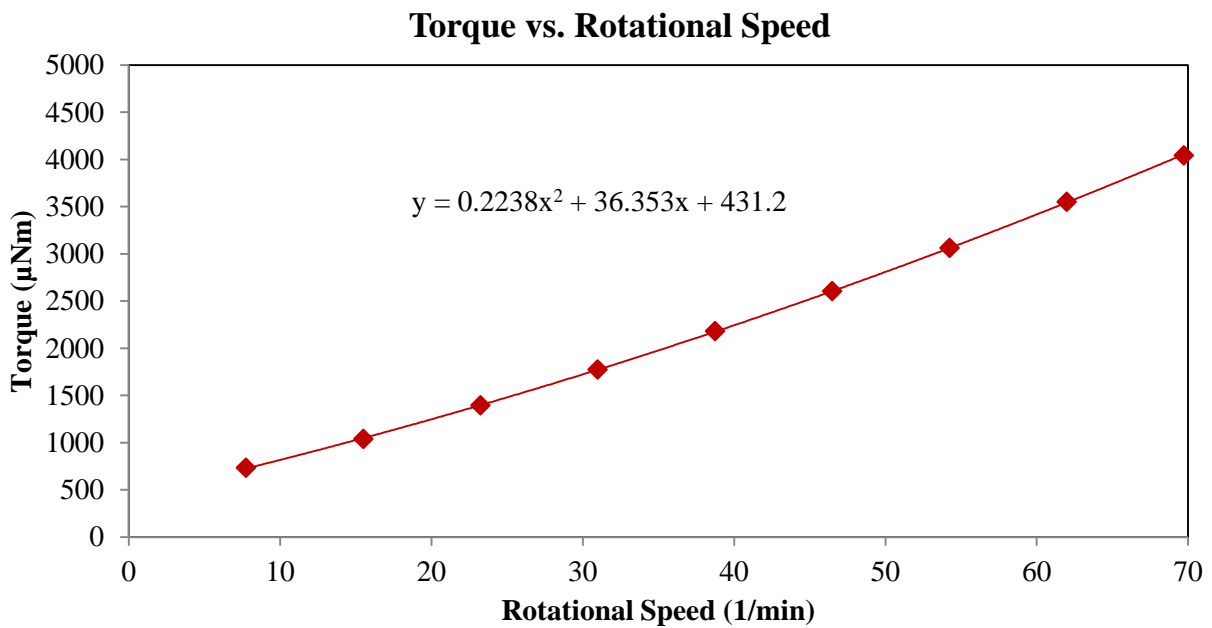


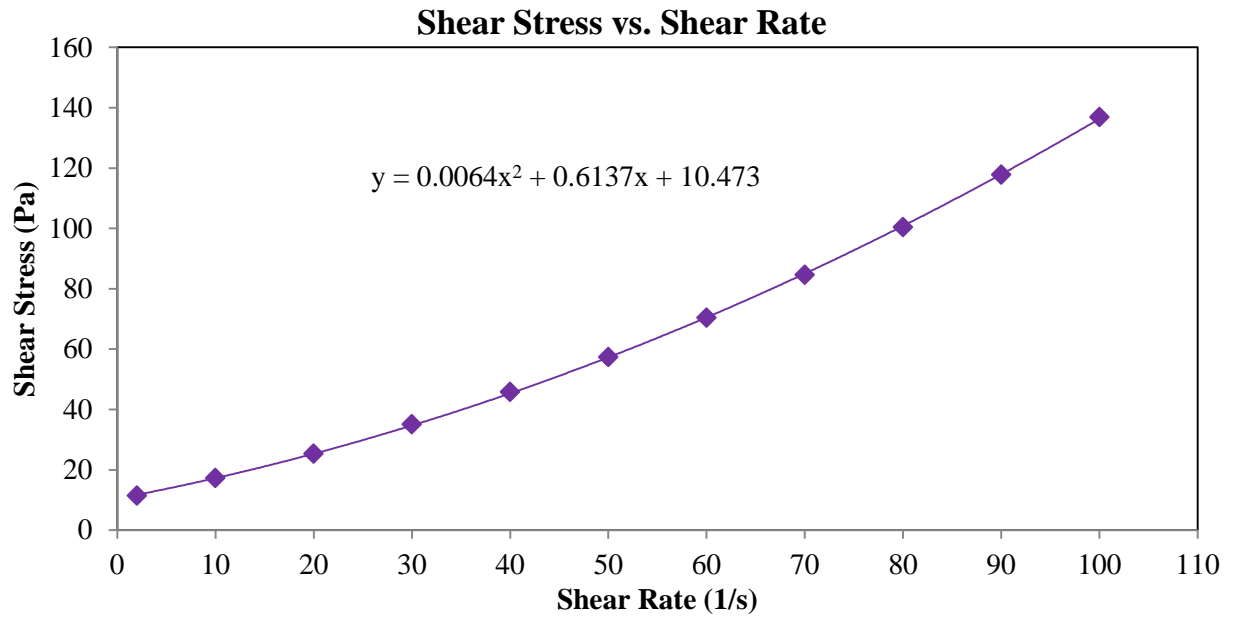Figure B.8.4 FAC40SF5: Torque versus rotational speed at 20 min

## Shear Stress vs. Shear Rate

$y = 0.0039x^2 + 0.5902x + 10.581$
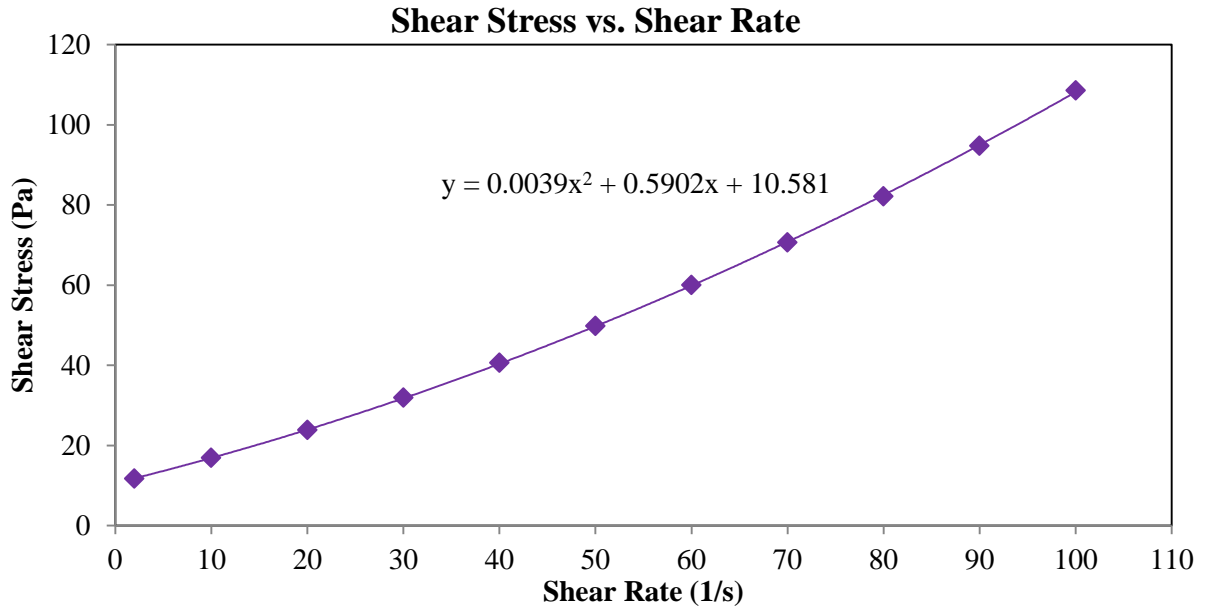
Figure B.8.5 FAC40SF5: Shear stress versus shear rate at 40 min

## Torque vs. Rotational Speed

$y = 0.3443x^2 + 40.174x + 567.79$
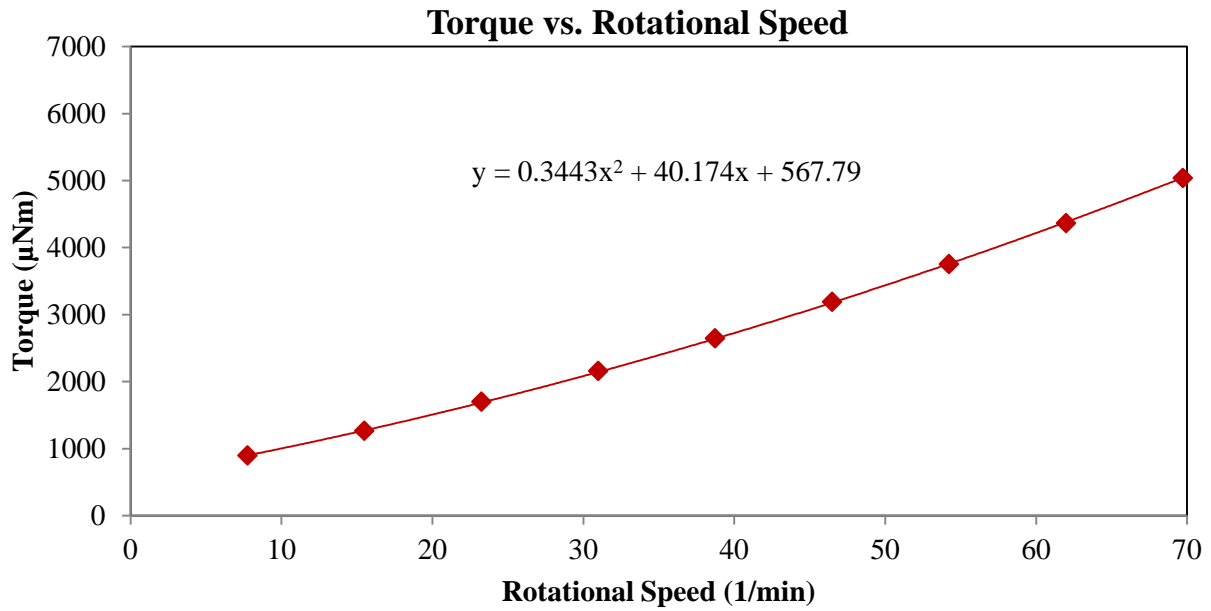
Figure B.8.6 FAC40SF5: Torque versus rotational speed at 40 min

**Shear Stress vs. Shear Rate**

$y = 0.0044x^2 + 0.6525x + 12$
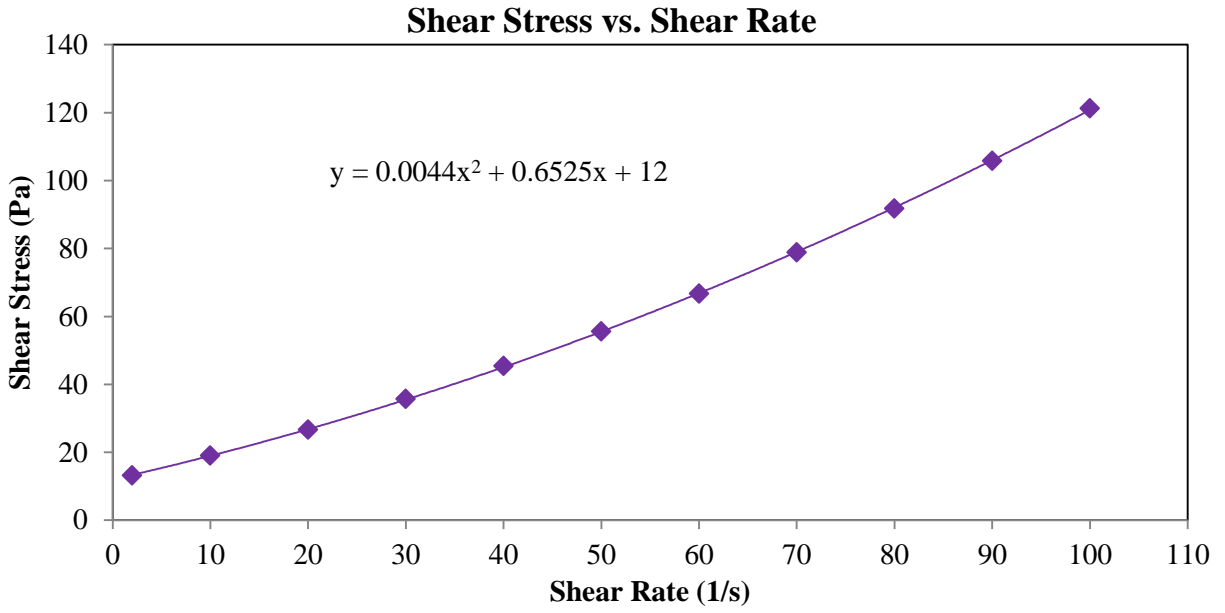
Figure B.8.7 FAC40SF5: Shear stress versus shear rate at 60 min



**Torque vs. Rotational Speed**

$y = 0.3911x^2 + 44.155x + 649.55$
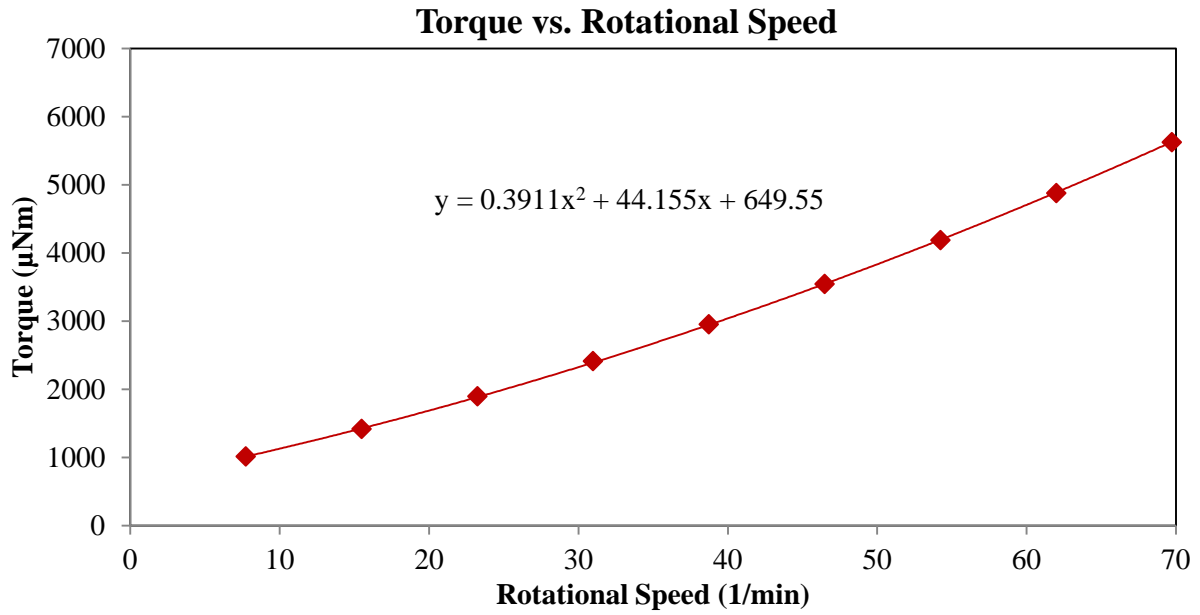
Figure B.8.8 FAC40SF5: Torque versus rotational speed at 60 min

## Shear Stress vs. Shear Rate

$$y = 0.007x^2 + 0.8311x + 15.574$$
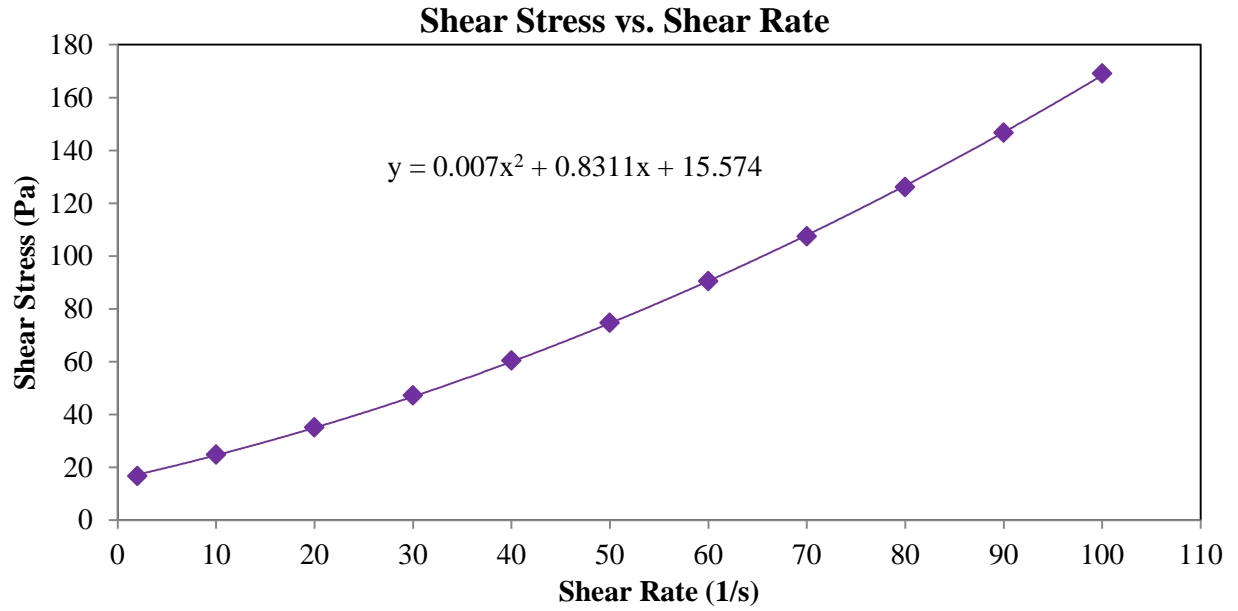
Figure B.8.9 FAC40SF5: Shear stress versus shear rate at 90 min

## Torque vs. Rotational Speed

$$y = 0.6169x^2 + 56.97x + 827.3$$
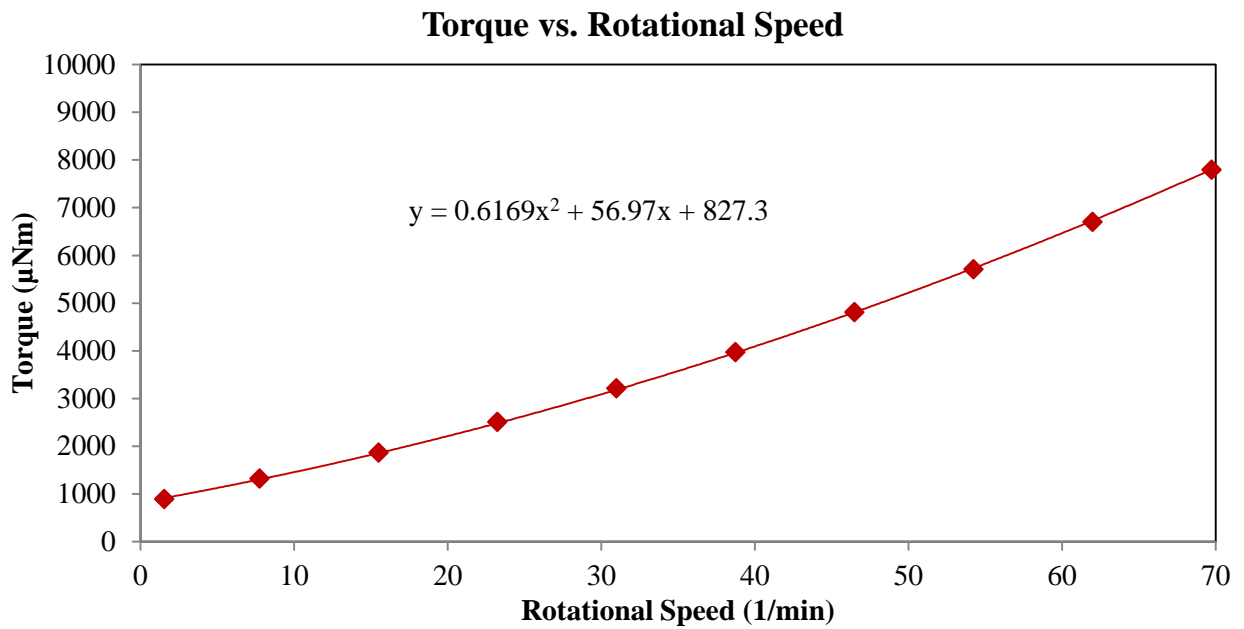
Figure B.8.10 FAC40SF5: Torque versus rotational speed at 90 min

Figure B.9.1 FAC40: Shear stress versus time at 40 min
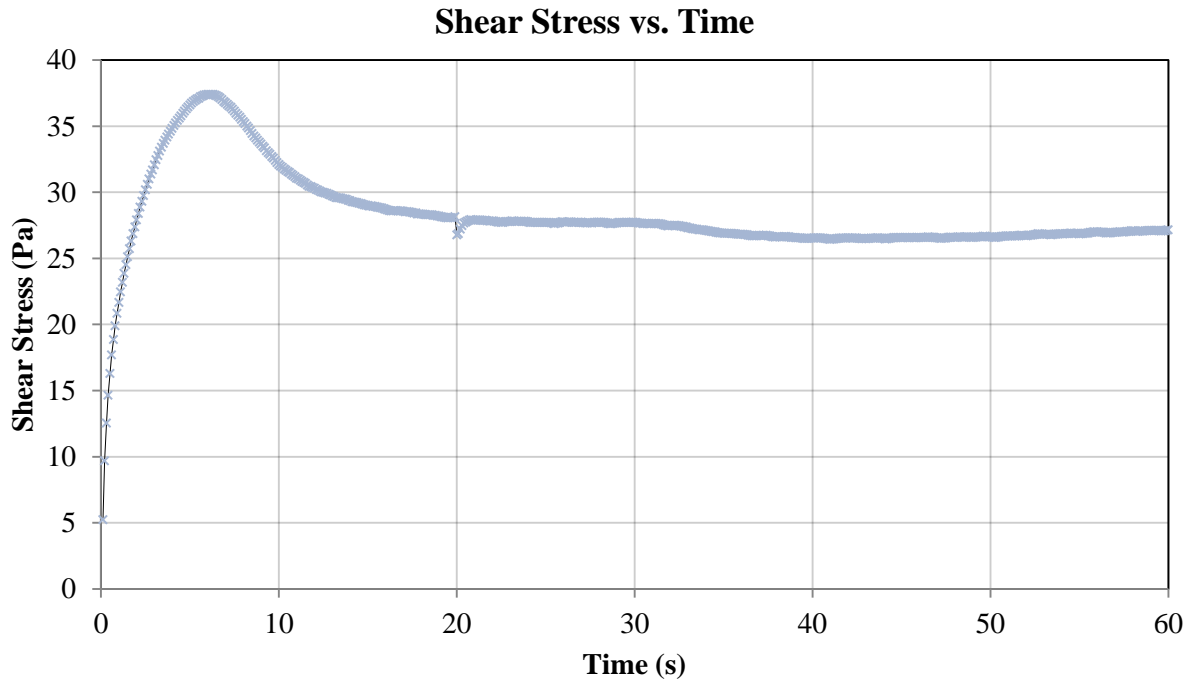


Figure B.9.2 FAC40: Static yield stress at 40 min

## Shear Stress vs. Shear Rate

$$y = 0.0033x^2 + 0.4343x + 6.7334$$
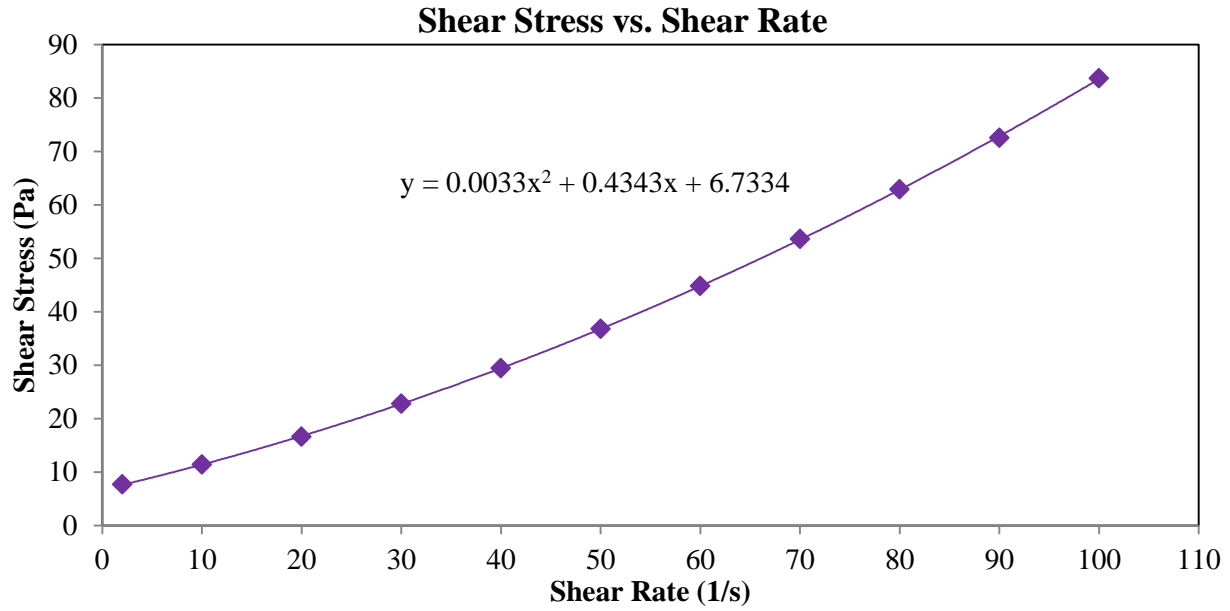
Figure B.9.3 FAC40: Shear stress versus shear rate at 20 min

## Torque vs. Rotational Speed

$$y = 0.2926x^2 + 30.058x + 351.58$$

Figure B.9.4 FAC40: Torque versus rotational speed at 20 min

145

## Shear Stress vs. Shear Rate

$$y = 0.0046x^2 + 0.4938x + 7.9356$$
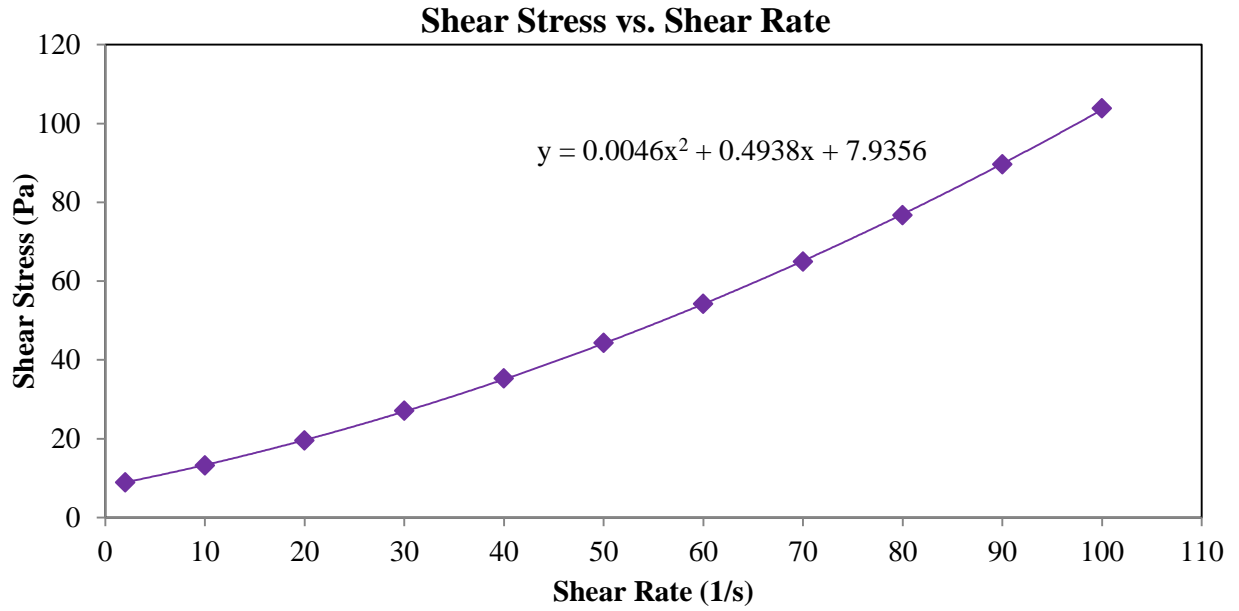
Figure B.9.5 FAC40: Shear stress versus shear rate at 40 min

## Torque vs. Rotational Speed

$$y = 0.409x^2 + 33.801x + 422.48$$
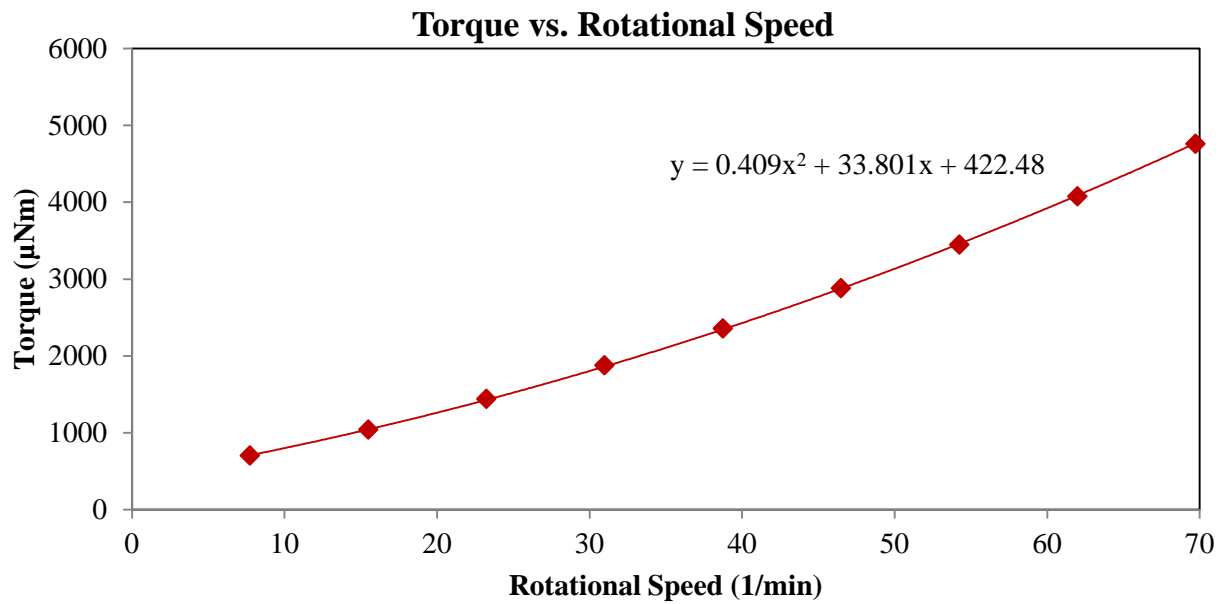
Figure B.9.6 FAC40: Torque versus rotational speed at 40 min

**Shear Stress vs. Shear Rate**

$y = 0.0053x^2 + 0.5238x + 8.7319$
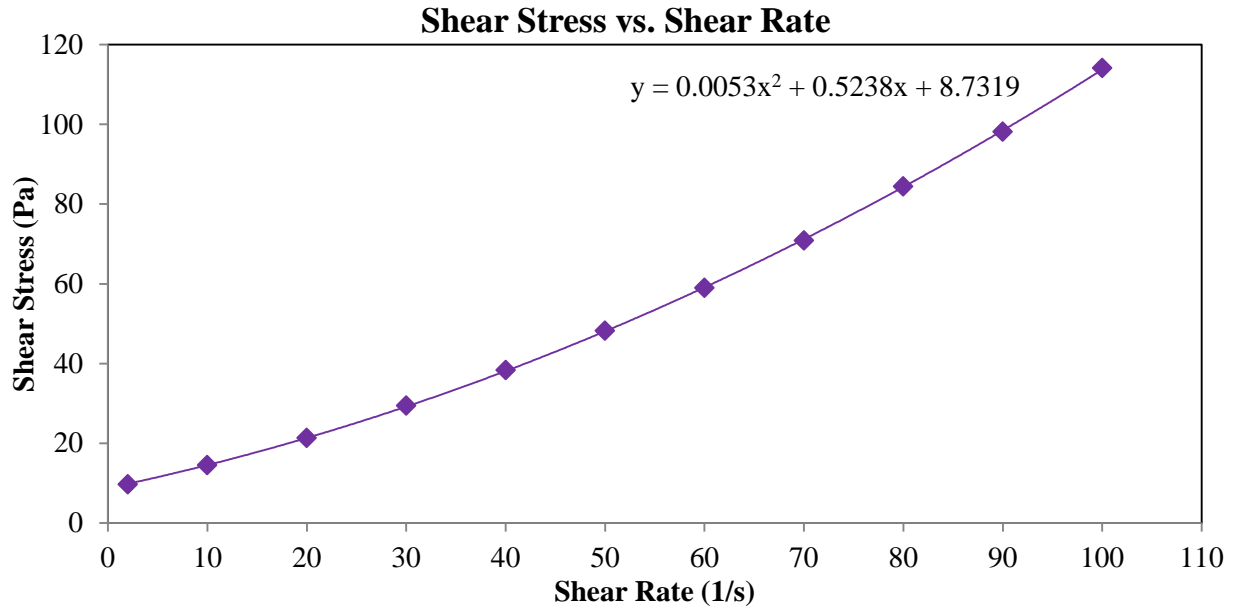
Figure B.9.7 FAC40: Shear stress versus shear rate at 60 min



**Torque vs. Rotational Speed** $-0.9698x^2 + 35.486x + 472.53$
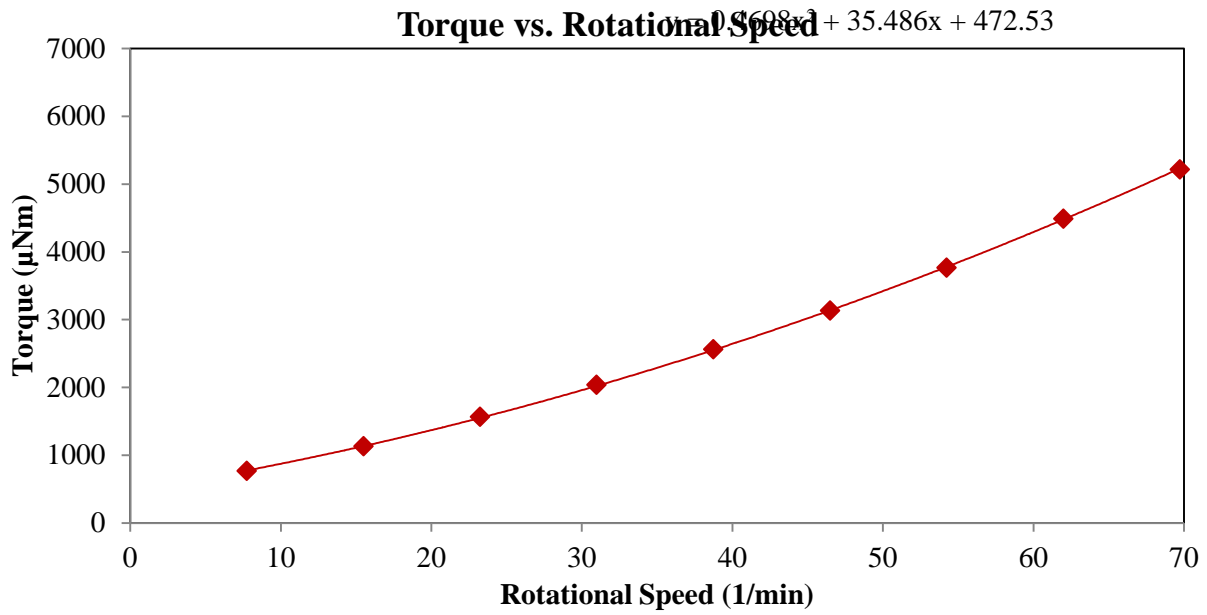
Figure B.9.8 FAC40: Torque versus rotational speed at 60 min

Figure B.9.9 FAC40: Shear stress versus shear rate at 90 min

$y = 0.0064x^2 + 0.6137x + 10.473$
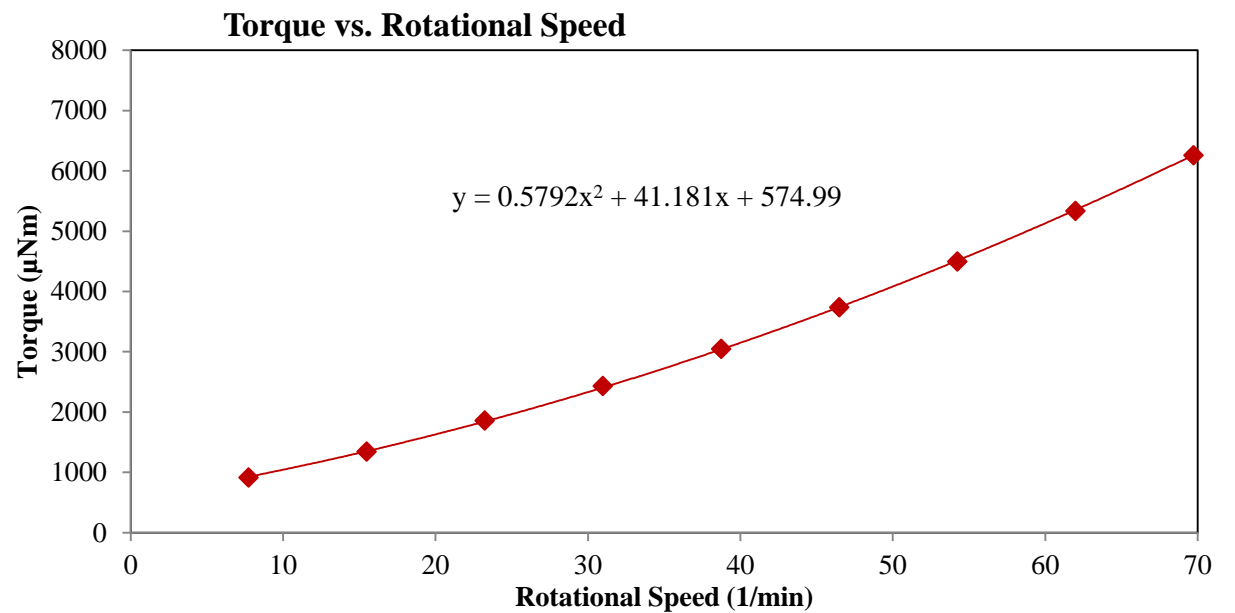


Figure B.9.10 FAC40: Torque versus rotational speed at 90 min

$y = 0.5792x^2 + 41.181x + 574.99$

# APPENDIX C RHEOLOGY RESULT FOR UHPC MIX DESIGN USING CONTECH VISCOMETER 5

## Torque vs. Time
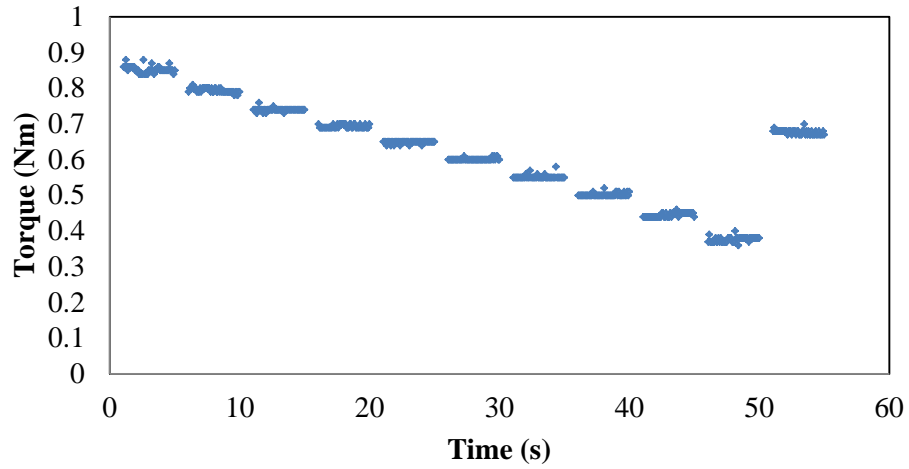


Figure C.1 Reference Ductal: Shear stress versus time at 20 min.

## Ductal-20 min.



$$y = 1.4x + 0.1276$$
$$R^2 = 0.995$$

$$y = -2.871x^2 + 1.8649x + 0.1126$$
$$R^2 = 0.9993$$
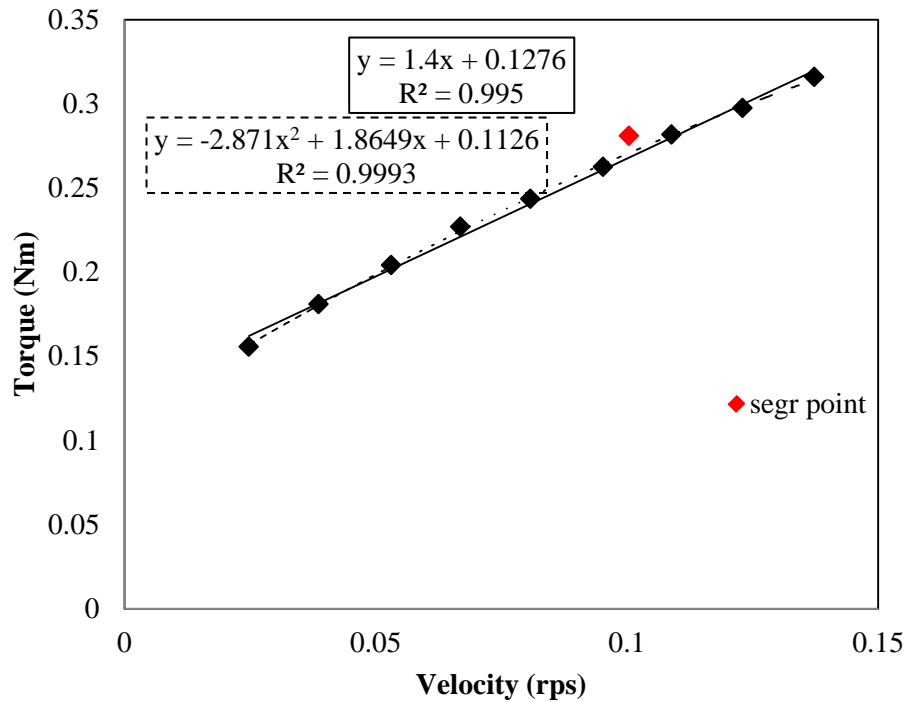
Figure C. 2 Reference Ductal: Torque versus rotational speed at 20 min
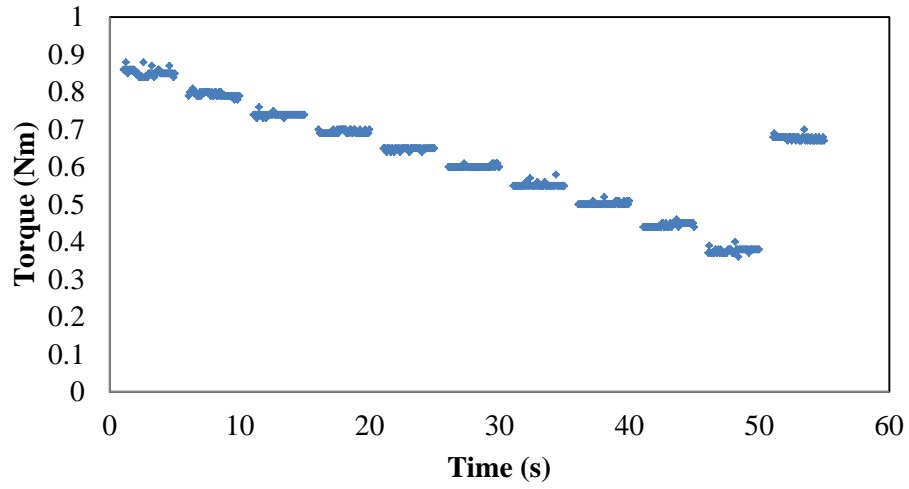
## Torque vs. Time



Figure C. 3 Reference Ductal: Shear stress versus time at 40 min.

## Ductal-40 min.



$y = 2.4731x + 0.2089$
$R^2 = 0.9969$

$y = -3.3831x^2 + 3.0187x + 0.1914$
$R^2 = 0.9988$

◆ segr point
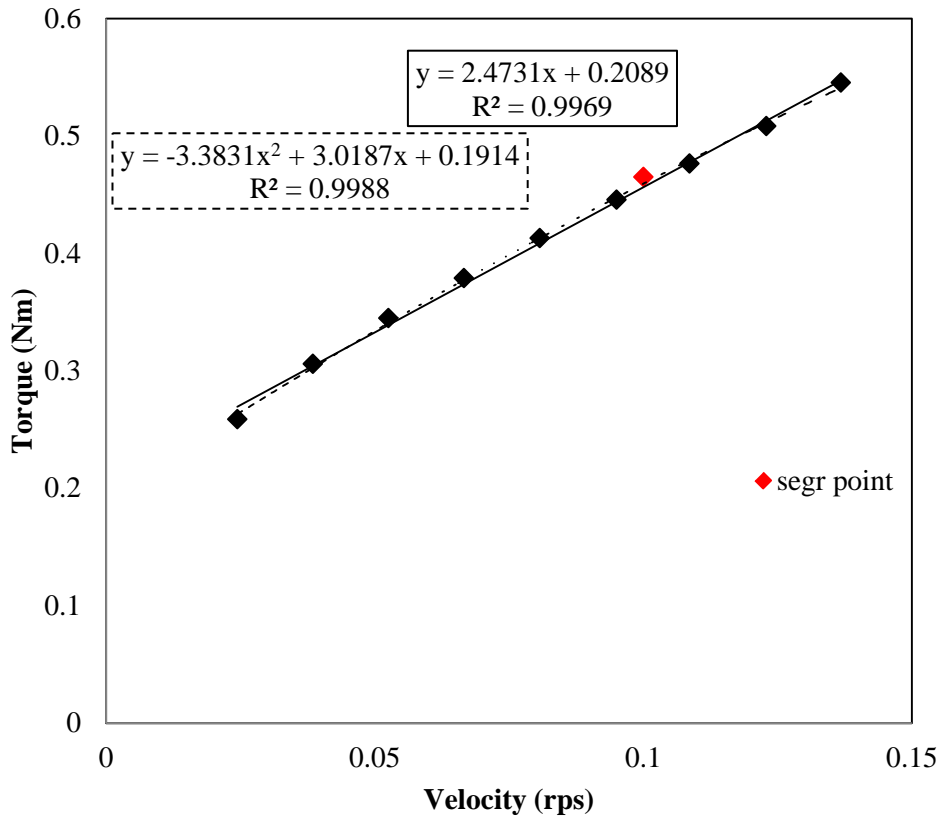
Figure C. 4 Reference Ductal: Torque versus rotational speed at 40 min

## Torque v. Time
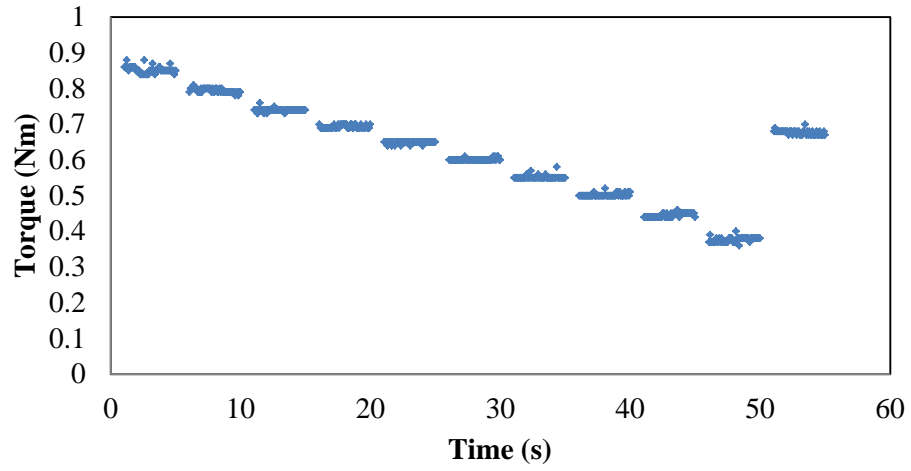


Figure C. 5 Reference Ductal: Shear stress versus time at 40 min.

## Ductal-60 min.



$y = 3.1617x + 0.2771$
$R^2 = 0.9975$

$y = -3.8571x^2 + 3.7837x + 0.2571$
$R^2 = 0.999$

◆ segr point
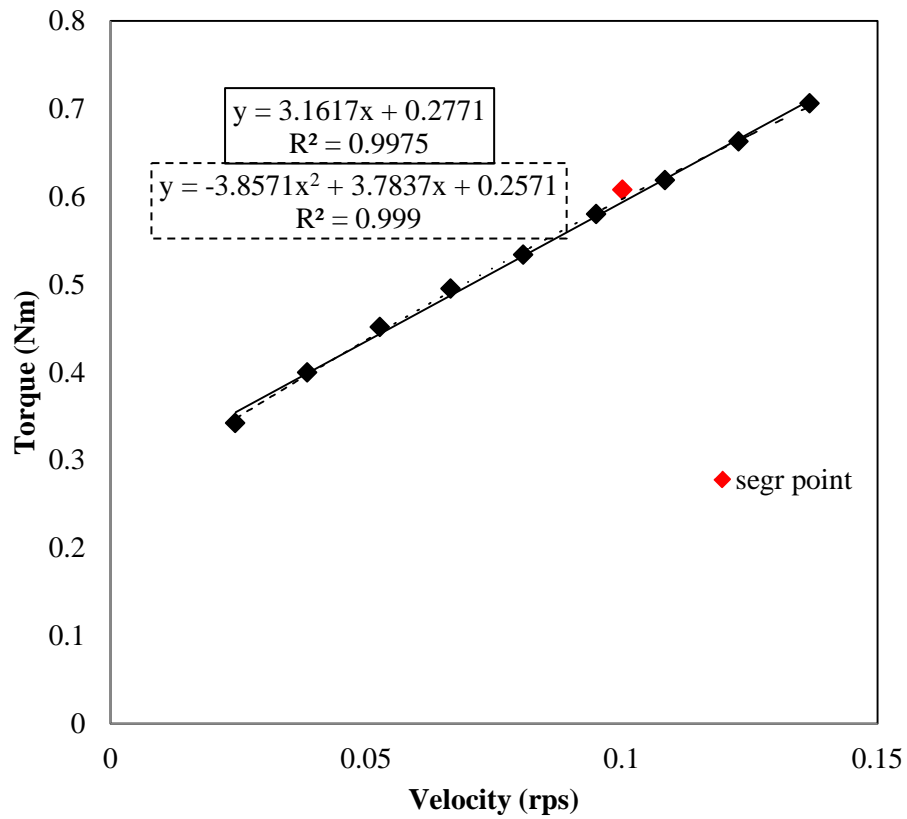
Figure C. 6 Reference Ductal: Torque versus rotational speed at 60 min
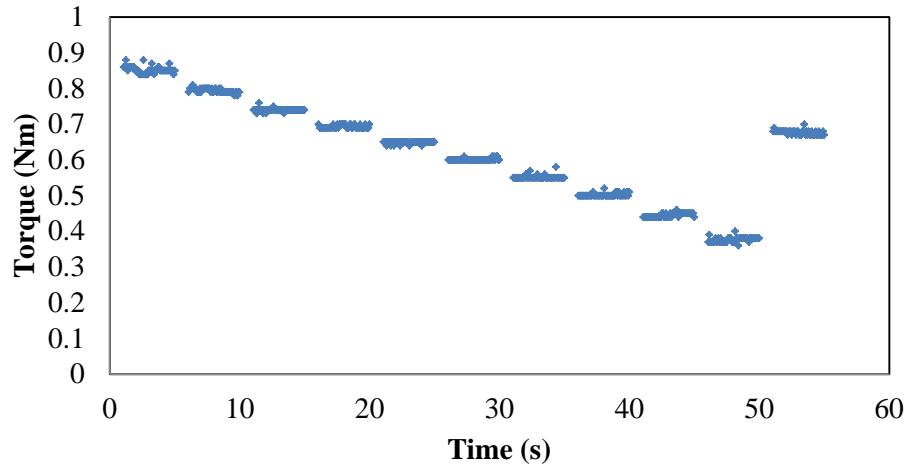
## Torque vs. Time



Figure C.7 G50SF5: Shear stress versus time at 20 min.

## G50SF5-20 min.



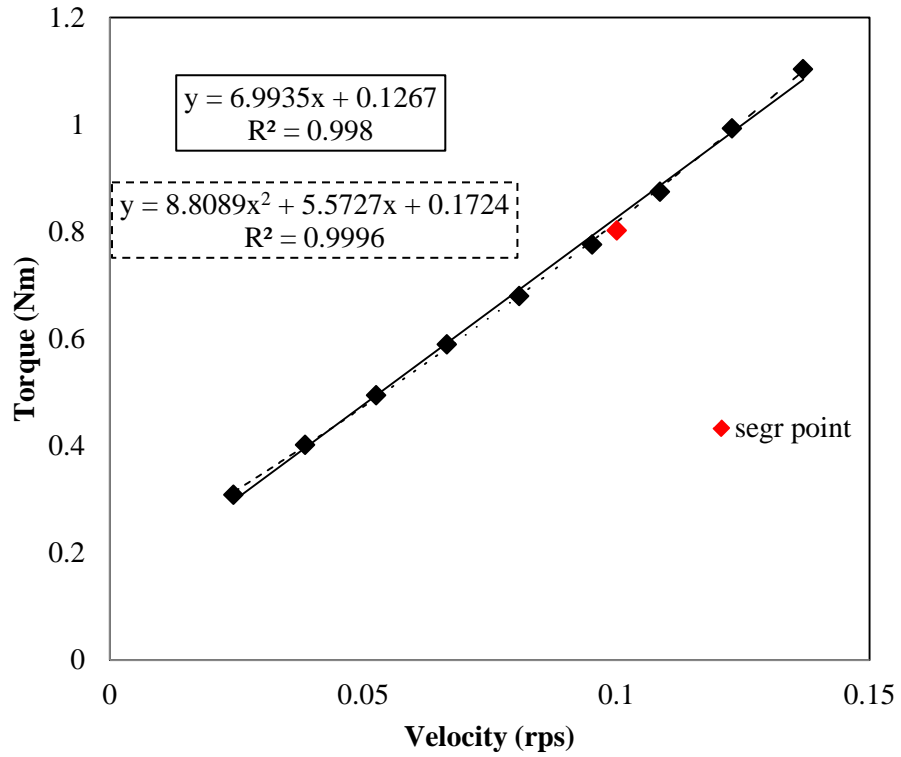$y = 4.9852x + 0.117$
$R^2 = 0.9991$
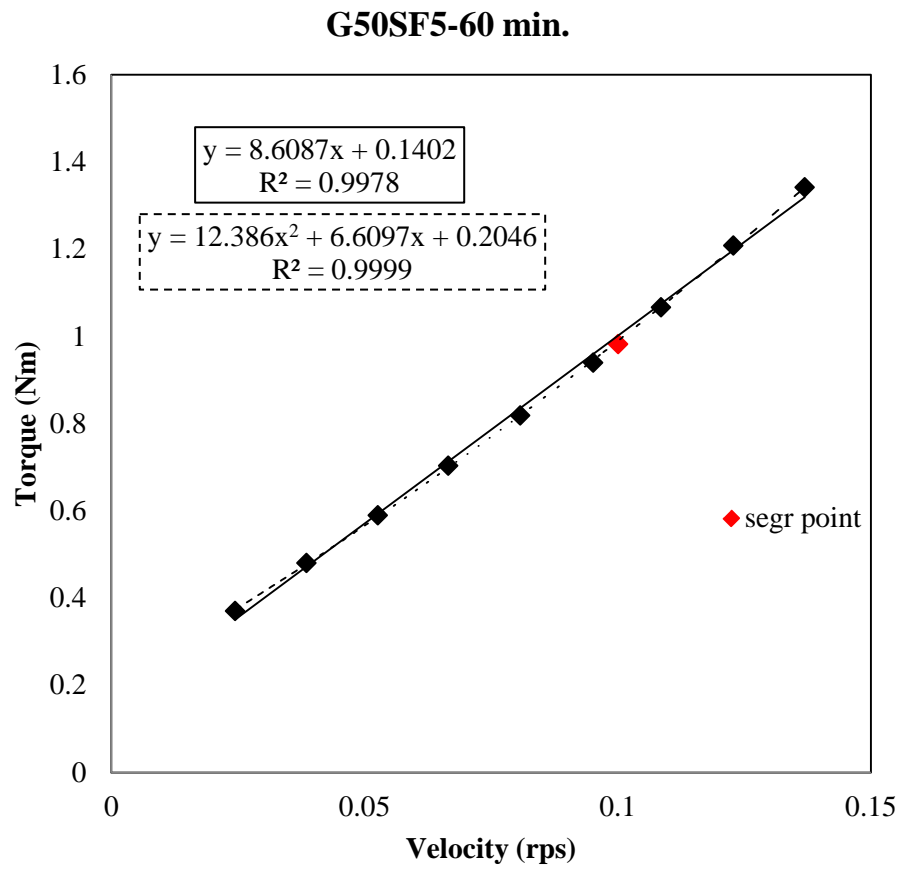$y = 4.5482x^2 + 4.25x + 0.1407$
$R^2 = 0.9999$

◆ Bingham

◆ segr point
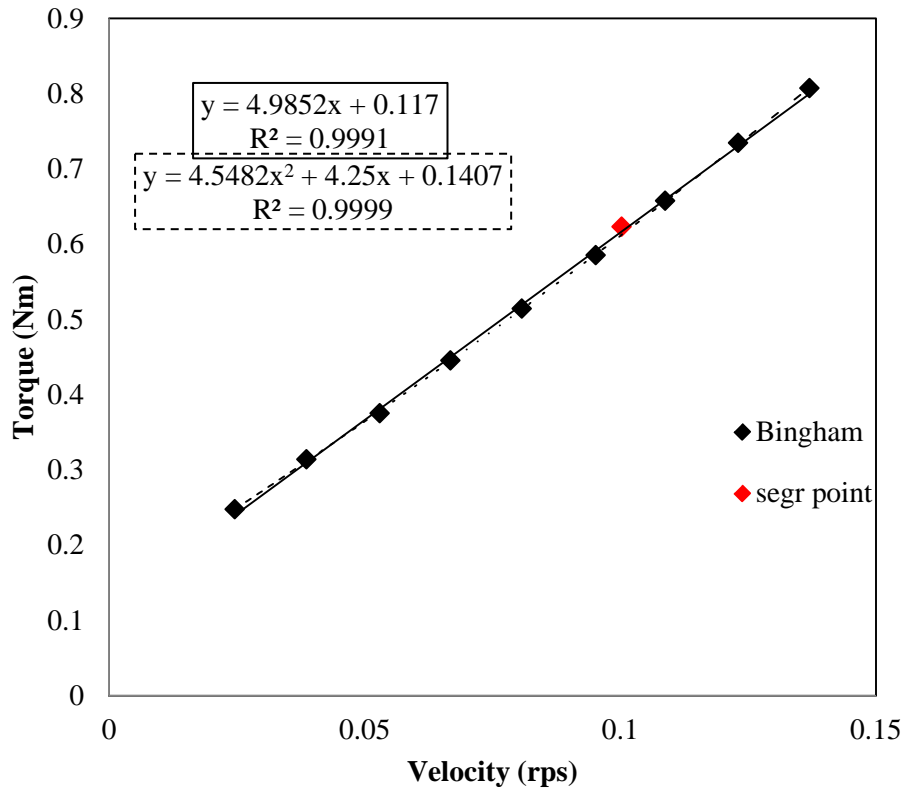
Figure C.8 G50SF5: Torque versus rotational speed at 20 min
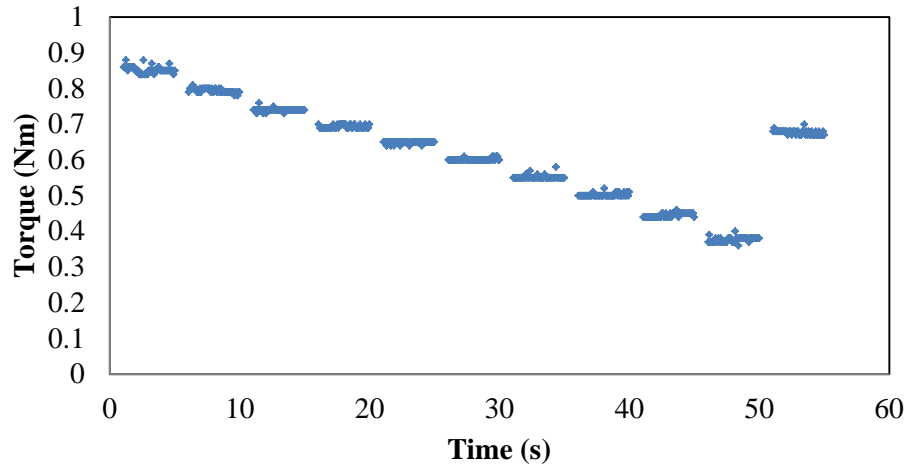
## Torque vs. Time



Figure C.9 G50SF5: Shear stress versus time at 40 min.

## G50SF5-40 min.



$$y = 6.9935x + 0.1267$$
$$R^2 = 0.998$$

$$y = 8.8089x^2 + 5.5727x + 0.1724$$
$$R^2 = 0.9996$$

◆ segr point

Figure C.10 G50SF5: Torque versus rotational speed at 40 min
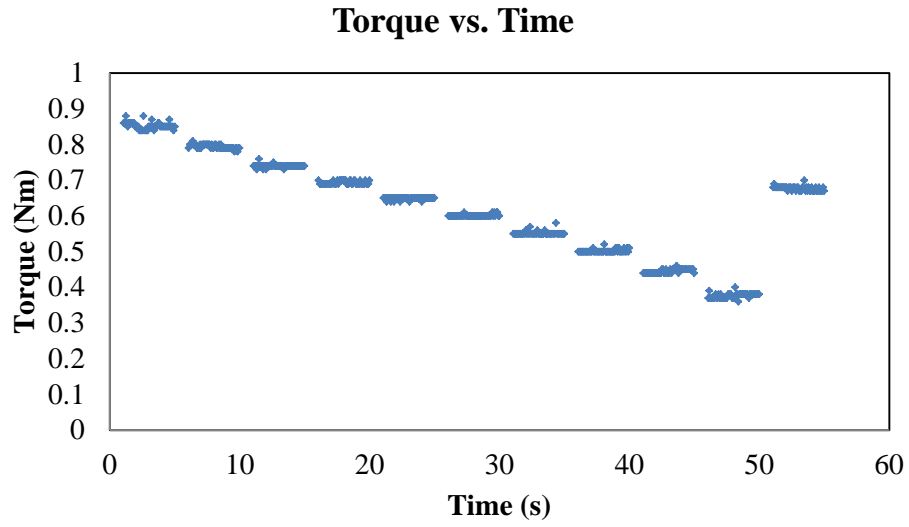
## Torque vs. Time



Figure C.11 G50SF5: Shear stress versus time at 60 min.

## G50SF5-60 min.



$$y = 8.6087x + 0.1402$$
$$R^2 = 0.9978$$

$$y = 12.386x^2 + 6.6097x + 0.2046$$
$$R^2 = 0.9999$$

◆ segr point

Figure C.12 G50SF5: Torque versus rotational speed at 60 min
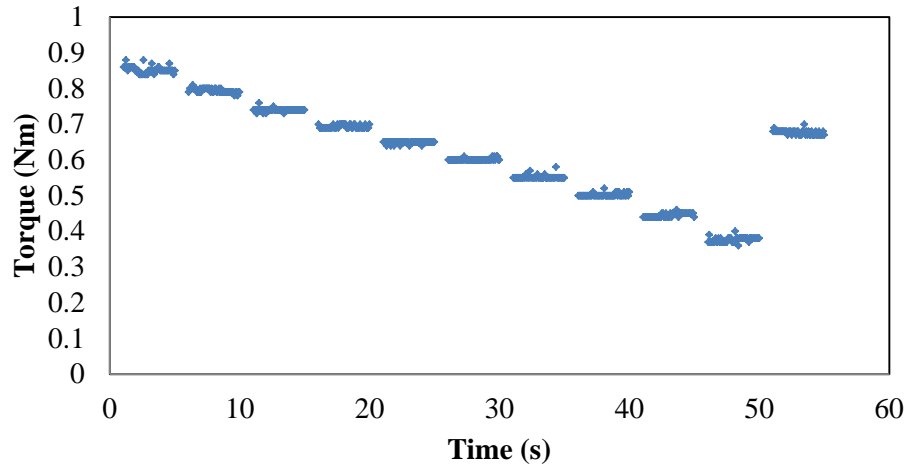
**Torque vs. Time**



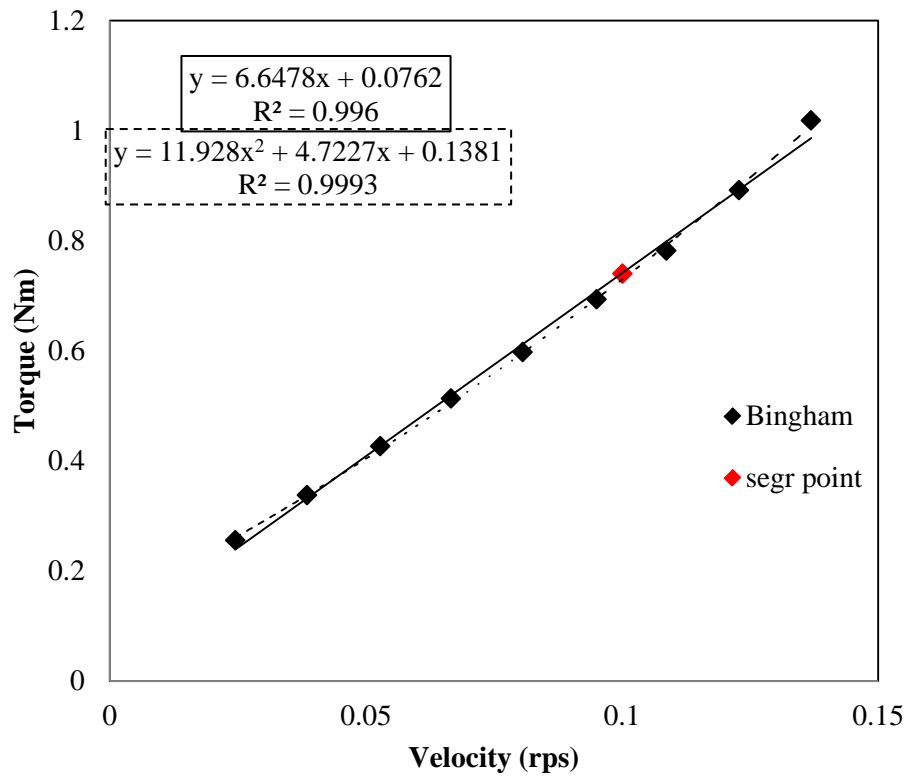Figure C.13 FAC40SF5: Shear stress versus time at 20 min.

**FAC40SF5**



$$y = 6.6478x + 0.0762$$
$$R^2 = 0.996$$

$$y = 11.928x^2 + 4.7227x + 0.1381$$
$$R^2 = 0.9993$$

Figure C.14 FAC40SF5: Torque versus rotational speed at 20 min
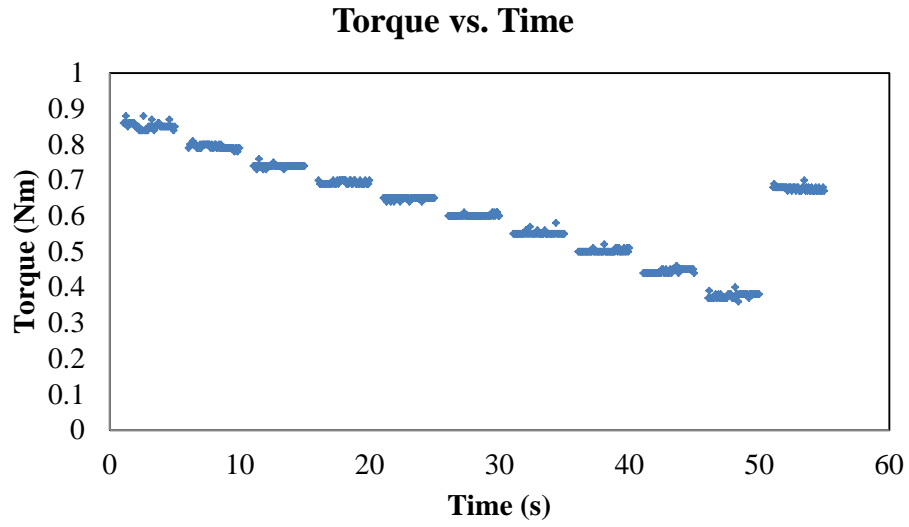
## Torque vs. Time



Figure C.15 FAC40SF5: Shear stress versus time at 40 min.

## FAC40SF5-40 min.



$y = 12.216x + 0.1092$
$R^2 = 0.9961$

$y = 16.781x^2 + 9.5144x + 0.1958$
$R^2 = 0.998$

◆ segr point
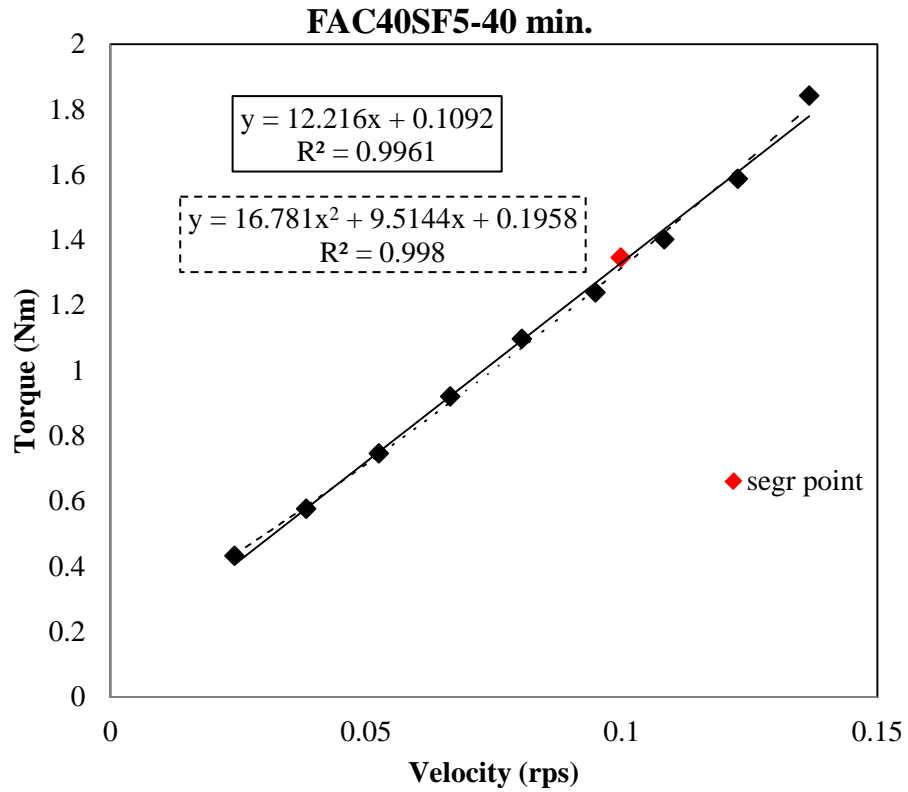
Figure C.16 FAC40SF5: Torque versus rotational speed at 40 min
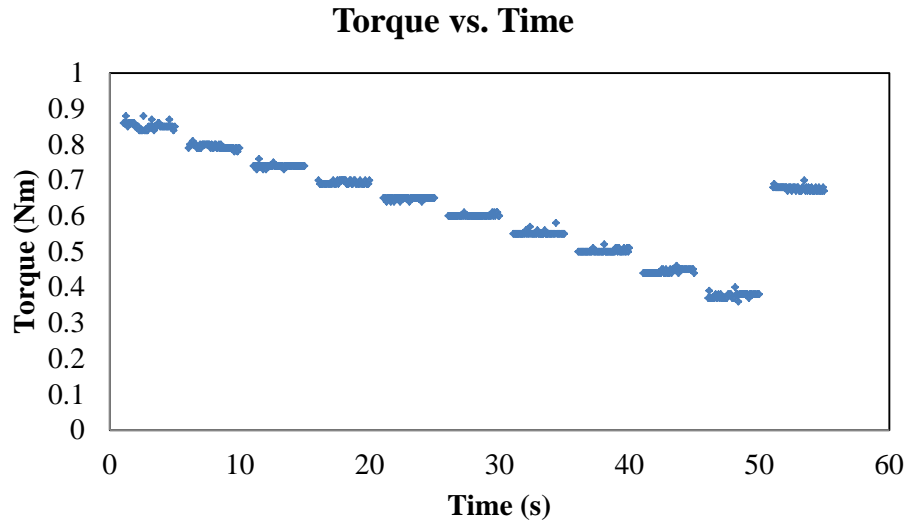
## Torque vs. Time



Figure C.17 FAC40SF5: Shear stress versus time at 60 min.

## FAC 40- 60 min.

$$y = 14.915x + 0.1294$$
$$R^2 = 0.9988$$
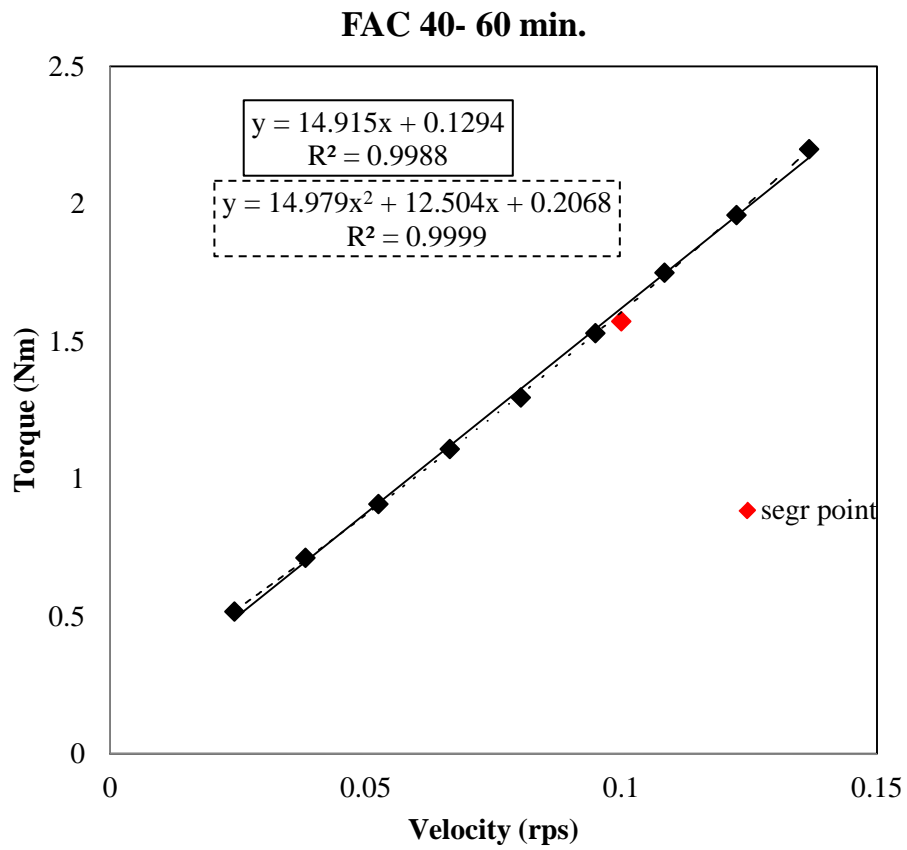
$$y = 14.979x^2 + 12.504x + 0.2068$$
$$R^2 = 0.9999$$

◆ segr point



Figure C.18 FAC40SF5: Torque versus rotational speed at 60 min